Impacts of Ethanol in Gasoline on Subsurface Contamination

by

Juliana Gardenalli de Freitas

A thesis
presented to the University of Waterloo
in fulfillment of the
thesis requirement for the degree of
Doctor of Philosophy
in
Earth Sciences

Waterloo, Ontario, Canada, 2009

Author's Declaration

I hereby declare that I am the sole author of this thesis. This is a true copy of the thesis, including any required final revisions, as accepted by my examiners.

I understand that my thesis may be made electronically available to the public.

Abstract

The increasing use of ethanol as a gasoline additive has raised concerns over the potential impacts ethanol might have on groundwater contamination. In North America, 10% ethanol is commonly being added to gasoline (termed E10). Ethanol is usually denaturated with gasoline compounds before being transported; consequently E95 (95% ethanol) mixtures are also common. Therefore, spills with compositions ranging from E10 to E95 can be anticipated. The compounds of main concern associated with gasoline spills are benzene, toluene, ethylbenzene and xylenes (BTEX), trimethylbenzenes (TMBs) and naphthalene, due to their higher mobility and potential risks to human health. Ethanol is thought to increase mobility of the NAPL, create higher hydrocarbon concentrations in groundwater due to cosolvency, and decrease the rate of gasoline hydrocarbon biodegradation, with consequent increase in the length of the dissolved plumes. The objective of this research was to improve the knowledge about ethanol fate in the subsurface and the impacts it might have on the fate of gasoline compounds. To investigate that, laboratory experiments and controlled field tests supported by numerical modeling were conducted.

To evaluate the impact of ethanol on dissolved hydrocarbon plumes, data from a controlled field test were evaluated using a numerical model. The mass discharge of BTEX, TMB and naphthalene from three sources (E0, E10 and E95) emplaced below the water table was compared to simulation results obtained in the numerical model BIONAPL/3D. It was shown that if ethanol fuel mixtures get below the water table, ethanol is dissolved and travels downgradient fast, in a short slug. Mass discharge from the E0 and E10 sources had similar hydrocarbon decay rates, indicating that ethanol from E10 had no impact on hydrocarbon degradation. In contrast, the estimated hydrocarbon decay rates were significantly lower when the source was E95. The aquifer did not have enough oxygen to support the mass loss observed assuming complete mineralization. Assuming a heterogeneous distribution of hydraulic conductivity did little to overcome this discrepancy. A better match between the numerical model and the field data was obtained assuming partial degradation of hydrocarbons to intermediate compounds, with consequent less demand for oxygen. Besides depending on the concentration of ethanol in the groundwater, the impact of ethanol on hydrocarbon degradation appears to be highly dependent on the aquifer conditions, such as availability of electron acceptors and adaptation of the microbial community.

Another concern related to ethanol biodegradation is formation of explosive levels of methane. In this study, methane $\delta^{13}C$ from toluene and ethanol as substrates was evaluated in microcosm tests. It was shown that methane is enriched in $\delta^{13}C$ when ethanol is the substrate. Ethanol derived methane $\delta^{13}C$ is in the range of -20‰ to -30‰, while methane from gasoline is around -55‰. The different ranges of $\delta^{13}C$ allow it to be used as a tool to identify methane's origin. This tool was applied to seven ethanol-gasoline contaminated sites. Methane origin could be clearly distinguished in five of the seven sites, while in the other two sites methane appears to have been produced from both ethanol and gasoline. Both ethanol and gasoline were identified as the source of methane in hazardous concentrations.

The behaviour of ethanol fuels in the unsaturated zone was evaluated in 2-dimensional (2-D) lab tests and in a controlled field test. In the 2-D lab tests, dyed gasoline and ethanol were injected in the unsaturated zone simulated in a transparent plexiglass box packed with glass beads. Tests were performed under both static conditions and with horizontal groundwater flow. It was confirmed that some ethanol can be retained in the unsaturated zone pore water. However, most of the ethanol went through the unsaturated zone and reached the pre-existing gasoline pool. Ethanol displaced the NAPL to deeper positions, and it was shown that for large ethanol releases much of the gasoline can be displaced to below the water table. The ethanol that reaches the capillary fringe was shown to travel downgradient rapidly at the top of the capillary fringe, while ethanol was also retained in the unsaturated zone.

The behaviour of ethanol fuel spills was further evaluated in a controlled field test. 200L of E10 containing around 5% MTBE was released into the unsaturated zone. Groundwater concentrations of ethanol, MTBE, BTEX, TMB and naphthalene above and below the water table were monitored downgradient of the source in multilevel wells. Lab tests were performed to evaluate the applicability of these samplers for volatile organic compounds. It was shown that volatilization losses might be significant when bubbles formation in the sampling line could not be avoided. A method for losses estimation and correction of the concentrations was developed. Concentrations in the source zone were measured in soil samples. Despite the thin (35 cm) unsaturated zone at the site, most of the ethanol was retained in the unsaturated zone pore water, above the capillary fringe. Being in zones of low effective hydraulic conductivity, ethanol was not transported downgradient, and remained in the unsaturated zone for more than 100 days. Ethanol mass discharge was much lower than would be anticipated based solely on the ethanol fraction in the gasoline and on its solubility. Oscillations in the

water table, particularly when a shallow position was maintained for prolonged periods, flushed some ethanol to zones with high water saturation, where horizontal transport occurred. The ethanol that reaches the saturated zone appears in the downgradient wells as a slug, with relatively low concentrations. No effect of ethanol on gasoline hydrocarbons was observed, a consequence of most of the ethanol being retained in the unsaturated zone.

In summary, spills of ethanol fuels might have two different outcomes, depending on whether most of the ethanol is retained in the unsaturated zone or if most reaches the capillary fringe and the saturated zone. The relation between the ethanol volume spilled and the retention capacity of the unsaturated zone will control the spill behaviour. The volume of ethanol that can be retained in the unsaturated zone is a function of the volume of water that is contacted by the infiltrating NAPL. Therefore, the type of soil, heterogeneities, depth to the water table and area of the spill will be determinant factors.

If a relatively large volume of ethanol reaches the capillary fringe, ethanol will travel rapidly in the groundwater possibly in high concentrations, potentially enhancing dissolved hydrocarbon plumes. However, when most of the ethanol is retained in the unsaturated zone, it will likely be detected downgradient only in low concentration, and in pulses spread in time. In this scenario, impact on hydrocarbon plumes will be minor.

Acknowledgements

Looking back, I remember when the idea of getting into the University of Waterloo and completing a PhD seemed a distant and almost impossible task. Many amazing events happened since then that helped me in my goal, and all these were only possible because of the people I met along the way. You all made this adventure for me extremely rewarding, exciting and, I dare say, fun.

My first thanks go to my supervisor, Jim Barker. Jim has dedicated uncountable hours along these years providing the conditions that made everything run smoothly. Besides all the insightful technical advice, Jim has offered all the guidance and support I needed, particularly when things didn't go as planned. I am really glad I had the chance to learn from him and have him at my side to help me finish this research. Working with Jim has been really inspiring; he is the best example of what a supervisor should be. Jim, thanks for everything. I will always be in debt with you.

I also want to thank my committee members: Jim Smith, Barbara Butler, John Chatzis and Mario Ioannidis for making time to discuss my research and for providing invaluable comments and suggestions since my first year here. Thanks also to my external examiner, Susan Powers, for offering her time. Her name is already on all my references lists, so her presence at my defense puts the last touch on this journey.

Thanks to the three Brazilians that helped me to get here: Vicente Aquino Neto, Everton de Oliveira and Sidney Ferreira Filho were the first people to make it all possible. I am really grateful to them.

I also want to thank Luc Tousignant and Émilie Évrard (LPT Enviro Inc.) for providing access and assistance to the Ontario Site. Thanks also to Jennifer Lambert who twice agreed to help me with the long driving and sampling, despite the cold winter and the smell of butyrate in the groundwater (and in our clothes). Thanks to Dr. Elizabeth Edwards, Eve Moore and Marianne Vandergriendt for all the advice with the microcosm setup and for helping me in keeping those little bugs alive. Thanks to Ramon Aravena and Barbara Fletcher for all the interesting conversations about what the isotope data could possibly mean.

I also had the pleasure to work and learn a lot from John Molson. John introduced me to the world of numerical modeling and he always made himself available to discuss all my ideas. Thanks also for the code modifications and the several reviews. Thanks also to Marian Mocanu and José Luiz Gomes Zoby.

The geophysics group added a new perspective to my research, allowing me see things that would be impossible otherwise (although I am not sure if they were really there…). Thanks to Tony Endres, Cameron McNaughton and Scott Piggott.

Marianne Vandergriendt and Shirley Chatten spend long hours working on my thousands samples, besides answering all my questions on analytical techniques and laboratory procedures. Thanks for your patience! Wayne Noble, Manjula Ravindran and Min Zhang also had the patience to deal with my samples, which sometimes were not so nice and clean…

I also need to acknowledge the two guys that can make everything possible: Paul Johnson and Bob Ingleton. My field work would have been impossible without the suggestions and hard work of both of you. Thanks also to Greg Friday, Sue Fisher and Lorraine Albrecht, for guiding me through the university regulations and procedures.

Many people contributed by answering my random email questions, giving me good suggestions and chatting about hydrogeology and ethanol. Thanks to Bruce Bauman, Bill Rixey, Mette Broholm, Bernadette Conant, Ed Cey and many others.

All the field work, from making the wells to getting more than 2000 samples, was not an easy task, but a lot of people have helped over the years and even made it an enjoyable experience. My thanks to Claudia Naas, Scott Piggott, Cameron McNaughton, Colby Steelman, Melissa Bunn, Daniel Gardner, Colin McCarter, Reynold Chow, Ben Doulatyari, Bobby Katanchi, Marcelo Sousa, Jiri Beranek, Jon Rigg, Neelmoy Biswas, Kammy Sra, Miguel Madrid, Giulia De Santis, John Mosquera, and the list goes on.

Thanks to Marcelo, who agreed to leave a job, family and friends back in Brazil to enjoy a 4+ years long "vacation" with me in Canada, even though I am sure he would prefer if I had chosen the University of Hawaii. Thanks for your support through this whole time. You encouraged me and you made me believe that I can go as far as I want. You made me laugh even in the hard days; at your side everything seemed fun and easy.

Thanks to all my friends: Maricris, Miguel, Paulinho, Ju, Jesse, Soon Young, Reza, Jordi, Barb, Emilio, Sylvia, Bobby and Neelmoy, Erika, Claudia, Michelle, Jenny, Fatemeh, Leif and many others. Because of you these years were awesome (!). In the end, Waterloo proved to be a much more exciting place than I expected.

Finally, I want to acknowledge the financial support of the Brazilian Government (CAPES - Brazil), American Petroleum Institute, NSERC CRD program, the Canadian Petroleum Products Institute, Water and Earth Science Associates Ltd. (WESA), Conestoga Rovers and Associates (CRA) and the Ontario Ministry of Environment.

Dedication

To Vicente de Aquino Neto, for inspiring me and many others.

Table of Contents

List of Figures

List of Tables

Chapter 1
Introduction

1.1 Background

Oxygen-containing organic compounds (oxygenates) have been added to gasoline for decades (Nadim et al. 2001). In North America, tetraethyl lead was one of the first additives to be added to the gasoline. It was used in the US until 1973, when it started being phased out due to the health risks posed by lead. By 1990, tetraethyl lead use in gasoline in the US was almost zero. In 1990, the Clean Air Act established that gasoline should contain at least 2% oxygen. Besides improving octane rating, it was aimed at decreasing air pollution, especially in urban areas. After the Clean Air Act, methyl *tert*-butyl ether (MTBE) use as gasoline additive increased. Then, in July 1999, the Blue Ribbon Panel organized by the USEPA suggested that MTBE use should be substantially reduced and eventually eliminated. Although the health impacts of MTBE were not clearly established, one of the motivations for this recommendation was that MTBE was being frequently detected in surface and ground water reservoirs, as described in Deeb et al. (2003). Ethanol started to rise as a suitable replacement for MTBE after that, and its use has been increasing in North America since then. The increased use of ethanol and biofuels in general, may also have economic and energy security benefits (Granda et al. 2007).

Ethanol use in Brazil followed a different path. According to the Brazilian National Petroleum, Gas and Biofuels Agency - ANP (2009), Brazil started using 4.5% sugarcane derived ethanol in the gasoline in 1977. The percentage increased to 15% in 1979 and then to 22% in 1985. Also, in 1974, the Brazilian government started a program of incentives for the use of hydrated ethanol as a fuel. By 1983, more than 90% of the vehicles sold were ethanol powered. Following oscillations in the petroleum market, the proportion of ethanol powered vehicles decreased until 2003, when flex-fuel vehicles were introduced. In 2008, the consumption of hydrated ethanol and gasoline (with 20 to 25% ethanol) was similar.

The overall environmental impact of ethanol use is controversial (Scharlemann and Laurance 2008; Goldemberg 2008). One of the issues in dispute is the potential that the increase in land use for ethanol production would result in higher prices of food crops due to competition (Luque et al. 2008; Fraiture et al. 2008; Muller et al. 2008) or result in deforestation (Leite 2008). Other issues involve net energy (Granda et al. 2007; Fraiture et al. 2008) and water consumption for biofuels production

(Muller et al. 2008; Fraiture et al. 2008; Dominguez-Faus et al. 2009). Clearly, a complete life cycle analysis of biofuel use needs to consider many aspects and will be complex.

One particular aspect, which is the main interest of this study, is the impact that ethanol fuels might have on groundwater contamination. When gasoline is spilled it moves downwards in the unsaturated zone. Due to its lower density it accumulates at the top of the capillary fringe, the region above the water table that is virtually fully water saturated (Parker 1989; Pantazidou and Sitar 1993; Schroth et al. 1995). If ethanol is present, it can cause further depression of the capillary fringe due to its lower surface tension (Jawitz et al. 1998; McDowell et al. 2003). Also, due to its low density and high solubility, ethanol is likely to accumulate and be transported at the top of the capillary fringe. Several studies indicated that significant horizontal flow and transport can happen in the capillary fringe (Ronen et al., 1997; Henry and Smith 2003; Berkowitz et al. 2004). Berkowitz et al. (2004) emphasized that although the capillary fringe represents only a minor fraction of regional flow, it may play a very important role for shallow contaminant transport at the local scale.

Also, ethanol can facilitate the displacement of NAPLs (non-aqueous phase liquids). Because of this, ethanol injection has been considered as a remediation technique in some studies, particularly for DNAPL's (dense non-aqueous phase liquids) (Oliveira 1997; Jawitz et al. 2000; Palomino and Grubb 2004; Brooks et al. 2004). In the case of ethanol fuel spills, it can modify the shape of gasoline pools, locally increasing gasoline saturation, and mobilize existing gasoline residual phase (McDowell et al. 2003; Stafford et al. 2009). One of the mechanisms by which ethanol can mobilize NAPL is by creating interfacial tension gradients. The interfacial tension between the aqueous phase and NAPL decreases exponentially as the concentration of ethanol in the aqueous phase increases (Oliveira 1997; McDowell et al. 2003). Also, ethanol increases the solubility of hydrocarbon compounds (Morris et al. 1988; Heermann and Powers 1998; Corseuil et al. 2004) and at concentration higher than 70% causes the system ethanol-water-gasoline to be comprised of a single phase (Oliveira 1997; Powers et al. 2001).

Organic compounds in the NAPL are slowly dissolved into the groundwater, threatening groundwater quality. Ethanol cosolvency effects might increase the dissolved hydrocarbon concentrations (Morris et al. 1988; Heermann and Powers 1998; Corseuil et al. 2004). In gasoline contaminated sites, the compounds of main interest are benzene, toluene, ethylbenzene, xylenes (BTEX), trimethylbenzenes (TMBs) and naphthalene, based on their higher mobility and potential health risks; for example, BTE and naphthalene are defined by the USEPA as priority pollutants

(Phelps and Young 1999; Frazer et al. 1995). Monitored natural attenuation, which relies on biodegradation for mass removal, is a common remediation technique applied at gasoline contaminated sites (Wilson et al. 2004). As a consequence, one of the major concerns related to ethanol use is the impact it might have on hydrocarbon biodegradation. Microcosm and column studies have indicated that under aerobic and anaerobic conditions ethanol will be preferentially degraded and will exert a high electron acceptor demand, resulting in a decrease in hydrocarbon biodegradation rates (Corseuil et al. 1998; Da Silva and Alvarez 2002; Deeb et al. 2002; Lovanh et al. 2002; Chen et al. 2008). A review of other potential effects of ethanol on hydrocarbon biodegradation is presented by Powers et al. (2001).

Numerical modeling studies suggested that the decrease in hydrocarbon biodegradation rates due to preferential electron acceptor consumption for ethanol biodegradation could result in longer plumes, which could potentially compromise the efficacy of monitored natural attenuation (Deeb et al. 2002; Molson et al. 2002; Gomez et al. 2008). Hubbard et al. (1994) conducted one field test at CFB Borden, ON, where three solutions were injected in the saturated zone, representing plumes from three different gasoline sources: pure gasoline, gasoline with 10% MTBE and gasoline with 85% methanol. Methanol is considered to have an impact similar to ethanol. BEX were found to be more persistent in the plume with 85% methanol than in the plume from pure gasoline, in agreement with the findings from laboratory tests. In another field study (Mackay et al. 2006), two side-by-side injections of BTX solution were conducted, with one containing 500 mg/L of ethanol. A decrease in the hydrocarbon degradation rates was observed when ethanol was present.

Although several studies investigated impacts of ethanol on gasoline contamination, most were conducted at laboratory scale and focused on particular effects. All the controlled field experiments so far were limited to the saturated zone. The lack of field investigations including the unsaturated zone and capillary fringe is likely due to difficulties associated with sampling in negative gauge pressure conditions above the water table (Ronen et al. 1997; Berkowitz et al. 2004).

1.2 Objectives

The main objective of this thesis is to provide a better understanding of the consequences for groundwater contamination of ethanol addition to gasoline. To achieve that, different potential impacts of ethanol were investigated, including biodegradation and fate in the unsaturated zone and capillary fringe. Ultimately, the goal was to understand how the different processes interact at field scale. Specific objectives of this research are to:

- improve our ability to estimate the impact of 10% and 95% ethanol in gasoline on hydrocarbon degradation near sources in the saturated zone;
- assess the potential for methane generation in ethanol fuel contaminated sites and to develop and test an isotopic tool to identify the source of methane;
- develop and apply a method for groundwater sampling in the capillary fringe suitable for volatile organic compounds;
- evaluate at field scale the significance of organic compounds transport in the capillary fringe;
- evaluate the behaviour of ethanol in the source zone and ethanol transport downgradient and the consequences to gasoline hydrocarbon transport following an E10 spill in the unsaturated zone.

1.3 Thesis Organization

This thesis is organized in 7 chapters, with 5 core chapters (Chapter 2 to 6) written as manuscripts, in the sense that they are stand-alone documents. Each Chapter discusses the ethanol behaviour and its impacts on groundwater contamination by gasoline focusing on a different process or applying different methods. A conceptual model of a gasoline spill and potential impacts of ethanol is shown on Figure 1.1. As discussed in Subsection 1.1, in the event of a gasoline spill in the unsaturated zone, the gasoline will move downwards until it reaches the capillary fringe where it will tend to accumulate. Solubilization of gasoline compounds into the groundwater and transport downgradient will result in the formation of a dissolved plume. One of the main concerns associated with the presence of ethanol in groundwater is that it might decrease hydrocarbons biodegradation rates, resulting in longer dissolved plumes. This issue was dealt with on Chapter 2. Following on the discussion of ethanol impacts on biodegradation, Chapter 3 presents a study on the formation of byproducts, particularly methane. As is discussed on Chapter 2, oxygen is likely to be depleted from the aquifer by ethanol biodegradation, and therefore methane production is likely to happen. A discussion of methane formation and fingerprinting is presented on Chapter 3.

However, the formation of dissolved plumes is dependent on how contaminants behave in the source zone, including the unsaturated zone and capillary fringe. Chapter 4 and 5 discuss how ethanol changes the source zone behaviour and the consequences to the formation of dissolved plumes. To introduce this issue, in Chapter 4 small scale 2D visualization tests were used to develop a conceptual framework of the fate of ethanol and gasoline following spills in the unsaturated zone. One issue that is recognized in Chapter 4 is the transport of volatile organic compounds on the capillary fringe. Since sampling in the capillary fringe at field scale is not trivial, a methodology for sampling in the capillary fringe is developed at Chapter 5.

To finish, Chapter 6 presents a comprehensive investigation of a controlled E10 release at field scale, involving source zone behaviour and the formation of dissolved plumes in the saturated zone. Methods and concepts developed in previous chapters were applied in this field investigation to allow a comprehensive assessment of the impact of ethanol in gasoline. In Chapter 7, the main findings are revisited and an overall conceptual understanding of ethanol and hydrocarbons fate following spills of gasoline with ethanol is presented.

Some chapters had the collaboration of other authors. In Chapter 2, the impact of ethanol on hydrocarbon biodegradation was evaluated in a controlled field test. The field data used in this study

were derived from the work of previous students, Marian Mocanu and Jose Luiz Zoby (Mocanu 2007; Zoby 2006). The data were assessed using a numerical model, BIONAPL/3D (Molson 2007), with the advice and model code developments of Prof. John Molson (Laval University).

The study of methane production and isotopic fingerprinting (Chapter 3) is co-authored by Barbara Fletcher, who performed the ethanol microcosm test and the initial interpretation of the ethanol results, which is the subject of her master thesis (Fletcher 2008). This study was completed with support also from Prof. Ramon Aravena (University of Waterloo). My contributions were the realization and interpretation of the toluene microcosm test, integration of the results from the ethanol microcosm test with Fletcher's interpretation, the assessment of 7 field sites in Ontario and in Brazil and the discussion based on all the data collected. This Chapter is presented as it was submitted to the journal *Ground Water* in July 2009 (Freitas et al. in submission).

Chapter 4 presents the results from two-dimensional laboratory tests to investigate the behaviour of gasoline and ethanol spills in the unsaturated zone and capillary fringe. This study had support from Prof. John Chatzis (University of Waterloo). Part of the results described in this chapter was previously used in the development of a numerical model by Soon Young Yu, and was published in the *Journal of Contaminant Hydrology* in 2008 (Yu et al. 2008).

In Chapter 5 a groundwater sampling technique for volatile compounds in the vadose zone was evaluated. This study is presented in the same format as it was published in *Ground Water Monitoring and Remediation*, in 2008 (Freitas and Barker 2008).

Chapter 6 presents the results and discussion of a controlled E10 release. The discussion of this release encompasses several issues, but it emphasizes two aspects: behaviour in the source zone and consequences to downgradient transport.

Finally, Chapter 7 reviews the main conclusions, discusses the overall implications and provides recommendations for future research.

1.4 Figures

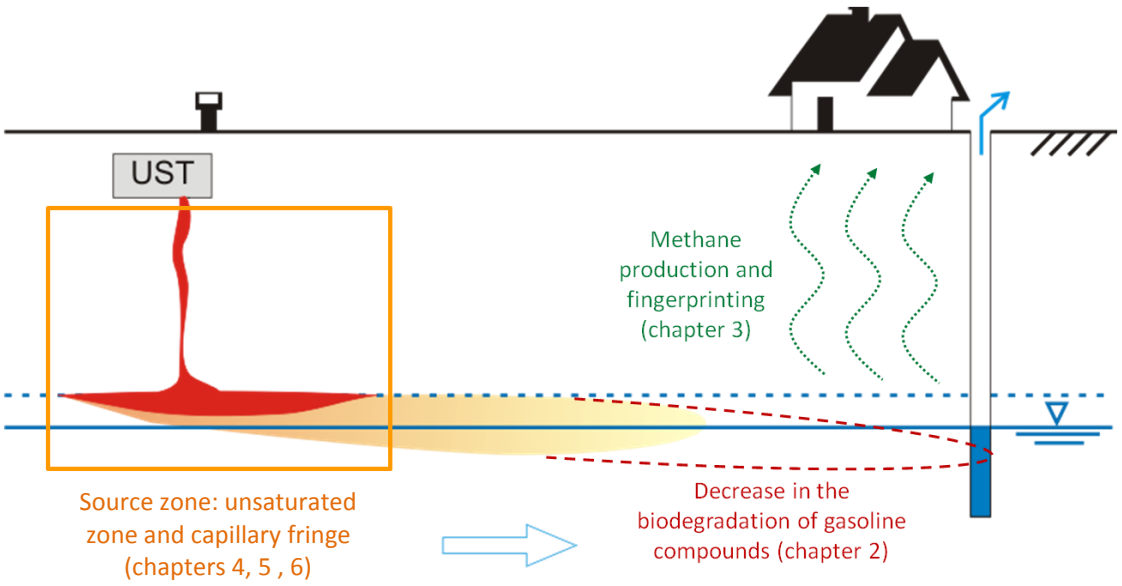

Figure 1.1: Conceptual model of a gasoline-ethanol spill and processes evaluated in this research

Chapter 2
Effect of Ethanol on Gasoline Hydrocarbon Degradation at a Field Site [1]

2.1 Introduction

Leakage from underground storage tanks is recognized as one of the main sources of groundwater contamination throughout the world. Many leaks involve gasoline hydrocarbons, to which oxygenate compounds are commonly added aiming to improve combustion and improve air quality. As oxygenated fuels are released to the environment, it is important to understand the fate and impact of these additives on groundwater quality. MTBE (methyl *tert*-butyl ether) was used as a gasoline additive throughout North America, and has become a significant groundwater contaminant (Deeb et al. 2003). More recently, ethanol has started to replace MTBE as a gasoline additive and its use is increasing in North America. According to the Renewable Fuels Association (2008), more than 50% of the gasoline sold in the United States in 2007 was blended with ethanol, most in mixtures of 10% ethanol and 90% gasoline (E10). Ethanol is transported to be blended with gasoline in mixtures of 95% ethanol and 5% gasoline (E95 – denaturated ethanol). Therefore, E10 and E95 blends are likely to become common sources of groundwater contamination.

The potential effects of ethanol on the biodegradation of aromatic hydrocarbons in groundwater have been discussed in the literature (Williams 2007; Alvarez et al. 2002; Lovanh et al. 2002; Powers et al. 2001; Corseuil et al. 1998). Most concern has focused on the mobile, toxic monoaromatic hydrocarbons: benzene, toluene, ethylbenzene, xylenes (termed BTEX), and on trimethylbenzenes and naphthalene (TMB + naph). These effects include ethanol toxicity to aquifer microorganisms, depletion of electron acceptors and nutrients due to preferential ethanol biodegradation, and alteration of microbial communities (Powers et al 2001).

In a field study by Mackay et al. (2006), dissolved compounds were injected into an aquifer and it was verified that ethanol increased the persistence of hydrocarbons, resulting in longer plumes. This effect had also been predicted in numerical models (Molson et al. 2002a; Deeb et al. 2002; Gomez et al. 2008). This was considered to increase the risks of exposure of potential receptors to the contamination (Lovanh et al. 2002), and eventually could compromise monitored natural attenuation as a remediation strategy at some sites.

[1] The field data used in the analysis were derived from the theses of Marian Mocanu (M Sc, University of Waterloo, 2007) and Jose Luiz Zoby (Ph D, Universidade de São Paulo, 2006).

In this study, the effect of ethanol on the mass discharge of aromatic hydrocarbons leaving a gasoline residual source was evaluated by applying a numerical model to field data obtained from a controlled test in the Borden research aquifer. The effect of aquifer heterogeneities on the mass discharge estimates and on biodegradation was also assessed.

2.2 Field Site and Numerical Model

Three sources composed of around 50 L of API 91-01 gasoline (Prince et al. 2007) with different fractions of ethanol were emplaced below the water table as part of a field experiment conducted at the Borden aquifer, in Ontario (Mocanu 2007; Zoby 2006). The source compositions were: E0: gasoline without ethanol, but with about 9.8% MTBE and 0.2% TBA (*tert*-butyl alcohol); E10: gasoline with 10% ethanol; and E95: gasoline with 95% ethanol. The site monitoring was performed in four transects perpendicular to groundwater flow (Figure 2.1), each with 6, 15 sampling point multilevel wells. The mass of contaminants migrating through each transect per unit time (mass discharge) was calculated using equation 1.

$$Mass\ discharge = \sum_{i=1}^{n} q_i \cdot C_i \cdot A_i \quad (1)$$

q_i: Darcy flux at sampling point i; average of 0.03 m/day assumed equal for all points;

C_i: concentration at sampling point i;

A_i: cross sectional area attributed to sampling point i, perpendicular to flow direction.

A_i was assumed to be a rectangle with dimensions equal to half the distance to the closest sampling points in all directions. The area values were 0.216 m^2 for all points, except for the two deepest points in each well, which were assigned areas of 0.864 m^2.

The numerical model BIONAPL/3D (Molson 2007) was used to simulate groundwater flow, contaminant transport and decay in each gate. It was assumed that the contaminant distribution is symmetrical with respect to the vertical xz-plane through the source centre, so only half of each gate was simulated in the transverse y-direction. Unless otherwise noted, all the dimensions and source parameters discussed below refer to the half-source. The model domain is 20 m in the x-direction (along the groundwater flow direction), 3.5 m in the y-direction and 5.0 m in the vertical or z-direction. The grid elements were defined as 0.2 m in the x-direction and 0.1 m in the y- and z-directions. Three fences for mass discharge calculation were defined with positions corresponding to rows 2, 3 and 4 of the field site (Figure 2.2).

The dimensions of the E0 and E10 residual NAPL sources were based on results from soil samples collected in the gates (Yang 2008). After 980 days there was no indication of gasoline residuals 30 cm upgradient of the injection points, so gasoline spreading from the injection wells in the

x-direction was therefore defined as 0.4 m. The source was taken to be 1.6 m in the z-direction based on the position of the injection screens and on the soil analysis. The cores did not provide enough information to characterize the residual distribution in the y-direction, so it was defined as 3.3 m (1.65 m for the half-source), the lateral distance covered by the injection wells plus 0.6 m to each side. These dimensions result in an estimated half source volume of 1.065 m^3 (total volume = 2.13 m^3) and an average gasoline saturation of 6.8% for the E0 gate and 5.4% for the E10 gate. While this average is reasonable, considerable inhomogeneity of residuals was inferred from analysis of soil samples (Yang 2008).

A different configuration of the E95 source was expected, since ethanol is completely miscible with water. During the source emplacement, water was injected to minimize buoyancy effects. It was assumed that ethanol was instantly mixed with all the injected water, leaving the gasoline trapped in the pores close to the injection points. To simulate this configuration, an initial concentration of 10.057 kg/m^3 of ethanol was applied to a region with dimensions of 2 m x 1.65 m x 1.6 m (x-, y- and z-direction, respectively), totaling 5.28 m^3. The consequences of this assumption and its adequacy are discussed in Subsection 2.3.2. The volume of gasoline in the E95 spill was only 2.4 L. Therefore, a smaller source volume for the gasoline hydrocarbons was assumed: 0.2 m in the x-direction, 1.05 m in the y-direction and 1.3 m in the z-direction (half source volume of 0.273 m^3), dimensions similar to the distance between the injection wells in all directions. With this configuration, the gasoline saturation in the E95 source zone was 1.3%.

For the E10 and E95 gates, 6 components were simulated: benzene, toluene, o-xylene, 1,2,3-trimethylbenzene, all other chemicals present in the gasoline (here termed “bulk”), and ethanol. For the E0 gate, 7 components were included in the numerical model: benzene, toluene, o-xylene, 1,2,3-trimethylbenzene, TBA, MTBE, and bulk. Table 2.1 presents the chemical properties used in the model. The mass of each component in each source zone (Table 2.1) was calculated from the volume injected and the gasoline composition (Prince et al. 2007; Williams 2007).

The aquifer properties adopted in the numerical model are presented in Table 2.2. Initially, the aquifer was assumed to be homogeneous. Gasoline hydrocarbons were considered to be affected by sorption following a linear isotherm model. Ethanol, MTBE and TBA sorption was neglected. The values adopted for the sorption distribution coefficient (Table 2.1) provided retardation factors in the same range as observed in previous field tests at the Borden aquifer (Hubbard et al. 1994; Patrick 1986).

The organic compound degradation was simulated by applying both first-order decay and Monod-type kinetic degradation. The first-order decay rates were based on the values determined by Hubbard et al. (1994) for gasoline without additives and gasoline with 85% methanol in the Borden aquifer (Table 2.3). Methanol and ethanol are expected to behave similarly and to have similar impacts on hydrocarbon biodegradation. For the Monod-type kinetic biodegradation, different combinations of parameters were tested, within the range reported in the literature (Bekins et al. 1998; Lovanh et al. 2002; Alvarez et al. 1991; Schirmer et al. 2000).

The effect of a heterogeneous distribution of the hydraulic conductivity in the biodegradation using Monod-type kinetics was also assessed for the E10 and E95 gates. Five realizations of spatially variable and structurally correlated hydraulic conductivity were tested. The conductivity fields were generated as described in Molson et al. (2008).

The simulation results were compared to the field test data using the mass discharge calculated at each fence by the model and the value calculated from groundwater analyses at the corresponding monitoring row. The comparison between the field data and numerical model results was qualitative only. Statistical methods to compare different simulation results were not adopted due to the uncertainty associated with the field data, as discussed in Subsection 2.3.1. The total mass discharge was calculated through the complete lateral extent, therefore the model results were multiplied by two to allow the comparison.

2.3 Results and Discussion

2.3.1 Uncertainty in the Field Data Derived Mass Discharge Values

To estimate the mass discharge from the field data, several assumptions are made and different variables are involved. Therefore there are many potential sources of uncertainties in the calculated mass discharge values. Although it is not possible to estimate the uncertainties from all the variables involved, statistical data are available for some of the variables, allowing us to estimate the standard deviation on our mass discharge estimates.

One assumption that is made when equation 1 is applied is that each sampling point corresponds to a certain area where the concentration and Darcy flux are constant. The error associated with this assumption is not easily quantifiable, but a numerical study performed by Kubert and Finkel (2006) indicated that this method compares well with other methods for estimating mass discharge. The effect of assuming a constant Darcy flux is further discussed in Subsection 2.3.4.

In equation 1, there are two variables that are likely sources of error, the Darcy flux (q) and the concentration (C). The Darcy flux can be further separated in two: the hydraulic conductivity (K) and the hydraulic gradient (dh/dx). Statistical data from the hydraulic conductivity at the Borden aquifer are available from Sudicky (1986). The variance (σ^2) of $\ln K$ was calculated as 0.29. The hydraulic gradient is also variable in both magnitude and direction (Sudicky 1986), but no statistical data is available. However, our study was conducted in a controlled test cell isolated by sheet pilling on the sides, which likely minimized the variations in the hydraulic gradient.

The uncertainties in the concentration values are of two sources: 1) bias caused during sampling; 2) analytical uncertainties. The samples were obtained using a peristaltic sampling pump in glass vials positioned before the pump head to minimize sorption and volatilization (Einarson 2001). Although it is known that suction sampling can result in the loss of VOC's due to degassing (Barcelona et al. 1984; Parker 1994), the losses by volatilization are expected to be minimal (Barker et al. 1987) in comparison with other hydrogeological uncertainties. Due to the lack of statistical data on the accuracy of the sampling technique, the uncertainties associated with it were not included in the uncertainty analysis. On the other hand, there are statistical data on the uncertainties of the chemical analysis. Quality control in the laboratory was based on standards at five or more concentrations, which were run in triplicate. The relative standard deviation (σ) was always below 14%, for all the ranges evaluated.

The standard deviation of the mass discharge estimates was calculated considering uncertainties associated with the hydraulic conductivity and the analytical technique (Appendix A). The calculated relative standard deviation was around 54%, mainly a consequence of the large variance in the hydraulic conductivity, with the analytical uncertainty causing a negligible uncertainty, no more than 0.5%.

According to Kubert and Finkel (2006), the site geometry that is more similar to our site (σ^2_{lnK} = 0.25, vertical distance between sampling points of 0.25 m and distance between wells of 1.0 m) results in a mean error of mass discharge of around 0.1. The values derived here should not be compared directly to the values estimated by Kubert and Finkel (2006), as they estimated the mean relative errors and the value derived here is an estimate of the standard deviation. Besides, the mean error estimated by Kubert and Finkel (2006) is relative to a time integrated mass discharge crossing a fence, while our standard deviation is derived for a time specific value of mass discharge. Li et al. (2007) applied a geostatistical model to estimate the uncertainties associated with mass discharge estimation using multilevel well measurements. They indicated that the concentrations distribution pattern has a significant effect on the uncertainties in the model estimate. Sampling densities from 1 to 25% were found to produce accurate estimates for continuous and concentrated concentration distribution, and sampling densities higher than 6 to 7% were necessary to produce accurate results when concentrations are scattered with small hot spots. Sampling densities of 6 to 7% were identified by Li et al. (2007) as corresponding to approximately 50 to 60 samples over a cross sectional area of 77 m^2. In our case, 90 samples were collected in an area of 35 m^2, which yields a sampling density higher than stipulated by Li et al (2007). However, the calculation by Li et al. (2007) considered sampling through a 30 cm long screen, while the sampling ports used in this study were point measurements, which results in a lower sampling density.

The uncertainties associated with the mass discharge calculation are further discussed in Subsection 2.3.4, where the numerical model is used to evaluate different scenarios of K distribution.

2.3.2 Linear Degradation

Simulations without considering mass loss in general produced a higher mass discharge than that estimated from the field data, suggesting that some degradation had occurred in the field experiment. The first-order decay rates determined by Hubbard et al. (1994) were then applied to all gates to examine the apparent degradation rates for all components. A TMB degradation rate was not

determined by Hubbard et al. (1994), so the value of 0.004 d^{-1} was initially applied. Simulation results and field data are presented in Figure 2.3.

For benzene in both the E0 and E10 gates, the numerical model results agreed well with the field data assuming a linear decay rate of 0.004 d^{-1}, which was determined by Hubbard et al. (1994) for a gasoline without additives. At the E95 gate the benzene slug had a shorter duration so only a limited number of "snapshots" from the field test were available. Although it is not possible to conclude which degradation rate better fits the field data in the E95 gate, the rate of 0.001 d^{-1} seems to reasonably match the mass discharge data. Therefore, it seems that ethanol did not interfere with benzene biodegradation in the E10 gate, but the higher ethanol concentrations in the E95 gate might have had some impact on it.

The assumption of linear degradation did not provide a good match to the calculated toluene and o-xylene mass discharge in the E10 and E0 gates for any of the decay rates tested. In both gates at later times, the observed toluene and o-xylene mass discharge curves declined at rates faster than predicted by the model. For toluene, the linear decay rates estimated by Hubbard et al. (1994), both with and without methanol, resulted in a higher mass loss than was apparent in all gates, especially for earlier times. A lower biodegradation rate (0.006 d^{-1}) seemed to better simulate the field results from the E0 and E10 gates. For the E95 gate, the linear decay rate of 0.006 d^{-1} also over-estimated the apparent mass loss.

For o-xylene, the "best-fit" mass discharge curve was obtained using a decay rate smaller than found by Hubbard et al. (1994). The data from the E0 and E10 gates seem to present a similar trend, indicating that ethanol did not have a major impact on o-xylene degradation. For the E95 gate, the no-degradation curve fitted the field data relatively well, indicating that o-xylene degradation was negligible. The difference in the E95 gate compared to the other two gates is likely a consequence of the presence of high ethanol concentrations in the E95 gate.

The simulation results for 1,2,3-TMB with linear degradation rates from 0.004 d^{-1} to 0.006 d^{-1} agree reasonably well with the flux estimates from groundwater samples from the E0 and E10 field test. Within the uncertainties in the mass discharge calculations and modelling assumptions, the ethanol in the E10 gate had little impact on the degradation of 1,2,3-TMB. On the other hand, at the E95 gate, 1,2,3-TMB appears to be more persistent. The simulation results did not represent the observed trend at the E95 gate, where the simulated results showed a decrease in mass discharge through time, even under the no-degradation scenario, due to the declining mole fraction of 1,2,3-TMB in the source

residual. This decline was not observed in the groundwater-based mass discharge. It also seems that TMB had a later arrival than predicted by the model. A decrease in groundwater velocity in the model produced a better fit for 1,2,3-TMB, but the higher value adopted seems to be best considering all compounds. It is also possible that 1,2,3-TMB was more affected by sorption than considered in the model. The sorption coefficient adopted results in retardation factors within the range expected for TMB in the Borden aquifer, but a higher value could result in a better match to the field data.

Ethanol would be expected to impact the hydrocarbon compounds biodegradation only when ethanol or its byproducts, that exert a significant BOD (biochemical oxygen demand), co-exist with the compound. For the more retarded compounds, such as o-xylene and 1,2,3-TMB, that implies that ethanol impact would only be seen early, before the unretarded ethanol and byproducts move ahead. This could be one of the reasons why ethanol had no significant impact on the biodegradation of o-xylene and 1,2,3-TMB at the E10 gate. In the E95 gate, the ethanol slug was longer and ethanol and byproducts were likely more persistent due to the higher BOD. From Figure 2.3, even though the ethanol slug was short and not completely delimited in both the E10 and E95 gates, it appears that in the E95 gate the slug was delayed in time, and had a larger overlapping with the other hydrocarbons. Therefore, ethanol and byproducts more likely interfered with hydrocarbon biodegradation at the E95 gate.

Due to the limited number of groundwater sampling events capturing the evolution of the ethanol mass discharge over time for both the E10 and E95 releases, the ethanol degradation rates were not determined. However, in both releases it appears that the degradation rate was lower than the value determined by Hubbard et al. (1994) for methanol, of 0.019 d^{-1} (Figure 2.3).

The simulations for ethanol in the E95 gate were also a relatively poor match with the mass discharge calculated from the field data. The numerical model indicated an earlier breakthrough than was evident in the field (Figure 2.3). This could be caused by a slower groundwater velocity in the field. However, the simulated groundwater velocity produced results that seemed to agree with most of the hydrocarbon field data, which suggests that the groundwater velocity used in the model was reasonable. Another uncertainty in the model input is the size of the source zone. For the E95 release, it was assumed that the ethanol was instantly mixed with the injected water, resulting in a large source volume (8.64 m^3). To verify the implication of this assumption on the model results, another simulation was done decreasing the source volume to 0.48 m^3, using the same dimensions that were assumed for the hydrocarbons. The results obtained are very similar to the results with the larger

source volume. Therefore, the ethanol distribution in the source zone has only a minor impact on the model results and does not explain the discrepancy between the field data and model results.

Enhanced solubility of BTEX (cosolubility) was expected if the ethanol fraction locally exceeded 10%. Corseuil et al. (2004) found that >10% ethanol induced significant cosolvent effects with BTEX. The cosolvency effect was included in the modelling of both the E10 and E95 cases using the formulation described in Molson et al. (2002a). A cosolvency power of 2 was assumed for all compounds, which is in the range of the values determined empirically for gasoline hydrocarbons (Corseuil et al. 2004; Morris et al. 1988). However, including cosolvency did not produce any significant difference in the simulation results. This result was expected for the E10 gate, where the maximum ethanol concentrations in groundwater at row 2 was only 2.4 g/L. For the E95 release, there was a greater potential for ethanol to exert a significant cosolvent effect, depending upon the effective mixing volume ratios of water and ethanol (Poulsen et al. 1992). But high ethanol concentrations were not evident in the field data (highest ethanol concentration at row 2 was 12.8 g/L). Nor was significant cosolvency generated in the model, a consequence of assuming that the injected ethanol was instantaneously mixed with all the co-injected water, which leads to ethanol concentrations in the groundwater in the source zone of around 15 g/L. This value seems to be in agreement with the concentrations of less than 13 g/L in the monitoring wells. For these low ethanol concentrations, cosolvency effects are expected to be negligible (Schwarzenbach et al. 2003).

In summary, the linear degradation model was capable of representing some of the trends observed in the field (e.g., benzene), but the behaviour of toluene and o-xylene, for example, in the E0 and E10 gates, as well as 1,2,3-TMB in the E95 gate, could not be represented using the linear decay assumption. Nevertheless, the simulations with linear decay provided a basis for comparing the mass discharge of the different aromatics. In general, the mass losses in the E0 and E10 gates were similar, indicating that the ethanol impact on their degradation, if any, was minimal. In the E95 gate, all compounds seemed to be more persistent. This result agrees with previous results from Hubbard et al. (1994), which indicated that at high fractions of methanol, the hydrocarbon biodegradation rates were lower.

2.3.3 Monod-Type Kinetic Biodegradation

Numerical simulations of biodegradation assuming first-order decay provided a good match to the mass discharge curves calculated from field data only for some compounds, particularly benzene. Next, Monod-type kinetic biodegradation was applied to evaluate its ability to simulate the fate of the

organic compounds at the field site and improve the comparison of degradation rates between the gates.

Monod kinetic models recognize that electron acceptor availability may limit the rate of biodegradation. The rate of dispersive mixing of oxygen in uncontaminated groundwater with contaminants in the plumes has been shown to control the rate of biodegradation (Cirpka et al. 1999; Grathwohl et al. 2000; Molson et al. 2002b; Cirpka and Valocchi 2007). This has also been shown in the Borden experiments with BTEX and gasoline sources (Hubbard et al. 1994; Schirmer et al. 2000).

In the first scenario tested, complete mineralization of all compounds was assumed and the kinetic parameters were chosen from the range reported in the literature (Bekins et al. 1998; Lovanh et al. 2002; Alvarez et al. 1991; Schirmer et al. 2000) in order to create the maximum degradation (Table 2.4 and Table 2.5). Based on the site groundwater chemistry, with limited concentrations of nitrate and no evidence of sulfate utilization, oxygen was considered as the only electron acceptor. Fraser et al. (2008) also noted oxygen as the sole electron acceptor in a nearby plume in the shallow Borden aquifer.

In the E0 and E10 gates, assuming Monod-type kinetics and complete mineralization, only minor mass loss for all compounds was predicted. In fact, the results were very similar to the simulations without degradation (Figure 2.4). Oxygen was quickly depleted as the contaminants travelled downgradient, and so microbial growth was limited to the few areas where oxygen and contaminants were available: in the source zone and on the dispersive fringe of the plume. The restriction of biodegradation to peripheral zones of the plume where transverse dispersion causes mixing of electron acceptors and the substrate was also shown by Grathwohl et al. (2000), Tuxen et al. (2006); Cirpka and Valocchi (2007) and Bauer et al. (2009).

The E95 gate showed a different trend (Figure 2.4). In this case, although the mass discharge for benzene and ethanol were not significantly altered (as in the E0 and E10 gates), the other compounds showed a significant decrease in the mass discharge at later times. In this gate, ethanol is present in much higher mass. While ethanol is present, oxygen is quickly depleted, and biodegradation is limited. But ethanol travels out of the system quickly, and therefore biodegradation of only the more mobile compounds, like benzene, are impacted by ethanol. As ethanol leaves the system, the availability of oxygen increases, resulting in a sharp decrease in hydrocarbons mass discharge, especially in the simulated curves for TMB and xylene. The mass discharge values from the field data for these two compounds were higher than the simulations with biodegradation, and similar to the

results with no biodegradation, indicating that there was no significant mass loss due to biodegradation in the field. Based on these results, it seems that biodegradation of TMB and xylene was not limited by oxygen availability. Biodegradation of these compounds could have been limited by nutrient availability. Nutrient transport and reaction were not included in the numerical model simulation. Nutrient availability could also have limited the biodegradation of other compounds such as benzene and ethanol, but based on the model results, oxygen was already a limiting factor for biodegradation of these compounds and, therefore, it is not possible to infer if other factors were limiting their reaction.

However, in the model oxygen availability appeared to be limiting the mass loss due to biodegradation in both the E0 and E10 gates. The model formulation used does not consider the availability of nutrients, although that could be a factor in the field. Since insufficient oxygen was available to support the mass loss measured during the field test assuming complete mineralization, it is possible that biodegradation stopped at intermediate compounds. The presence of organic acids as hydrocarbon breakdown products at field sites has been reported by Barcelona et al. (1995) and Fang et al. (2000). King et al. (1999) described the formation of organic acids from the biodegradation of coal tar creosote in the Borden aquifer. In a study of natural attenuation of organic compounds from the same creosote source, Fraser et al. (2008) showed that, assuming complete mineralization, oxygen availability was not sufficient to account for the apparent mass reduction, and so the possibility of partial degradation was also considered. Unfortunately, no typical intermediates were analyzed in the field experiment discussed here.

Yu et al. (2001a) reported catechol, 3-methylcatechol and 3,6-dimethylcatechol as the major intermediates for benzene, toluene and p-xylene degradation under aerobic conditions. They found that that under oxygen-limited conditions, phenol and cresols accumulated in the system, from benzene and toluene, respectively. They also verified that biomass growth was largely controlled by the degradation of the intermediates. The formation of catechol, phenol and other biodegradation intermediate products described in the literature (Smith 1990; Tao et al. 2004; Yerushalmi et al. 2002), result in different utilization ratios of oxygen to organic substrate. The reactions describing toluene biodegradation to different products (but neglecting carbon conversion to biomass) are shown in equations 2 to 5. For those reactions, the stoichiometric mass ratios of oxygen to toluene are 3.13, 0.52, 0.35 and 0.17; a difference of almost 20.

toluene mineralization: $C_7H_8 + 9\ O_2 \rightarrow 7CO_2 + 4H_2O$ (2)

toluene to benzoic acid: $C_7H_8 + 1.5\ O_2 \rightarrow C_7H_6O_2 + H_2O$ (3)

toluene to 3-methylcatechol: $C_7H_8 + O_2 \rightarrow C_7H_8O_2$ (4)

toluene to p-cresol: $C_7H_8 + 0.5\ O_2 \rightarrow C_7H_8O$ (5)

benzene to catechol: $C_6H_6 + O_2 \rightarrow C_6H_6O_2$ (6)

benzene to phenol: $C_6H_8 + 0.5\ O_2 \rightarrow C_7H_6O$ (7)

xylene to 3,6-dimethylcatechol: $C_8H_{10} + O_2 \rightarrow C_8H_{10}O_2$ (8)

Based on this information, two scenarios were tested for the E0 and E10 gates. Scenario 1 was defined to simulate degradation of benzene, toluene and xylene to catechol (equation 6), 3-methylcatechol (equation 4) and 3,6-dimethylcatechol (equation 8). Scenario 2 simulated degradation of benzene, toluene and xylene to phenol (equation 7), cresols (equation 5) and 3,6-dimethylcatechol (equation 8). In Scenario 2 the microbial yield coefficient was also decreased to values in the lower range described in the literature, since biomass growth is said to be strongly related to the degradation of the intermediates (Yu et al. 2001a). Table 2.6 presents the values adopted in each simulation.

Although methane was not identified at the site in significant concentrations in three monitoring dates (Mocanu 2007), it is possible that ethanol was degraded anaerobically to intermediate products such as acetate, propionate and butyrate (Chen et al. 2008; Wu and Hickey 1996; Kim et al. 1994). In the simulations for the E10 gate considering partial degradation of hydrocarbons, it was arbitrarily assumed that only 15% of the ethanol was degraded aerobically and exerted a demand for oxygen, with the remaining being degraded anaerobically. The simulation results and field data are presented in Figure 2.4.

In the partial degradation Scenario 1, the simulated mass loss rate was still lower than that estimated from field data for benzene and toluene, indicating that oxygen availability might still be more limiting in the model than in the field. For toluene, the slope of the mass discharge curve after the peak seems to represent the trend in the field data better than the linear model (Figure 2.3), showing a faster decrease in the mass discharge with time than the linear decay model. For benzene in the E0 gate, the simulation was closer to the calculated field mass discharge data than at the E10 gate.

For o-xylene, the results from partial degradation Scenario 1 provided a good match with the field data for both E0 and E10 gates. The Monod-type kinetic model was able to capture the decrease in mass at later times, which was not well represented by the linear decay model. For 1,2,3-TMB, the numerical model match to the field data was poor. The result for the E0 gate seems to follow the field

data better than the E10 gate, where the mass loss in the simulations was too small in comparison to the field data for the earlier times, similar to what was observed for benzene.

Since partial degradation Scenario 1 suggested that oxygen was more limiting in the model than in the field, the ratios of oxygen to substrate consumed were lowered further in partial degradation Scenario 2, as presented in Table 2.6.

In partial degradation Scenario 2, a higher mass loss was observed for all compounds. The simulation represented benzene well in the E0 gate, but not in the E10 gate. The difference in the simulation results is likely a consequence of the oxygen consumption by ethanol. In both the E0 and E10 gates, a good match was obtained for toluene, while for o-xylene the mass discharge from the numerical model was lower than observed in the field. The numerical model was still unable to represent the field trend observed for 1,2,3-TMB.

The partial degradation products of gasoline hydrocarbons are known to be easily degradable. It is normally assumed that the initial substrate degradation is the limiting step of the mineralization reaction. However, Yu et al. (2001b) pointed out that a two-step model incorporating that intermediates control cell growth might be more appropriate to simulate BTEX aerobic degradation. The Monod-kinetic model applied here assumes that cell synthesis is based on the biodegradation rate of the initial substrate. While this was shown to be adequate in some cases (Schirmer et al. 2000), other studies have indicated that biomass growth presents a lag phase to the biodegradation of the initial substrates and it persists growing until after all the substrate has been removed (Chang et al. 1993). This indicates that the oxygen consumption could be more distributed in time in comparison to assuming that the reaction happens in a single-step.

Another simulation was performed for the E10 gate with the same parameters as in partial degradation Scenario 1, but maintaining the ratio of oxygen to ethanol consumed of 2.09, which means that all ethanol was mineralized (Figure 2.5). For benzene, the increase in oxygen consumption by ethanol biodegradation resulted in a higher peak mass discharge. For the more hydrophobic compounds, the assumption of ethanol mineralization created only a small deviation from the curve with less oxygen demand exerted by ethanol (a small peak with short duration at an earlier time), indicating that the impact of ethanol on the hydrocarbon mass discharge is limited to a short period of time when ethanol or ethanol-derived BOD is still close to the BTEX plumes. Molson et al. (2002a) illustrated this influence of such a “slug” of ethanol migrating at the front of BTEX plumes.

2.3.4 Effect of Heterogeneous K Field on Mass Discharge Values and Biodegradation

In the previous simulations the aquifer was considered homogeneous with respect to hydraulic conductivity. However, all aquifers have some degree of heterogeneity, which can modify the plume behaviour and impact the mass discharge through time. In addition, in the simulations using Monod-type kinetics, oxygen dispersion into the plume was identified as the step limiting the mass loss. In a heterogeneous aquifer the rate of mixing between uncontaminated groundwater and the contaminants might be higher, increasing the oxygen availability for biodegradation (Werth et al. 2006; Bauer et al. 2009). To address these two questions, the two simulations for the E10 and E95 gates, one without biodegradation and the other assuming complete mineralization were redone using heterogeneous K fields.

Five realizations of spatially variable and structurally correlated hydraulic conductivity were used in the simulations. The conductivity fields were previously described in Molson et al. (2008) and are based on properties of the Borden aquifer. The simulation results for the E10 and E95 gates are presented in Figure 2.6 and Figure 2.7, respectively.

Based on the non degradation scenarios it can be seen that the heterogeneous K had a major impact on the mass discharge values over time in both the E10 and E95 gate. In general, the contaminants arrived earlier at the fence in the heterogeneous scenarios. In the E10 gate, benzene and ethanol had lower peak mass discharges than the homogeneous scenario for all K realizations. However, for the other compounds the homogeneous scenario resulted in intermediate peak concentrations. Similarly, in the E95 gate, the heterogeneous scenarios resulted in both lower and higher peaks of mass discharge.

The contours of the plumes were significantly altered in the heterogeneous K distribution, as highlighted in Figure 2.8. With the random field K2, a much earlier arrival was noticed, which was caused by a relatively thick and continuous high conductivity layer (Figure 2.9). The heterogeneous K distributions seem to have also impacted the rate of oxygen dispersion into the contaminated groundwater. The mass biodegraded in different K fields can be inferred from the distance between the curves without biodegradation and assuming mineralization (Figure 2.6 and Figure 2.7). For most but not all of the scenarios tested, more mass was degraded in the heterogeneous scenarios in comparison to the homogeneous scenario (Figure 2.10 and Figure 2.11).

To compare the results with lab studies in the literature, we calculated the reaction enhancement factor (REF): the ratio between the mass degraded in the heterogeneous and homogeneous conditions,

as defined by Bauer et al. (2009). Values for toluene ranged from 0.87 to 1.34 for the E10 gate. The highest value, 2.04, was obtained for TMB. The values are in the same range as reported in Bauer et al. (2009), for a 2D microcosm test using toluene (REF from 1.23 to 1.82).

Although in general there was an increase in the hydrocarbon compounds mass biodegraded in the heterogeneous scenarios, in the E10 gate the mass degraded was still low in comparison to the mass injected (Table 2.7). The cumulative benzene mass apparently removed by biodegradation in the field test was estimated as the difference between the total benzene mass injected and the benzene mass that crossed Row 4. To estimate the benzene mass that crossed Row 4, the data points were integrated using the trapezoid rule and assigning values of zero for the mass discharge at times 100 days and 700 days. Benzene was the only compound to which this estimate was made since it was the only hydrocarbon that more clearly approached the zero mass discharge within the 600 days. The benzene mass degraded was estimated in 38% of the total mass. This value is more than two times the values calculated in the heterogeneous scenarios. Therefore, while heterogeneities do increase the extent of biodegradation, the difference is not great enough to explain all the mass loss observed in the field test in the E10 gate.

In the E95 gate, no mass loss of any of the hydrocarbons was evident considering the heterogeneous K simulations (Figure 2.7). The same estimate of cumulative mass of benzene biodegraded in the field was done for the E95 gate. The mass biodegraded was estimated in 10%, which agrees with the values calculated in the heterogeneous scenarios. Ethanol mass discharge curves were strongly influenced by the heterogeneous K distributions in both the E10 and E95 gates. Considering the limited number of mass discharge points from the field, it is not possible to reliably assess if ethanol was biodegraded and, if so, to what extent.

The concentration distributions in the simulations with the heterogeneous K are likely closer to the field test than the distributions generated in the simulations with the homogeneous K. While the numerical model calculates the mass discharge based on a unique Darcy flux at each node, the mass discharge from the field data was calculated assuming a homogeneous flux throughout the section. The extent of variation in the Darcy flux can be assessed by considering how groundwater velocity varies through the section. In the K3 field, the velocities at row 4 ranged from 27 to 2 cm/day, while the average velocity is 6.75 cm/day. Variations of velocity in this range have been measured at the site (Devlin et al. 2009). To better understand the errors caused by the assumption of an average

Darcy flux in the whole section, the mass discharge values were recalculated using the numerical model results of concentration, but using the average Darcy flux.

In general the mass discharge calculated using the average Darcy flux was lower than the mass discharge considering the heterogeneous hydraulic conductivity distribution (Figure 2.12 and Figure 2.13). This is expected as most of the mass travels through high conductivity zones, where velocities are higher. In some cases (ethanol and benzene in Figure 2.12) at later times the mass discharge calculated using the average velocity was higher. This is a consequence of the delayed transport in the less permeable zones. This indicates that the values calculated from field data using an average value of Darcy flux more likely will underestimate the overall mass discharge, but may extend the time of significant flux of "slugs".

For the heterogeneous fields simulated, the error in the peak mass discharge due to the use of an average Darcy flux exceeded 50% for benzene, which is in the same order of magnitude as the standard deviation estimated in Subsection 2.3.1. Considering the 5 scenarios simulated, the mean relative error in the peak mass discharge was 0.3. This value is higher than the value of 0.1 determined by Kubert and Finkel (2006), for the scenario that closer represents the Borden aquifer. The difference is likely due to differences in the geometry of the problem, and also because Kubert and Finkel (2006) adopted a constant source and looked at the steady-state concentrations distribution, representing a time integrated value of mass discharge. In contrast, a transient source and mass discharge varying with time was considered in this study.

2.4 Conclusions

A comparison of the mass discharge obtained from the field data and numerical simulations indicate that significant monoaromatic mass loss occurred in both the E0 and E10 releases. Although the first-order decay model matched the field data imperfectly, the modeled decay rates that provided the best fit to the field data were similar for the two gates, indicating that 10% ethanol had no more than a minor impact on hydrocarbon biodegradation. On the other hand, the observed mass loss was significantly lower when the initial mixture contained 95% ethanol.

These results contrast with the study by Mackay et al. (2006), where relatively low ethanol concentration, 500 mg/L versus 2300 mg/L in the E10 gate in our study, resulted in a significant increase in monoaromatic plume length and mass discharge. In that study site, sulfate was the main electron acceptor and the site had been previously contaminated by gasoline compounds, with indications that the microbial community was already adapted to anaerobic monoaromatics degradation. In our field experiment, there was no previous exposure to hydrocarbons and the aquifer was initially mildly aerobic. Besides that, the dissolved hydrocarbon concentrations in the Mackay et al. (2006) experiment were around 1-3 mg/L, around ten times less than the concentrations found in our study. According to Mackay et al. (2006), the BTX concentrations injected did not deplete sulfate substantially when ethanol was not present, but with ethanol present, sulfate was consumed causing a shift in geochemical conditions. As a consequence of these factors, the biodegradation rates reported by Mackay et al. (2006) were significantly different with and without ethanol, but in both cases they were higher than inferred in our study. Mackay et al. (2006) estimated benzene biodegradation rates of 1.18 d^{-1} and 0.06 d^{-1}, for the scenario without and with ethanol, respectively. Both decay rates are higher than the values estimated in our tests: 0.04d^{-1} for the E0 and E10 sourced plumes. Therefore, it appears that in our test biodegradation was limited by the availability of electron acceptors even when ethanol was not present (which was not the case in Mackay et al. 2006), possibly by nutrient availability and perhaps by an unacclimated microbial community. Therefore, the addition of ethanol did not cause any evident change in the mass discharge at the Borden test as it didn't significantly change the conditions controlling hydrocarbon biodegradation, in contrast with what was reported by Mackay et al. (2006). The Mackay et al. (2006) experience might be most relevant to a release of ethanol or ethanol-fuel into a pre-existing, anaerobic plume, while our experiment may be more relevant to a release of ethanol-fuel into a pristine, aerobic aquifer.

Incorporating different heterogeneous distribution of hydraulic conductivity results in significantly different mass discharge over time. This casts some doubt on the biodegradation rates inferred from models based on a homogeneous K field. Monod type kinetic models in the homogeneous scenario indicated that there was not enough oxygen to support the observed mass loss at the E0 and E10 gates. Heterogeneous K distributions provide only a slight increase in electron acceptor availability, not sufficient to provide a good match to the field estimates of mass discharge. Further, assuming partial degradation of hydrocarbons to intermediate compounds resulted in less demand for oxygen and an improved fit to the field data.

In conclusion, ethanol reduced the attenuation of gasoline hydrocarbons only when present in high fraction, as in the E95 release. In the E10 release, no impact of ethanol on hydrocarbon biodegradation was evident.

2.5 Figures and Tables

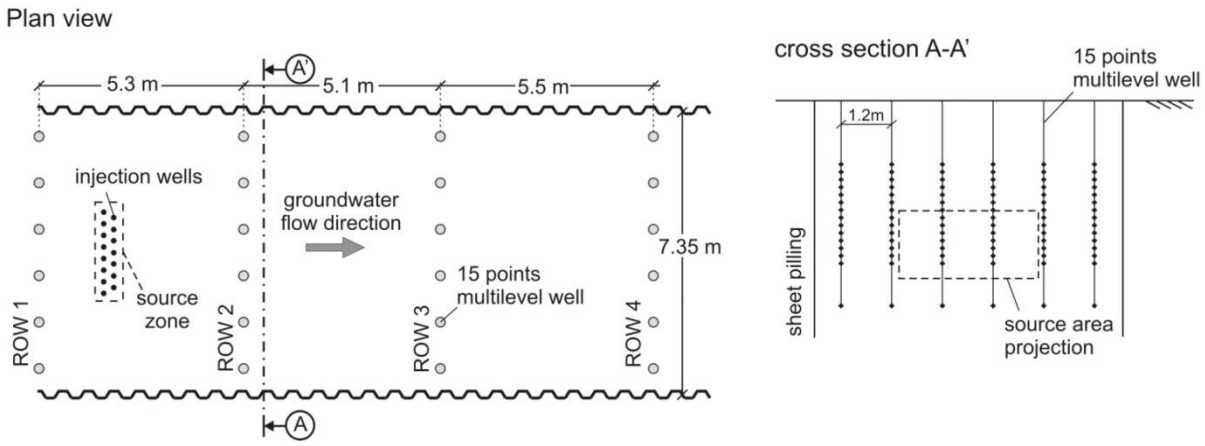

Figure 2.1: Field setup.

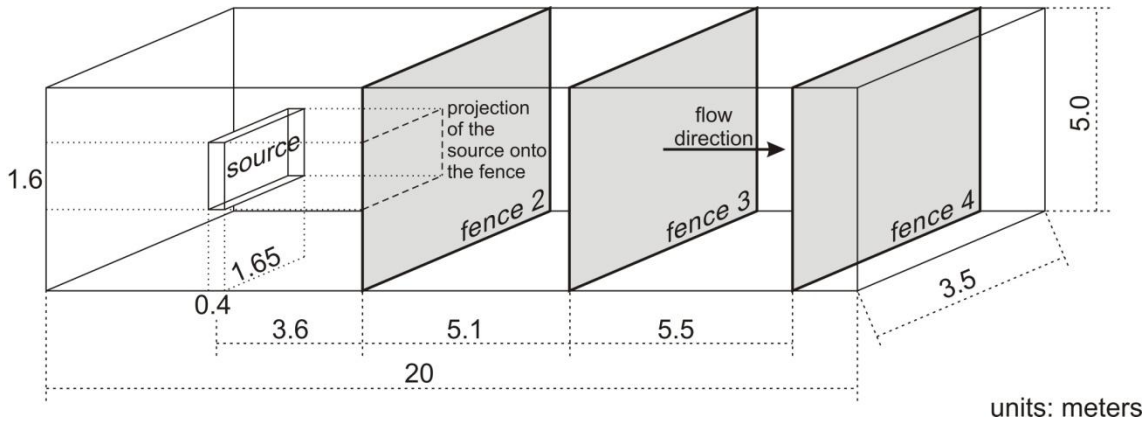

Figure 2.2: Model domain for the E10 and E0 simulations, representing half of each gate, and showing the corresponding half-source.

Figure 2.3: Comparison of field data (dots), non-degradation (λ=0; continuous line) and linear degradation simulation results at Row 4. Mass discharge (g/day) is on the y-axis and time (days) on the x-axis. Error bars represent 2 standard deviations. Note changes in flux scale for the E95 gate results.

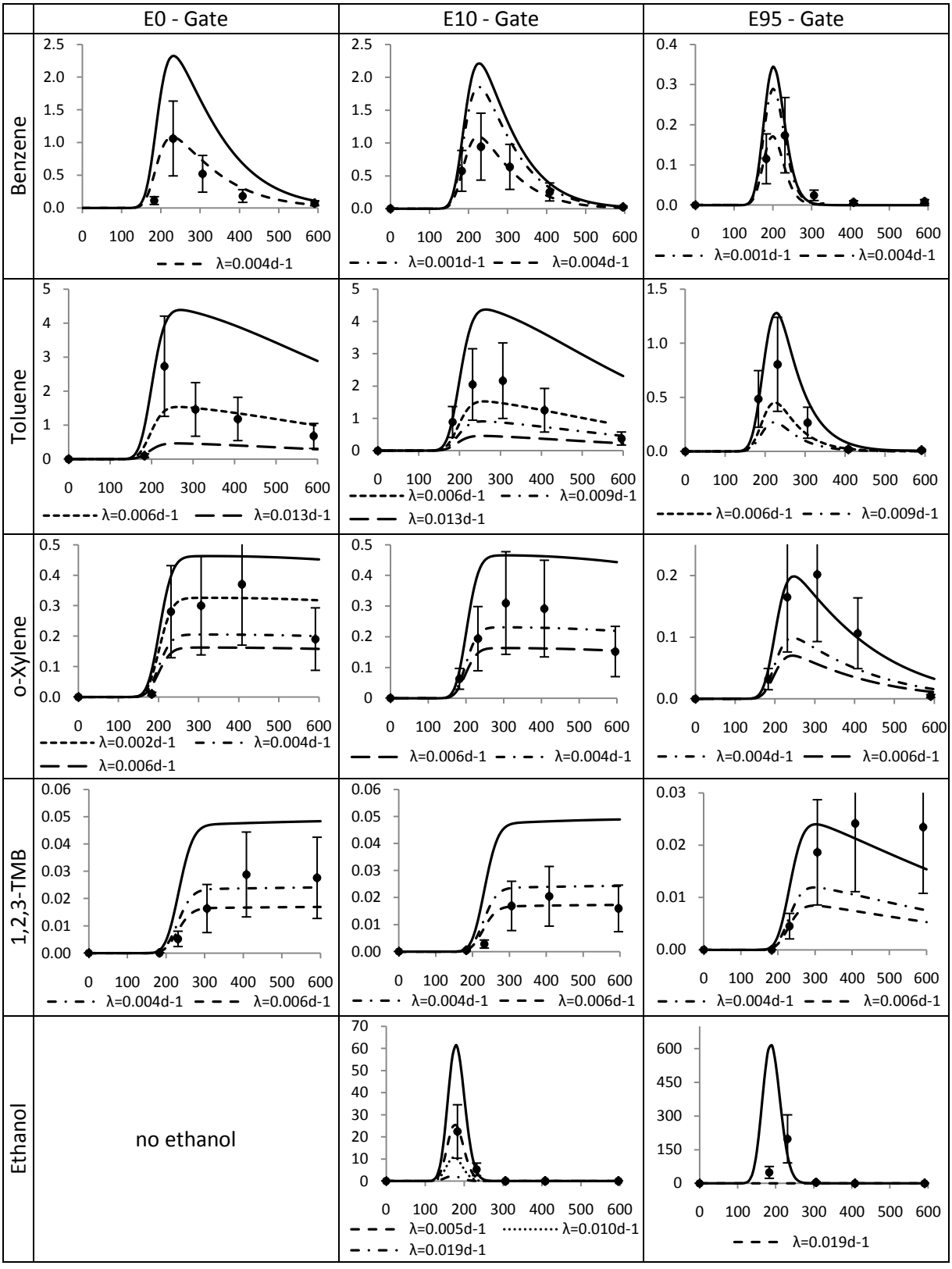
E0 - Gate
E10 - Gate
E95 - Gate
Benzene
Toluene
o-Xylene
1,2,3-TMB
Ethanol
no ethanol
λ=0.004d-1
λ=0.001d-1
λ=0.006d-1
λ=0.009d-1
λ=0.013d-1
λ=0.002d-1
λ=0.005d-1
λ=0.010d-1
λ=0.019d-1

Figure 2.4: Comparison of field data (dots) and Monod-type kinetic degradation simulation results with different ratios of oxygen to substrate at Row 4. Mass discharge (g/day) is on the y-axis and time (days) on the x-axis. Error bars represent 2 standard deviations. Note changes in flux scale for the E95 gate results.

Legend:

——— base case

– · – · mineral.

— — Partial 1

····· Partial 2

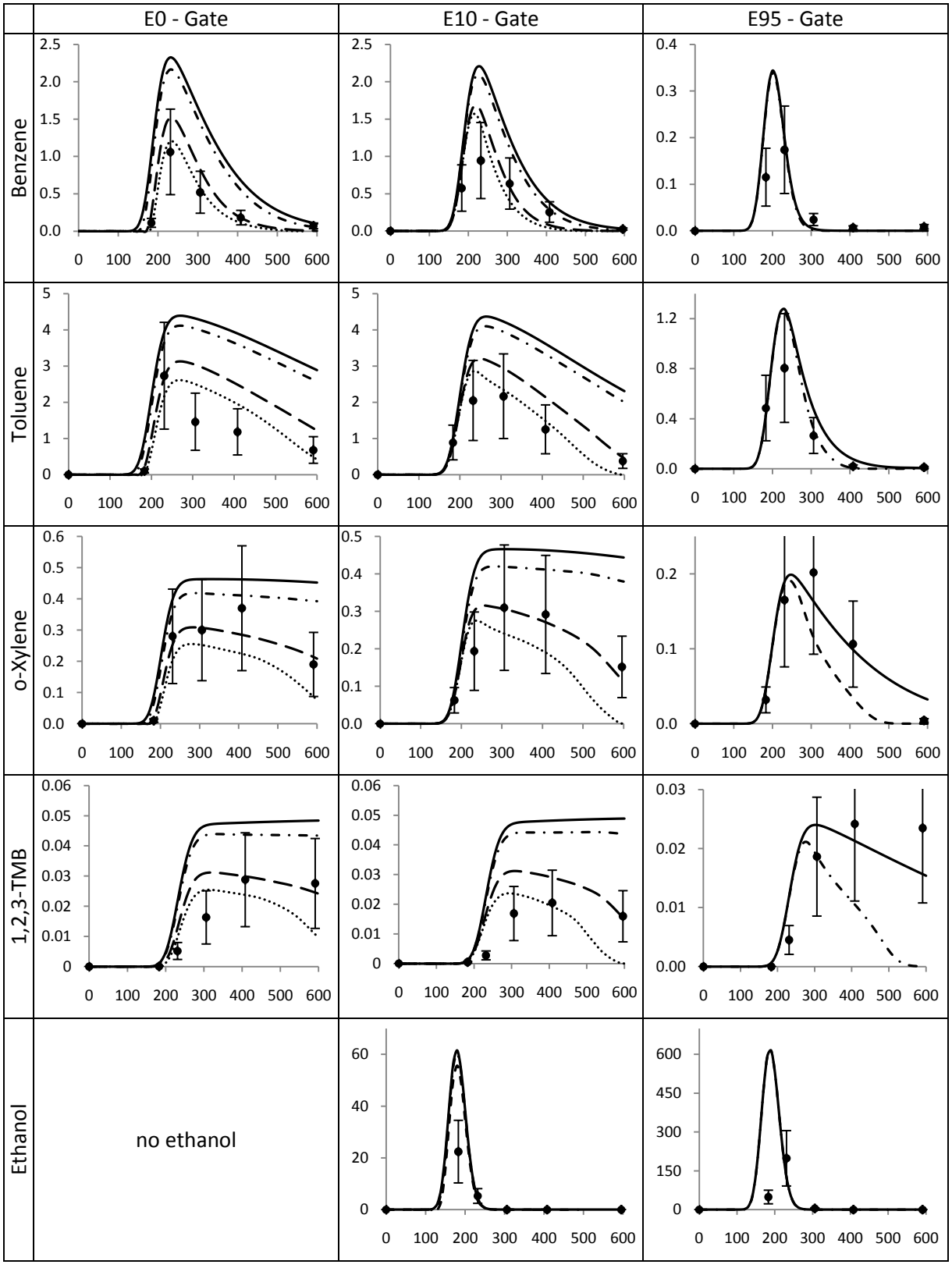
E0 - Gate
E10 - Gate
E95 - Gate
Benzene
Toluene
o-Xylene
1,2,3-TMB
Ethanol
no ethanol

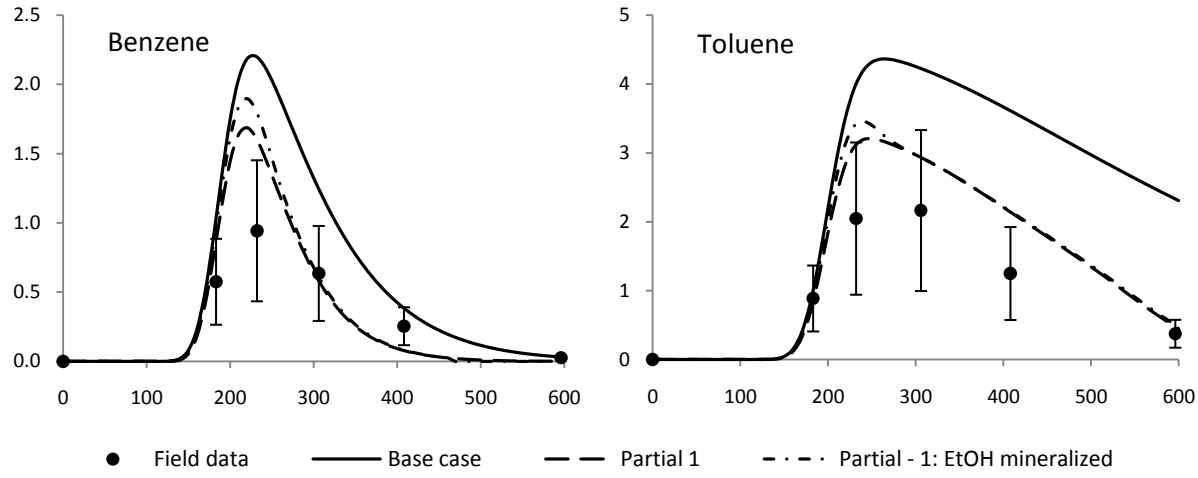

Figure 2.5: Impact of ethanol biodegradation on benzene and toluene mass discharge curves at the E10 gate, Row 4. Mass discharge (g/day) is on the y-axis and time (days) on the x-axis. Error bars represent 2 standard deviations.

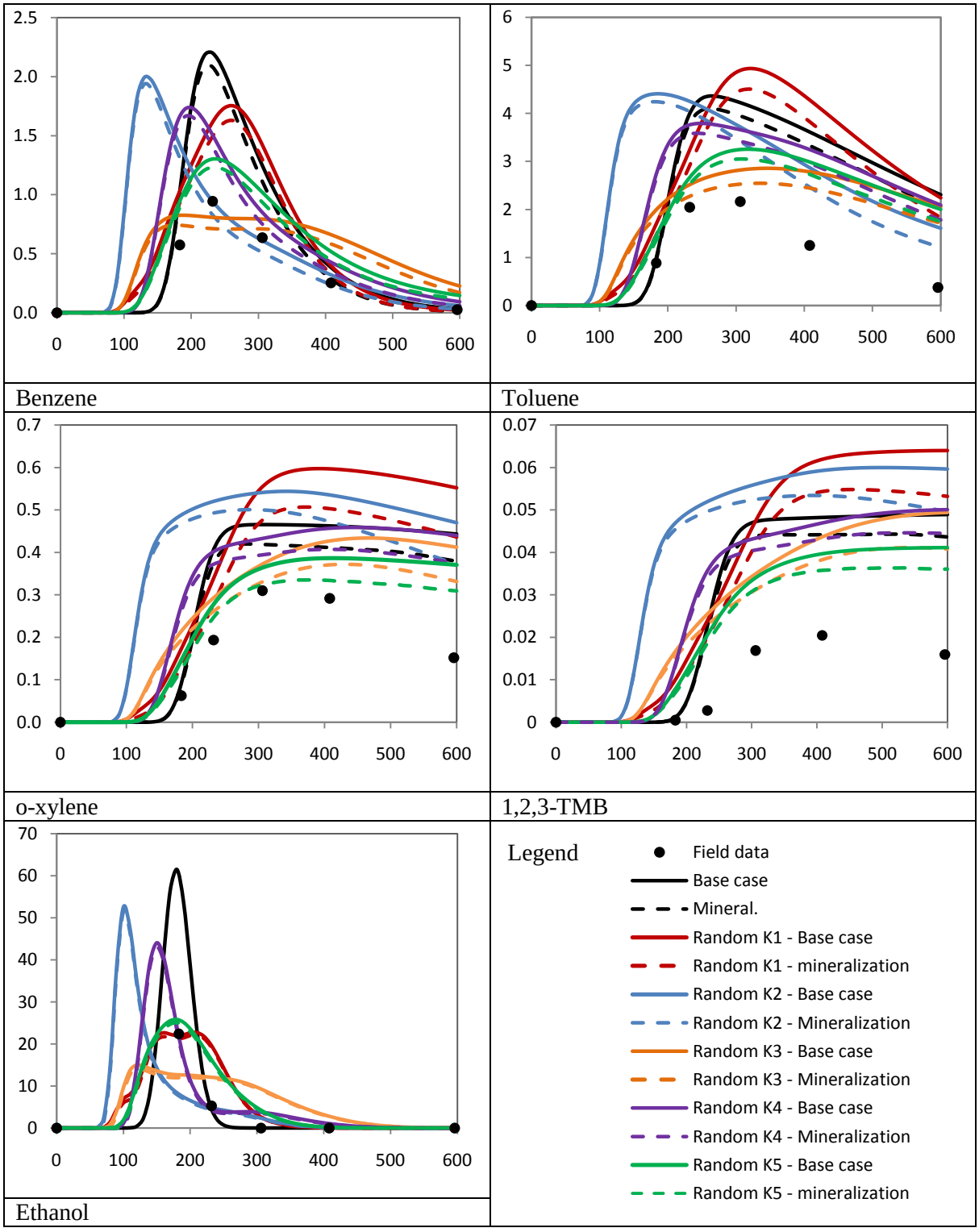

Figure 2.6: E10 gate: Results for heterogeneous scenarios. Mass discharge (g/day) is on the y-axis and time (days) on the x-axis.

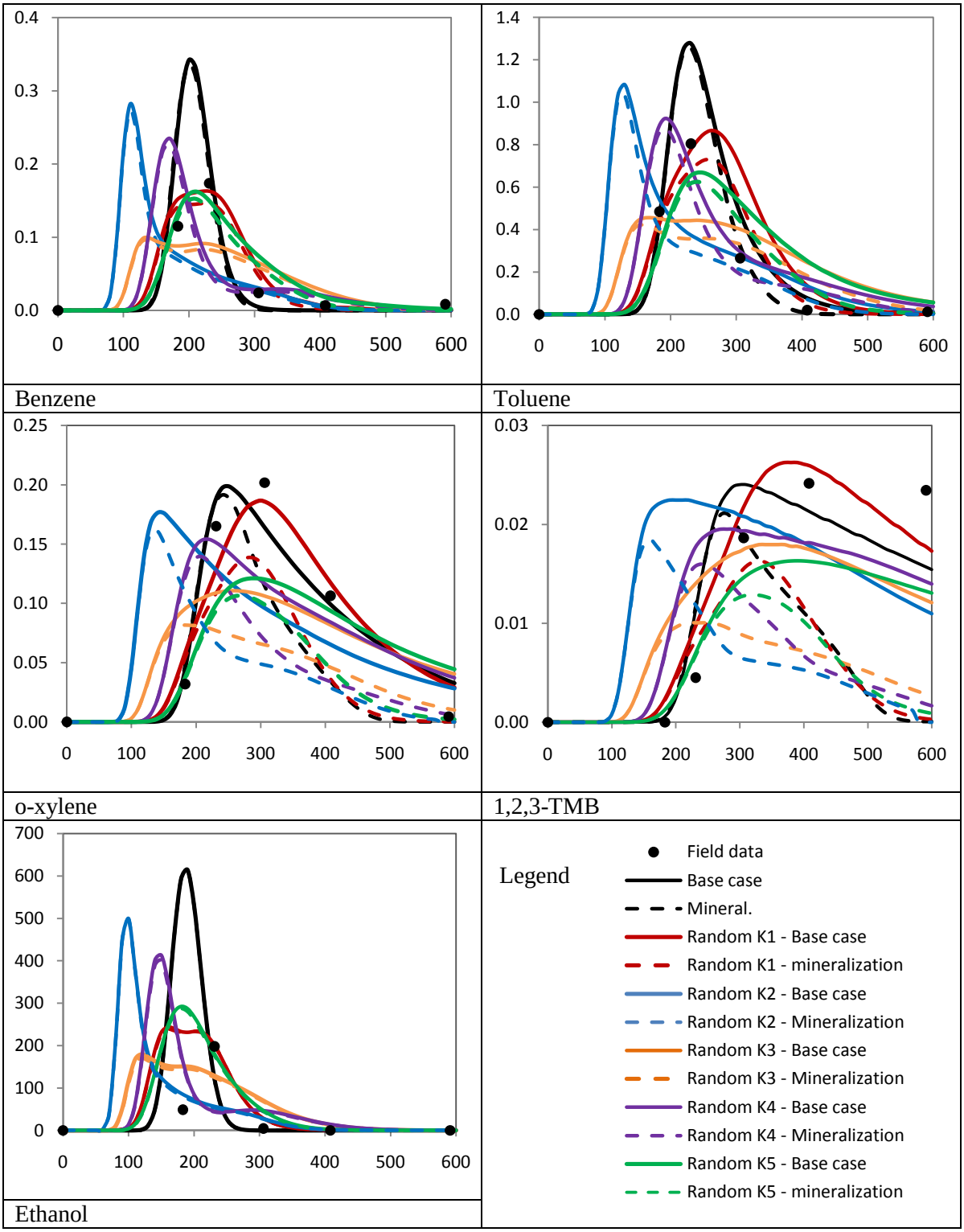

Figure 2.7: E95 gate: Results for heterogeneous scenarios. Mass discharge (g/day) is on the y-axis and time (days) on the x-axis.

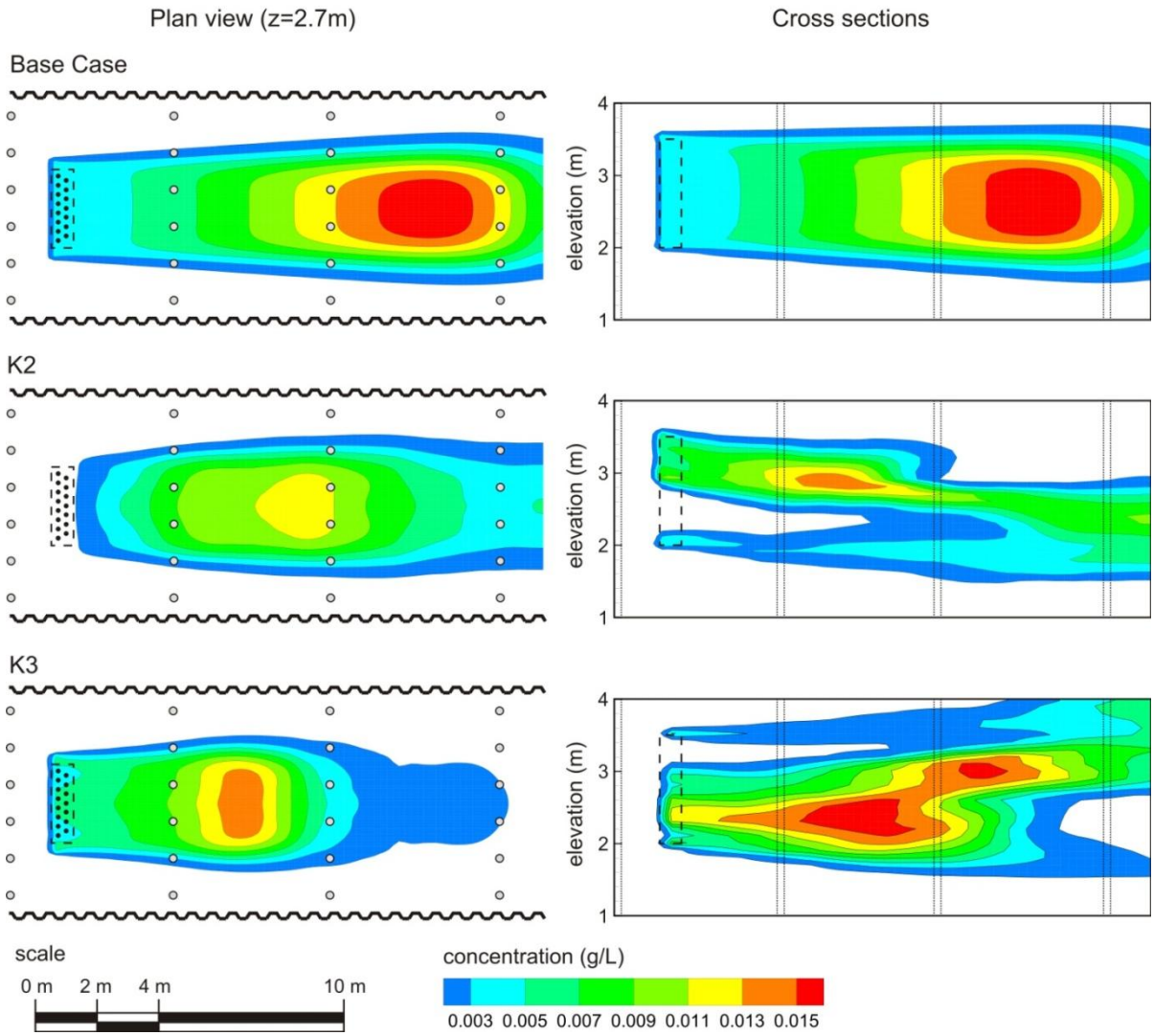

Figure 2.8: E10 gate - Comparison of the benzene plume at 200 days for the homogeneous (Base case) and heterogeneous K2 and K3 scenarios. Plan views are shown on the left and cross sections on the right. Groundwater flows from left to right. Dashed line indicates the position of the source zone.

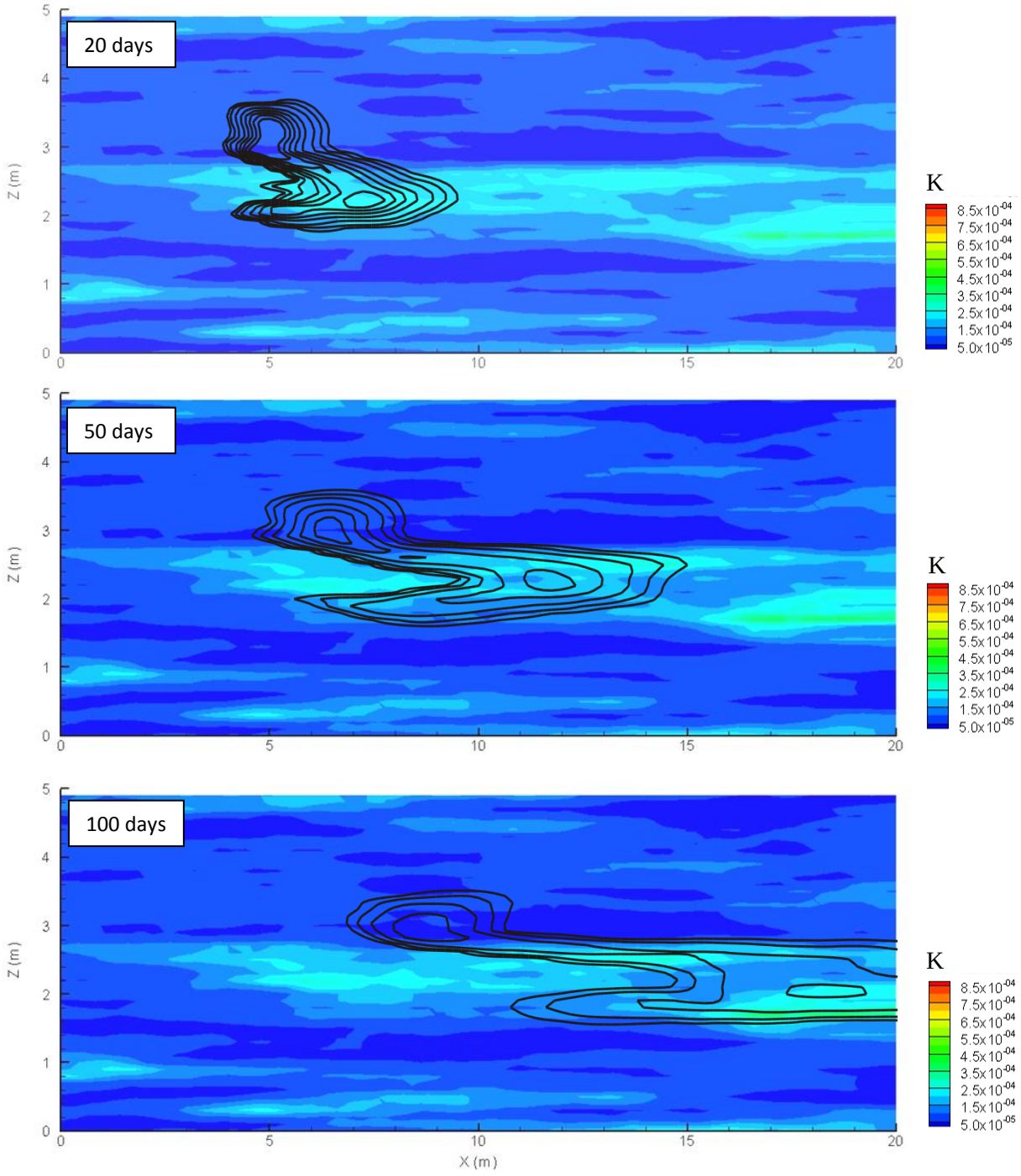

Figure 2.9: E10 gate, random K field 2, ethanol contours at 20, 50 and 100 days. Contours lines extend from 0.05 to 1.2 kg/m^3.

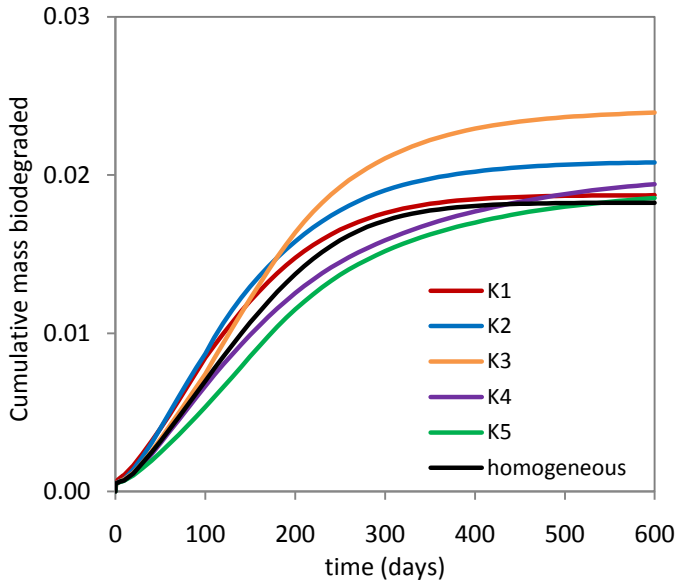

Figure 2.10: Cumulative mass of benzene (kg) biodegraded at the E10 gate, considering half source.

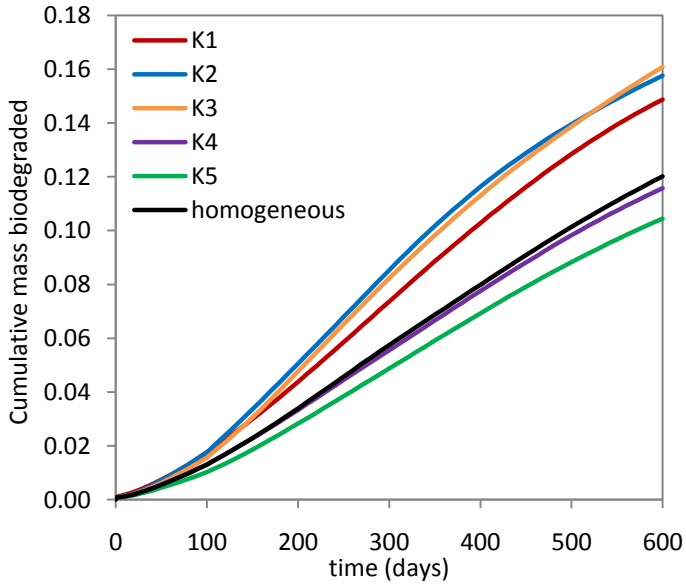

Figure 2.11: Cumulative mass of toluene (kg) biodegraded at the E10 gate, considering half source.

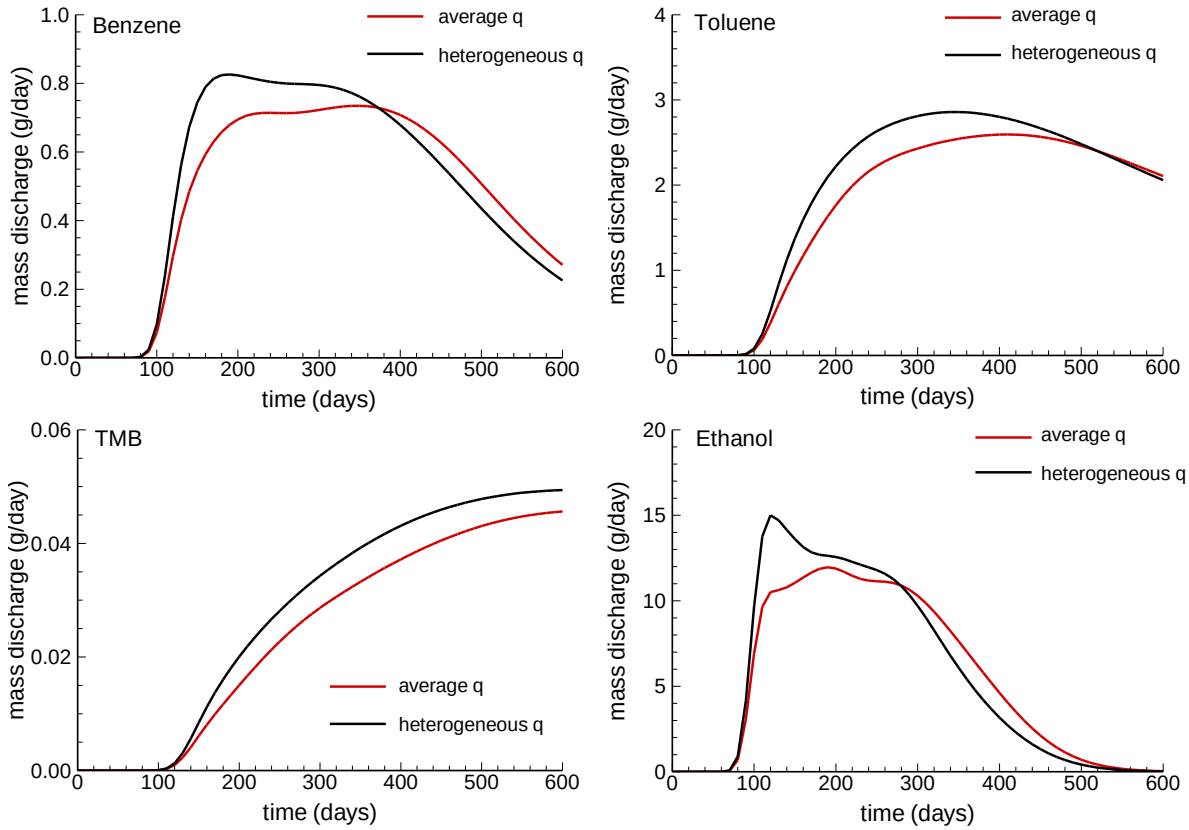

Figure 2.12: E10 gate, K3 field: Impact of averaging the Darcy flux on the mass discharge.

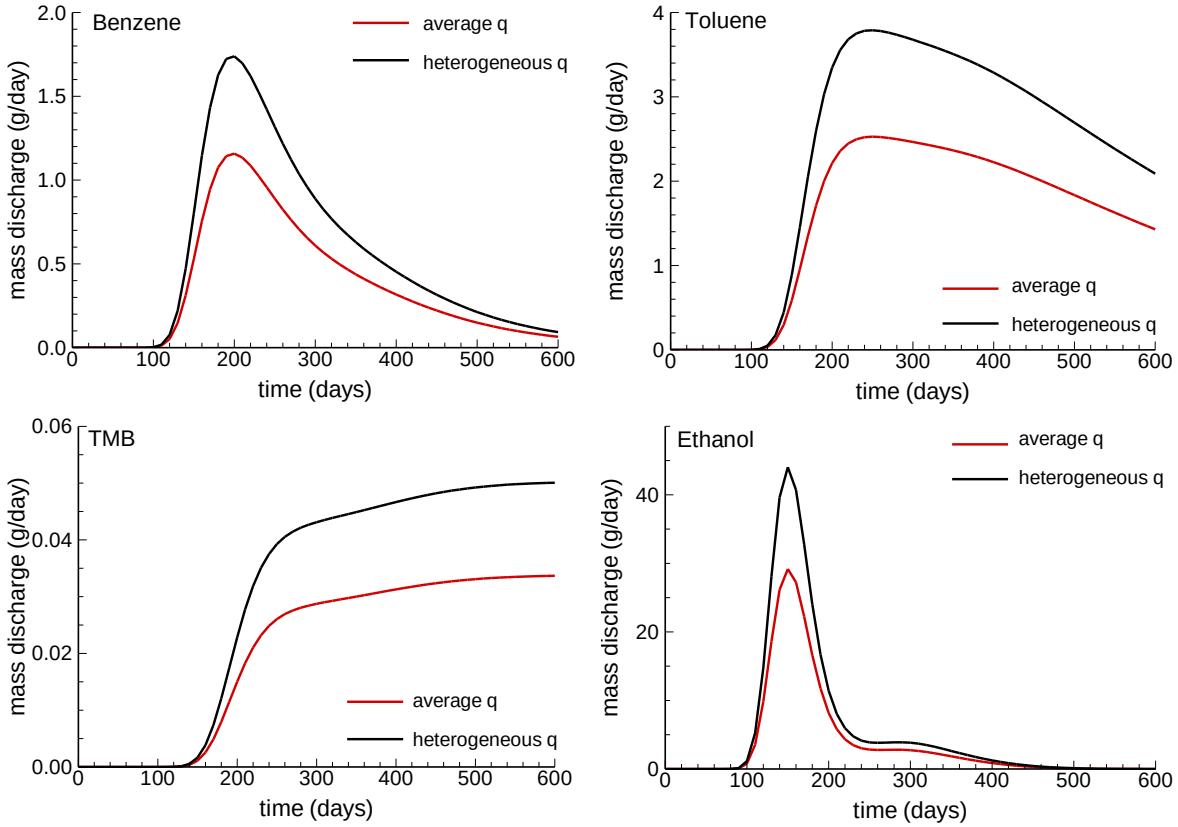

Figure 2.13: E10 gate, K4 field: Impact of averaging the Darcy flux on the mass discharge.

Table 2.1: Chemical properties and source composition.

component	molecular weight (g/mol)	density (kg/m^3)	aqueous solubility (kg/m^3)	sorption coefficient (m^3/kg)	diffusion coefficient (m^2/s)	total moles in source zone		
						E0	E10	E95
benzene	78	878.6	1.78	1.5×10^{-5}	7.7×10^{-10}	4.98	3.95	0.28
toluene	92	867	0.53	2.7×10^{-5}	6.2×10^{-10}	26.6	21.1	1.48
o-xylene	106	880	0.18	2.9×10^{-5}	6.2×10^{-10}	7.95	6.30	0.44
1,2,3-TMB	120	894	0.08	6.1×10^{-5}	6.2×10^{-10}	1.82	1.45	0.10
bulk	90	890	0.02	3.3×10^{-4}	6.2×10^{-10}	381	302	21.1
TBA	74	790	59	0.0	11.5×10^{-10}	1.02	-	-
MTBE	88	740	48	0.0	11.5×10^{-10}	39.3	-	-
ethanol	46	789	infinite	0.0	11.5×10^{-10}	-	63.8	762

Table 2.2: Aquifer physical properties (after Mackay et al. 1986; Sudicky 1986; Molson et al. 2008).

porosity	0.33
bulk density (g/cm^3)	1.81
hydraulic conductivity (m/s)	9×10^{-5}
hydraulic gradient	0.0034
recharge (mm/year)	200
mean grain diameter (d_{50}) (mm)	0.15
longitudinal dispersivity (m)	0.1
transverse horizontal dispersivity (m)	0.01
transverse vertical dispersivity (m)	0.001

Table 2.3: Linear decay rates (d^{-1}) from Hubbard et al. (1994).

component	gasoline without additives	85% methanol
benzene	0.004	0.001
toluene	0.013	0.009
o-xylene	0.006	0.004
methanol	-	0.019

Table 2.4: Compound specific Monod-type kinetic biodegradation parameters: Mineralization.

	benzene	toluene	xylene	TMB	bulk	EtOH
maximum organic utilization rate: k (d^{-1})	8.4	10.68	6	6	0.1	11
microbial yield coefficient: Y (-)	1.5	1.22	1.3	1.3	1	1
organic half rate util. concentration: K (mg/L)	0.3	0.1	0.0007	0.3	0.3	0.088
ratio of oxygen to substrate consumed: F (-) *	3.08	3.13	3.17	3.2	3.5	2.09

* based on reaction stoichiometry

Table 2.5: Monod-type kinetic biodegradation parameters: Mineralization.

description	value
microbe decay rate (b) (d^{-1})	1.00E-12
initial oxygen concentration (mg/L)	6.5
initial microbe concentration (kg/m^3)	0.0015

Table 2.6: Partial degradation: Monod-type kinetic biodegradation parameters altered in comparison to the mineralization scenario.

		benzene	toluene	xylene	TMB	bulk	EtOH
1	microbial yield coefficient: Y (-)	1.5	1.22	1.3	1.3	1	1
	ratio of oxygen to substrate consumed: F (-)	0.41	0.35	0.3	0.3	0.05	0.35
2	microbial yield coefficient: Y (-)	1	0.5	1	1.3	1	1
	ratio of oxygen to substrate consumed: F (-)	0.21	0.17	0.3	0.3	0.01	0.35

* based on reaction stoichiometry

Table 2.7: Relative cumulative mass biodegraded in the mineralization scenarios (%) up to day 600, in the whole model domain

		benzene	toluene	xylene	TMB	bulk	ethanol
E10 Gate	homogeneous	12%	12%	31%	11%	0.2%	4.2%
	K1 field	12%	15%	26%	13%	0.2%	6.1%
	K2 field	14%	16%	20%	22%	0.3%	6.2%
	K3 field	12%	11%	55%	8.6%	0.1%	6.1%
	K4 field	16%	17%	17%	17%	0.3%	7.2%
	K5 field	13%	12%	32%	10%	0.2%	6.9%
E95 Gate	homogeneous	3.8%	17%	47%	74%	8.1%	0.7%
	K1 field	11%	24%	52%	78%	10%	0.9%
	K2 field	10%	22%	51%	76%	11%	0.7%
	K3 field	14%	31%	54%	70%	5.4%	1.0%
	K4 field	12%	26%	52%	76%	8.5%	1.0%
	K5 field	11%	23%	50%	75%	7.4%	0.9%

Chapter 3
Methane Production and Isotopic Fingerprinting in Ethanol Fuel Contaminated Sites [2]

3.1 Introduction

The increasing use of ethanol as a gasoline additive and as a fuel itself has raised concerns over the potential impacts it might have on groundwater quality in the events of accidental spills. Some potential effects include mobilization of NAPL (McDowell et al. 2003; Yu et al. 2008), enhanced solubility of gasoline compounds (Powers et al. 2001) and decrease of hydrocarbon biodegradation rates (Alvarez et al. 2002; Powers et al. 2001; Corseuil et al. 1998).

One issue that has been hypothesized is the formation of methane in concentrations that might lead to potential explosion hazards (Powers et al. 2001). This concern arises from the fact that in aquifers contaminated with gasoline-ethanol mixtures, the biochemical oxygen demand is usually higher than the available oxygen within the plume, and anaerobic conditions are likely to develop (Powers et al. 2001). Anaerobic ethanol biodegradation happens in two stages: in the first stage acetate is produced (reaction 1) and in the second stage mineralization is accomplished by methanogens (reactions 2 and 3).

ethanol to acetate: $CH_3CH_2OH + H_2O \rightarrow 2H_2 + CH_3COO^- + H^+$ (1)

acetate to methane: $CH_3COO^- + H^+ \rightarrow CH_4 + CO_2$ (2)

carbon dioxide to methane: $CO_2 + 4H_2 \rightarrow CH_4 + 2H_2O$ (3)

The overall conversion of ethanol to methane is given in reaction 4.

ethanol to methane – overall reaction: $2CH_3CH_2OH \rightarrow 3CH_4 + CO_2$ (4)

However, as pointed out by Kim et al. (1994), under stressed conditions, such as severe ethanol loadings, other reactions are involved. In this case, butyric and propionic acids may be formed (reaction 5) and then degraded to acetate as the stress conditions recede, in a reverse reaction (Wu and Hickey 1996; Chen et al. 2008).

ethanol and acetate to butyrate: $CH_3CH_2OH + CH_3COO^- \leftrightarrow CH_3CH_2CH_2COO^- + H_2O$ (5)

[2] The ethanol microcosm test and initial interpretation of the ethanol microcosm results were performed by Barbara Fletcher and are reported in her M Sc thesis (University of Waterloo, 2008).

The production of methane is a concern since it can migrate in the subsurface and reach indoor or confined spaces, such as basements and underground piping systems, where it can accumulate leading to explosion risks. For methane, the lower explosive limit is 5% and the upper explosive limit is 15% by volume in air. This means that a flame can propagate at any concentration of methane in this range (Lide 2007). According to Gooddy and Darling (2005), although the definition of a methane concentration in groundwater that will lead to explosive hazard is dependent on the confined space properties, hazard potential exist if methane partial pressure is greater than 0.05 bars, which is equivalent to 1600 μg/L.

Ethanol is used as an additive in gasoline in proportions ranging from 5% to 25% and it is denaturated with around 5% gasoline before being transported. Therefore, in most sites where groundwater is impacted by ethanol, hydrocarbons will also be present, which can also be a source of biogenic methane. To distinguish the source of methane between ethanol and hydrocarbons, an isotopic tool was developed and tested in real sites. It is based on the fact that ethanol is enriched in ^{13}C in comparison with gasoline hydrocarbons.

The main ethanol producers are the United States and Brazil, which together account for around 70% of the 49 billion liters of ethanol produced in the world per year (Fraiture et al. 2008; F.O. Licht, cited in RFA 2008). In most of North America, ethanol is derived from corn and in Brazil it is derived from sugar cane (Granda et al. 2007; Müller et al. 2008). Both corn and sugar cane are C_4 plants, having $^{13}C/^{12}C$ ratios, reported as $\delta^{13}C$ values (see equation 6), ranging from -9 to -17‰ (Boutton 1996; Pessenda et al. 2004; O'Leary 1981). Compounds present in fossil fuels, on the other hand, present much more depleted $^{13}C/^{12}C$ ratios and so more negative $\delta^{13}C$ values. Widory (2006) evaluated 28 samples of liquid fuels, including regular gasoline, unleaded gasoline, diesel and fuel oil. All samples were within a narrow $\delta^{13}C$ range from -26.4 to -28.6‰. Smallwood et al. (2002) evaluated 19 gasoline samples, and among the 16 compounds evaluated, the $\delta^{13}C$ values ranged from around -23‰ to -28‰. Other studies (Harrington et al. 1999; Kelley et al. 1997; Dempster et al. 1997) have reported similar $\delta^{13}C$ values for gasoline hydrocarbons. Therefore, based on the significant carbon isotope difference between ethanol and gasoline hydrocarbons, methane generated from ethanol biodegradation is likely to have a significantly different carbon isotope signature than the methane generated from biodegradation of gasoline hydrocarbons.

Methane in groundwater can have origins besides ethanol and hydrocarbons biodegradation. The sources of methane are usually classified into three major categories, biogenic, thermocatalytic and abiogenic (Clark and Fritz 1997; Jenden and Kaplan 1986; Schoell 1980). Biogenic, or microbial, refers to the methane derived from the biodegradation of organic matter. Methane generated by the alteration of organic matter at elevated temperatures is classified as thermocatalytic or thermogenic, even thought it might involve microbial reactions. The last category, abiogenic, is relative to the methane produced without microbial activity and not generated from organic matter.

Carbon isotopes have been used extensively to identify the source of methane (Aravena et al. 1995; Aravena and Wassenaar 1993; Coleman et al. 1988; Cramer et al. 1999). In this study, the $\delta^{13}C$ in methane produced from ethanol and toluene substrates was evaluated in controlled microcosm experiments. This study is the first to determine $\delta^{13}C$ in methane derived from ethanol. The microcosm results were then applied at seven field sites contaminated by gasoline and ethanol to evaluate the origin of methane and verify the applicability of the isotopic tool.

3.2 Experimental Section

3.2.1 Ethanol Carbon Isotope Fingerprinting

The range of ethanol carbon isotopic signature was evaluated using 13 samples of commercially available ethanol. All samples, except for one, were corn derived ethanol from North America. The other sample was sugar cane derived ethanol from Brazil. The carbon isotopic analysis was performed as described in the next section.

3.2.2 Anaerobic Microcosms Experiments

The carbon isotopic signature of methane derived from ethanol and toluene biodegradation was assessed in anaerobic microcosm experiments. For the ethanol biodegradation test, the microcosm was composed of anaerobic soil and groundwater collected at the Canadian Forces Base Borden, located in Ontario, and modified Bushnell-Haas Medium (MBH). Ethanol was added to a target concentration of 150 mg/L. The tests were conducted in 1140 mL glass bottles with mininert valves, filled with 1000 mL of aqueous phase and 182 mL of soil. The MBH was sterilized in the autoclave and composed 10% of the aqueous phase. The experiments were run in duplicate. Control bottles were poisoned with mercuric chloride. Headspace samples were collected and analyzed for methane concentration and methane $\delta^{13}C$. Aqueous samples were collected for ethanol and dissolved inorganic carbon (DIC) quantification and $\delta^{13}C$ analysis. Aqueous samples were also collected for acetate analysis.

The evaluation of the isotopic signature of methane generated from petroleum hydrocarbons was carried out during biodegradation of toluene under methanogenic conditions. The culture was kindly provided by Dr. E. Edwards (Department of Chemical Engineering & Applied Chemistry, University of Toronto) and is a mixed consortium, which was described elsewhere (Edwards and Grbic-Galic 1994; Ficker et al. 1999; Ahad et al. 2000; Ward et al. 2000).

Four, 1150 mL glass bottles with screw caps and black butyl rubber stoppers were used as microcosms. Two bottles were prepared with 200 mL of culture and 200 mL of medium and are referred to as active 1 and 2. The medium contains no other carbon source and its composition is described in Edwards and Grbic-Galic (1994). Two controls were prepared with 400 mL of medium and 0.4 mL of 10% sodium azide solution. 35 μL of filter-sterilized toluene was added to all bottles, bringing the concentration of toluene to around 50 mg/L. The bottles were kept in an anaerobic glove

box with an atmosphere of 5% carbon dioxide, 5% hydrogen and 90% nitrogen. Headspace samples were collected and analyzed for toluene and methane concentration and $\delta^{13}C$ values.

All headspace samples were collected using gastight syringes fitted with Hamilton® miniature inert plug valves. Methane and toluene analyses were performed within one hour. Methane and toluene samples for $\delta^{13}C$ were transferred into glass serum vials with BD Vacutainer® red stoppers, which were previously flushed with helium gas. Samples were stored at 4°C until analysis. Aqueous samples for ethanol and DIC were collected from microcosms using sterile syringes. The ethanol sample (0.2-1 mL) was transferred to a glass autosampler vial with Teflon-lined septa, preserved with sodium azide and stored at 4°C until analysis. Ethanol samples were analyzed within 2 days of removal from the microcosm. The DIC aqueous sample for quantification was transferred to a 1 mL glass vial with Teflon-lined septa, preserved with mercuric chloride and stored at 4°C until analysis. For DIC carbon isotope analysis, the aqueous sample was transferred to a 10 mL glass VOA vial with Teflon-lined septa, preserved with mercuric chloride and stored at 6°C until analysis. For the analysis of acetate, a 2.0 mL sample was removed from the microcosm and added to a plastic 5 mL Dionex IC autosampler vial.

Methane, ethanol and toluene quantification analyses were performed at the Organic Chemistry Laboratory, Department of Earth and Environmental Sciences, University of Waterloo. Toluene headspace samples were analyzed with a Shimadzu 9A capillary gas chromatograph (GC) and a flame ionization detector. A 500 µL vapor sample was pushed from the collection syringe into a gas sampling valve (Valco Instruments) and 100 µL was loaded into a split injection port and then on column. The column was a 0.32 mm inner diameter, 60 m length, Supelcowax 10 (Supelco) with a 0.5 µm stationary phase of carbowax 20. The helium carrier gas column flow rate was 5 mL/min with a make-up gas flow rate of 50 mL/min. Detector/injector temperatures were 200^{o}C and column oven temperature was 105^{o}C. Data integration was completed with a Shimadzu CR3A integrator. The detection limit was 1.0 µg/L.

For methane headspace analysis, a 5 mL aliquot of the gas phase from the syringe was injected, via an automated gas sampling valve, into a Varian 3800 GC equipped with a flame ionization detector and capillary injection port. The automated gas injection utilises a 6 port gas sampling valve with a 2 mL sample loop, a vacuum pump, and a 16 port stream selector valve, to draw the sample from the syringe into the sample loop and on column. Data integration is completed with the Varian Star chromatography workstation software. The methane detection limit was 0.3 µg/L. Laboratory control

samples and matrix spikes were prepared with known quantities of C1-C3 gases and method recovery of the gases was measured daily. Recovery limits for quality assurance samples were 80-120%. Laboratory duplication on 10% of field samples was performed, and results were considered acceptable when they fell within 15% of their average.

For ethanol analysis, the autosampler vial was placed on a 7673A HP autosampler GC for chromatographic analysis. The GC was equipped with a flame ionization detector and a 3 m length, 0.318 cm inner diameter column packed with 3% SPI500 on Carbopack B (80/100 mesh). The detection limit for ethanol was 0.05 mg/L.

Dissolved inorganic carbon (DIC) was analyzed using a DC-190 TOC Analyzer (Dohrmann Division of Rosemount Analytical Inc.). Samples were run in inorganic carbon mode giving total CO_3^{2-}, HCO_3^- and $CO_{2(aq)}$ concentrations in the sample. The analytical precision was +/- 2% of the measured value.

Acetate analyses were performed at the Groundwater Laboratory from the Institute for Groundwater Research at the University of Waterloo. The sample was placed on a Dionex AS-40 autosampler. A 25 µL sample was then injected onto a Dionex ICS-2000 Ion Chromatograph equipped with an Ion-Eluent Generator and conductivity detector. A Dionex IonPac AS18 column (4x250 mm) was used. The mobile phase used was 30 mM KOH at a flow rate of 1.0 mL/min. The chromatograph was obtained on a Dell p4-3GHz computer using Dionex Chromeleon 6.5 software. Acetate detection limit was 1.0 mg/L.

Carbon isotopes analyses were performed at the Environmental Isotope Laboratory, Department of Earth and Environmental Sciences, University of Waterloo. Samples for ethanol carbon isotopes were analyzed using a PT-GC-IRMS system. The PT-GC-IRMS system consisted of a Tekmar 3000, Purge and Trap Concentrator (Tekmar Company, Cincinnati, Ohio), a Trace GC (Thermo Finnigan, San Jose,CA interface), a GC–Combustion III interface operating at 940°C for ^{13}C and a Delta^{plus} XL isotope ratio mass spectrometer (Thermo Finnigan MAT, Bremen, Germany). The trap used was Purge Trap K (Vocarb TM 3000) (Supelco, Bellefonte, PA). A 60 m, DB-624 column with 0.32 mm internal diameter and 1.8 µm film thickness was used. Blank runs were done to remove the carryover effect of ethanol.

Methane and toluene carbon isotope ratios were determined using a GC-C-IRMS system consisting of an Agilent 6890 GC (Agilent, Palo Alto, USA) with a split/splitless injector, a Micromass

combustion interface operated at 850°C, a cold trap cooled to -100°C using liquid nitrogen, and a Micromass Isoprime isotope-ratio mass spectrometer (Micromass, Manchester, U.K.). For methane carbon isotope analysis, the GC was equipped with a CARBONPLT column (30 m length, 0.32 mm internal diameter, 3 μm stationary phase, from J&W Scientific, Folsom, CA, and U.S.A.). The GC analysis of toluene was done using a 30 m long RTX-5 column with an internal diameter of 0.25 mm and a film thickness of 1 μm (Restek Corp., USA). For all samples, injections were done such as to obtain peak heights close to the height of the reference gas of the system. The $\delta^{13}C$ of the samples were determined with a precision of 0.5‰ for all compounds.

For DIC $\delta^{13}C$ analysis, the sample solution was acidified with Ortho-Phosphoric acid in a Helium atmosphere in 10 mL Vacutainers®. The Vacutainer® had 80% solution and 20% headspace. After acidification, the Vacutainers® were agitated in a mechanical shaker for about 20 minutes to ensure equilibration of the gas between the two phases. The CO_2 gas from the headspace was then injected into the GC following the method for $\delta^{13}C$ analysis of methane. The stable carbon isotopic concentrations are reported using the delta notation (equation 6), calculated relative to the VPDB (Vienna Peedee Belemnite) reference value (Clark and Fritz, 1997).

$$\delta^{13}C_{sample} = \left(\frac{\left({}^{13}C/{}^{12}C\right)_{sample}}{\left({}^{13}C/{}^{12}C\right)_{reference}} - 1 \right) \cdot 1000 \qquad (6)$$

3.2.3 Field Sites

Seven contaminated sites were selected to test the isotopic tool to identify the origin of methane and to evaluate the risks associated with methane production due to ethanol biodegradation.

The first site is located in Ontario, and was contaminated with approximately 100 m^3 of denaturated ethanol (2 to 5% gasoline) in 2005, as a consequence of an accident with a train tanker car. Twelve monitoring wells had been installed at the site (Figure 3.1), with screens around 1.5 m long, positioned across the water table (LPT Enviro Inc. 2006). Five wells in which ethanol had been found were selected to be analyzed in this study. On February 18-19, 2008 wells BH-2, 3, 5, 9 and 14 were sampled using dedicated Waterra pumps. Wells BH-9 and BH-14 were also sampled on November 14th, 2007. Wells BH-2, 3 and 5 are likely in the source zone and wells BH-9 and BH-14 are somewhat downgradient of the spill.

The other six sites (BR1 to BR6) are located in Sao Paulo, Brazil, where ethanol was previously identified in groundwater or soil samples. One site is a fuel distribution terminal (BR5) and the others are fuel stations. All sites in Sao Paulo were contaminated by E20 (gasoline with 20 to 24% ethanol) and possibly E90 (minimum ethanol content of 90%). Groundwater samples were collected from existing monitoring wells where ethanol was more likely to be found based on historical data. At sites BR3 to BR6, two monitoring wells, labeled A and B, were sampled. Samples were collected by CETESB (Environmental Agency of São Paulo State) technicians and shipped to the University of Waterloo for chemical and isotopic analysis. Samples from sites BR1 to BR4 were collected in November 2007 and the remaining sites were sampled in September 2008.

Samples from all sites were analyzed for ethanol, methane, acetate, butyric acid, BTEX (benzene, toluene, ethylbenzene, p,m-xylenes and o-xylene), TMBs (1,2,4-trimethylbenzene, 1,3,5-trimethylbenzene and 1,2,3-trimethylbenzene), naphthalene, and $\delta^{13}C$ for ethanol and methane. Groundwater samples for methane $\delta^{13}C$ analysis were collected in 120 mL serum vials with BD Vacutainer® red stoppers. Groundwater samples for all other parameters were collected in 40mL VOA vials with Teflon-sealed screw caps and preserved with sodium azide.

Ethanol, methane and the carbon isotope analysis were performed as described previously. Monoaromatic hydrocarbon analyses were also performed at the Organic Chemistry Laboratory, Department of Earth and Environmental Sciences, University of Waterloo. The analyses were performed by solvent extraction with methylene chloride followed by gas chromatography. The solvent was placed in a Teflon-sealed autosampler vial for injection into the GC. Samples were analyzed with a HP 5890 capillary GC equipped with 0.25 mm × 30 m length DB5 capillary column with a stationary phase film thickness of 0.25 μm, a HP7673A autosampler, and a flame ionization detector. Extraction duplicates were performed on samples and results were acceptable when they agreed within 10%. The method detection limits for the monoaromatics tested were below 2.2 μg/L. The relative standard deviation was below 5% for all chemicals in the range of concentrations tested. A detailed description of the method can be found at Freitas and Barker (2008).

Acetate and butyric acid analyses were performed at the Groundwater Laboratory of the Institute for Groundwater Research at the University of Waterloo, following the procedure described previously. Detection limits were 1.0 mg/L for acetate and 1.3 mg/L for butyric acid.

3.3 Results and Discussion

3.3.1 Ethanol Fingerprinting

The $\delta^{13}C$ values for the ethanol samples ranged from -11 to -13‰, with a mean value of -12.3‰. The highest and lowest $\delta^{13}C$ value corresponds to a Canadian and a Brazilian ethanol sample, respectively. These values are within the range of $\delta^{13}C$ values for C_4 plants (-9‰ to -17‰; Boutton 1996; Pessenda et al. 2004), which are the precursors of the ethanol.

3.3.2 Methane Fingerprinting

3.3.2.1 Ethanol microcosm experiments

The ethanol used in the microcosm experiment had an initial $\delta^{13}C$ value of -11.1‰. Ethanol degradation was followed by an increase in acetate concentrations and methane production only became apparent after all the ethanol was converted to acetate (Figure 3.2a). Based on the stoichiometric reaction of ethanol conversion to methane (equation 4), around 73.6% of the expected methane was produced in the microcosm. After 20 days, DIC concentrations increased following the same trend as methane, as would be expected.

The observed sequential reactions, with ethanol being converted to acetate, and then acetate being converted to methane and carbon dioxide, contrast with previous studies (Conrad et al. 1985; Wu and Hickey 1996; Powers et al. 2001). The conversion of ethanol to acetate is thermodynamically unfavorable (standard Gibbs free energy, ΔG^0=2.3 kcal/mol, Thauer et al. 1977), unless it is coupled with a hydrogen consuming reaction, like methane formation from acetate (reaction 2), which has a ΔG^0=-8.6 kcal/mol (Thauer et al. 1977). It is likely that some hydrogen consuming reaction was taking place simultaneously to the acetogenesis in the microcosm, without resulting in methane formation.

During the first days of the test, the DIC had a sudden drop in concentration (Figure 3.2a) correlated with a large carbon isotopic enrichment from +9.4‰ to +21.6‰ (Figure 3.2b). This is likely a consequence of a reaction with the DIC as the substrate. One possibility is that the DIC initially present in the system reacted with the H_2 that was being produced by the ethanol degradation (reaction 1), resulting in the formation of methane with consequent DIC enrichment (equation 3). That would remove the hydrogen from the system, making the ethanol conversion to acetate thermodynamically favorable. However, no methane was detected during the first days of the

experiment. Therefore, it is more likely that the DIC was being transformed into acetate by autotrophic acetogens (reaction 7). This reaction also results in hydrogen consumption and is thermodynamically favorable, ΔG^0=-25 kcal/mol (Thauer et al. 1977). Gelwicks et al. (1989) reported a large carbon isotopic enrichment in DIC during acetogenesis. After peaking at earlier time, the DIC $\delta^{13}C$ value decreased progressively until it reached values closer to the initial values. During the increase in concentrations at later time, the DIC $\delta^{13}C$ remained constant with values around -6‰.

DIC to acetate: $2HCO_3^- + H^+ + 4H_2 \rightarrow CH_3COO^- + 4H_2O$ (7)

The carbon isotope data for ethanol showed an unexpected trend during biodegradation. The ethanol became more depleted in ^{13}C as biodegradation proceed (Figure 3.2b), reaching $\delta^{13}C$ values as low as -27.6‰ (Figure 3.2b). Acetate $\delta^{13}C$ was not measured, but based on the ethanol results it would be expected that acetate would start with more enriched $\delta^{13}C$ values and then it would decrease, tending towards the initial carbon isotopic value of the ethanol. Sugimoto and Wada (1993) monitored the acetate isotopic signature from the anaerobic biodegradation of organic matter from a rice paddy field soil and verified a similar trend. The soil total organic carbon had an initial $\delta^{13}C$ value of -26.5‰, and it was verified that the acetate produced had an isotopic signature of -24‰ after two weeks, becoming more depleted with time.

A value of 5.7 was determined for the carbon enrichment fractionation factor (ε) for ethanol biodegradation to acetate using the microcosm data and the Rayleigh equation as presented in equation 8 (Clark and Fritz 1997), where *f* is the fraction remaining of ethanol.

$$\ln\left(\frac{\delta^{13}C + 1000}{\delta^{13}C_0 + 1000}\right) = (\alpha - 1)\ln f = \frac{\varepsilon}{1000}\ln f \quad (8)$$

The methane showed $\delta^{13}C$ values around -31.4‰ during the first days of the reaction and became more enriched as the reaction proceeded and methane concentration increased. After all the acetate was transformed, methane concentration and isotopic signature remained stable (Figure 3.2). The final methane $\delta^{13}C$ value was around -19.2‰, which is about 9‰ more depleted in ^{13}C in comparison to the original ethanol. On the other hand, the final $\delta^{13}C$ value of DIC, -5.8‰, was enriched in ^{13}C compared to the initial ethanol $\delta^{13}C$ value.

The difference in the isotopic signature of methane and DIC is likely due to the position of the enriched carbon in the ethanol and to the reaction pathway. According to Schink et al. (1985), when the ethanol degradation pathway involves only acetate and butyrate as intermediate products, methane is formed from the methyl carbon of ethanol. During ethanol conversion to acetate, the methyl group and carbon are transferred without cleavage of the carbon bond. Previous studies (Sugimoto and Wada 1993; Penning et al. 2006) have shown that the methyl carbon in acetate is usually depleted in comparison to the carboxyl carbon. Therefore, the more depleted carbon tends to form methane while the enriched carbon goes to the carbon dioxide, which explains the fractionation between the DIC and methane observed.

3.3.2.2 Toluene microcosm experiments

The evolution of the mass of toluene and methane in the toluene degradation microcosm tests can be seen in Figure 3.3a. The mass balance error was calculated based on the stoichiometric toluene degradation reaction as presented in Ahad et al. (2000). The error was less than 17% for the active bottles. The toluene used in the experiments had an initial $\delta^{13}C$ value of -28.5 ± 0.2‰, which is within the range determined in other studies. Harrington et al. (1999) analyzed toluene from 13 different samples and found $\delta^{13}C$ values from -25.8‰ to -29‰. Dempster et al. (1997) found toluene values that ranged from around -26.5‰ to -28.5‰.

The carbon isotopic signature of toluene was not altered significantly after about 80% of the toluene was biodegraded (Figure 3.3b), which is in agreement with Ahad et al. (2000), who showed small isotope fractionation for toluene during anaerobic degradation. Methane obtained from toluene anaerobic degradation (Figure 3.3b) had a $\delta^{13}C$ value of -55.3 ± 1.8‰, which remained fairly constant throughout the duration of the test.

The observed isotopic difference in the microcosm between toluene and methane was around 27‰, while in the ethanol microcosm the isotope difference between the initial $\delta^{13}C$ of ethanol and the final methane $\delta^{13}C$ was only 8‰. The methane $\delta^{13}C$ value from toluene was around -55‰, which is much more depleted than the $\delta^{13}C$ values of methane obtained from ethanol, which were in the range of -19‰ to -31‰. This difference confirms that stable carbon isotope can be used as a tool to identify methane generated from ethanol or from hydrocarbons. However, the distinction between gasoline, ethanol and other methane sources based solely on $\delta^{13}C$ may not be possible due to overlap of the carbon isotope signature between some ranges (Figure 3.4). Carbon isotope data for methane derived from ethanol overlap with methane of thermocatalytic and abiotic origin, and carbon isotope data for

methane derived from petroleum hydrocarbons tend to overlap with methane of biogenic origin, including landfills and wetlands.

3.3.3 Methane Fingerprinting at Field Sites

The field samples have methane $\delta^{13}C$ values distributed over a wide range, from around -80‰ to -10‰ (Figure 3.5).

3.3.3.1 Ontario site

The groundwater analytical results at the Ontario site for ethanol and its biodegradation products are presented in Table 3.1 and hydrocarbons concentrations are presented in Table 3.2. The presence of organic acids in high concentration in some samples interfered with the hydrocarbons analysis, so that concentrations could not be determined due to overlap of peaks in the chromatogram. In all samples the methane concentrations in groundwater were above 1600 μg/L, and so are indicative of potential explosive hazard (Gooddy and Darling 2005). Acetate and butyrate were found in all wells excepting BH-5 (Figure 3.1), even though ethanol was detected at only two wells. This shows that the biodegradation products can persist in the groundwater even after all the ethanol has been degraded.

The presence of butyrate is likely a consequence of the high ethanol loading in the groundwater. As the stress condition recedes, butyrate will probably be converted to acetate and then to methane, reaching conditions more similar to those at well BH-05. The results from well BH-14 collected in November, 2007 illustrates the situation of a highly stressed condition, where butyrate is present and acetate and methane also appear, but methane does not appear at such high concentrations as observed in the sample collected in February, 2008. The sample collected from Well BH-9 in November, 2007, which is generally upgradient of BH-14, is less stressed by high loadings. In this well ethanol is no longer detected, butyrate concentrations are lower and acetate and methane appear in higher concentrations. In the sample collected in February, 2008, methane concentration in well BH-14 increased significantly and ethanol and butyrate decreased, indicating that the concentrations in this well are switching from a high ethanol loading condition to a less stressed condition.

In this site, methane was expected to come primarily from ethanol biodegradation, since hydrocarbons were present in much lower quantity. The $\delta^{13}C$ values for methane ranged between -12 and -35‰ (Table 3.1), which is consistent with the range expected for methane originating from ethanol (Figure 3.4).

The most enriched $\delta^{13}C$ values are observed in the sample from well BH-14, which is the farthest downgradient well (Figure 3.1). The methane carbon isotope value measured at the first sampling event at this well was -12‰, similar to what would be expected to be the initial value for ethanol $\delta^{13}C$. This value is more enriched than would be expected based on the microcosm test, which indicated methane $\delta^{13}C$ should be depleted in comparison to the initial ethanol $\delta^{13}C$ value. The same sample also presented relative high concentration of ethanol, indicating that not all the ethanol had been converted to acetate. High concentration of acetate and butyrate were also observed in this sample. Based on the microcosm results, acetate produced from partial conversion of ethanol is probably more enriched in ^{13}C than the ethanol and until all the ethanol is converted, the acetate $\delta^{13}C$ trends towards the initial ethanol $\delta^{13}C$ value as the ethanol to acetate reaction proceeds. Since not all the ethanol has been converted to acetate, it is likely that the acetate present in the groundwater was still more enriched in ^{13}C than the initial ethanol. Even though methane is depleted in comparison to the acetate, since it was being produced from this enriched acetate, it is possible that it has a $\delta^{13}C$ value in the same range as ethanol, as appears to be the case at BH-14.

The effect of partial conversion of ethanol to acetate and acetate to methane is also observed in the ethanol carbon isotope data at well BH-14. The groundwater collected in November, 2007 showed a $\delta^{13}C$ value of -14‰ for ethanol and became more depleted in the groundwater collected in February 2008, when it was measured to be -18‰. A drop in concentration was also observed during this period (Table 3.1). The ^{13}C pattern for ethanol is in agreement with the microcosm results, which showed ethanol becoming more depleted in ^{13}C as biodegradation proceeds. The extent of ethanol biodegradation can be estimated applying Rayleigh equation and the enrichment factor determined in the microcosm experiment. Since the initial ethanol $\delta^{13}C$ is unknown, it was considered to be in the range of -11‰ to -13‰, which is the range previously determined for ethanol based on the analysis of 13 ethanol samples. The ethanol fraction remaining was determined to be between 60% and 84% by November, 2007 and decreased to between 27% and 40% by February, 2008.

The more depleted $\delta^{13}C$ values found in methane in the upgradient wells are still in the range of ethanol biodegradation, but might also be affected by some input of hydrocarbons biodegradation. Although the contaminant at the site was mainly ethanol (95% in volume), a considerable volume of gasoline was also spilled. From the concentration data it can be seen that most of the ethanol had left the source zone by the middle to the end of 2007, but hydrocarbons were still present (Table 3.2). The only well that still had ethanol was well BH-2. This is also the well where methane is more enriched

in ^{13}C, as in well BH-14. Therefore, it is possible that the more depleted values of methane at wells BH-3 and BH-5 reflect some input of methane from hydrocarbon degradation.

3.3.3.2 Sites in Brazil

In only two of the six Brazilian sites was ethanol found in high concentrations (Table 3.1). This was unexpected, since ethanol is present in all gasoline sold in Brazil and it is completely miscible with water. Ethanol biodegradation is likely one of the reasons for the lack of ethanol in most of the Brazilian groundwater samples collected.

The ^{13}C values for methane range between -11 and -78‰. In the three wells where ethanol was found (BR5-B and BR6-A and B), the carbon isotopic values varies between -11 and -26 ‰ which clearly is within the range expected for methane from ethanol (Table 3.1). In sample BR5-A no ethanol was detected and the methane concentration was much lower than the concentration measured in BR5-B. The $\delta^{13}C_{methane}$ value of -60‰ obtained in this sample is consistent with gasoline hydrocarbons biodegradation (Figure 3.4). This sample presented evidence of contamination by petroleum hydrocarbons (Table 3.2), with 305 µg/L of benzene. Therefore, it is likely that hydrocarbons are the source of the methane in BR5-A.

The most enriched $\delta^{13}C$ value of -11‰ was found in the site (BR-6A) that has the highest ethanol concentration (83,100 mg/L) among the Brazilian sites (Table 3.1). This sample also has the highest concentration of acetate and butyrate (Table 3.1). Similarly to well BH-14 at the Ontario site, the high ethanol concentration indicates that not all the ethanol had been converted to acetate, and therefore acetate was likely enriched in ^{13}C compared to ethanol, resulting in a methane with a more enriched $\delta^{13}C$ value of -11‰.

At site BR2, the methane concentration was high (5300 µg/L), with a carbon isotopic signature of -42.6‰, which is between the gasoline and ethanol origin ranges. This site showed the highest concentration of petroleum hydrocarbons (Table 3.2) and so both ethanol and hydrocarbons likely contributed to the relative high concentration of methane observed at this site.

The most depleted $\delta^{13}C$ values for methane, ranging between -78 and -65‰, were obtained at the fuel stations BR1 and BR4, indicating that ethanol biodegradation is not the source of the methane at these sites. In these two fuel stations, the maximum reported ethanol concentrations measured in 2005 and 2006 were less than 3 mg/L (CETESB 2007a; CETESB 2007b). In our recent sampling, ethanol was not detected in either of the sites. Acetate was found only in one of the samples at the BR4 fuel

station and in very low concentration (2.8 mg/L). The low hydrocarbons concentration and the $\delta^{13}C$ of -78‰ obtained for methane at site BR-1 suggested the methane may be derived from a biogenic source other than gasoline. In the case of site BR4, particularly at sample B, hydrocarbons and methane were found in higher concentrations and methane had a mean $\delta^{13}C$ value of -64‰, falling within the range of gasoline biodegradation. This suggests that methane at site BR-4 was most likely from gasoline biodegradation.

A contrasting scenario is observed at the fuel station BR3, where the methane $\delta^{13}C$ values from two different wells deviate significantly (16.3‰). Sample A had a value closer to the range expected for ethanol-derived methane (-37.2‰) while sample B was closer to the range of gasoline derived methane (-53.5‰), in agreement with the presence of hydrocarbons in well B (Table 3.2). Both samples are characterized by the lowest methane concentration measured in the Brazilian sites. The results also agree with previous ethanol concentrations measured in soil samples. In the location where sample A was collected, an ethanol concentration of 107 g/kg was measured in the soil water, while no ethanol was found previously in the location where sample B was collected (CETESB 2007c), indicating that the contamination in the two wells might be from different fuel sources.

3.4 Summary and Conclusions

High concentrations of methane (> 1600 μg/L) were found in both the gasoline and the ethanol sites, indicating biodegradation of both ethanol and gasoline were capable of generating methane in potentially dangerous concentrations. This research shows that organic acids, the byproducts of ethanol biodegradation and precursors for methane, can persist in groundwater even two years after an ethanol spill. In microcosms tests it was verified that the methane derived from gasoline hydrocarbons will present $\delta^{13}C$ values of around -55‰, which are more depleted than $\delta^{13}C$ values obtained in methane derived from ethanol, which was in the range of -20‰ to -30‰.

Contrary to the microcosm results in which methane was generated only after all the ethanol was transformed, ethanol and methane commonly co-occurred in field samples (Table 3.1). The field results agree with other studies which indicated that ethanol conversion to acetate occurs together with methanogenesis (Conrad et al. 1985; Wu and Hickey 1996; Powers et al. 2001). In the laboratory microcosm, the elevated DIC likely make the ethanol conversion to acetate thermodynamically feasible. In aquifers with different geochemical conditions, methanogenesis appears to become significant before all the ethanol has been removed.

Another reason for the simultaneous presence of ethanol and methane in the groundwater in the field samples is that field samples represent an average of the aquifer conditions where the well screen is installed. Therefore, it might include water from regions in different stages of ethanol transformation.

In the field samples methane $\delta^{13}C$ tended to greater enrichment as ethanol concentration increased (Figure 3.6). This correlation becomes even stronger when intermediate biodegradation products of ethanol anaerobic biodegradation are included, such as acetate and butyrate (Figure 3.7). A significant number of samples had methane $\delta^{13}C$ values indicative of ethanol origin ($\delta^{13}C$ higher than -40‰) although no ethanol was detected. This indicates that in some sites, although most or all of the ethanol was already degraded, the biodegradation products still persist in the groundwater.

In the microcosm experiment methane became more enriched as the sum of ethanol and acetate concentrations decreased; the opposite trend was noticed in the field samples (Figure 3.7). This difference is likely a consequence of the sequential reaction verified in the microcosm versus the simultaneous reactions that might have happened in the field. In the microcosm test, ethanol become isotopically depleted as the reaction proceeded, which indicates that the produced acetate started more

enriched in ^{13}C compared to the ethanol. When all the ethanol was converted to acetate, the acetate isotopic signature must have been the same as the initial ethanol, since all carbon was transferred from ethanol to acetate. The methane production started only after that, likely causing acetate to become enriched again, and so causing the methane $\delta^{13}C$ to also become enriched as the acetate was converted to methane.

However, if methane production happens simultaneously with ethanol conversion to acetate, the initial methane will be generated from acetate which is enriched in comparison to the ethanol, and therefore the methane will also be more enriched. As the reaction proceeds, ethanol becomes more depleted, and so does the acetate and resulting methane. This would generate a trend in methane $\delta^{13}C$ versus ethanol and acetate concentrations which is the opposite of what was measured in the microcosm.

Clearly, the methane isotopic signature is dependent on the microbial reactions involved and on the stage of ethanol biodegradation. For example, methane carbon isotopic signature can be modified by other processes, which could lead to a misinterpretation of the methane's origin. Microbial oxidation of methane leads to a decrease in concentration and enrichment in ^{13}C (Barker and Fritz 1981a; Clark and Fritz 1997). The methane from BR-3A could have been enriched by microbial methane oxidation. Therefore, in establishing the source of methane as either hydrocarbon or ethanol fermentation, the $\delta^{13}C$ value of methane should not be used in isolation. One additional approach is to evaluate the ^{14}C content of the methane. Fossil fuel hydrocarbons are free of ^{14}C while ethanol from biomass has modern levels of ^{14}C (Clark and Fritz 1997; Conrad et al. 1997). While ethanol and the methane originated from its biodegradation should have modern ^{14}C levels, methane from hydrocarbons should not contain significant ^{14}C.

Even with these caveats, the difference in $\delta^{13}C$ between methane from ethanol and from gasoline is significantly large to allow the $\delta^{13}C$ of methane to be used to identify its source. In the ethanol/gasoline sites evaluated, the methane $\delta^{13}C$ tool provided a clear source of the methane in 5 of 7 cases.

3.5 Figures and Tables

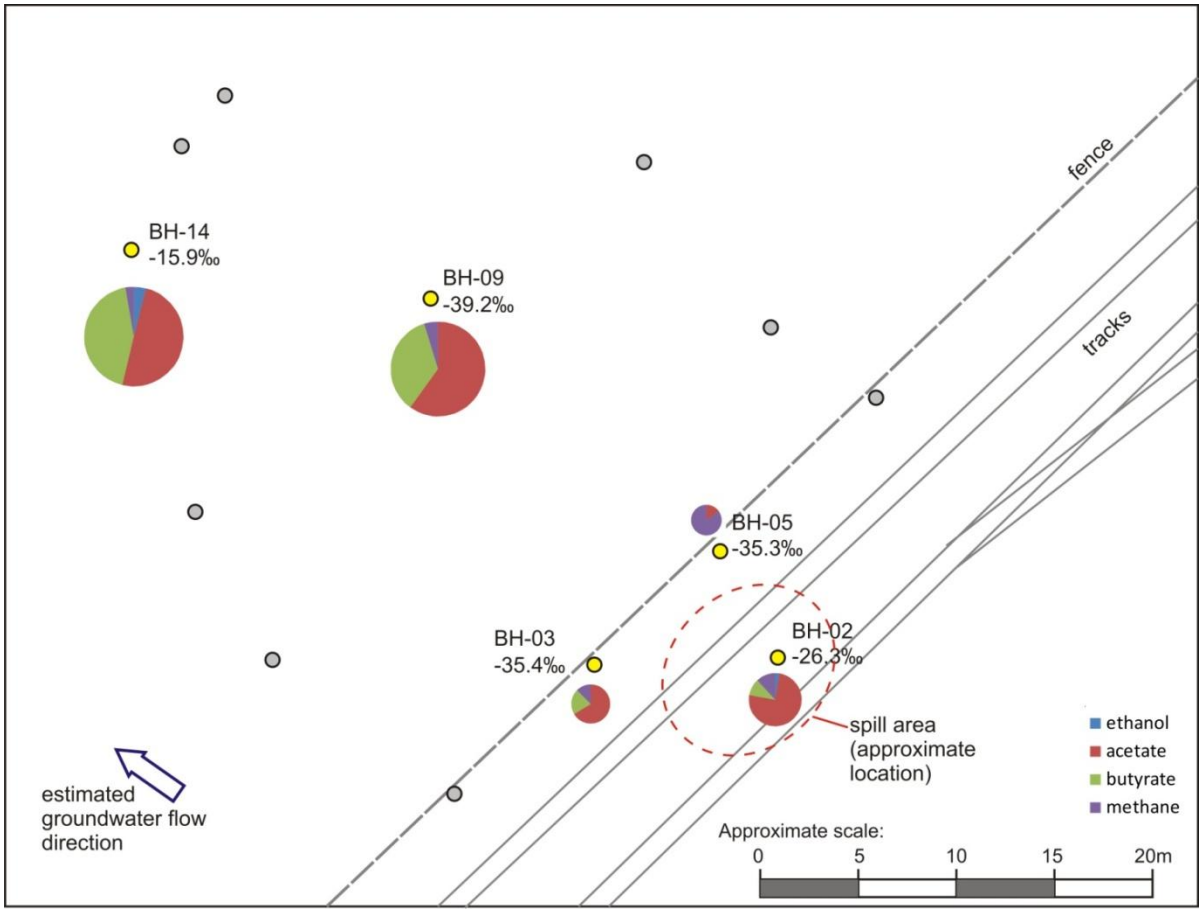

Figure 3.1: Ontario site - Methane $\delta^{13}C$ (‰) values and concentrations (mol/L) in February 2008. Pie charts diameters are proportional to concentration of ethanol plus biotransformation products. BH-05 chart was amplified five times to illustrate the presence of acetate. Wells highlighted in yellow were sampled in this study.

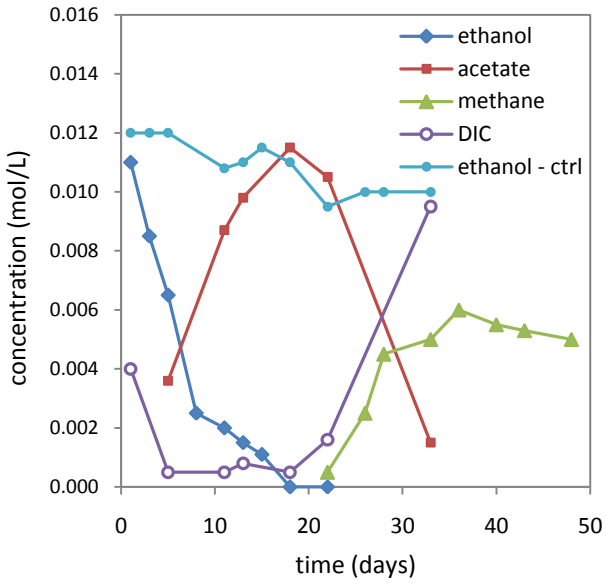

a) concentration in the aqueous phase

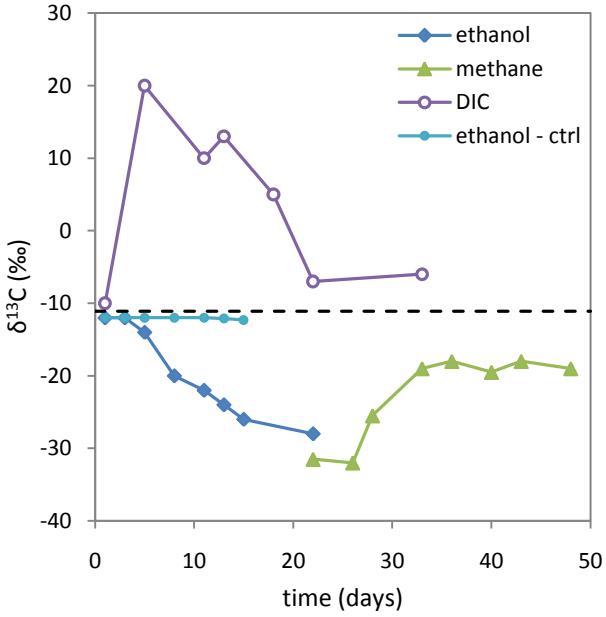

b) Carbon isotope (dashed line represents initial ethanol $\delta^{13}C$ value)

Figure 3.2: Results from the ethanol degradation microcosm. Repeat tests had similar results (not shown).

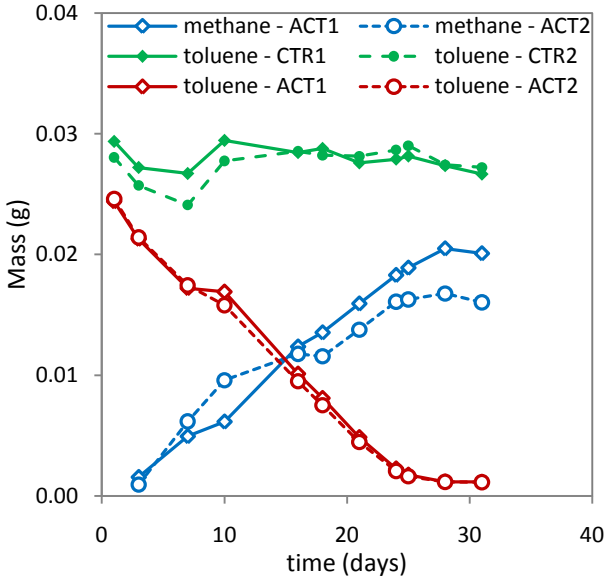

a) mass in the system

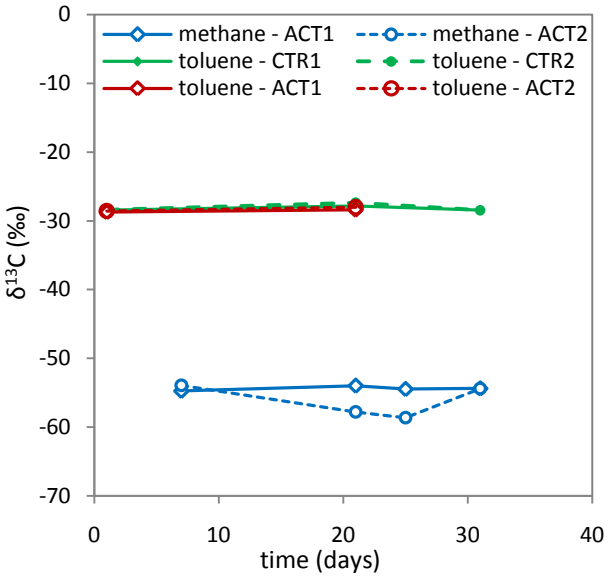

b) Carbon isotope

Figure 3.3: Results from the toluene degradation microcosm. (ACT: active bottles, CTR: control bottles)

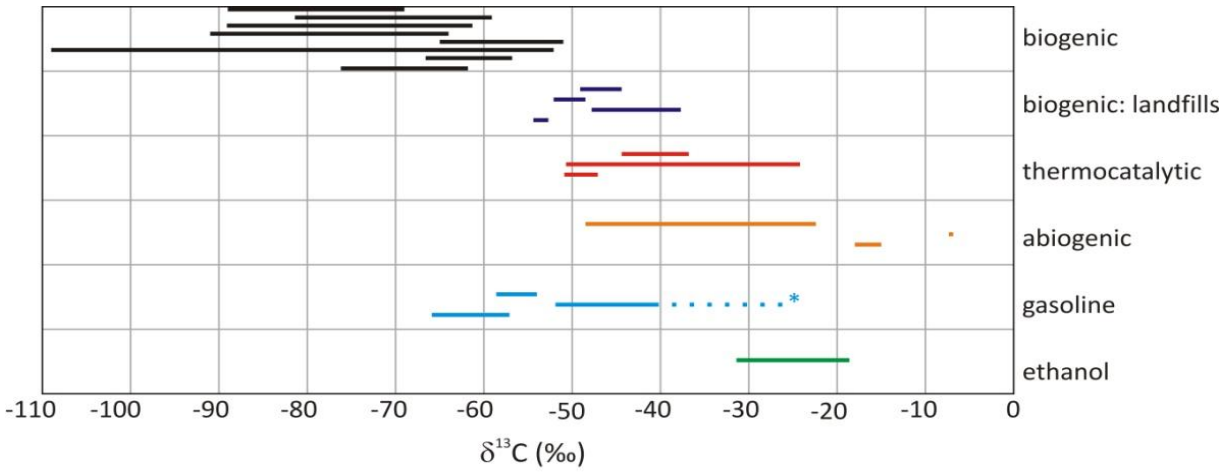

Figure 3.4: Methane $\delta^{13}C$ values according to attributed source. Biogenic: Aravena et al. 1995; Barker and Fritz 1981b; Coleman et al. 1988; Schoell 1980; Aravena et al. 2003; Whiticar et al. 1986; Strapoc et al. 2007; Kelley et al. 1992. Biogenic – landfills: Barker and Fritz 1981b; Whiticar et al. 1986; Games and Hayes 1974; Van Breukelen and Griffioen 2004. Thermocatalytic: Barker and Fritz 1981b; Schoell 1980; Strapoc et al. 2007. Abiogenic: Sherwood Lollar et al. 1993; Abrajano et al. 1990; Welhan 1988. Gasoline: this study (toluene); Conrad et al. 1999; Fletcher 2007. Ethanol: this study. *Enriched values were hypothesized to be caused by methane oxidation resulting in a shift in carbon isotope ratio (Conrad 1999).

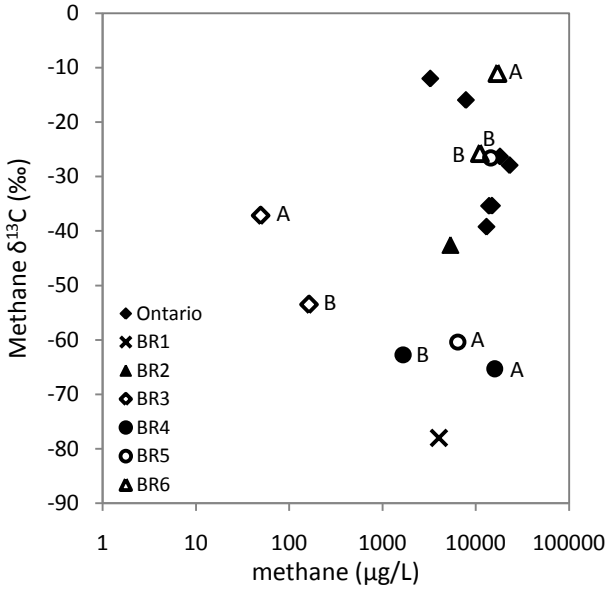

Figure 3.5: Methane $\delta^{13}C$ (‰) versus methane concentrations (A and B indicate samples from the same site but different wells)

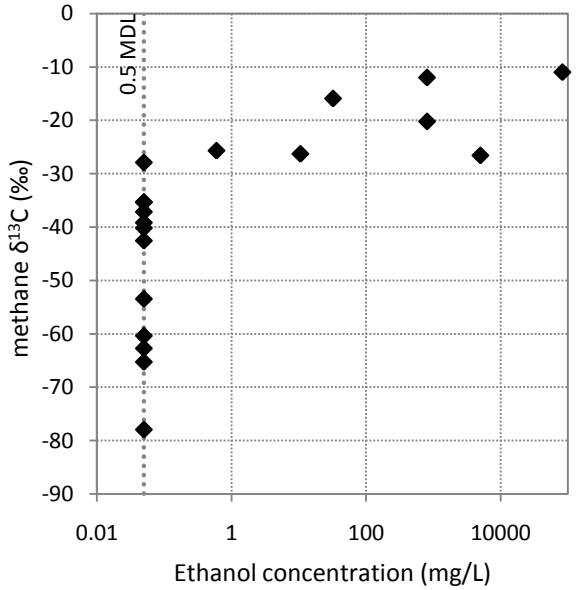

Figure 3.6: Methane $\delta^{13}C$ (‰) and ethanol concentration from field samples. Correlation coefficient = 0.68 (including all points). When ethanol was non-detect, groundwater concentration was assumed as 0.5MDL (0.05 mg/L).

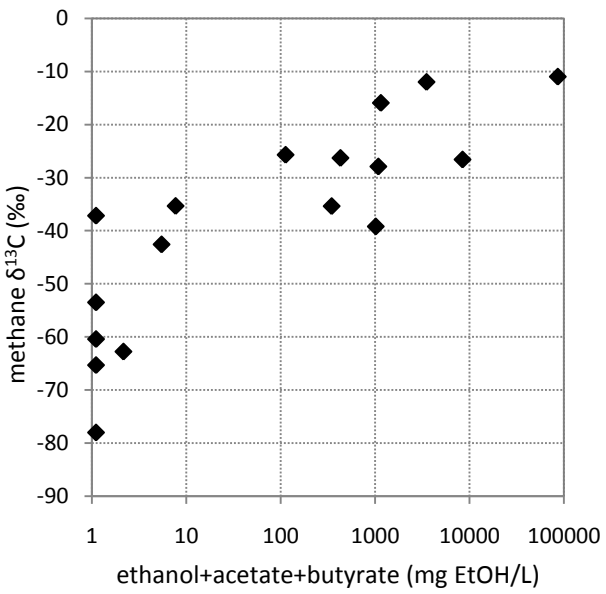

Figure 3.7: Methane $\delta^{13}C$ (‰) versus ethanol and biodegradation products. All concentrations were converted to equivalent ethanol. Correlation coefficient = 0.84 (including all points). Non-detected compounds were assumed as 0.5MDL.

Table 3.1: Ethanol and biodegradation products concentrations (A and B indicate samples from the same site but different wells).

	Sample	sampling date	ethanol (mg/L)	methane (μg/L)	acetate (mg/L)	butyrate (mg/L)	methane $\delta^{13}C$ (‰)
Ontario, CA	BH2	19-Feb-08	10.6	18100	428	86	-26.3
	BH3	19-Feb-08	ND	13900	275	129	-35.4
	BH5	19-Feb-08	ND	14870	10	ND	-35.3
	BH9	14-Nov-07	ND	23000	600	594	-27.9
	BH9	18-Feb-08	ND	13000	608	525	-39.2
	BH14	14-Nov-07	808	3250	557	2170	-12.0
	BH14	18-Feb-08	32.4	7820	529	680	-16.0
BRAZIL	BR1	12-Nov-07	ND	4020	ND	ND	-78.0
	BR2	12-Nov-07	ND	5350	7.1	ND	-42.6
	BR3-A	13-Nov-07	ND	49.3	ND	ND	-37.2
	BR3-B	13-Nov-07	ND	163	ND	ND	-53.5
	BR4-A	13-Nov-07	ND	1660	2.8	ND	-62.7
	BR4-B	13-Nov-07	ND	15900	ND	ND	-65.3
	BR5-A	23-Sep-08	ND	6430	ND	ND	-60.4
	BR5-B	23-Sep-08	5020	14400	934	2590	-26.6
	BR6-A	25-Sep-08	83100	17100	3580	449	-11.0
	BR6-B	25-Sep-08	0.6	11100	34.7	81.5	-25.7

ND: non detected

Table 3.2: Hydrocarbons concentrations

		sampling date	benzene	toluene	ethyl-benzene	m,p-xylenes	o-xylene	1,3,5-TMB	1,2,4-TMB	1,2,3-TMB	naphthalene
MDL			0.8	1	1	2.2	2.1	1.1	1.1	1.3	2.1
LOQ			2.5	3.1	3.1	6.6	6.2	3.2	3.3	3.8	6.4
Ontario, CA	BH2	19-Feb-08	48	17.1	ND	10.3	7.1	ND	2.6	ND	ND
	BH3	19-Feb-08	103	5.7	ND	2	2.5	ND	ND	ND	ND
	BH5	19-Feb-08	21	4.9	ND	2.4	ND	ND	ND	ND	ND
	BH-9	14-Nov-07	190	66	14.5	24.8	26.2	N/A	N/A	N/A	N/A
	BH-9	18-Feb-08	136	68.5	ND	64.1	ND	ND	ND	ND	ND
	BH-14	14-Nov-07	13400	837	N/A	N/A	67.2	N/A	N/A	N/A	N/A
	BH-14	18-Feb-08	117	42.4	ND	9.2	ND	ND	ND	ND	ND
BRAZIL	BR1	12-Nov-07	1.1	0.6	0	0.5	0	0	0	0	0
	BR2	12-Nov-07	4830	4130	498	2760	1560	204	678	231	185
	BR3-A	13-Nov-07	3.2	0	0	1.3	0.7	0	4.2	0.9	0
	BR3-B	13-Nov-07	326	403	146	543	217	55	194	54	59.7
	BR4-A	13-Nov-07	0	1.2	6.3	1.7	1.4	0	0	0	4
	BR4-B	13-Nov-07	54.1	0.5	1.3	5.6	1.7	0	0	1.7	7.8
	BR5-A	23-Sep-08	305	0	0	2.7	8.3	0	4	0	2.4
	BR5-B	23-Sep-08	N/A	N/A	N/A	N/A	N/A	N/A	N/A	N/A	N/A
	BR6-A	25-Sep-08	N/A	N/A	N/A	N/A	N/A	N/A	N/A	N/A	N/A
	BR6-B	25-Sep-08	1120	180	240	249	220	67	153	62	161

concentrations in µg/L

N/A: not analyzed due to interfering peaks

Chapter 4
2-D Laboratory Evaluation of Gasoline and Ethanol Spills in the Unsaturated Zone

4.1 Introduction

The behaviour of LNAPL's (light non-aqueous phase liquids) following a spill in the unsaturated zone has been evaluated in several laboratory tests (Pantazidou and Sitar 1993; Schroth et al. 1995; Sharma and Mohamed 2003; Kechavarzi et al. 2005). In general, LNAPL mainly migrates vertically in the unsaturated zone and then accumulates on the saturated/quasi saturated zone below the top of the capillary fringe. The resulting water saturation profile in this three-phase system is dependent on the capillary pressure between water and NAPL; and the total saturation profile is dependent only on the capillary pressure between NAPL and air (Leverett 1941; Parker 1989).

Ethanol can interfere significantly with the NAPL distribution in the source zone, as it modifies several properties of the system. As the concentration of ethanol increases, the interfacial tension between the aqueous and the NAPL decreases exponentially (Oliveira, 1997; McDowell et al. 2003). Similarly, the water surface tension decreases as the ethanol fraction in the aqueous phase increases (McDowell et al. 2003). When present in high fractions, ethanol also decreases the density and increases the viscosity of the aqueous phase (Ageno and Frontali 1967; Belda et al. 2004).

The effect of ethanol releases on top of gasoline contamination was first assessed by McDowell et al (2003). In 2D visualization experiments, the shape and area of the gasoline pool was significantly altered following an ethanol release. Capiro et al. (2008) and Stafford et al. (2009) showed that ethanol is transported at the capillary fringe and shallow groundwater and can displace a hydrocarbon residual phase located downgradient.

In this study, the behaviour of gasoline and ethanol released in the unsaturated zone was further evaluated. Two-dimensional (2-D) tests were conducted under different flow conditions. These tests add to previous research by considering the effect of different spill volumes and the consequences of water level fluctuations.

4.2 Methods

Gasoline and ethanol spills were simulated in a transparent plexiglass box 48 cm long, 40 cm high and 2.5 cm thick, which was packed with 390 μm glass beads, representing a medium to coarse sand. The glass beads were packed underwater in lifts of 2 cm to prevent air entrapment. Porosity was measured as 40%. The water was then drained to establish the water table and capillary fringe. In this study, the top of the capillary fringe was defined as the visually observed interface between the regions with high and low water saturation. The visible interface corresponds to a point in the transition zone, between fully saturated and the residual saturation (Pantazidou and Sitar 1993; Schroth et al. 1995; Sharma and Mohamed 2003). The box was covered with plastic film to minimize losses due to volatilization, but a small opening was created to maintain atmospheric pressure inside the box.

Gasoline and ethanol were injected with a glass syringe, in the center of the box, 1 cm below the glass bead surface. The gasoline used (API 91-01; Prince et al. 2007) was dyed red with Sudan IV (80% dye content, from Sigma Aldrich) to allow a better visualization of the NAPL. Ethanol (99.9% purity, from Commercial Alcohols Inc.) was dyed with fluorescein, except for test 1. Fluorescein is a yellow, hydrophilic dye and has been used by other researches as an indicator of ethanol distribution (McDowell et al. 2003). In the interpretation, the presence of the dyes was considered as indicators of the presence of gasoline and/or ethanol. The gasoline and ethanol densities were 0.773 g/cm^3 and 0.789 g/cm^3, respectively. The contaminant behavior was recorded in pictures and the volume of water drained from the box was monitored over time. Three tests were done under static conditions and test four was done with horizontal groundwater flow (Table 4.1).

For the first three tests, three hoses were connected to the bottom of the box (Figure 4.1). Glass beads were packed to a height of 22 cm. The water level was kept constant at 5 cm from the bottom of the box and the top of the capillary fringe was situated 9.5 cm above the water table. Gasoline was injected and approximately one day later ethanol was injected. The volumes injected ranged from 25 to 50 mL (Table 4.1). In the third experiment, when steady state was reached after the ethanol injection, the water level was raised to 12.5 cm above the bottom of the box, to simulate the effect of a rising water table on the contaminants distribution. Water was injected through the middle hose at a flow rate of approximately 1.2 mL/s.

In the fourth test, two vertical sheets of stainless steel mesh were used to create two constant-head reservoirs at the sides of the box (Figure 4.2). The head difference between the reservoirs was fixed at

1 cm, resulting in a hydraulic gradient of 0.024, and inducing horizontal flow. The use of stainless steel mesh to create the reservoirs resulted in a perturbation in the flow condition at the sides of the box, as it does not allow flow in and out of the capillary fringe directly to the reservoir. This results in vertical flow components at the limits of the box, upwards at the inlet (left) side and downwards at the outlet (right) side. The streamlines close to the reservoirs are expected to have steep slopes (Wyckoff et al. 1932); therefore this perturbation in flow is expected to be limited to a small distance from the sides of the box, with essentially horizontal flow at the middle of the box. The results obtained in the experiments seem to indicate that this was the case. The gasoline and ethanol injection volumes were decreased to 15 mL to constrain the gasoline pool within the reduced length of the box. The time between the gasoline and ethanol injections was 20 minutes.

4.3 Results and Discussion

4.3.1 Ethanol and Gasoline Injection under No-Flow Conditions

4.3.1.1 Gasoline Injection

In the three static tests the behavior of the gasoline was very similar, despite the changes in the conditions of the tests. In general the observations are in agreement with previous studies about LNAPL infiltration and distribution in the unsaturated zone (Pantazidou and Sitar 1993; Schroth et al. 1995; Sharma and Mohamed 2003; Kechavarzi et al. 2005). The gasoline moved downwards with a circular front until it reached the top of the capillary fringe. Then, it mainly spread laterally on the top of the capillary fringe with some fingering. Some gasoline was left in the unsaturated zone, but its saturation decreased with time and by the end of the test the red color indicative of gasoline presence was really subtle.

Following the gasoline injection, the capillary fringe was depressed between 30% and 40% (Table 4.2). The reduction was expected, considering the lower values of gasoline surface tension (Parker et al. 1987; Parker 1989). At earlier times, the gasoline moved laterally at the elevation of the depressed capillary fringe, extending below the top of the original capillary fringe. As the gasoline spread, it decreased the surface tension, causing drainage of the water just above it. As a consequence, a small tension-saturated zone above a low water-saturation zone was formed at the corners of the gasoline pool (Figure 4.3a). Similar behaviour was reported previously by Henry and Smith (2001) in the study of butanol injection.

Later, the gasoline lateral spreading slowed and appeared to follow a different pattern. Instead of the gasoline spreading laterally and causing a depression in the capillary fringe, first the capillary fringe was depressed, and then the gasoline spread on top of it (Figure 4.3b). At the end of all tests, the gasoline was distributed over the entire length of the box (Figure 4.4). The depression of the capillary fringe in some regions before gasoline was noted could simply be caused by the presence of gasoline in lower saturation that could not be seen at the plexiglass front.

Another possibility for the depression of the capillary fringe before NAPL reached it is that the water at the top of the capillary fringe was increasingly being contaminated by gasoline compounds that dissolve from the NAPL into the water or from compounds that volatilized into the gas phase and later partitioned to the clean water (Conant et al. 1996; Grathwohl et al. 2002). The presence of

dissolved hydrocarbons in water could cause a significant decrease in the water surface tension, and consequent decrease in the capillary rise. Jajuee et al. (2006) measured o-xylene saturated water surface tension and found it to be around 20% less than pure water. Since the box used was a closed system, as time progressed the concentrations in the water and vapor would tend to equilibrium conditions. The gasoline used has a relatively high fraction of highly volatile compounds such as pentane and hexane (around 3% each, mass based) which have low values of surface tension, from 15 to 20 mN/m (Lide 2008). It also contains compounds with relatively high solubility and low surface tension, such as benzene, with solubility of 1780 mg/L and surface tension of 28 mN/m (Lide 2008). This contrast with previous studies (Pantazidou and Sitar 1993; Schroth et al. 1995; Sharma and Mohamed 2003; Kechavarzi et al. 2005) where the LNAPLs tested were of low solubility and low volatility. It appears more likely that dissolved hydrocarbons caused the depression of the capillary fringe. Even though it is possible that some NAPL was not seen, it would have to be in low saturations and therefore it would have only a minor effect on the capillary fringe height.

The volume drained over time due to the gasoline injection was around 180 mL in each test (Figure 4.5), more than the volumes injected. The volume injected had no noticeable influence on the total drained volume. The volume drained reflects the decrease in the capillary fringe height, which was similar for all tests. The depression in the capillary fringe (h_d) was estimated based on the drained volume (V_d) using equation 1, where: V_i: injected volume; L: length of the box; t: thickness of the box; n: porosity (40%) and S_{wr}: residual water saturation (assumed 5%). A good balance was obtained between the volume drained and the observed depression in the capillary fringe height (Table 4.2).

$$h_d = \frac{V_d - V_i}{L \cdot t \cdot n \cdot (1 - S_{wr})} \quad (1)$$

4.3.1.2 Ethanol Injection

Approximately one day after the gasoline injection, ethanol was injected following the same procedure as for gasoline. The injected ethanol moved downwards in the unsaturated zone without significant lateral spreading and with high saturation, as evidenced by the strong green color (Figure 4.6). When the injection stopped, the ethanol from the center of the injection, where the saturation was highest, started to drain, as can be seen comparing the pictures from time 55 s and 210 s. Unlike in McDowell et al. (2003), no significant mobilization of gasoline residuals from the unsaturated zone

was noticed. This difference was likely due to the low gasoline residual saturation in the glass beads, which made it difficult to visualize gasoline in the unsaturated zone.

The ethanol front reached the gasoline pool and continued moving down due to further decrease in surface tension and due to its higher density relative to gasoline. As it moved down, it carried the gasoline, forming a circular ring of high gasoline saturation (a strong red) in front of it. As ethanol depressed the capillary fringe and moved the gasoline deeper in the center of the box, the gasoline saturation on the sides decreased. The depression of the capillary fringe at the center of the box induced the gasoline to collect in the center. The same behaviour was described by McDowell et al (2003). No gasoline residuals could be seen behind the ethanol front, indicating that ethanol was able to mobilize the gasoline without a significant residual entrapment. Ethanol can displace the gasoline by immiscible displacement, in an imbibition process, or by miscible displacement, if ethanol concentrations are high enough.

When ethanol concentrations are higher than 70% on a mass basis, the ternary system ethanol-water-gasoline is composed of one single phase (Oliveira 1997; Powers et al. 2001). For miscible displacement of gasoline residuals a minimum of 88% ethanol would be required according to Oliveira (1997). Although pure ethanol was injected, as it travel downwards it mixes with the pore water in the unsaturated zone. However, the mixing in our test was likely not sufficient to bring the ethanol concentrations to less than 88% given the short distance between the top of the box and the gasoline pool and the limited ethanol spreading in the unsaturated zone. The total volume of water in the unsaturated zone in the region where ethanol infiltrated was estimated to be above 3 mL, assuming an initial average residual water saturation of 5%. If all the ethanol was mixed equally with all the water the ethanol mass fraction would be around 87%. Considering the high affinity of ethanol for water, the initial concentrations of ethanol to reach the gasoline pool were probably more depleted in ethanol, but the concentrations likely exceeded 88% as the water was taken up by the infiltrating ethanol.

Immiscible displacement of gasoline by ethanol-rich water is also facilitated by the lower interfacial tension between the aqueous phase and NAPL. Oliveira (1997) showed that a reduction of 0.33 to 0.66 in the interfacial tension can result in the mobilization of gasoline residuals due to interfacial tension gradients. A reduction in interfacial tension of this magnitude would be generated by ethanol mole fractions in the aqueous phase of around 0.07 to 0.2 (16 to 40% mass fraction). Therefore, even if ethanol concentrations were less than required for miscible displacement when it

reached the gasoline pool, the gasoline could still have been mobilized effectively by ethanol. Numerical model by Yu et al. (2009) indicated that ethanol likely reached the gasoline pool with its mole fraction higher than 0.55, which could promote gasoline residuals mobilization by interfacial tension gradients.

At around 200 seconds, ethanol stopped moving down and started to spread horizontally, with the gasoline moving up and accumulating in the center. Pure ethanol is only slightly denser than gasoline, but as it mixes with water its density increases. The difference in density between the ethanol solution and gasoline likely caused the gasoline to move above the ethanol-rich water and accumulate in the center of the box, on top of the capillary fringe. In test 3, which had a smaller injection volume (25 mL), ethanol lateral spreading started when the front of the gasoline ring was approximately at the water table. However, in the tests with larger injection volumes (tests 1 and 2) the gasoline ring moved below the static water table (Figure 4.7). This indicates that the volume of ethanol injected has a great effect on the amount of hydrocarbons that will reach the water table and the saturated zone below it.

As ethanol moved laterally, an area with an opaque pink color developed at the deepest positions reached by the gasoline ring (Figure 4.8). The color observed could not be replicated in the laboratory by simply mixing water, dyed gasoline and dyed ethanol. Besides, the occurrence of this zone in the first test indicates that the color was not a consequence of the fluorescein dye. It appears that as most of the ethanol left that region, the hydrocarbons solubility decreased and some of it precipitated, resulting in the formation of residual NAPL with the reddish color. The formation of this zone was more pronounced in the tests with higher injection volumes. This behavior is analogous to what was observed by Capiro et al. (2008) during the injection of E95 (95% ethanol, 5% hydrocarbons) at the water table: the NAPL separated and was left behind the ethanol which moved upwards.

When ethanol moved horizontally and upwards due to its low density, it reached the top of the capillary fringe on the sides of the gasoline. Ethanol spread laterally on the top of the capillary fringe on the sides of the gasoline, causing the capillary fringe to be further depressed (Table 4.2), due to a reduction in surface tension. Ethanol also moved horizontally in the unsaturated zone, above the capillary fringe. Ethanol spreading in the unsaturated zone might have been caused by diffusion in the aqueous phase or volatilization with subsequent partitioning to clean pore water. Henry and Smith (2003) also showed that flow would be induced from contaminated regions toward clean regions in the presence of organic compounds that decrease the surface tension of water, such as ethanol. At the

end of the experiments, ethanol had spread over the entire length of the box in both the capillary fringe and unsaturated zone.

Most of the gasoline accumulated at the top of the capillary fringe, in the middle, where the capillary fringe was first depressed. Some of the gasoline was also dispersed over the whole capillary fringe. The color of the gasoline pool was much stronger than before the ethanol injection and the area of the pool was smaller, indicating higher NAPL saturation. The same observation was made by McDowell et al. (2003), and it was justified as a consequence of the lower interfacial tension allowing the gasoline to fill smaller pores.

Similarly to what was observed following the gasoline injection, the volume of ethanol injected didn't affect the volume of water drained (Figure 4.9). The total volume drained after the ethanol injection was less than the volume drained after the gasoline injection. This was expected since the capillary fringe was already depressed because of the gasoline when ethanol was injected. The calculated depression of the capillary fringe based on the volume drained matched the observed depression (Table 4.2).

4.3.2 Test 3: Water Table Rise

One day after the ethanol injection the water level was raised 7.5 cm over about 270 seconds, reaching 12.5 cm (Figure 4.10). After the water level was raised, the capillary fringe was thinner, around 2 cm. This is likely due to hysteresis in the capillary pressure-saturation curve.

Ethanol moved up as the water table rose, always staying at the top of the capillary fringe. The gasoline pool was also displaced upwards, but at 80 seconds it divided in two parts. The first was relatively flat and stayed on top of the upward moving capillary fringe. The second high saturation zone had a circular shape and was less mobile, being retained in the region where the gasoline was initially present. This second zone decreased in area with time and eventually it disappeared. Sharma and Mohamed (2003) reported a similar NAPL disconnection during lowering of water table in 2D experiments using mineral oil as the NAPL. They hypothesized that the NAPL had travelled through invisible pathways. It is possible that the same happened at our test and the two NAPL regions were never disconnected. The NAPL present in the lower zone might have just slowly migrated upwards due to buoyancy through pathways that could not be perceived at the plexiglass front, mainly due to low NAPL saturation. This behaviour is evidenced by the increase in the area of the NAPL pool on

top of the capillary fringe as the area of the second NAPL zone decreased, indicating that NAPL was being transferred from one zone to the other.

Besides these two regions with high gasoline saturation, the amount of gasoline distributed over the entire length of the box seems to have increased with the water table rise. The presence of gasoline in lower saturation could be seen over a thick zone close to the top of the capillary fringe, coinciding with the high ethanol concentration zone. The ethanol contaminated zone also seems to have thickened with the water table rise. An increase in the ethanol contaminated area could indicate a decrease in its concentration, which would also lead to a decrease in hydrocarbons solubility. It is possible that NAPL precipitated as ethanol concentration declined. This would account for the increase in the scattered red color in the shallower zones. However, the increase in the ethanol contaminated area in the capillary fringe could also reflect an increase in ethanol mass, as the ethanol that was previously in the unsaturated zone is incorporated into the rising capillary fringe. By the end of the test, the amount of ethanol in the unsaturated zone was less than before the water table rise.

The zone that was previously identified by the opaque pink color did not move with the water table rise, consistent with the previous inference that gasoline residuals were formed in that location. After the water table rose, this region appears to be completely depleted of ethanol and disconnected from the high ethanol zones and from the gasoline pool. In summary, an ethanol release moves the NAPL deeper and leaves residual NAPL with low ethanol below the gasoline pool. When the water table rises, these residuals are unlikely to be mobilized due to the low ethanol, resulting in a gasoline residual zone completely disconnected from the gasoline pool. In a real situation, this could result in two source zones, at different depths, disconnected from each other.

4.3.3 Test 4: Behaviour with Groundwater Flow

In the fourth experiment a hydraulic gradient of 0.024 was established to induce horizontal flow in the box. The flow rate was stable at 0.24 mL/s before the injections. Close to the constant head reservoirs a significant vertical component of flux was anticipated, due to the flux of water in and out of the capillary fringe. To minimize the influence of this artificial condition on the results, the injection volumes were decreased and the contaminant behavior in the corners was not considered representative.

The gasoline was injected at 20 seconds and ethanol was injected after twenty minutes (Figure 4.11). Their behaviors were similar to the previous tests. The gasoline moved vertically in the

unsaturated zone until it reached the capillary fringe, where it accumulated. The capillary fringe was depressed over the whole extent of the box, but mostly at the center and downgradient side (Figure 4.12). Visual gasoline did not reach the limits of the box, and was still concentrated in the center of the box when ethanol was spilled. As in the previous tests, the capillary fringe depression where gasoline was not seen could have been caused by dissolved hydrocarbons.

Ethanol moved the gasoline pool deeper into the capillary fringe, but ethanol and gasoline didn't reach the water table (Figure 4.11; time = 22 min). As in the other tests, ethanol reached the capillary fringe on the sides of the gasoline pool and started spreading laterally. However, due to the flow conditions established in the box, ethanol moved preferentially downgradient of the gasoline source, and was transported in a very thin layer on top of the capillary fringe. When ethanol reached the limit of the box, it migrated downwards to the water table and left the box. The downward movement at the outlet is a consequence of the constant head reservoir constructed with the stainless steel mesh, which does not allow flow directly into it from the capillary fringe. Therefore, the downward transport of ethanol at the limit of the box does not represent a situation that would be seen in a continuous porous media, but like around a pumping well. After two hours most of the ethanol that reached the capillary fringe had migrated out of the system leaving the gasoline behind. Below the high saturation gasoline pool, an area with the opaque pink color started being formed at around 40 minutes and increased with time (Figure 4.11). This opaque area was formed as ethanol left the region. As discussed previously, this likely indicates that NAPL was precipitated as ethanol concentrations decreased.

Downgradient of the gasoline pool the capillary fringe was further depressed by ethanol, while on the upgradient side this effect was not so pronounced (Figure 4.12). The capillary fringe height remained relatively stable from 90 min until the end of the test. Similar to the tests performed under no-flow conditions, ethanol also spread significantly in the unsaturated zone, as is evidenced by a thick green zone above the capillary fringe. Ethanol persisted in the unsaturated zone without significant change for one day, when the test was ended (Figure 4.13). At the end of the test ethanol could be seen only in the unsaturated zone, with no evidence of its presence in the capillary fringe or below the water table.

The volume of water that flowed through the system was measured over time and the flow rate was calculated (Figure 4.14). The peaks following the injections are due both to water displacement by gasoline and then by ethanol, and by drainage of the capillary fringe in both cases. The peak was

higher after the gasoline injection, but was also significant after the ethanol injection. This difference is consistent with the results obtained in the experiments 1 to 3.

4.4 Conclusions

The behaviour of gasoline and ethanol releases in the unsaturated zone was evaluated in 2D tests. The capillary fringe height was lowered 37% (3.5 cm in average) by gasoline injection and an additional 22% by ethanol injection (around 2 cm), due to lowering of surface tension. It appears that volatilization and dissolution of gasoline hydrocarbon might contribute to the capillary fringe depression, facilitating NAPL spreading on top of the saturated zone.

Ethanol release on top of gasoline resulted in NAPL being displaced to deeper positions. Most of the gasoline accumulated in the center of the box, where ethanol first reached the capillary fringe. The final elevation of the gasoline pool was dependent on the ethanol volume released. For large ethanol spills, much of the gasoline source might be displaced to below the water table.

Ethanol, on the other hand, did not accumulate in a small area. After moving downwards and displacing the gasoline, ethanol was redistributed around the gasoline pool on top of the capillary fringe and occupied the whole extension of the box. With groundwater flow, all the ethanol that reached the capillary fringe was transported downgradient quickly. Independent on the flow conditions established in the saturated zone, some fraction of the ethanol did not reach the capillary fringe. Due to ethanol's high solubility in water, a significant fraction was dissolved in the unsaturated zone pore water and was retained there during the duration of the test.

When the water level rose, some gasoline was trapped in the saturated zone. Gasoline residuals that formed below the NAPL pool when ethanol was released remained in the same position. Ethanol appeared to be distributed over a thicker zone after the water table rose, which is likely associated with decrease in concentrations. The decrease in ethanol concentration could have caused NAPL formation, resulting in the scattered gasoline appearing over the complete extension of the box in the first few centimeters of the capillary fringe.

4.5 Figures and Tables

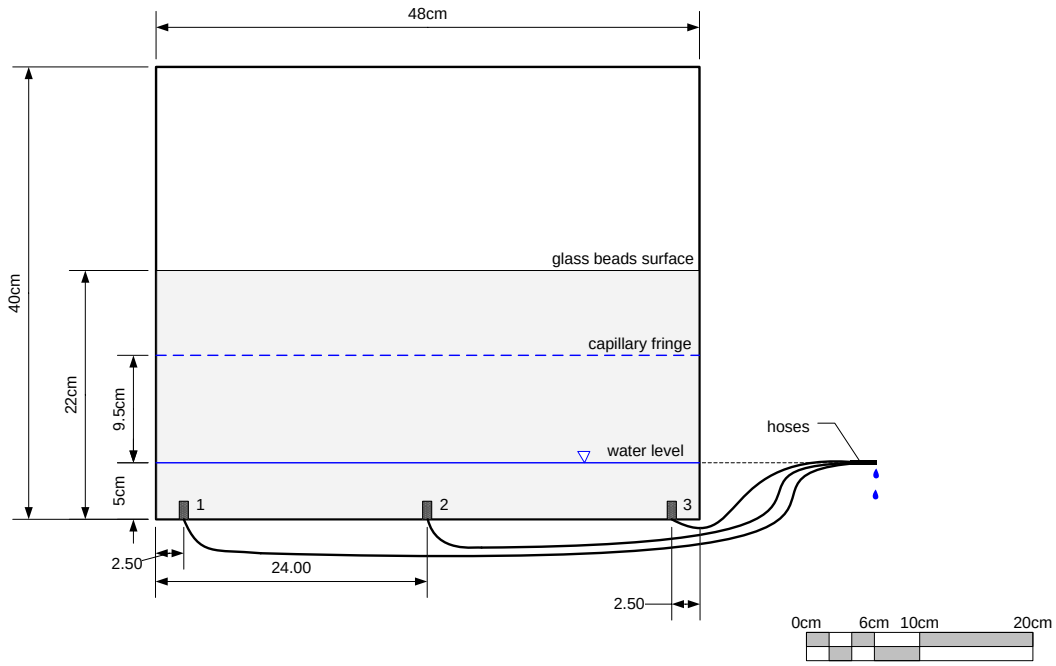

Figure 4.1: Setup for tests 1 to 3

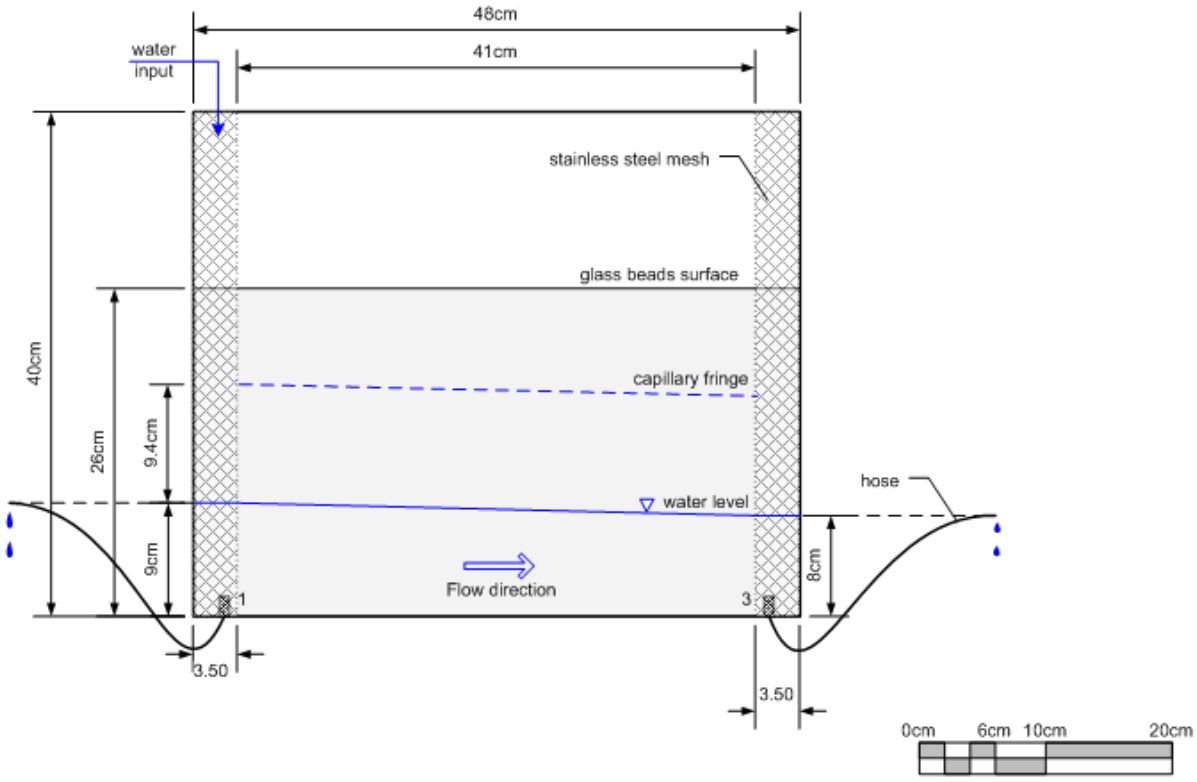

Figure 4.2: Setup for test 4

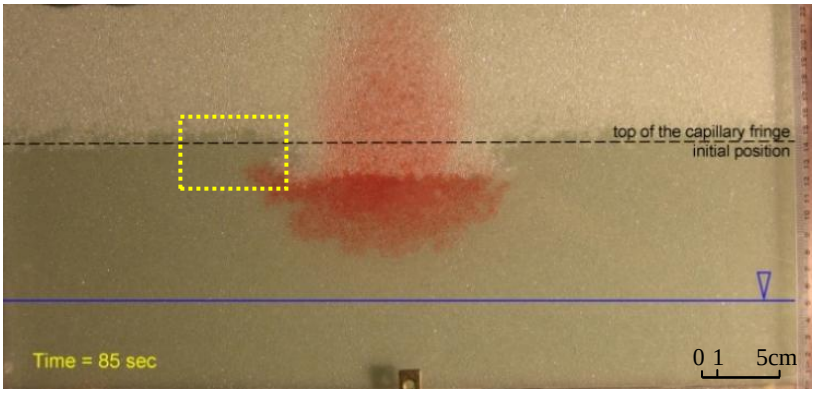

a) Earlier times: gasoline spreading laterally with formation of tension saturated zones above low water-saturation regions

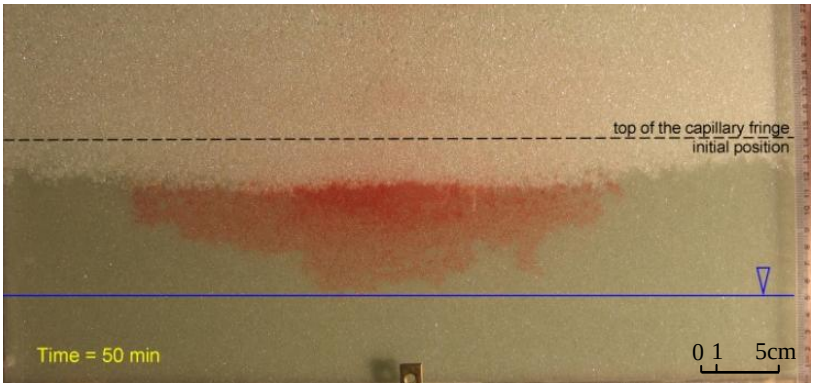

b) Later times: gasoline spreading is preceded by capillary fringe collapse

Figure 4.3: Gasoline configuration through time at test 3. Blue line represents the position of the water level and the black dashed line represents the initial position of the capillary fringe.

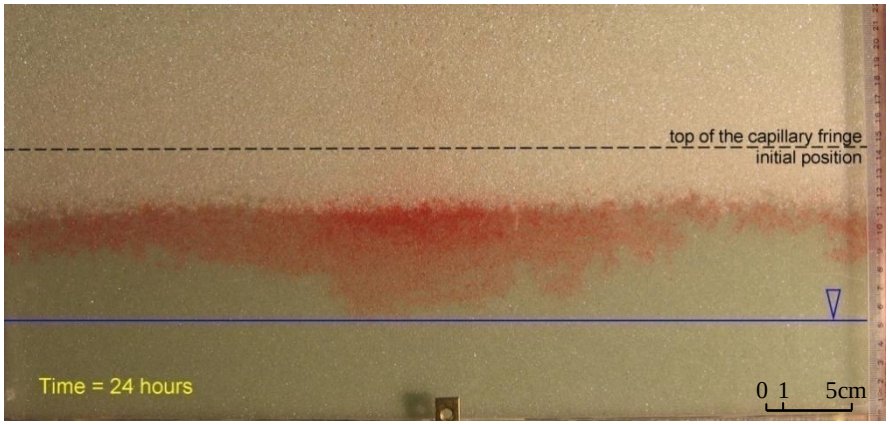

Figure 4.4: Gasoline configuration for test 3, 1 day after injection. Gasoline was seen on top of the depressed capillary fringe over the whole box extension.

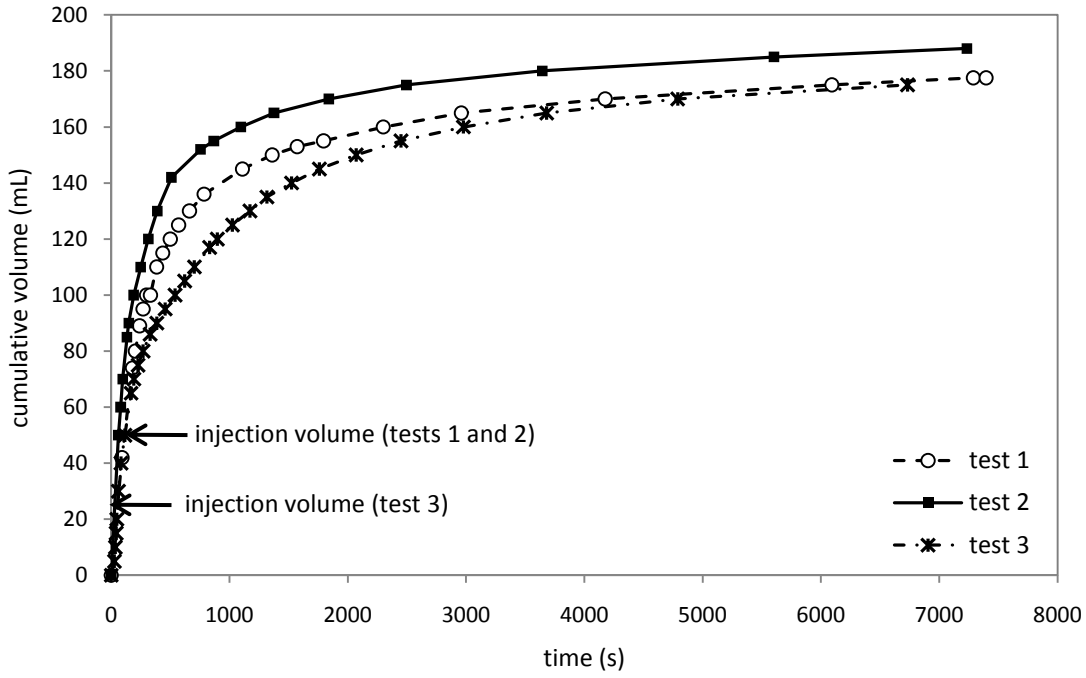

Figure 4.5: Cumulative volume drained versus time after gasoline injection.

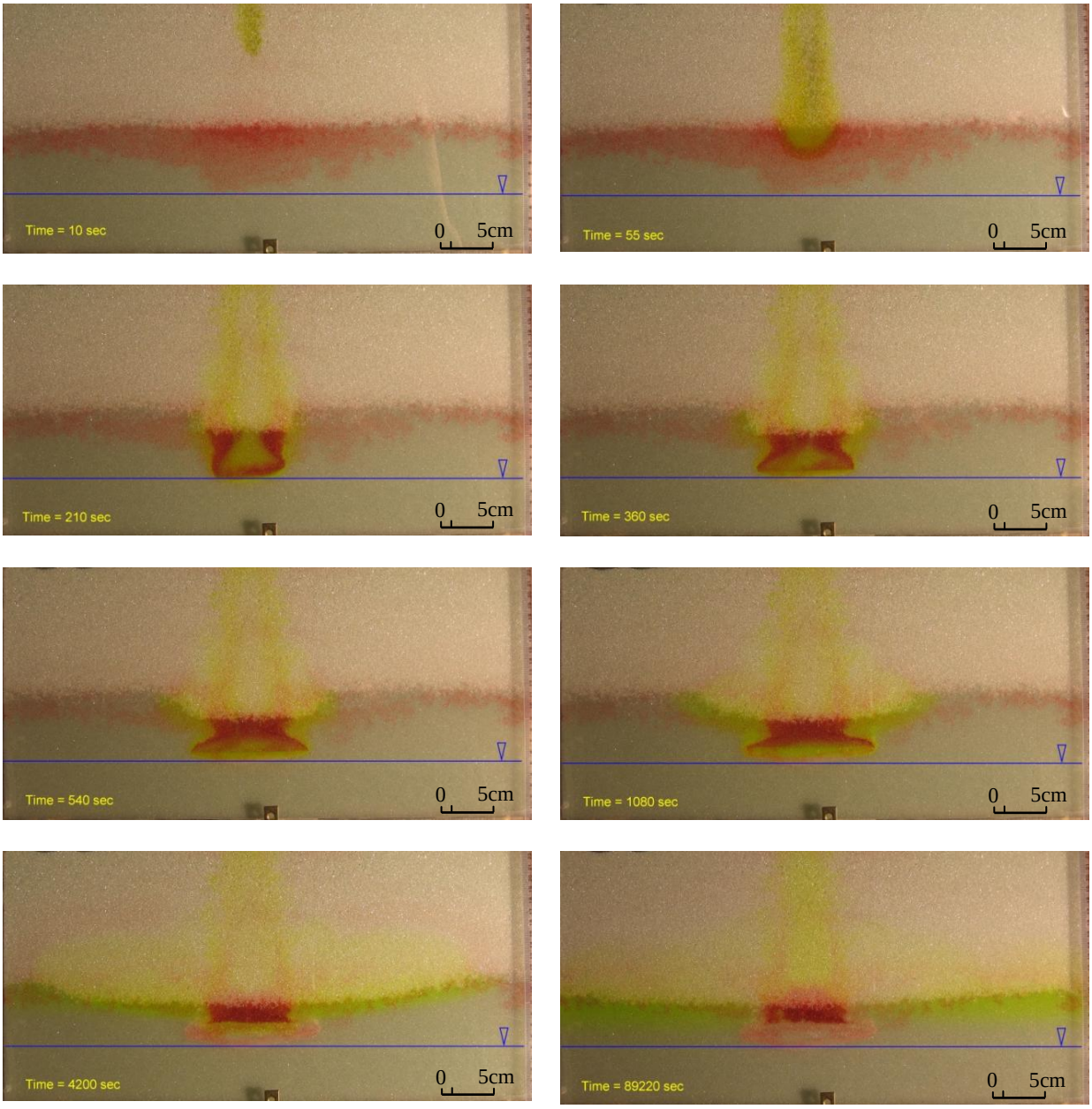

Figure 4.6: Ethanol injection (green) on top of gasoline (red), test 3. Blue line represents the position of the static water level.

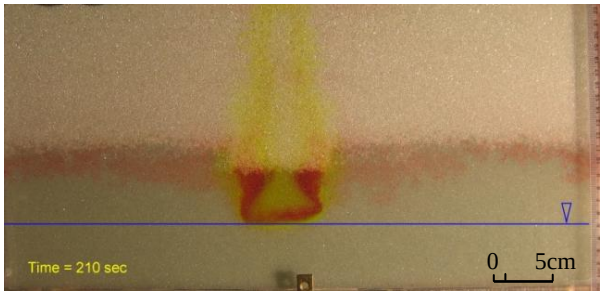

Test 3: Injection volume of 25 mL. The gasoline ring stops at the static water level

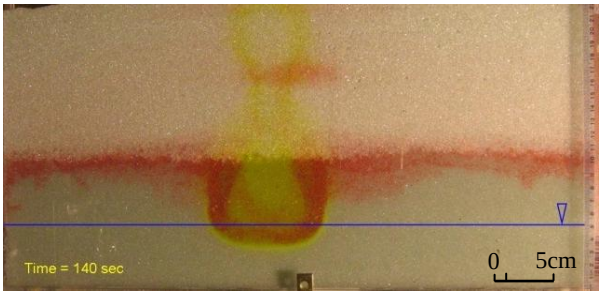

Test 2: Injection volume of 50 mL. The gasoline ring moves below the static water level

Figure 4.7: Ethanol Injection – Comparison between tests 2 and 3: the blue line represents the position of the static water level

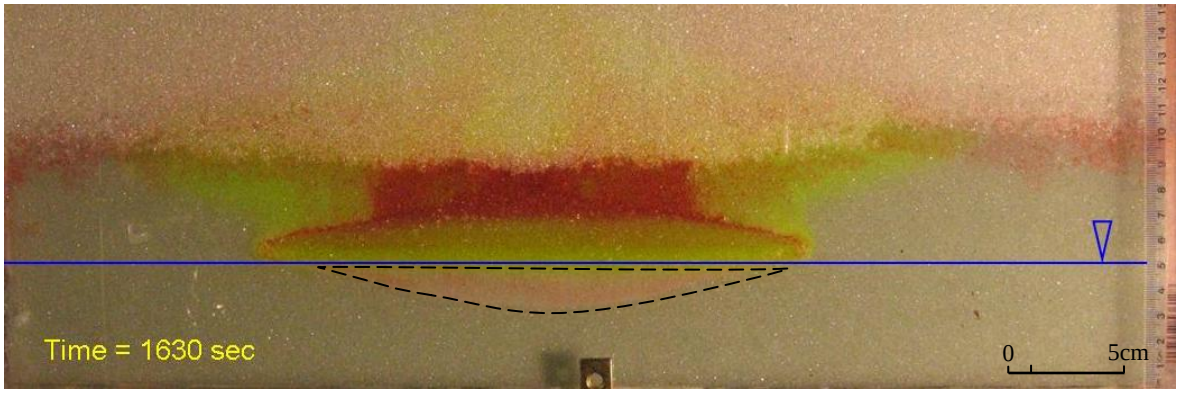

Figure 4.8: Formation of gasoline residuals (reddish color outlined by the dashed line) after ethanol started to spread horizontally during test 2

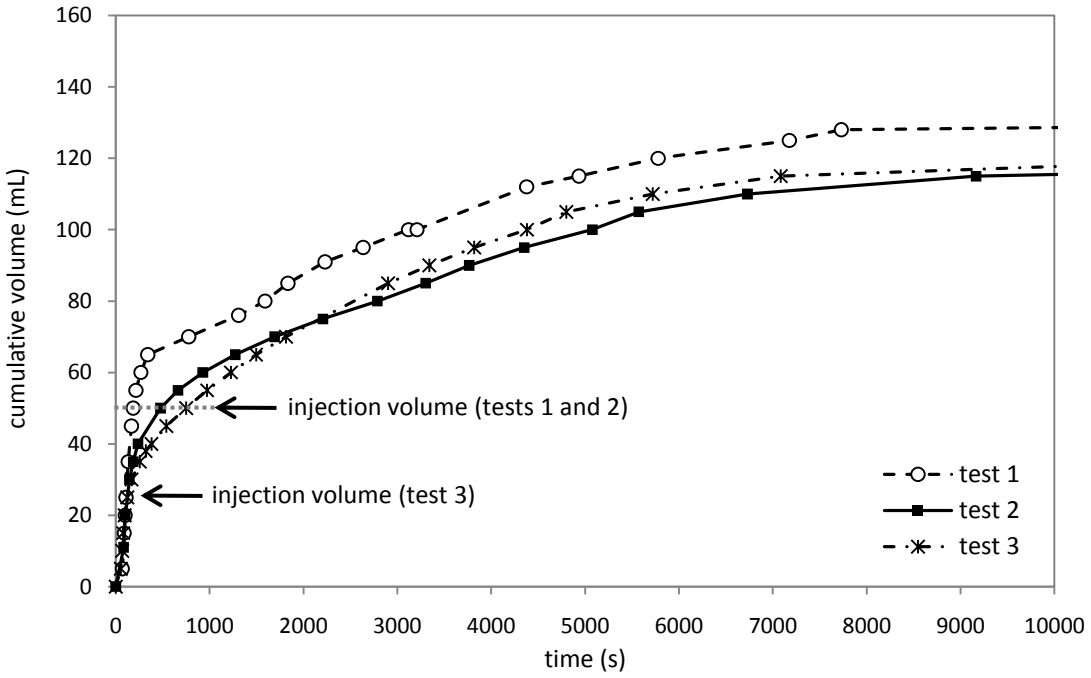

Figure 4.9: Ethanol Injection: Cumulative volume drained versus time

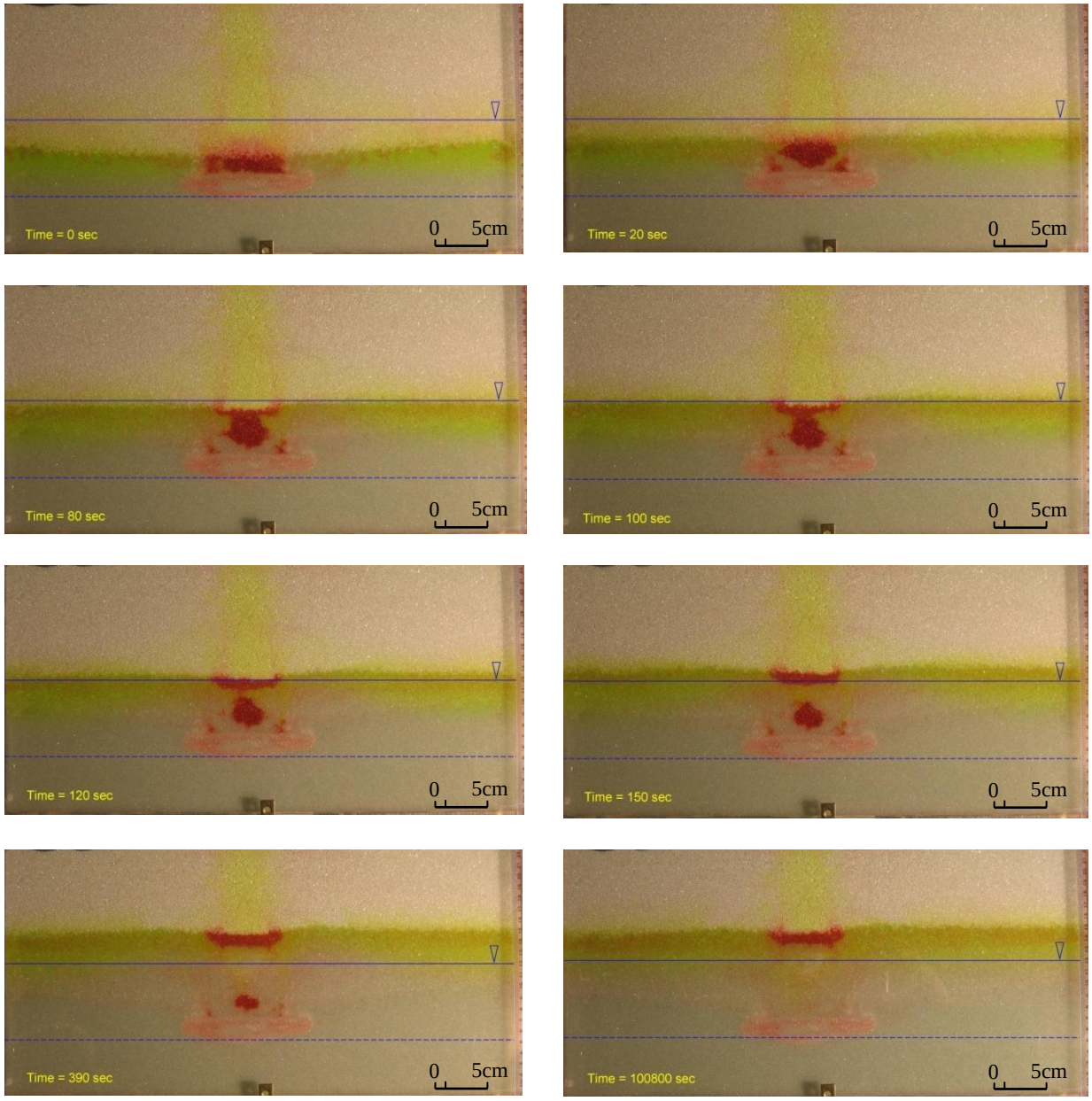

Figure 4.10: Water Level Raise - Experiment 3: the dotted blue line represents the initial position of the water level and the continuous blue line represents the position of the final water level

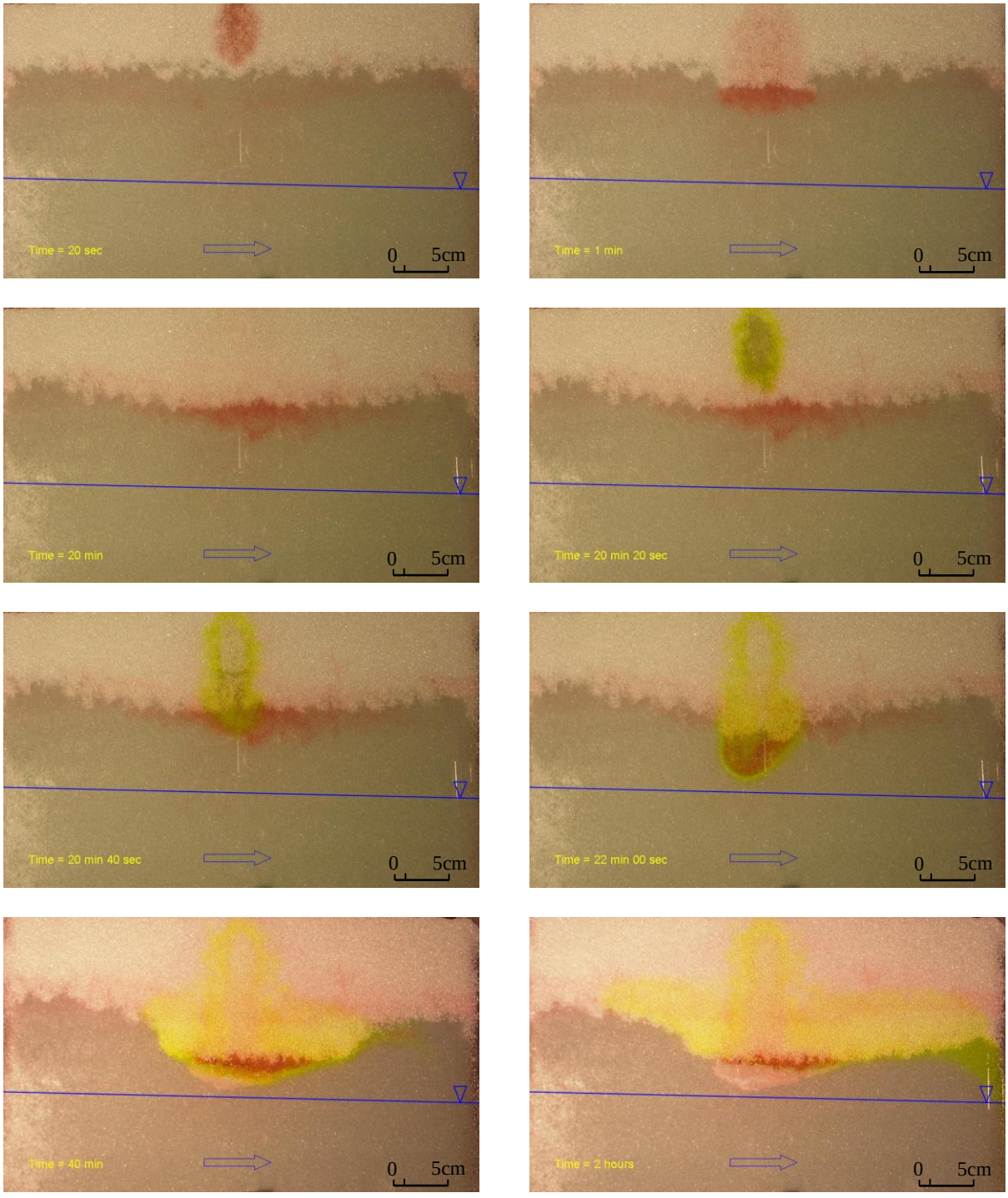

Figure 4.11: Gasoline and ethanol distribution after injections in the unsaturated zone during test 4. The blue line represents the position of the water level, water flows from left to right

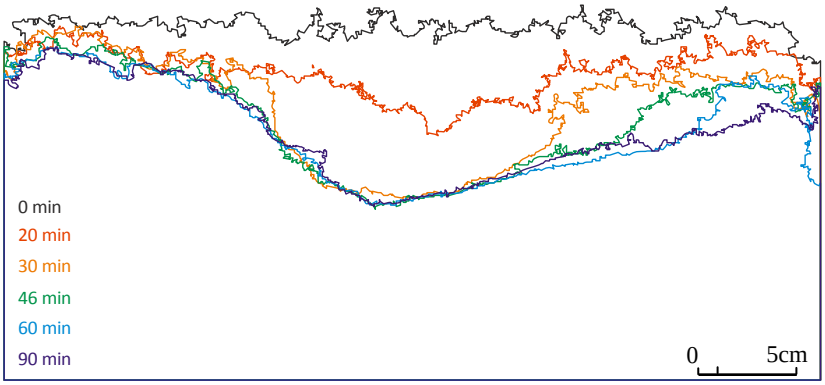

Figure 4.12: Capillary fringe evolution with time. Gasoline reached the top of the capillary fringe at 25 seconds and ethanol at 20 minutes and 25 seconds.

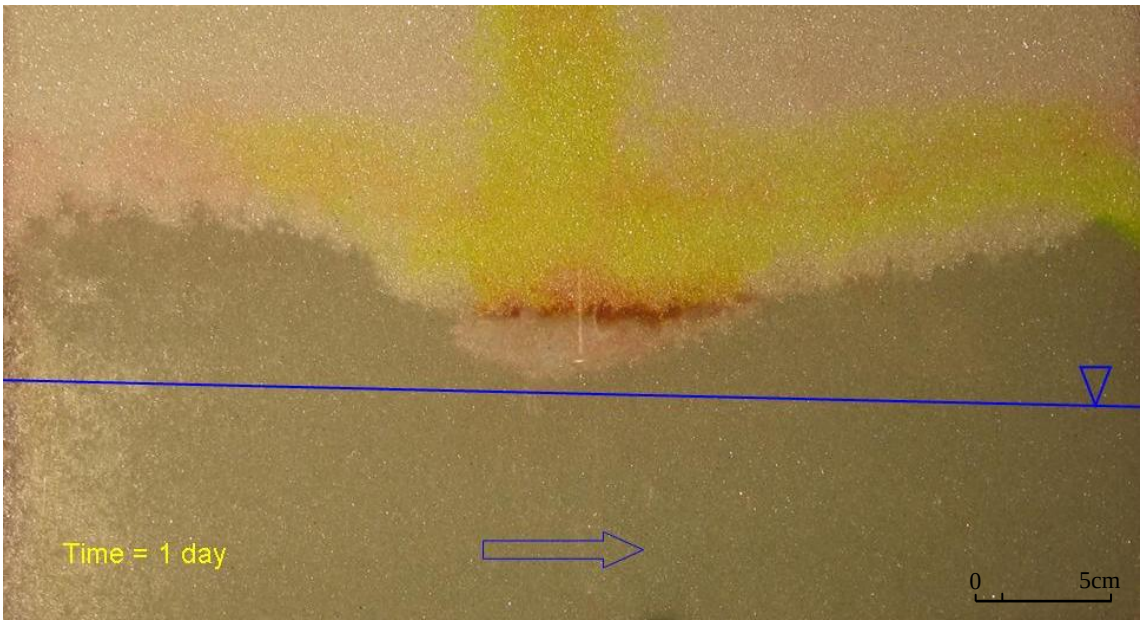

Figure 4.13: Contaminant distribution one day after injections.

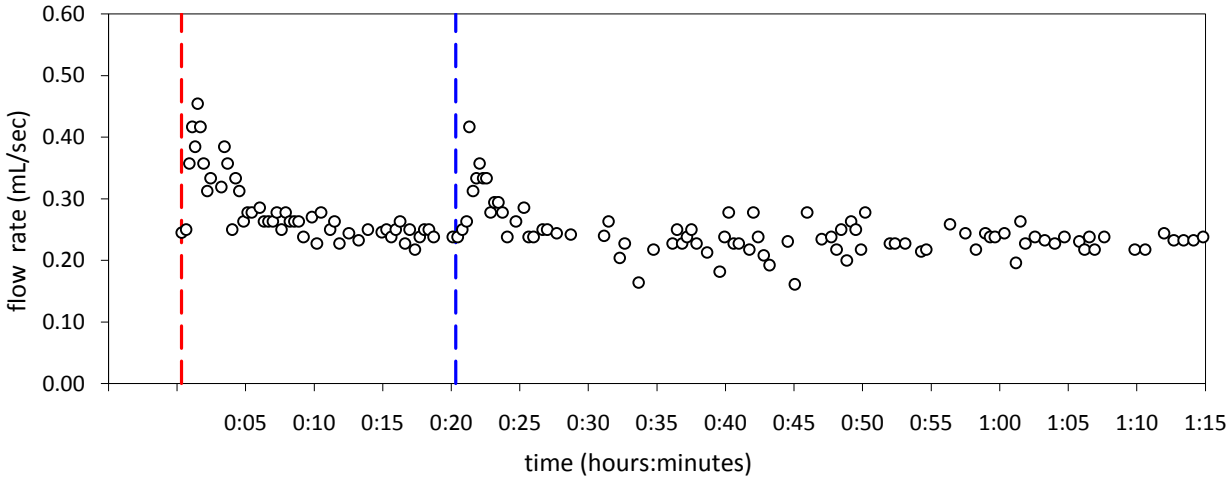

Figure 4.14: Flow rate versus time during test 4. Dashed red line indicates the time of gasoline injection and dashed blue line the time of ethanol injection.

Table 4.1 - Conditions of the tests performed

	Hoses used for drainage	Ethanol and gasoline injection volume (mL)	Injection rate (mL/min)
Test 1	2	50	35
Test 2	1, 2 and 3	50	50
Test 3	1, 2 and 3	25	35
Test 4	-	15	30

Table 4.2: Comparison of measured and calculated depression of the capillary fringe

	V_i (mL)	V_d (mL)	calculated h_d (cm)	measured h_d (cm)
Gasoline spill				
test 1	50	188	3.0	3.0
test 2	50	196	3.2	4.0
test 3	25	175	3.3	3.5
Ethanol spill				
test 1	50	147	2.1	2.5
test 2	50	119	1.5	2.0
test 3	25	125	2.2	2.0

Chapter 5
Sampling VOCs With Porous Suction Samplers in the Presence of Ethanol: How Much Are We Losing?

5.1 Introduction

Sampling volatile organic compounds (VOCs) in water from the capillary fringe and unsaturated zone may be of great interest when dealing with contaminations by LNAPLs (light non aqueous phase liquids), such as gasoline and hydrocarbon solvents. While sampling of VOC's below the water table presents challenges due to the potential losses that may be caused by the sampling techniques (Parker 1994), the difficulties increase when samples are to be withdrawn from the vadose zone, where a negative gauge pressure must be applied to overcome the tension that holds the pore-liquids.

Wilson et al. (1995) presented a general overview of the techniques to sample the unsaturated zone. According to this work, there are two ways to get water samples from the vadose zone: 1) using direct water sampling methods, using porous suction samplers, or 2) through indirect methods such as collecting soil cores and extracting pore-water. Porous suction samplers have been widely used and allow for the collection of repetitive samples and so are considered in this paper. General information about porous suction samplers and their operation can be found in the review papers by Grossmann et al. (1991), Everett et al. (1985), and Wilson et al. (1995).

Different designs of and materials for porous suction samplers have been discussed in the literature (Everett et al. 1988; Grossmann et al. 1991; Silkworth et al. 1981; Smith et al. 1992). Factors that may interfere with the representativeness of samples were identified and include: degassing (Grossmann et al. 1991; Suarez 1986), sorption (Grossmann et al. 1991; Silkworth et al. 1981), filtration of colloids (Grossmann et al. 1991) and biodegradation (Grossmann et al. 1991; Lewis et al. 1992).

The main concern associated with the use of suction samplers for VOCs sample collection is degassing since, to create flow from the porous medium into the sampler through the sampler porous wall, a lower pressure than the unsaturated zone pressure must be applied (Smith et al. 1992). Smith et al. (1992) compared the results of four different techniques to obtain samples of water contaminated with trichloroethylene (TCE), and concluded that the method using a syringe was better than the others tested based on precision, accuracy and ease of use. Everett et al. (1988) evaluated the loss of organic compounds using ceramic cup samplers with a PVC body versus all-PTFE porous

cups. Tests were conducted on API (American Petroleum Institute) separator sludge, containing 30 to 36% aromatics. In the PTFE suction samplers VOCs were almost totally lost, which was attributed to the need to reestablish vacuum in the suction samplers. No trend was identified between the increase in the pressure applied during sampling and loss of VOCs. Broholm et al. (2002) evaluated the loss of methyl-cyclopentane and naphthalene using seven pore-water suction samplers of different sizes and materials. They concluded that steel and ceramic samplers were better for the chemicals tested. For naphthalene the loss was around 40%. Jonge et al. (2003) compared results obtained using two different suction samplers (steel and PTFE/quartz), equilibrium calculations based on pore-gas measurements and soil extraction. The chemicals evaluated were benzene, MTBE, phenanthrene, TCE and gasoline (total hydrocarbons). Steel porous suction samplers were considered by the authors to provide consistent and accurate results.

When evaluating monitoring techniques for gasoline contaminated sites one should anticipate the presence of oxygenates, particularly ethanol, due to its increasing use worldwide. Previous studies (Cápiro et al. 2007; McDowell et al. 2003) showed that ethanol accumulation and migration are likely to happen mainly in the capillary fringe, thus the importance of considering its impact on capillary fringe and vadose zone monitoring techniques. Cosolvency of hydrocarbons in the presence of ethanol (Corseuil et al. 2004; Heermann et al. 1998; Morris et al. 1988) may result in high concentrations of dissolved hydrocarbons accompanying high ethanol concentrations in the capillary fringe. Because of its cosolvent effect and high vapor pressure compared to water, the presence of ethanol can significantly alter the representativeness of groundwater samples.

The objectives of this work are (1) to evaluate the loss of VOCs when ceramic porous-cup suction samplers are used in the presence of ethanol, and (2) to develop methods for estimating those losses a priori based on parameters that can be easily measured in the field.

5.2 Materials and Methods

A mixture of benzene, toluene, ethylbenzene, xylenes, naphthalene and trimethylbenzenes in methanol was spiked into deionized water in a 4 L glass amber bottle. The volume of methanol added was around 1 mL in 4 L of water (0.025%, v/v), so was not sufficient to interfere with the tests. The individual hydrocarbon concentrations in the spiked solution ranged from 1,400 to 1,600 mg/L, totaling around 15,000 mg/L. Four tests were made with similar hydrocarbons concentrations but different percentages of ethanol in the aqueous phase: 0%, 10%, 20% and 50% (by volume). The properties of the chemicals used are presented in Table 5.1. Two transparent Teflon® tubes, 3.18 mm (1/8") OD x 1.58 mm (1/16") ID and 1m long, were placed into the solution in the bottle to permit samples to be obtained. A round bottom, straight wall porous ceramic cup was connected to the end of one tube, the other tube was left open. The porous ceramic cups were from Soil Moisture®, 2.858 cm long, with an external diameter of 0.635 cm and an internal diameter of 0.160 cm. The ceramics used were high flow with 1 bar air entry pressure, maximum pore size of 2.5μm and saturated hydraulic conductivity of 8.6×10^{-6} cm/s (Soil Moisture 2006). Before the test, the porous cups were saturated with deionized water.

The same sampling procedure was applied to collect water samples from the tubing with and without the porous cup. The samples were obtained using a peristaltic pump and were collected in 22 mL glass vials positioned before the pump head, to minimize losses due to sorption to the flexible tubing in the pump head and to avoid exposure of the sample to the atmosphere and consequent losses due to volatilization (Einarson 2001). Similar setups were described elsewhere (Suarez 1986; Smith et al. 1992; Jonge et al. 2003; Broholm et al. 2002; Kohne 2005; Wessel-Bothe et al. 2000). The samples were collected in glass vials fitted with Teflon®-lined septa and preserved with 0.4 mL, 10% sodium azide. A volume of 20 mL was purged before the collection of each sample. Different nominal pumping rates were tested, with flow rates of 0.7 mL/s (low flow) and 4.4 mL/s (high flow), measured while pumping distilled water.

In each test 4 groups of 5 samples were collected, in the following order: 1) from the tubing without the porous cup, using low flow; 2) from the tubing with the porous cup, using low flow; 3) from the tubing with the porous cup, using high flow; 4) repeat of the first group (5 samples from the tubing without the porous cup, using low flow) in case decline in concentrations in the sampled solution during the experiment could be caused by the increasing headspace volume in the bottle as samples were collected.

Although the materials and procedures adopted for sampling were chosen to minimize losses, it is expected that negative bias could occur due to sorption to Teflon® tubing and volatilization. To evaluate this, additional water samples were collected by carefully pouring water from the bottle to the sampling vials. These results are considered to be representative of the actual concentration in the test solution and were compared to the results obtained from the samples collected from the tubing alone to establish the losses due to sorption onto the Teflon® tubing and volatilization caused by the use of the peristaltic pump.

The results of the samples collected from the tubing with the porous cup were compared to the results obtained from the samples collected with the tubing alone. Since the samples were collected using the same procedure, this comparison provided information about the bias due only as a consequence of the use of the porous suction samplers.

At the end of the tests with 0% and 10% ethanol, the porous cup was transferred to a vial with deionized water and five water samples were collected sequentially, using the same sampling procedure described previously, to determine possible biases caused by retention of chemicals onto the ceramic cup. This part of the test was done in approximately one hour with the purging volume decreased to 5 mL, in order to allow the collection of more samples but still being enough to purge twice the tubing volume.

The analysis for monoaromatics and ethanol were performed at the Organic Chemistry Laboratory, Department of Earth and Environmental Sciences, University of Waterloo. For ethanol analysis a 2 mL aliquot of the aqueous solution was transferred to an auto-sampler vial and placed on a 7673A HP Autosampler Gas Chromatograph (GC) for chromatographic analysis. The GC was equipped with a flame ionization detector and a 3 m length by 0.318 cm inner diameter column packed with 3% SPI500 on Carbopack B (80/100 mesh). The detection limit for ethanol was 0.05 mg/L. The analyses for monoaromatics were performed by solvent extraction followed by gas chromatography. The Teflon® sealed screw cap of the vial was quickly removed and 5.0 mL of sample was discarded with a glass/stainless syringe. This was followed immediately by the addition of 1.0 mL of methylene chloride containing internal standards m-fluorotoluene and fluorobiphenyl (25 mg/L).The vial was quickly resealed and agitated on its side at 350 rpm on a platform shaker for 20 min. After shaking, the vial was inverted and the phases were allowed to separate for 30 minutes. Approximately 0.7 mL of the methylene chloride phase was removed from the inverted vial with a gas tight glass syringe, through the Teflon septum. The solvent was placed in a Teflon® sealed autosampler vial for injection

into the gas chromatograph. Samples were analyzed with a HP 5890 capillary gas chromatograph, a HP7673A autosampler, and a flame ionization detector. Three microliters of methylene chloride was injected in splitless mode onto a 0.25 mm x 30 m length, DB5 capillary column with a stationary phase film thickness of 0.25 μm. Data integration was completed with a HP 3396A integrator. Calibrations were made in internal standard mode and standards were run in triplicate at five (or more) different concentrations, covering the expected sample range. Standards were prepared by spiking water with concentrated methanolic stock standards (purchased and certified from Ultra Scientific Analytical Solutions). Standards were extracted and analyzed in the same way as samples. Extraction duplicates were performed on samples and results were acceptable when they agreed within 10%. The method detection limits for the monoaromatics tested were below 2.2 μg/L. The relative standard deviation was below 5% for all chemicals in the range of concentrations tested.

5.3 Results and Data Analysis

5.3.1 Measured Losses

The loss of chemicals due to the sampling procedure using Teflon® tubing and the peristaltic pump was evaluated by comparing the results of the samples collected by carefully pouring the test solution from the bottle into the sample vial with the results from the samples obtained by pumping the water from the tubing alone. Losses were below 5%. The maximum loss measured was for 1,3,5-trimethylbenzene: 4.3% ± 2.3%. Higher losses were found for the more hydrophobic compounds (higher octanol-water partition constant, K_{ow}). This indicates that the losses were probably caused by sorption to the sampling tube. The biases are low if compared to the bias caused by the use of the porous suction samplers (discussed later).

The loss of VOC's due to the use of the porous suction samplers was calculated as follows:

$$measured\ loss = \frac{c_{iq} - c'_{iq}}{c_{iq}} = 1 - \frac{c'_{iq}}{c_{iq}} \quad (1)$$

where:

c_{iq}: Concentration of chemical *i* in the aqueous phase measured by sampling with tubing alone [M/V];

c'_{iq}: Concentration of chemical *i* in the aqueous phase measured by sampling with tubing and the porous cup [M/V].

The losses are presented in Figure 5.1. Ethanol losses were not significant, ranging from 0 to 0.9% (not shown). Of all hydrocarbons tested, naphthalene had the smallest measured loss resulting from the use of the porous cup. This is an indication that volatilization is the main process causing the sample bias, since naphthalene is the least volatile compound tested, and therefore less susceptible to significant losses due to partition to the vapor phase. In general this trend was observed for all compounds for the same ethanol volume fraction and flow rate.

When ethanol was not present, the losses were smaller for the low flow rate, likely a consequence of lower suction pressure resulting in less volatilization. Surprisingly, in the presence of ethanol the opposite trend was found for all compounds tested.

For all chemicals, highest losses were found at intermediate ethanol volume fractions. This is a consequence of two different and opposing phenomena. First, as the ethanol concentration increases, the headspace in the tubing increases leading to higher losses by volatilization. On the other hand, as the ethanol concentration increases, the aqueous activity coefficient of hydrocarbons decreases and the hydrocarbons tend to partition more to the aqueous phase. These are discussed below.

5.3.2 Loss Prediction Models

Two main processes are likely to interfere with the accuracy of the results when using porous suction samplers: 1) sorption and 2) volatilization. Sorption of metals and inorganic ions to the ceramic material has been reported (Grossmann et al. 1991; Rais et al. 2006; Silkworth et al. 1981). Sorption of organic chemicals has been studied by Perrin-Ganier et al. (1993), Wessel-Bothe (2000) and Patterson et al. (2000). Perrin-Ganier et al. (1993) concluded that pesticides could be retained by the ceramic material by sorption, but the reactions were found to be limited to the beginning of the sampling. Wessel-Bothe et al. (2000) also evaluated sorption of pesticides to the ceramic and a correlation between retention of the pesticides and hydrophobicity (as log K_{ow}) was described. Finally, Patterson et al. (2000) concluded that naphthalene did not sorb significantly to the ceramic material. Based on that, sorption was not included in the models developed here to estimate the losses but, in the last section, the retention of the organic compounds to the ceramic cups is discussed.

Pankow (1986) discussed the effects of bubbles and headspace in the collection of water contaminated with VOCs based on partitioning of analytes between air and water. However, previous studies were unable to establish a correlation between the volume of bubbles and the loss of VOC's (Barker and Dickhout 1988), as anticipated by Pankow (1986).

During each sampling, the length of the bubbles inside the tubing (L_g) and the length of the continuous aqueous phase (L_q) were measured (Figure 5.2). At least 3 pairs of bubble and aqueous segments were measured in each case. A volume fraction of bubbles (b) was calculated as:

$$b = \frac{V_g}{V_t} = \frac{V_g}{V_q + V_g} = \frac{L_g}{L_q + L_g} \tag{2}$$

$$\frac{L_g}{L_q} = \frac{b}{1 - b} \tag{3}$$

where:

V_g: Volume of the gas phase [V];

V_q: Volume of the aqueous phase [V];

V_t: Total volume [V].

An increase in the volume fraction of bubbles inside the tubing was observed as the ethanol volume fraction in the test solution increased. This was expected since ethanol has a higher vapor pressure than water. At 20°C, water vapor pressure is 2.34 kPa (Lide 2008) while ethanol vapor pressure is 5.86 kPa (Linstron et al. 2005). The vapor pressure of the water-ethanol mixtures tested was estimated using the equation derived in Strey et al. (1999), which takes into consideration the system deviation from ideality. The values obtained are 3.06, 3.64 and 4.77 kPa for 10%, 20% and 50% ethanol, respectively, representing an increase of more than 100% in the solution vapor pressure for 50% ethanol. Pankow (1986) identified that the condition for bubble formation due to sample depressurization is that the sum of the vapor pressures of all constituents is greater than the hydrostatic pressure. The presence of dissolved gases in the sampling solution was not determined, so a quantitative assessment of the pressure required for bubble formation as suggested in Pankow (1986) was not done. No bubbles were observed during sampling from the tubing only.

The loss expected from equilibrium partitioning to the vapor phase present in the tubing was calculated following procedures developed by Pankow (1986).

$$c_{iq} \cdot V_q = c_{ig} \cdot V_g + c'_{iq} \cdot V_q \tag{4}$$

$$\frac{c'_{iq}}{c_{iq}} = \frac{1}{\frac{c_{ig}}{c'_{iq}} \cdot \frac{V_g}{V_q} + 1} = \frac{1}{\frac{c_{ig}}{c'_{iq}} \cdot \left(\frac{b}{1-b}\right) + 1} \tag{5}$$

$$calculated\ loss = 1 - \frac{1}{\frac{c_{ig}}{c'_{iq}} \cdot \left(\frac{b}{1-b}\right) + 1} \tag{6}$$

The concentration in the gas phase inside the tubing (c_{ig}) was calculated assuming equilibrium between phases. The partial pressure of a compound above a liquid solution or liquid mixture is given by Equation 7 (Schwarzenbach et al. 2003), and therefore the concentration in the gas phase can be obtained as presented in Equation 8.

$$p_i = \gamma_{il} \cdot x_{il} \cdot p^*_{iL} \quad (7)$$

$$c_{ig} = \frac{p_i \cdot MW}{R \cdot T} = \frac{\gamma_{il} \cdot x_{il} \cdot p^*_{iL} \cdot MW}{R \cdot T} \quad (8)$$

where: p_i: Equilibrium partial pressure of compound *i*;

γ_{il}: Activity coefficient of compound *i* in the solution or mixture;

x_{il}: Mole fraction of compound *i* in the solution or mixture;

p^*_{iL}: Vapor pressure of compound *i* (relative to the pure liquid compound);

MW: Molecular weight of compound *i*;

R: Gas constant [P V mol^{-1} T^{-1}];

T: Temperature [T].

Therefore, the calculated loss (Equation 6) is dependent on the value of the activity coefficient, which adds complexity to the application of the equilibrium equation, particularly in the presence of an organic solvent such as ethanol. It is commonly assumed that the solution or mixture is ideal and therefore the activity coefficient is one (Raoult's law) or that the activity coefficient is constant (Henry's Law) as assumed in the equations developed by Pankow (1986). However, in the presence of ethanol the activity coefficients for hydrocarbons are neither one nor constant, as discussed by Harley et al. (2000). Therefore, for the tests without the presence of ethanol, Henry's law and tabulated values of Henry's law constant were applied, while for the tests in the presence of ethanol two different methodologies were applied to estimate the activity coefficient values, as discussed below.

5.3.2.1 No ethanol

Without ethanol a strong correlation between Henry's law constant and loss was noticed (Figure 5.3), with correlation coefficients of 0.96 for both the low flow and high flow conditions.

In this situation Henry's law was used to estimate the equilibrium partial pressure of compound *i* (p_i in Equation 9), which was converted to the concentration in the gas phase (c_{ig} in Equation 8) used to calculate the loss (Equation 6).

$$H_i = \frac{p_i}{c_{iq}} \quad (9)$$

The loss calculated using Henry's law matched the measured loss much better in the low flow rate than with the high flow rate experiments (Figure 5.4, Table 5.2). With the high flow rate the calculated losses were higher than measured. It appears that with the high flow rate equilibrium between the vapor and aqueous phase was not reached.

The good agreement between the measured and calculated losses indicates that, for the selected compounds under the conditions tested, the main mechanism responsible for the additional losses when using porous suction samplers was volatilization and not processes such as sorption to the ceramic material or filtration.

5.3.2.2 Ethanol present: Log-linear model estimate of activity coefficients

The log-linear model is one approach commonly used to quantify the effects of cosolvents such as ethanol on the aqueous concentrations of organic chemicals (Heermann et al. 1998; Poulsen et al. 1992; Schwarzenbach et al. 2003). The log-linear model is described by the following equations (Schwarzenbach et al. 2003), where f_v is the volume fraction of ethanol:

$$\log \gamma_{il}(f_v^1) = \log \gamma_{il}(f_v^2) - \sigma(f_v^1 - f_v^2) \tag{10}$$

$$\sigma = \frac{\log \gamma_{il}(f_v^2) - \log \gamma_{il}(f_v^1)}{f_v^1 - f_v^2} = \frac{\log \gamma_{il}^w - \log \gamma_{il}(f_v^1)}{f_v^1} \tag{11}$$

As described in Equation 11, for any given value of the cosolvency power (σ), the activity coefficient can be determined. Since the loss is calculated using the activity coefficient (Equations 6 and 8), the calculated loss is dependent on the cosolvency power. Applying Equations 6, 8 and 11, the value of the cosolvency power that minimized the difference between the measured and calculated losses was determined for each chemical. The values obtained (Table 5.3) are in agreement with values presented by other research (Corseuil et al. 2004; Morris et al. 1988), considering that the value is dependent on the range of cosolvent used in its determination.

The calculated versus measured loss using the fitted values of the cosolvency power are presented in Figure 5.5. It can be seen that the log-linear model predicted the losses reasonably well, with maximum difference between measured and calculated loss of 5.2% with a residual mean of 0.5%.

From Figure 5.5, it appears that the results for 50% ethanol deviate significantly, perhaps following a different line. This is a consequence of the fact that the log-linear model works better within smaller

ranges of volumetric fractions of the cosolvent (Schwarzenbach et al. 2003), while in this study a wider range was considered.

The log-linear model can also be applied in a predictive way, without fitting the data to obtain the cosolvency power. For example, one value that is commonly assumed to represent the cosolvency power for gasoline chemicals in the presence of ethanol is 2 (Molson et al. 2002), which is within the range of experimental values reported in the literature (Table 5.3). Applying the value of 2 for all compounds the agreement between measured and calculated loss is only slightly poorer (Table 5.4), the main difference being an increase in the maximum residual.

To compare the differences in the calculated losses using fitted values of the cosolvency power or using a fixed value of 2, a linear regression analysis of measured versus calculated losses was performed for both scenarios and the slope and standard error were calculated. The slopes obtained were 0.887±0.020 and 0.875±0.024, for the fitted cosolvency power and for the fixed value of 2, respectively. A t-Test analysis revealed that the slopes do not differ significantly (95% confidence) (Helsel and Hirsch 2002).

5.3.2.3 Linear / Log-linear Model estimate of activity coefficients

As discussed in Heermann et al. (1998), deviations from the log-linear model have been reported and a linear/log-linear model was identified as a more precise way of describing the cosolvent effects. The linear/log-linear model was applied in this study using equations 12 and 13 (Heermann et al. 1998) to obtain activity coefficients for each chemical, that were then used to calculate the loss (Equations 6 and 8).

$$\frac{1}{\gamma_{il}\bar{V}_m} = \left(1 - \frac{f_v}{\beta}\right)\frac{1}{\gamma_{il}^{w}\bar{V}_w} + \frac{f_v}{\beta}\frac{1}{\gamma_{i\beta}\bar{V}_\beta} \qquad ;f_v < \beta \qquad (12)$$

$$\ln\left(\frac{1}{\gamma_{il}\bar{V}_m}\right) = \left(1 - \frac{f_v - \beta}{1 - \beta}\right)\ln\left(\frac{1}{\gamma_{i\beta}\bar{V}_\beta}\right) + \left(\frac{f_v - \beta}{1 - \beta}\right)\ln\left(\frac{1}{\gamma_{ie}\bar{V}_e}\right) \qquad ; f_v \geq \beta \qquad (13)$$

The parameter β represents the volume fraction of ethanol where the model changes from linear to log-linear. In Equations 10 and 11 $\bar{V}$ is the molar volume [V/mol] and the subscript *e* indicates pure ethanol. The three parameters β, γ_β, and γ_e that minimized the difference between the measured and calculated losses were calculated for each chemical, following similar procedure as described

previously to obtain the cosolvency power in the log-linear model. The values obtained for β compare well with the values presented by Heermann et al. (1998) (Table 5.5). The comparison of measured versus calculated losses is presented in Figure 5.6.

The linear/log-linear model was capable of representing the losses throughout the range of volume fraction of ethanol tested with good precision. A comparison between log-linear and linear/log-linear results is presented on Table 5.6. Overall, the linear/log-linear model better predicted the losses, but only slightly. The linear regression analysis resulted in a slope of 0.953±0.038. The value is closer to one than the slope obtained with the log-linear model (Subsection 5.3.2.2), confirming that a better match was obtained. The slope was found to differ significantly from the slopes obtained with the log-linear model, with 95% confidence.

5.3.3 Bias Due to Retention of Chemicals by the Porous Cup

After sampling the water spiked with chemicals, the porous suction samplers were transferred to a vial with deionized water which was sampled sequentially via the porous cup and tubing. Initially the concentrations were around 6% of the concentrations to which they were exposed previously, that is, the value measured in the samples collected using the tubing only. The concentrations decreased rapidly as the volume of water pumped through the cup increased (Figure 5.7).

Different mechanisms can explain the apparent retention of analytes. First, the ceramic is a porous material, with porosity of around 45% (Soil Moisture 2006), resulting in a pore volume of 0.3 mL for one ceramic cup. During sampling in the spiked water this volume was filled with the test solution containing hydrocarbons and ethanol, so when the porous ceramic cup was moved to the deionized water, this water was retained within the cup. Second, chemicals might have been retained due to sorption to the ceramic material.

The mass of contaminants that could have been retained within the cup as defined in the first hypothesis was calculated by multiplying the pore volume of the porous cup (0.3 mL) by the concentrations in the spiked solution previously sampled with the porous cup. This mass was compared to the mass of chemicals removed in pumping distilled water (M_p), obtained by integrating the data in Figure 5.7 according to Equation 14.

$$M_p = \sum_{j=1}^{5} \left(c_j \cdot \left(V_p + V_v \right) \right) \tag{14}$$

where: j: sample number;

c_j: concentration in sample j;

V_p: volume purged before each sample (5 mL);

V_v: volume of the vial (22 mL).

It appears that the mass dissolved in the water inside the cup accounted for a maximum of 26% of the mass recovered in the sequential sampling of organic-free water. In general, for the more hydrophobic hydrocarbons (higher values of K_{ow}) the percentage of the mass that could have been attributed to the water inside the pores of the ceramic cup was smaller (Figure 5.8), implying that more mass of these chemicals was sorbed rather than simply retained, as would be expected (Schwarzenbach et al. 2003, Wessel-Bothe et al. 2000). Therefore, sorption was likely the more significant mechanism responsible for the retention of VOC's by the porous cup.

Also, ethanol concentrations decreased at a faster rate than all the other compounds (Figure 5.7). Considering that ethanol has less potential to sorb, this is another indication that sorption played a major role in the observed carry over.

Therefore, a sufficient volume of water must be purged before collecting the samples to minimize bias caused by the retention and later release of chemicals by the porous cup, especially in conditions of decreasing pore water concentrations through time. However, for the porous cups tested, the concentrations decreased very fast, with approximately 70% of the total hydrocarbon mass being removed with 27 mL of purging. For ethanol, 95% was removed in 27 mL. It is expected that for porous cups with larger dimensions the purge volume should be greater to minimize the bias associated with the retention of chemicals. Similar results were described by Perrin-Ganier et al. (1993) in tests performed with a solution containing pesticides and ceramic cups with bigger size (6.3 cm diameter and 9 cm long). In that study it was concluded that the first 20-50 mL of the sampled solution should be discarded in order to obtain representative samples.

Therefore, although organic compounds are retained by the ceramic material, this effect can be overcome by purging a small volume before the sample collection. The good agreement obtained previously between the measured losses and calculated losses using models that consider only volatilization also indicates that sorption has a minor influence on the samples accuracy when purging is performed.

5.4 Conclusions

The use of porous ceramic suction samplers for sampling volatile organic chemicals can cause considerable negative bias in groundwater samples due to volatilization to the gas phase formed in the sampling tubing as a consequence of depressurization. Up to 30% loss was measured for ethylbenzene, the most volatile (i.e., highest Henry's law constant) chemical tested. However, in the absence of a cosolvent in the aqueous phase, the loss can be easily estimated based on Henry's law and field observations of the ratio of gas to water in the sampling line.

The presence of a cosolvent such as ethanol has a significant impact, negative and positive, on the bias during sampling. With 10% ethanol a significant increase in the loss was noticed (maximum of 30% for ethylbenzene). On the other hand, with 50% ethanol the losses were minimized (maximum of 13% for benzene). Two different models to assess the cosolvent effect of ethanol on hydrocarbon analytes were evaluated. Both the log-linear model and the linear/log-linear model estimated the losses with good precision and accuracy. The log-linear model is easier to apply, but the quality of the results obtained was slightly inferior to the ones obtained with the linear/log-linear model.

Since chemicals can be retained by the porous cup, sufficient purging before sample collection is important. For porous cups tested here, purging 27 mL removes around 70% of the analytes retained in the porous cup.

In conclusion, it is likely that significant bias will occur when using porous suction samplers to obtain samples for volatile compounds analysis. The volume of bubbles in the sampling tube was found to have major impact on the magnitude of the measured losses, and therefore efforts should be made to minimize bubbles formation during sampling. In the event that bubble formation in the sampling tubing can't be avoided, it is possible to account for volatilization losses and correct the values based on partition models and simple field observations, even where ethanol is present.

5.5 Figures and Tables

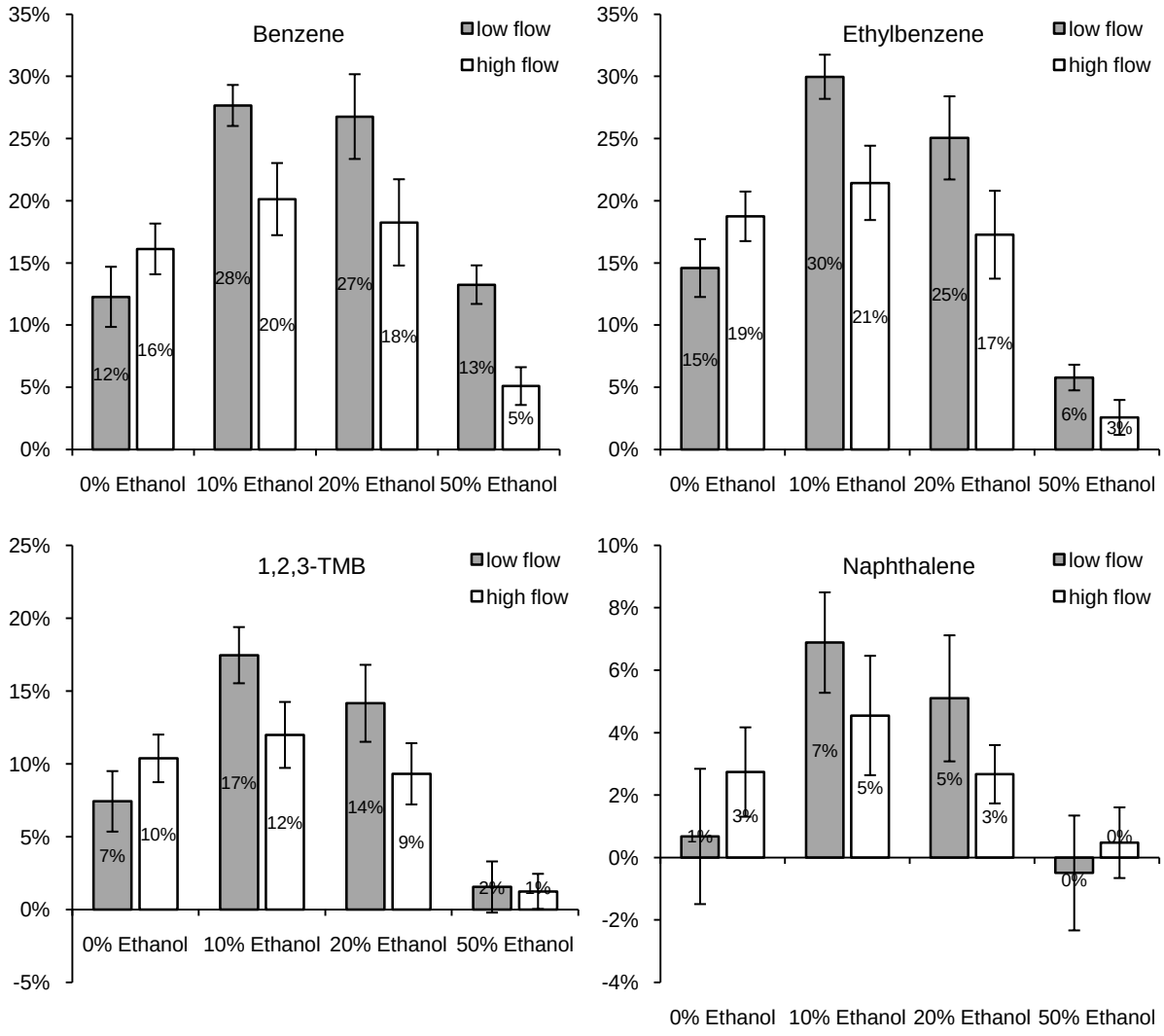

Figure 5.1: Measured losses using porous cups for four chemicals. Error bars size is 2 standard deviations, calculated from repetitive samples.

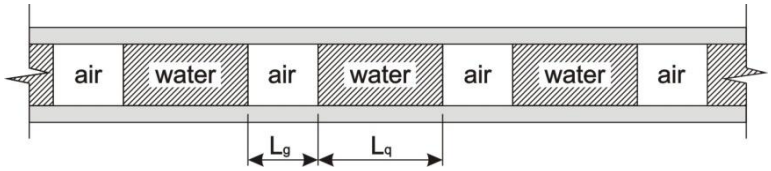

Figure 5.2: Bubbles distribution in sampling tubing

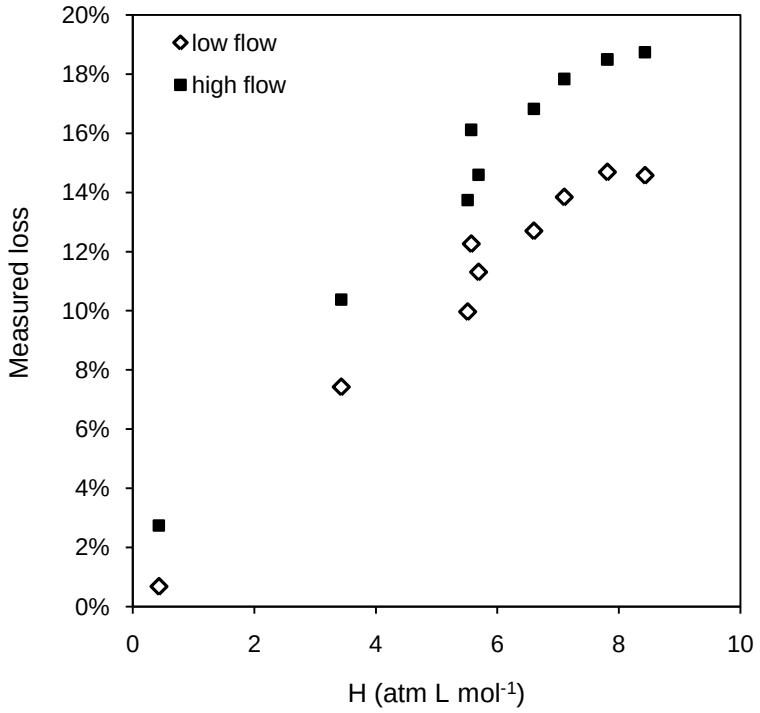

Figure 5.3: Measured loss versus Henry's law constant when ethanol was not present in the test solution.

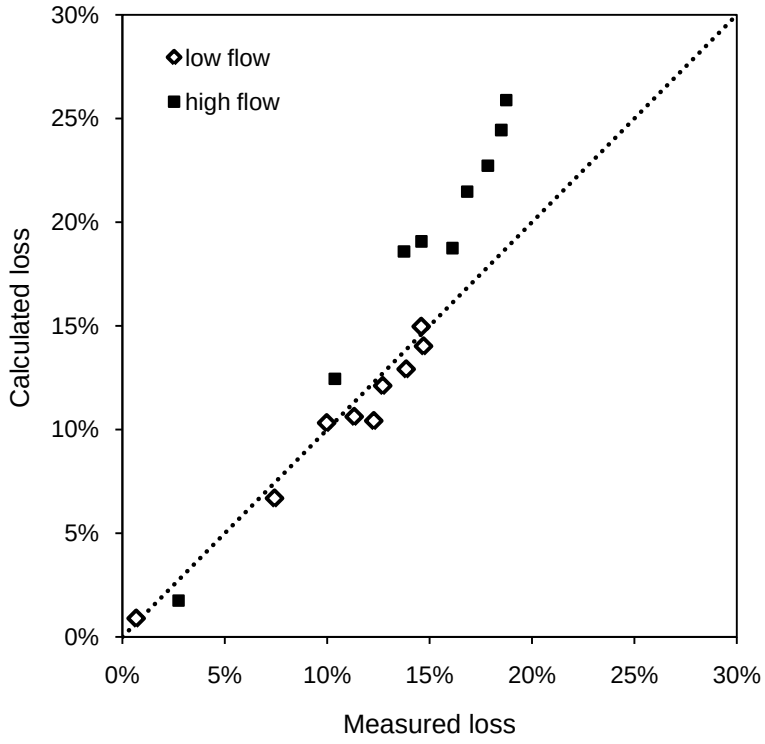

Figure 5.4: Measured versus calculated losses when ethanol was not present in test solution.

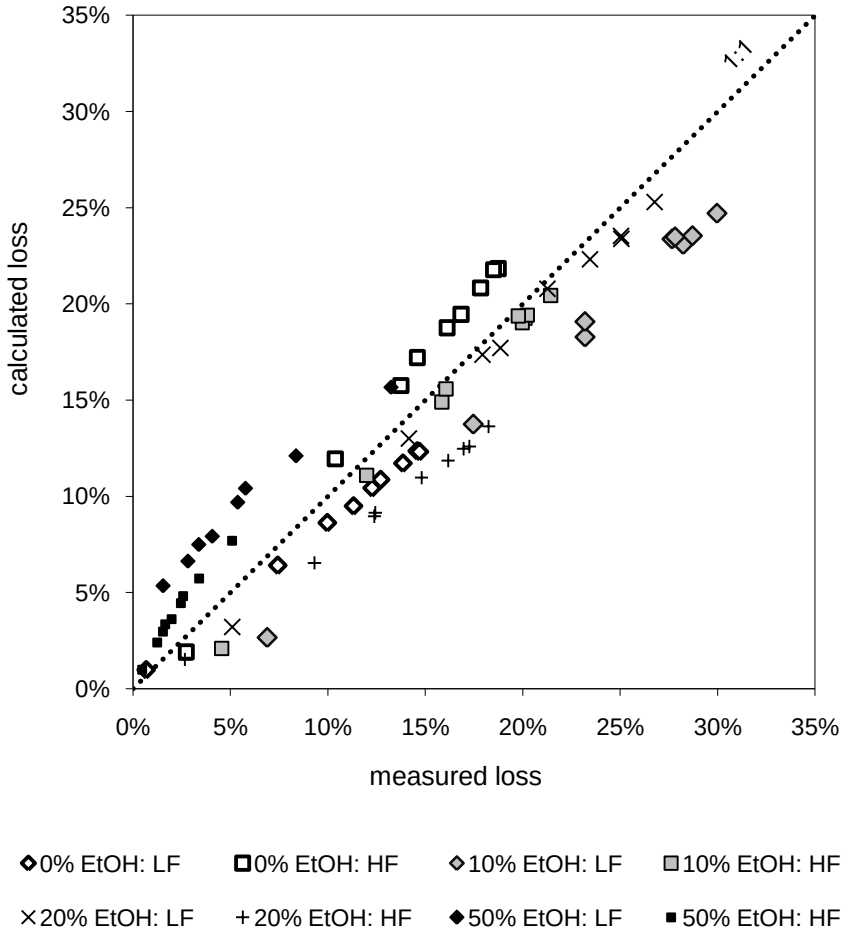

Figure 5.5: Log-linear model: Measured versus calculated losses for values of σ determined fitting the measured data. LF: low flow rate; HF: high flow rate.

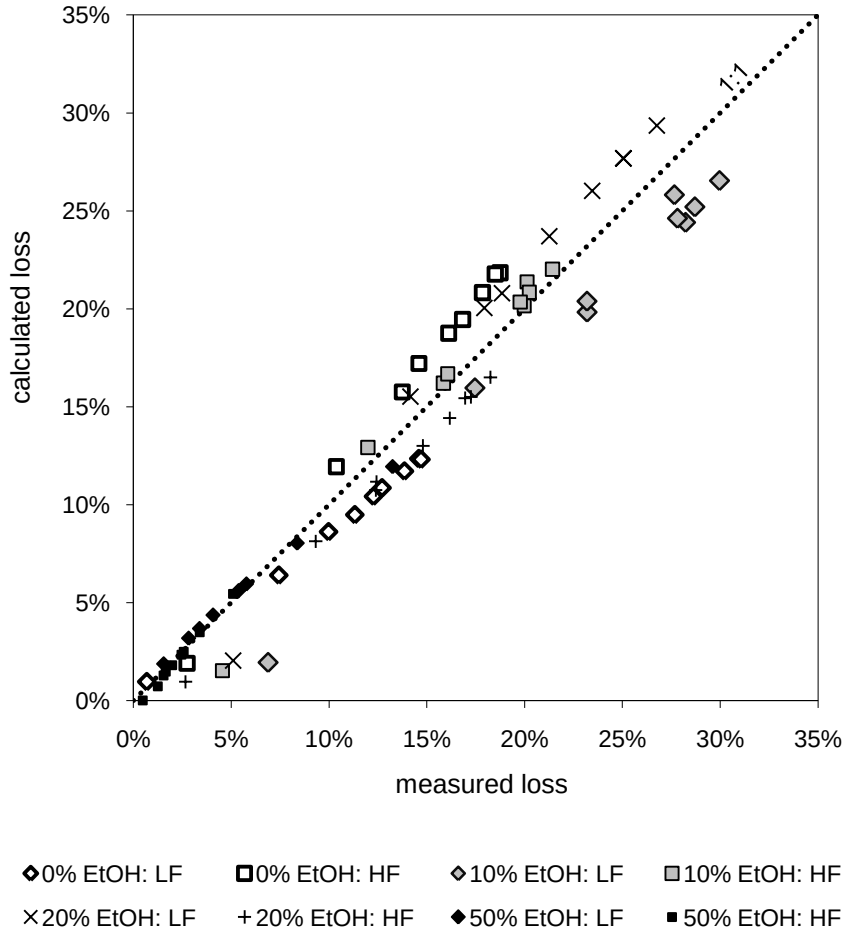

Figure 5.6: Linear/Log-linear model: Measured versus calculated losses.

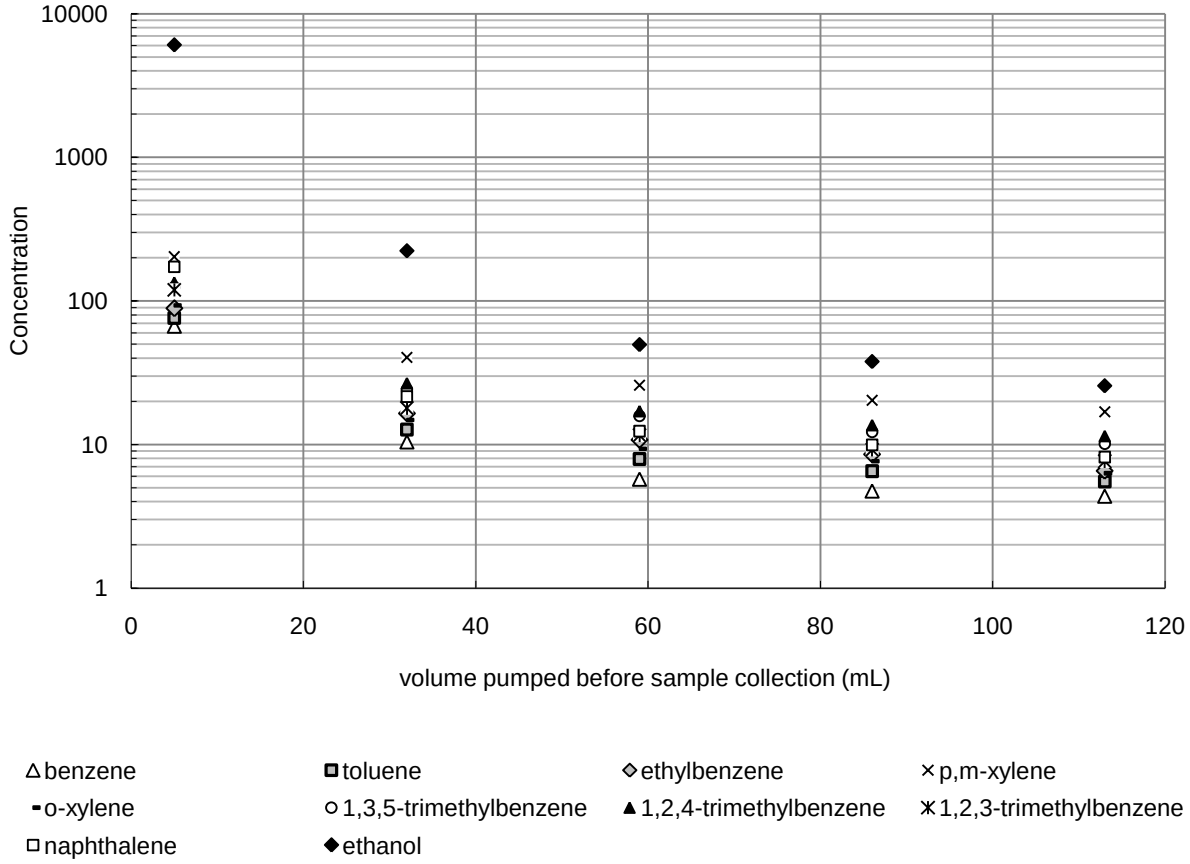

Figure 5.7: Measured concentrations when sampling deionized water. Ethanol volume fraction = 10%. Similar results were verified when ethanol was not present. Ethanol concentrations are in mg/L, aromatics concentrations are in µg/L.

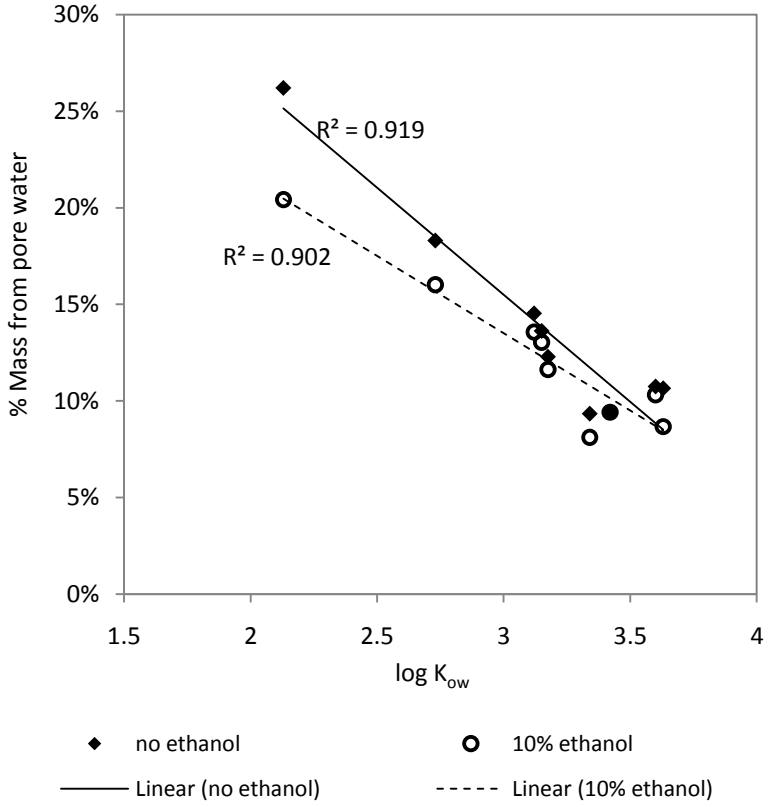

Figure 5.8: LogK_{ow} versus percentage of mass present in the water inside the pores.

Table 5.1: Physical properties of the chemicals tested

	H (atm L mol^{-1})	Solubility (kg/m^3)	log K_{ow}
benzene	5.57	1.78	2.13
toluene	6.60	0.531	2.73
ethylbenzene	8.43	0.161	3.15
p-xylene	6.90	0.181	3.15
m-xylene	7.30	0.161	3.20
o-xylene	5.51	0.171	3.12
1,3,5-trimethylbenzene	7.81	0.050	3.42
1,2,4-trimethylbenzene	5.69	0.057	3.63
1,2,3-trimethylbenzene	3.43	0.070	3.60
naphthalene	0.43	0.019	3.34
ethanol	0.0051	infinite	-0.30

Source: Lide (2008). H: Henry's Law Constant; K_{ow}: octanol-water partition coefficient.

Table 5.2: Correlation of measured with calculated loss obtained with low flow and high flow. Ethanol volume fraction = 0%.

	low flow	high flow
Num. of data points	9	9
Maximum residual [a]	1.8%	7.1%
Residual mean [b]	0.5%	-4.0%
Abs. residual mean [c]	0.7%	4.2%
Correlation coefficient	0.975	0.981

[a] $max|meas_i - calc_i|$

[b] $\frac{\sum_{i=1}^{n}(meas_i - calc_i)}{n}$

[c] $\frac{\sum_{i=1}^{n}|meas_i - calc_i|}{n}$

$meas_i$: measured loss for chemical *i*

$calc_i$: calculated loss for chemical *i*

Table 5.3: Comparison of cosolvency power values

chemical	**σ [a]**	**σ [b]**	**σ [c]**
benzene	1.56	0.65	2.05
toluene	1.82	1.27	-
ethylbenzene	2.05	-	-
p,m-xylene	2.06	-	-
o-xylene	1.97	1.66	-
1,3,5-trimethylbenzene	2.31	-	-
1,2,4-trimethylbenzene	2.19	-	-
1,2,3-trimethylbenzene	2.05	-	-
naphthalene	1.31	1.85	3.48

[a] this study (ethanol volume fraction ranging from 0 to 50%)
[b] Corseuil et al. 2004 (ethanol volume fraction ranging from 0 to 20%)
[c] Morris et al. 1988 (ethanol volume fraction ranging from 0 to 90%)

Table 5.4: Log-linear model: effect of cosolvency power on agreement between measured and calculated losses

	Fitted σ	σ = 2
Num. of Data Points	72	72
Max. Residual	5.2%	7.6%
Residual Mean	0.5%	0.7%
Abs. Residual Mean	2.5%	2.7%
Correlation Coefficient (R^2)	0.946	0.927

Table 5.5: Comparison of values for β

chemical	**β** [a]	**β** [b]
benzene	0.232	0.270
toluene	0.247	0.226
ethylbenzene	0.238	0.203
xylenes	0.236	0.204
1,3,5-trimethylbenzene	0.235	-
1,2,4-trimethylbenzene	0.234	-
1,2,3-trimethylbenzene	0.226	-
naphthalene	0.561	-

[a] from this study
[b] Heermann et al. 1998

Table 5.6: Comparison of agreement between measured and calculated losses for log-linear and linear/log-linear models

	Log-linear	Linear/log-linear
Num. of Data Points	72	72
Max. Residual	5.2%	4.6%
Residual Mean	0.5%	0.4%
Abs. Residual Mean	2.5%	1.6%
Correlation Coefficient (R^2)	0.946	0.975

Chapter 6
Ethanol Retention in the Unsaturated Zone and Implications to Oxygenated Gasoline Spills

6.1 Introduction

Oxygenates are typically added to gasoline aiming to improve urban air quality or decrease greenhouse gas emissions. Methyl *tert*-butyl ether (MTBE) was the most common additive in North America, but it is increasingly being replaced by ethanol, in around 10% (E10). Brazil has been using 20 to 25% ethanol as a gasoline additive for 30 years. Since fuels are a common source of groundwater contamination, one environmental concern associated with ethanol use is how it behaves in the subsurface and the potential impacts it might have on the fate of hydrocarbon contaminants from gasoline.

Ethanol is completely miscible with water, unlike the gasoline hydrocarbons, which have low solubility in water. When an E10 mixture contacts water, ethanol will partition between the aqueous and NAPL (non-aqueous phase liquid) phases, but it will prefer the aqueous phase (Powers et al. 2001; Oliveira 1997). Once dissolved, ethanol travels at the groundwater velocity, without being retarded by sorption (Zhang et al. 2006). Despite ethanol's high solubility and mobility, it is rarely found in high concentrations at gasohol impacted sites (Chapter 3; McDowell et al. 2003).

One of the main concerns associated with ethanol in groundwater is the impact on hydrocarbon biodegradation. Although ethanol can affect microbial activity by several mechanisms, one of the main impacts is the change in environment caused by its presence (Alvarez et al. 2002; Powers et al. 2001). Ethanol is very easily biodegraded and poses a high oxygen demand. In aquifers contaminated by ethanol the microorganisms will likely use most of the available oxygen and nutrients to degrade ethanol. This results in a depletion of both oxygen and nutrients, limiting hydrocarbon biodegradation. This effect has been shown in laboratory (Corseuil et al. 1998; Silva and Alvarez 2002; Lovanh et al. 2002) and field tests (Mackay et al. 2006). As ethanol travels through the groundwater at the front of the plume, it is expected to create a region of depleted electron acceptors and nutrients making the other gasoline compounds more persistent. As a direct consequence, benzene plumes, for example, are expected to be longer in the presence of ethanol (Deeb et al. 2002; Molson et al. 2002; Gomez et al. 2008).

However, the unsaturated zone and capillary fringe might play an important role in the fate of ethanol in the subsurface. In general, the capillary fringe is defined as the region above the water table where the pores are virtually saturated, but with negative gauge pressure (Berkowitz et al. 2004). The lower limit of the capillary fringe is consistently defined in the literature as the water table; however, different definitions of the upper limit of the capillary fringe have been proposed. A review is presented by Berkowitz et al. (2004). In this study, the common approach of defining the upper boundary based on water saturation of around 95% will be adopted. Visualization laboratory tests indicated that ethanol tends to accumulate on the top of the capillary fringe due to its low density (McDowell and Powers 2003; Capiro et al. 2007; Stafford et al. 2009; Chapter 4). Considering ethanol cosolvency properties, it is likely that high concentrations of hydrocarbons will be carried by ethanol-rich water. Horizontal velocities in the capillary fringe are expected to be similar to groundwater velocity immediately below the water table (Berg 2007), and horizontal transport in the capillary fringe has been shown in laboratory visualization tests (Ronen et al. 1997; Henry and Smith 2003; Berkowitz et al. 2004) and in one field test using bromide as a tracer (Abit et al. 2008). However, to date no study has evaluated the transport of organic compounds in the capillary fringe at field scale. Considering the ubiquity of sites contaminated by LNAPLs (light non-aqueous phase liquids) such as gasoline and diesel, which accumulate mainly on top of the capillary fringe and act as a constant source of dissolved contaminants, we believe that the importance of organic compounds transport in the capillary fringe has been under appreciated in the literature.

As the concentration of ethanol in the aqueous phase increases, both the surface tension between air and water and the interfacial tension between the aqueous phase and the NAPL decreases (Oliveira 1997; McDowell and Powers 2003). Some of the consequences of this decrease in surface tension include depression of the capillary fringe and induced flow by capillary pressure gradients (Jawitz et al. 1998; Smith and Gillham 1999; Henry and Smith 2003). The decrease in interfacial tension can decrease NAPL entrapment, increase NAPL saturation and make it more mobile (Oliveira 1997; McDowell and Powers 2003).

Besides the issues of transport in the capillary fringe and change in NAPL distribution, McDowell and Powers (2003) identified that the unsaturated zone above the capillary fringe will also impact the fate of ethanol. In one and two-dimensional experiments simulating E10 spills, they noticed that some of the ethanol partitioned out of the NAPL and was retained in the unsaturated zone. It was

hypothesized that ethanol retention in the unsaturated zone with slow release to the saturated zone could decrease the impacts of ethanol on hydrocarbon biodegradation (McDowell and Powers 2003).

To evaluate the fate and transport of ethanol and gasoline compounds after an E10 spill, a controlled release of E10 was performed at field scale. This is the first controlled field study to evaluate the fate of ethanol in the vadose zone, including retention and downgradient transport in the capillary fringe. Also, we evaluate the consequences of the ethanol for the transport of hydrocarbons.

6.2 Methods

6.2.1 Site Description

The field test was conducted in a controlled test cell at the Canadian Forces Base Borden, located 80 km northwest of Toronto. The Borden aquifer is an unconfined sand aquifer of glaciofluvial origin, composed of well sorted, fine to medium grained sand (Mackay et al. 1986; MacFarlane 1980). Distinct bedding features were identified by Mackay et al. (1986), primarily horizontal and parallel, with some cross bedding and convoluted bedding. The hydraulic conductivity geometric average is 7.2×10^{-5} m/s (10ºC), but it can vary spatially within one order of magnitude (Sudicky 1986). The water saturation profile for Borden sand is shown on Figure 6.1.

The test cell, which was also used in other studies (Mocanu 2007; Molson et al. 2008), is isolated on the sides by 7 m deep sheet pilling, but allows natural flow along the axis of the cell (Figure 6.2). The site was covered with a roof to avoid direct recharge.

6.2.2 Release

The NAPL mixture released was 171 L of API 91-01 gasoline (Prince et al. 2007; Williams 2007), 20 L of ethanol (99.9% purity, from Commercial Alcohols Inc.) and 9 L of MTBE (99.8% purity, from Sigma Aldrich). This resulted in an E10 mixture, with 10% ethanol and 4.5% MTBE. To aid in the identification of NAPL presence in soil samples, the gasoline mixture was dyed with 0.1 g/L of Oil-Red-O. Some concern has been raised on how dyes can interfere with NAPL properties (Tuck et al. 2003). The surface tension of the gasoline mixture with and without dye was measured by the pendant drop method (VCA 2500, AST Products, Massachusetts) at the Porous Media Laboratory, in the Department of Chemical Engineering, at the University of Waterloo. The surface tension without and with the dye were 21.2±0.2 dynes/cm and 21.5±0.1 respectively, indicating that there is no significant change due to the dye.

The release was made into a trench with dimensions of 1.5 m wide x 0.8 m in the flow direction and 20 cm deep. The sides of the trench were supported by steel sheets and the trench sides and bottom were lined with a plastic sheet. On August 21, 2008 (Day 0), the ethanol and the premixed gasoline and MTBE were poured into the trench, mixed, the plastic layer removed and the gasoline infiltrated into the unsaturated zone. To minimize losses by volatilization, the trench was covered immediately with plywood. To verify the gasoline composition during the period of infiltration, 8 NAPL samples were collected from the trench, one from the initial mixture and the others at intervals

between 20 to 50 minutes. After 5 hours, when all the gasoline mixture infiltrated, the steel sides were removed and the trench was refilled with Borden sand.

6.2.3 Site Monitoring

To assess the contaminant behaviour, multilevel wells for groundwater sampling were installed in three rows perpendicular to groundwater flow (Figure 6.2). Each row was composed of 11 wells, each well containing 15 to 24 sampling ports (Figure 6.3), totaling 594 points. To allow the collection of water samples above the water table, ceramic porous cups were used to construct the multilevel wells. The vertical distance between the center of the sampling points ranges from 6 to 10 cm. The ceramic cups are round bottom, straight wall, 2.86 cm long, 0.64 cm external diameter, and 0.16 cm internal diameter. They are high flow ceramic with 1 bar air entry pressure, maximum pore size of 2.5 μm and saturated hydraulic conductivity of $8.6x10^{-6}$ cm/s (Soil Moisture 2006). The ceramic cups were connected to Teflon® tubes, 3.18 mm (1/8") OD x 1.58 mm (1/16") ID and arranged outside a 2.54 cm (1") PVC SCH80 pipe.

The wells were installed by direct-push with an XD-1 Envirocore rig. An EC-4 Envirocore casing (4.76 cm ID, 6.03 cm OD) was driven to the desired depth and after the well was positioned inside the casing, the casing was removed and the aquifer sand collapsed around the well. The wells were installed in May and June of 2007, more than one year before the release. During this period, the water table oscillated all the way up to the ground surface ensuring the sand collapse and a good contact between the ceramic cups and the aquifer sand.

Groundwater samples were obtained using a peristaltic pump to apply suction, positioning the vial between the well and the pump to minimize losses by sorption in the pump and exposure to the atmosphere. Samples were collected in 20 mL VOA vials and preserved with 0.25 mL of 10% solution of sodium azide. The volume of bubbles in the sampling lines was monitored, and when the volume of bubbles exceeded 10% the hydrocarbons concentrations were corrected as described in Freitas and Barker (2008).

Three wells located downgradient of the source (RA-W06, RA-W07 and RB-W07) were sampled frequently to evaluate the groundwater and capillary fringe water concentration evolution with time. Also, on 27, 77, 117, 154 and 188 days after the release all wells at Row A were sampled to provide a detailed cross section of the dissolved plumes. Samples were analyzed for BTEX (benzene, toluene, ethylbenzene, p,m-xylenes and o-xylenes), TMB's (trimethylbenzenes), naphthalene, ethanol, MTBE

and TBA (*tert*-butyl alcohol). Their properties are presented in Table 6.1. Occasionally, samples were also collected for determination of ethanol biodegradation products: acetate, butyrate and methane; and methane carbon isotope signature. Samples for biodegradation products were collected from ports where concentrations were expected to be highest, usually in proximity to where the core of the ethanol plume was previously detected. Five samples were selected for methane stable carbon isotope analysis, to allow the distinction of the source of methane between ethanol and gasoline biodegradation (Chapter 3).

To evaluate the contaminant distribution in the source zone, soil cores were collected close to the source zone 14, 47 and 77 days after the release (Figure 6.2). A 2.8 cm ID aluminum tube was hammered to the desired depth; the tube with the core inside was retrieved and the holes were backfilled with sand or bentonite. The tube wall was drilled every 3 cm and around 2 mL of soil was collected using a 5 mL syringe with the tip removed (Hewitt 1996; Schumacher and Minnich 2000). The soil samples were inserted into 20 mL pre-weighted VOA vials with 5 mL of solvent. For hydrocarbons analysis the solvent was methylene chloride and for ethanol, MTBE and TBA analysis the solvent was water with 0.05 mL of 10% solution of sodium azide.

A fourth core was obtained 341 days after the release for saturated hydraulic conductivity (K_s) measurements. A 1.5 m core was collected in a 5.08 cm (2") aluminum pipe. The tube was cut in 10 cm segments and the soil collected, dried and homogenized before each test. Falling head permeameter tests (Reynolds 2008) were conducted in triplicate.

For 300 days, the depth to the water table was monitored in 6 hour intervals using pressure transducers installed in four piezometers.

6.2.4 Analytical Procedures

Oxygenates, hydrocarbons and methane were analyzed at the Organic Chemistry Laboratory, Department of Earth and Environmental Sciences, University of Waterloo. For ethanol, MTBE and TBA analysis a 2 mL aliquot of the aqueous solution was transferred to an auto-sampler vial and placed on a 7673A HP Autosampler Gas Chromatograph (GC). For the soil samples, the vials with soil and water were shaken by hand for 20 minutes and allowed to settle for 30 minutes before transferring the water aliquot to the auto sampler vial. The GC was equipped with a flame ionization detector and a 3 m length by 0.318 cm inner diameter column packed with 3% SPI500 on Carbopack B (80/100 mesh). The detection limits for the three compounds was 0.1 mg/L.

For methane determination in the water samples, a 15 mL aliquot was drawn from the sample bottle into a 30 mL glass syringe followed by 15 mL of helium. The syringe was shaken and allowed to equilibrate for 2 hours. A 5 mL aliquot of the gas phase from the syringe was injected, via an automated gas sampling valve, into a Varian 3800 GC equipped with a Megabore GS-Q, 30 m long column, a flame ionization detector and a capillary injection port. The automated gas injection utilizes a 6 port gas sampling valve with a 2 mL sample loop, a vacuum pump, and a 16 port stream selector valve, to draw the sample from the syringe into the sample loop and on column. Data integration was completed with the Varian Star chromatography workstation software. The dissolved concentrations in the original water samples were determined using Henry's Law. Laboratory control samples and matrix spikes were prepared with known quantities of C1-C3 gases and method recoveries of the gases were measured daily. Recovery limits for quality assurance samples are 80-120%. Laboratory duplication on 10% of field samples (which were chosen randomly) was performed, and results were considered acceptable when they agreed within 15% of their average. The detection limit for methane was 0.3 μg/L.

Hydrocarbons (BTEX, TMB's and naphthalene) analyses were performed by solvent extraction with methylene chloride followed by gas chromatography as described in Freitas and Barker (2008). For the soil analysis, the vials with the soil samples and methylene chloride were shaken vigorously (350 rpm) for 18 hours and then settled for around 3 weeks. The samples were reweighted to ensure there was no mass loss during this period. For both water and soil samples, after extraction solvent was placed in a Teflon-sealed autosampler vial and injected into a HP 5890 capillary GC equipped with 0.25 mm × 30 m length DB5 capillary column with a stationary phase film thickness of 0.25 μm, a HP7673A autosampler, and a flame ionization detector. The method detection limits for the monoaromatics tested were below 2.7 μg/L for water samples and 8.5 mg/kg for soil samples. The relative standard deviation of replicated standards was below 10% for all chemicals in the range of concentrations tested.

Groundwater analysis of acetate and butyrate was performed at the Institute for Groundwater Research at the University of Waterloo. A 2.0 mL sample was removed and added to a plastic 5 mL Dionex IC autosampler vial. The vial was then placed on a Dionex AS-40 autosampler, and a 25 μL sample was injected onto a Dionex ICS-2000 Ion Chromatograph equipped with an Ion-Eluent Generator, a Dionex IonPac AS18 column (4 x 250 mm) and a conductivity detector. The mobile phase was 30 mM KOH at a flow rate of 1.0 mL/min. The chromatograph was obtained on a Dell p4-

3GHz computer using Dionex Chromeleon 6.5 software. Analytical quality control involved method blanks which were carried through the entire analytical procedure, as well as water spiked with analytes from an independent source and the percent recoveries recorded. The two blanks and approximately eight spikes were analyzed along with samples. The detection limits were 1.0 mg/L for acetate and 1.3 mg/L for butyrate. The mean error of replicated standards was 8% and the relative standard deviation was below 25%.

Methane stable carbon isotope analyses were performed by the Environmental Isotope Laboratory of the University of Waterloo, following the method described on Chapter 3. Ratios are reported in the standard delta notation in reference to the VPDB (Vienna Peedee Belemnite) standard. The standard deviation was 0.5‰.

6.3 Results and Discussion

6.3.1 Potential for Ethanol Extraction from the E10 into the Pore Water

As gasoline with ethanol infiltrates in the unsaturated zone, it will contact the pore water retained in the soil by capillarity. Ethanol will tend to partition out of the gasoline into the water, in a liquid-liquid extraction process. When ethanol partitions from the gasoline into the groundwater, water drainage occurs, due to two factors. First, the volume of the aqueous phase, now composed of water and ethanol, will increase. Since the volume of aqueous phase that can be retained in the pore space is limited, the increase in volume alone results in drainage. Second, the increase in ethanol concentration in the aqueous phase results in a decrease in surface tension (McDowell et al. 2003), and consequent decrease in capillary pressure and water saturation (Leverett 1941; Kueper and Frind 1991; Smith and Gillham 1999).

To assess how much ethanol can be extracted from the gasoline into the unsaturated zone groundwater, a simplified mathematical model of the system was defined (Figure 6.4). It is one-dimensional (1-D), with E10 gasoline flowing downward. The water saturation profile was estimated assuming that the water saturation is a function of the capillary pressure between gasoline and water (Lenhard and Parker 1990), scaling the capillary pressure – saturation curve considering a decrease in surface tension from 72 dynes/cm (clean water surface tension) to 23 dynes/cm (water-gasoline interfacial tension), as presented in Figure 6.1. This profile was assumed to be constant in time, with the water table at the bottom of the column. This simplification does not consider a transient water saturation profile, as would be expected based on the dependence of the surface tension with ethanol concentration.

It was assumed that equilibrium between NAPL and aqueous phase is reached within each layer of height dz. An equation to estimate ethanol partitioning between the two phases was developed based on the ternary diagram presented in Oliveira (1997) (Appendix B). MTBE was also included in the model, considering that its partitioning to the aqueous phase follows Raoult's law. The cosolvent effect of ethanol on MTBE solubility was included using a log-linear model (Morris et al. 1988; Heermann and Powers 1998). MTBE solubility and cosolvency power were determined based on laboratory tests (Appendix C). Ethanol transport in the aqueous phase due to diffusion and surface tension gradient was not considered. Also, it was assumed that ethanol and water volumes are cumulative, while Oliveira (1997) showed some volume reduction when ethanol is added to water.

The solution scheme is presented in Appendix D, and the calculations were performed in a spreadsheet.

In the vertical direction, twenty layers of dz = 1.8 cm were used, totaling 36 cm, corresponding to the distance between the bottom of the trench and the water table when the E10 mixture was released at Borden. The source area was defined as 1.7 m^2, corresponding to the trench area plus 10 cm in each direction. The NAPL flux was set as 23.5 $L/m^2.h$ for 300 minutes and then decreased to zero. The flux was calculated from the time measured in the field to infiltrate the 200 L of E10. Porosity was defined as 0.33, representative of Borden sand (Mackay et al 1986). The calculations were done for a total time of 1500 minutes, to ensure steady state was reached.

Most of the ethanol (maximum ethanol concentration, 67%) remained in the top layers (Figure 6.5) over the 1500 minutes. Below 45 cm bgs ethanol concentrations were close to zero. Where ethanol concentrations were higher, MTBE was also found at higher concentrations, due to cosolvency (Figure 6.6). Unlike ethanol however, MTBE was present in all the profile with concentrations equal to and often greater than its effective solubility determined in the absence of ethanol. The volume of ethanol retained per layer at steady-state condition is shown in Figure 6.7. All the ethanol mass is in the aqueous phase, most of it above 40 cm bgs. Only 15% of the ethanol mass is below 40 cm, where the water saturation is higher and some horizontal transport would be anticipated (Figure 6.5). Only 7% of the MTBE is in the aqueous phase (Figure 6.7), the remaining 93% left the model domain (reached the depth of 55 cm) still in the NAPL. Of course, the MTBE retention in the unsaturated zone will be more significant in settings where the water table is deeper.

The results are consistent with the 1-dimensional column test performed by McDowell and Powers (2003). In 400 and 600 mL E10 releases into a 44 cm long column with water at residual saturation, at least 99% of the ethanol was retained in the unsaturated zone.

Although several simplifying assumptions were made, the model showed that the unsaturated zone has the potential to retain most of the ethanol mass released in this experiment above the capillary fringe. Non-equilibrium conditions could result in more ethanol being transported downwards towards the water table. Preferential flow through fractures, macropores or in high permeability zones could also result in more ethanol reaching the saturated zone.

6.3.2 Contaminant Distribution in the Source Zone

The resulting distribution of residual LNAPL in the field test was assessed by direct methods, such as coring, and also by the groundwater concentrations measured downgradient. Surface ground penetrating radar (GPR) was also used to assess the LNAPL infiltration and redistribution (McNaughton, in preparation).

6.3.2.1 Estimation of the source area

Around twenty four days after the E10 release there was a major precipitation event that resulted in a water table rise to around 22 cm bgs (Figure 6.8). In the presence of gasoline, the capillary fringe is expected to be around 15 cm thick, with the transition zone extending another 20 cm (Figure 6.1). Therefore, with the water table rise to 22 cm bgs the gasoline moved upwards close to the ground surface and a stain from the gasoline red dye was left on the ground. From one corner of the trench a finger of stain extended more than 0.5 m upgradient. This clearly shows that the contaminants distribution was not symmetrical; likely heterogeneities in the sand facilitated the NAPL movement in that particular direction. After that first event, the water table went back down to 60 cm bgs, and then in December, 2008 it moved up and stayed around 45 cm bgs. A stronger stain was noticed on the sides of the trench on December 03, possible caused by differences in packing when the trench was filled. In January, 2009, the water table rose slightly, reaching about 30 cm bgs. The dye pattern in the ground became stronger, following the water table oscillations. The evolving stain pattern in the ground is shown in Appendix E.

A good correlation between the lateral extent of gasoline occurrence in core (Subsection 6.3.2.2), surface stain transverse to groundwater flow and the lateral extent of the MTBE plume observed at Row A (Figure 6.9) indicates that the stain left on the ground represents the lateral source distribution. By inference, the longitudinal distribution of the source is taken to be represented by the distribution of the surface stain. Based on the surface stain the source area was estimated as 4.2 m^2. The GPR surveys indicate similar results, and also identified NAPL upgradient of the source where the stain was noticed (McNaughton, in preparation).

6.3.2.2 Ethanol, MTBE and hydrocarbon distribution based on soil cores

Three soil cores were collected in the source zone, around 20 cm outside the release trench walls (Figure 6.2). The number of cores and position were selected to minimize disturbance in the source. The first core was obtained 14 days after the release, while the water table was at 67 cm bgs. During

the period between the release and the first coring the water table had mainly moved downwards (Figure 6.8). Between the first and the second coring events (day 14 to day 47), the water table oscillated over a wide range, going from 70 to 20 cm bgs. The water table was at 53 cm bgs when the second core was collected. From the time of the second to the last coring (day 117) the water table continued oscillating, and was higher by the time of the third core (36 cm bgs).

The results for ethanol, MTBE and total hydrocarbons in the sand are presented in Figure 6.10. In the first core, the highest hydrocarbons concentrations were found around 32 to 41 cm bgs, about 26 cm above the water table, indicating a higher concentration of gasoline above the top of the depressed capillary fringe, as would be expected. In the second core, hydrocarbons were smeared from 12 to 30 cm bgs, a consequence of the water table oscillations before the coring. In the third core higher concentrations were measured at much shallower depths, from 12 to 2 cm bgs, indicating that the water table rise had mobilized the gasoline upwards. The range of highest hydrocarbon concentrations always started at around 24 cm above the water table, consistent with the estimated capillary fringe.

The MTBE concentrations in the soil cores always presented a vertical distribution similar to that of the hydrocarbons, with correlation factors as high as 0.9. On the other hand, ethanol appeared at higher concentrations where hydrocarbons were at lower concentration. The difference between ethanol and MTBE is likely a consequence of the higher affinity of ethanol for soil water. Although MTBE has a high solubility in comparison to gasoline hydrocarbons (Table 6.1), ethanol is completely miscible with water. So, as the gasoline moves in the unsaturated zone, both ethanol and MTBE partition to the pore water, but ethanol concentrations are expected to be much higher than MTBE concentrations. Consequently, most of the MTBE mass was still retained within the NAPL when the NAPL reached the capillary fringe. One NAPL sample was recovered from the site 21 days after the release, at 40 cm bgs, through a steel tube previously installed for vapor monitoring (Figure 6.9). The recovered sample was almost completely depleted of ethanol (only 0.02% compared to 10% in the initial E10) while it still contained 3% MTBE (4.4% in the initial mixture). This result is consistent with the estimate in Subsection 6.3.1, where most of the ethanol was retained above the capillary fringe and around 90% of the MTBE left the model in the NAPL.

Ethanol was found at higher concentrations in the soil at about the same depths in all soil cores (around 15 to 25 cm bgs). On the first two core dates, this range is clearly in the unsaturated zone, above the top of the capillary fringe. The depth where ethanol was found in higher concentration

corresponds to the depth of the trench (20 cm), indicating that most of the ethanol was retained close to where it was released. Ethanol presence at high concentrations at such high elevations outside the trench area suggests that ethanol moved laterally in the unsaturated zone. This behaviour has been observed in 2D lab tests (Chapter 4) and could have resulted from ethanol diffusion in the aqueous phase, volatilization or pressure gradients created by changes in surface tension (Henry and Smith, 2003).

The retention of ethanol at the same depth indicates that oscillations in the water table had minor impact on the ethanol distribution. Ethanol mobilization during water table oscillation could be minimized by ethanol's lower surface tension, lower density and higher viscosity. The lower surface tension can cause a lower saturation in the ethanol-rich zones in comparison to the adjacent zones. This can result in a lower hydraulic conductivity, which would direct groundwater flow around the rich ethanol zone. Also, solutions with high ethanol concentration would have lower density and higher viscosity. Although pure ethanol values of viscosity and density deviates only around 20% from pure water, solutions with intermediate fractions of ethanol have more than 2 times higher viscosity than water (Ageno and Frontali 1967; Belda et al. 2004). For ethanol fractions ranging from 30% to 60%, the changes in density and viscosity cause a decrease in hydraulic conductivity by around 65%.

Besides the changes in hydraulic conductivity, displacement of ethanol by water is subject of fingering due to the unequal viscosities and densities, which will cause a decrease in the mass of ethanol that is carried by the water (Dullien, 1979). Based on the viscosity and density differences between pure water and ethanol-water mixtures, downward displacement of ethanol by water will always be unstable while upward displacement might be stable, depending on the velocity of the displacement and on the ethanol fraction in the ethanol-water phase (Kueper and Frind, 1988).

The retention of ethanol in the unsaturated zone could also be facilitated by heterogeneities in the porous medium. Although fairly homogeneous, the Borden aquifer has horizontal bedding features, with the hydraulic conductivity varying within one order of magnitude (Mackay et al. 1986). In the unsaturated zone, a layer with smaller pore size, and consequent higher capillary pressure, would have higher water saturation, and therefore would be more likely to retain a higher fraction of the ethanol. The hydraulic conductivity measurements from the site (Figure 6.11) vary by a factor of 4. However there is no clear evidence of a significant contrast in hydraulic conductivity at the shallower depths, although thin or non-continuous lenses could have been missed.

6.3.2.3 Estimation of pore water concentrations, saturation and effective hydraulic conductivity

The soil concentration results were used to estimate pore water concentrations and NAPL saturations. Using the estimated saturation values (Figure 6.1) the wet soil concentrations were converted to dry soil concentrations (Appendix F.1). The mass of ethanol and MTBE present in the source was estimated based on the soil concentrations in the three cores. The source area was estimated in 4.2 m^2, based on the stain that was left on the ground. For each core, the mass in the source was estimated assuming that the source is completely homogeneous. The mass in the source was assumed to be an average of the results based on each core. While this estimation might not be accurate due to the limited number of cores and heterogeneities in the source, the difference between ethanol and MTBE is evident. The ethanol mass in the first 30 cm was estimated to be about twice as high as the mass of MTBE, while the inverse was observed from 30 to 58 cm bgs. Around 38% of the total ethanol was retained in the upper 30 cm and only 14% of the MTBE. None of the cores were collected in the area of the trench, where concentrations might be higher. Therefore, although we can't precisely define how much of the ethanol is still in the source, a significant portion is being retained in the unsaturated zone.

The presence of NAPL in the soil samples was assessed by two methods. The first method, from Feenstra et al. (1991), calculates the maximum concentration that could be present in the dissolved and sorbed phases for each sample for toluene, ethylbenzene and o-xylene (Appendix F.2). If the measured concentration is higher than the calculated value, then NAPL was likely present in the sample. For the samples where this method indicates NAPL presence, its saturation was calculated as described in Appendix F.3. It appears that the NAPL got smeared over time, likely due to the oscillations in the water table (Figure 6.12). In the last core, NAPL was also present below the water table at the time of coring. In general, the values are within the range expected for residual saturation in the unsaturated zone (3% to 7%; Parker et al. 1995) and saturated zone (12%; Oliveira 1997).

In the second method, the ratios of selected hydrocarbons in soil samples to the ratios in the released gasoline were calculated. The concentrations of organic compounds in the gasoline released were determined previously (Prince et al. 2007; Williams 2007), and so the initial ratios of each compound to the total hydrocarbons (BTEX + TMBs + Naphthalene) were calculated (termed expected ratio). Then, the same ratios were calculated for each soil sample (termed measured ratio). The results of the measured ratios over the expected ratios are presented in Figure 6.13 for the first

soil core. If NAPL is present in the sample it dominates the total mass of each hydrocarbon and so the measured ratio tends to be the same as the ratio in the initial gasoline, i.e., the values tend to one. Where NAPL is not present, the values deviate significantly from one, with the ratios for the compounds with higher effective solubility (like benzene and toluene) being higher than one, as they are present in higher concentrations in the dissolved phase. The results are consistent with the results obtained from the method described previously.

Ethanol pore water concentrations ($c_{e,q}$) were calculated assuming ethanol partitioning between NAPL and aqueous phases according to the ternary diagram shown in Appendix B (Appendix G). The ethanol concentration profiles in the first two soil cores were similar (Figure 6.14), with peak concentrations of around 8% occurring around 15 to 25 cm deep. The profile in the last soil core is significantly different, with the highest concentrations in the top 10 cm and reaching values around 14%. While the change in position of the maximum values can be easily attributed to the shallower water table when the core was collected, a two times increase in pore water concentration seems unlikely. The observed discrepancy could be a consequence of a heterogeneous source zone, as discussed previously.

The ethanol concentrations are lower than calculated by the simplified model described in Subsection 6.3.1. Several reasons can justify the relatively low ethanol concentrations measured in the soil. First, all the cores were collected outside the trench area (Figure 6.2). Also, lateral spreading of ethanol due to diffusion and surface tension gradients were not considered in the model and could cause a decrease in ethanol concentrations. Ethanol volatilization and biodegradation could also result in lower concentrations in the field. However, the concentration profiles do not suggest a significant mass loss over time, as would be expected if those processes were significant during the time period evaluated through soil cores (117 days). Microcosm tests using Borden aquifer material and groundwater, with excess oxygen and without nutrient addition, indicated no ethanol loss after 64 days when ethanol concentrations were 1.5% (Araujo 2000), suggesting that biodegradation would not have a great impact on ethanol concentrations in the source zone at early times. Volatilization is also not expected to be a significant process for ethanol mass loss due to its preferential partitioning to the aqueous phase, as is evidenced by its relatively low Henry constant (Table 6.1). Even though the magnitude of the concentrations measured in the field do not match the simple model values, the pattern of ethanol concentration with depth seems to agree with the model expectations.

Ethanol concentrations higher than 10%, as were estimated, are expected to increase the solubility of the gasoline hydrocarbons due to cosolvency effects. Hydrocarbon solubilities considering ethanol cosolvent effects (C_i^m) were calculated using the log-linear model (equation 1) and cosolvency power values (σ) from previous studies (Table 6.1). At the highest ethanol concentration (14%), benzene solubility increased from 1780 mg/L to 2890 mg/L (effective solubility going from 26.7 to 43.4 mg/L). More hydrophobic compounds have even greater relative increases; for example, o-xylene solubility increased from 205 to 391 mg/L (effective solubility going from 6.7 to 13 mg/L). The NAPL saturation was reassessed considering the new solubility values, but the changes were always less than 0.05%.

$$\log C_i^m = \log C_{i,dis}^{sol} + \sigma \cdot f^c \quad (1)$$

The effective hydraulic conductivity for the aqueous phase (K_q) is shown versus depth in Figure 6.15. To estimate the relative permeability (k_r) based on the water saturation, the combined van Genuchten-Mualem model (van Genuchten, 1980) was applied utilizing parameters from Mickle (2005) (Appendix F.4). To incorporate the effect of ethanol on the hydraulic conductivity, experimental data of density and viscosity as a function of ethanol concentration from Belda et al. (2004) was used to obtain a polynomial equation of the relative permeability (k_r) as a function of ethanol mass fraction (f_e) (equation 2). The relative permeability function reaches its minimum of 0.3 at around 40% ethanol, a decline to around 30% from the pure water.

$$k_r = 8 \cdot 10^{-8} \cdot f_e^4 - 2 \cdot 10^{-5} \cdot f_e^3 + 0.0015 \cdot f_e^2 - 0.0538 \cdot f_e + 0.9846 \quad (2)$$

It can be seen from Figure 6.14 and Figure 6.15 that the high ethanol concentrations were located in regions where the effective hydraulic conductivity was zero, caused mainly by the low aqueous saturation. Since the high ethanol concentrations were always located in regions with extremely reduced hydraulic conductivity due to the low water content, the additional reduction caused by the ethanol changes in viscosity and density were not significant. The presence of ethanol in regions where the hydraulic conductivity is essentially nil supports the inference that most of the ethanol is not being transported downgradient, and it is being retained in the unsaturated zone in the release region.

Ethanol mobility might increase when the water table rises and it could also be mobilized by recharge. Since the research site was under a roof, the effect of recharge on the source zone was not evaluated. This is not unrealistic as fuel stations and distribution terminals have recharge minimized

by the presence of roofs and pavement. Also, McDowell and Powers (2003) indicated that ethanol is not readily flushed by recharge; in a column test, several recharge events were necessary to mobilize ethanol retained in the unsaturated zone. The retention of ethanol even in the presence of recharge is likely a consequence of instabilities arising from the density difference between ethanol and water (Kueper and Frind, 1988). Soil core 3, which was collected when the water table was at a higher elevation, showed a high percentage of ethanol below 20 cm bgs (Figure 6.14), where the hydraulic conductivity starts to increase. It is possible for ethanol to be transported downgradient under these conditions. However, in this situation the low density and high viscosity due to ethanol's presence in the aqueous phase could still delay its transport. Also, if ethanol is in regions of lower hydraulic conductivity, a further delay in ethanol transport is possible.

The distribution of phases inferred from soil samples in the ternary diagram also reveals some information about the processes that took place in the unsaturated zone (Figure 6.16). The presence of some samples in regions with total ethanol fraction higher than 10% cannot be explained by simple dilution with water. If an E10 gasoline mixture was being mixed with water, the system composition would follow the dashed line shown on Figure 6.16. The presence of samples above this line indicates that after the gasoline mixture contacted water and two phases were formed (aqueous and oleic), the two phases were transported differently in the subsurface, resulting in system compositions that are different than what would be expected based solely on mixing with water. This is consistent with our conceptual model that the aqueous phase with high ethanol was retained in the unsaturated zone while the gasoline phase continued travelling downwards. The results from the model presented at Subsection 6.3.1 are also plotted on Figure 6.16, for 300 min, a time corresponding to the end of injection. The model results also don't match the field data, first because the modeled line in the figure shows the composition after 300 min, just when the gasoline infiltration stopped, while the cores were taken much later. This likely results in the modeled fraction of gasoline to be higher than what was found in the later cores. Also, the model does not consider gasoline retention in the unsaturated zone, which may contribute to the poor match. Even though the model results don't match the field data, the model supports the interpretation that overall ethanol fractions higher than 10% are produced when ethanol is retained in the unsaturated zone while the oleic phase migrates downward.

6.3.3 Downgradient Transport

6.3.3.1 Early behaviour: Low ethanol concentrations

The consequences of ethanol retention in the unsaturated zone to the downgradient transport were evaluated by examining groundwater concentrations in multilevel wells. Two wells at Row-A, 6 and 7 and one well at Row-B, 7, were monitored for 117 days in intervals of 2 to 7 days. The breakthrough curves for MTBE and ethanol at well RA-W07 are presented in Figure 6.17. The breakthrough curves at the other two wells are similar (Appendix H). In all wells earlier MTBE arrival was observed at greater depths, but at lower peak concentrations. The differences in time of arrival with depth likely reflect higher hydraulic conductivity at greater depths (Figure 6.11).

Ethanol was expected to behave similarly to MTBE. However, as can be seen in Figure 6.17, except for a few sampling ports (RA-W7-06 and RA-W7-07), ethanol was not detected or detected only at very low concentrations, despite being more soluble and being present in a higher fraction than MTBE in the original E10 gasoline. Where ethanol was detected, it was as early as the initial MTBE was detected, consistent with ethanol's high mobility in groundwater. However, the lack of ethanol in significant concentrations at early time indicates that ethanol was retained in the unsaturated zone. The later arrival of the more hydrophobic gasoline hydrocarbons (Figure 6.18) is expected due to their retardation (Thorbjarnarson and Mackay 1994).

In some sampling events the highest concentrations were detected above the water table (Figure 6.19), indicating that horizontal transport in the capillary fringe is significant. In situations like this, a conventional monitoring well, screened across the water table, wouldn't be able to capture the highest concentrations in the groundwater. Vapor transport from the source zone downgradient could also be a source of contamination of groundwater (Conant et al. 1996; Grathwohl et al. 2002). However, if that was the case the concentration in the shallower sampling ports, on the top of the capillary fringe, would be the highest, with concentrations decreasing progressively with depth. This is not consistent with the field observations, supporting the inference of transport in the capillary fringe.

6.3.3.2 Late behaviour: Correlation with water table oscillations

From 117 to 320 days, wells RA-W07 and RB-W07 were monitored about every 30 days. At around 150 days, both MTBE and ethanol concentrations increased at Row A (Figure 6.20 and Figure 6.21). To evaluate what conditions in the source zone led to this second increase in concentrations, the breakthrough curves from 4 sampling ports at well RA-W07 were used to calculate groundwater

concentrations at the source zone at different depths. Only advection was considered, shifting the breakthrough curves in time using the first MTBE breakthrough curves to estimate groundwater velocity at each depth.

The rise in concentrations at the source appears to be related with oscillations in the water table (Figure 6.22). At around day 91 (November 20, 2008), the water table started to rise and reached it shallowest depth since the release, 20cm bgs, and unlike the previous events where the water table oscillations happened in a couple of days, it sustained a shallow position of less than 40cm bgs for more than two months (Figure 6.22). Therefore, during a prolonged period the source zone was almost completely saturated, which could have increased the contaminants mobility, particularly ethanol and MTBE.

After reaching the peak, the concentrations dropped precipitously following the water table drop to 50 cm bgs. Another rise in the water table around day 178 (February 15, 2009) was not followed by an increase in concentrations downgradient. This could be a consequence of the winter conditions, with the ground frozen at shallower depths. Although the melting point of ethanol is -114ºC, in a solution with ethanol mol fraction of 10%, the melting point increases to around -13ºC (Ott et al. 1979). Ground temperatures were not measured, but the average daily temperature (-12ºC for January) was slightly higher than this, so water with high ethanol concentrations probably did not freeze. Even so, at lower temperatures, mixtures of ethanol-water will have higher viscosities, which could also reduce its transport (Ott et al. 1979).

Also, low concentrations of all analytes were noted during the spring snowmelt period (Figure 6.22; Appendix I), when the water table at the site rose to around 5 cm above ground surface. It is possible that the rise in the water table was associated with upward flow, moving the dissolved plumes to shallower zones, above the sampling ports. However, high concentrations were previously identified up to around 73 cm deep, and the decrease in concentration was noticed even in the shallower sampling ports (33 to 43 cm bgs). Therefore, a displacement of at least 30 cm upwards between sampling events would be necessary to cause the plume to be missed by the shallowest port. The water table during the spring snowmelt reached a maximum of around 10 cm above the ground surface and the water table was around 30 cm bgs when the peak concentrations were measured, with the capillary fringe likely extending almost to the ground surface. Considering that 10 cm of water above the ground surface corresponds to a change in height of 30 cm in the porous media, it is possible that the plume was displaced 30 cm upwards. Also, the decrease in concentration at the

shallowest sampling port was not so steep, indicating that it could be capturing the bottom of the plume.

At the shallower ports, hydrocarbon concentrations reached a plateau at early time (example: RA-W07-2; Appendix I) and the concentrations remained relatively constant, showing no later increase as did MTBE. In the deeper ports (example: RA-W07-5; Appendix I) the hydrocarbon concentrations followed the same trend as MTBE. It appears that the deeper ports are located below the source zone, and when the water table oscillates upwards and then downwards, it brings down some contaminated water, which later appears at the deeper monitoring ports as a pulse, in contrast with a continuous source as is anticipated when free product is present.

6.3.3.3 Assessment of biodegradation and consequences for hydrocarbon transport

Snapshots from Row A (Figure 6.23) show that ethanol usually appears in lower concentrations than MTBE, but in general the shapes of the plumes are very similar. Hydrocarbons followed a similar pattern (Appendix J). This similarity suggests that the ethanol detected in the wells downgradient was transported downwards in the source within the NAPL, similarly to MTBE. Therefore, the low ethanol concentrations in the groundwater samples are indicative of low ethanol content in the NAPL, as would be expected since most of the ethanol is believed to have been retained in the unsaturated zone in the source.

The low concentrations of ethanol in comparison to MTBE could also be caused by ethanol biodegradation. Even though MTBE degradation has been reported at the Borden aquifer in aerobic conditions, the degradation rates were low and a significant lag period was observed (Schirmer et al. 2003). MTBE biodegradation product, TBA (*tert*-butyl alcohol) was not identified in significant concentrations following the E10 spill, but higher rates of TBA degradation are expected (Schirmer et al. 2003), and therefore TBA would not accumulate in the aquifer even if MTBE was degrading. A review by Schmidt et al. (2004) also indicates that in general MTBE and TBA are not easily biodegraded in comparison to gasoline hydrocarbons. On the other hand, ethanol biodegradation under both aerobic and anaerobic conditions is faster than hydrocarbon biodegradation (Powers et al 2001; Alvarez and Hunt 2002). Aerobic degradation of ethanol exerts a high demand for oxygen, leading to the development of anaerobic conditions. Methane (Figure 6.24) was found in the groundwater (discussed below), indicating that anaerobic conditions developed.

The mass of ethanol that could have been lost by aerobic degradation was calculated assuming: 1) oxygen was used solely for ethanol biodegradation; 2) oxygen input occurs by clean groundwater flowing through the source zone with background concentrations of dissolved oxygen of 7 mg/L; 3) complete mineralization, with ethanol being converted to water and carbon dioxide as in equation 3. The first assumption likely overestimates the amount of ethanol that could be degraded, as previous research have shown that ethanol can be degraded simultaneously with gasoline hydrocarbons (Williams 2007; Araujo 2000). The second assumption does not consider that some of the ethanol mass was present in the unsaturated zone, where oxygen availability might be greater.

ethanol aerobic degradation: $CH_3CH_2OH + 3O_2 \rightarrow 2CO_2 + 3H_2O$ (3)

The ethanol mass that could have been degraded aerobically is fairly small, around 80 g (100 mL) in 300 days, which represents around 0.5% of the total ethanol released. Besides oxygen limitations, ethanol biodegradation at the Borden aquifer is likely to be limited also by the availability of inorganic nutrients (such as nitrogen and phosphorous). Araujo (2000) performed microcosm tests with Borden soil and groundwater in excess oxygen conditions, with 0.5% ethanol and 30 mg/L of BTEX, and verified that without the addition of nutrients there was no mass loss of ethanol after 64 days of incubation. When nutrients were added the ethanol mass loss was around 25% when ethanol concentration was 0.5% and decreased to 7.3% for ethanol concentration of 1.5%. So, nutrient availability could also limit biodegradation in the unsaturated zone, even if excess oxygen is present.

The concentrations of methane, acetate and butyrate were used to estimate the extent of the anaerobic biodegradation of ethanol, based on equations 4 to 8. Methane was found in low concentrations in the groundwater, but the concentrations are increasing with time (Figure 6.24). Methane background concentrations in the site at around 10 m bgs, where previous contamination exist, are below 300 μg/L, with no evidence of methane at shallower depths, where this research was conducted (Barker 1979). Therefore, the presence of methane indicates the occurrence of biodegradation. The distribution of methane and organic acids at Row A can be seen in Figure 6.25. The concentrations of the biodegradation products were converted to ethanol concentrations using equations 4 to 8, and the ethanol contour recalculated as if there had been no biodegradation (Figure 6.25). A significant increase in the contour concentrations is evident, indicating that some ethanol is likely being lost by anaerobic biodegradation.

ethanol to acetate: $CH_3CH_2OH + H_2O \rightarrow 2H_2 + CH_3COO^- + H^+$ (4)

acetate to methane: $CH_3COO^- + H^+ \rightarrow CH_4 + CO_2$ (5)

ethanol and acetate to butyrate: $CH_3CH_2OH + CH_3COO^- \rightarrow CH_3CH_2CH_2COO^- + H_2O$ (6)

carbon dioxide to methane: $CO_2 + 4H_2 \rightarrow CH_4 + 2H_2O$ (7)

ethanol to methane – overall reaction: $2CH_3CH_2OH \rightarrow 3CH_4 + CO_2$ (8)

However, the anaerobic biodegradation of hydrocarbons can also result in the formation of the organic acids and methane (Heider et al. 1999). Therefore, the assumption that all biodegradation products were ethanol-derived is likely overestimating the extent of ethanol biodegradation. To provide some insight on this issue, methane $\delta^{13}C$ values were determined for selected samples on two dates (Table 6.2). Methane derived from ethanol is expected to have more enriched values of $\delta^{13}C$ than methane from gasoline (Chapter 3). In one sample (V13-0.2), methane $\delta^{13}C$ was clearly within the range of ethanol-derived methane. Another sample (RA-W04-03) had a depleted methane $\delta^{13}C$ value, indicating that its source was mainly hydrocarbon biodegradation. All the other samples had intermediate values, indicating that both ethanol and hydrocarbons had contributed to methane production.

Besides limiting the downgradient transport of ethanol, the retention of ethanol in the unsaturated zone also appears to have limited the ethanol impacts on hydrocarbon behaviour. Although ethanol pore water concentrations higher than 10% have been measured in soil cores above the water table, with consequent increase in the hydrocarbon compounds solubility, there is no evidence in the downgradient groundwater that cosolvent effects were important. Hydrocarbon concentrations approached, but didn't exceed, their effective solubility from E0 (Figure 6.26). This is likely a consequence of ethanol being present in high concentrations in the unsaturated zone where the transport is limited, and limited ethanol presence where the hydrocarbons are being transported.

The mass discharge crossing row A was estimated for all compounds (Appendix K) and is shown for select compounds in Figure 6.27. The mass flux of MTBE was always greater than that of ethanol. For the last two samplings the ethanol mass flux was reassessed assuming that all biodegradation products were derived from ethanol. This resulted in an increase of 56% for day 154 and 78% for day 188 in the "ethanol" mass discharge (ethanol + biodegradation products). However, even then, the total ethanol mass that crossed Row A by 188 days is still only 6.3% of the total released. Based on the mass discharge, anaerobic biodegradation could have caused an ethanol loss of around 2% of the total mass, or around 300 g. During the same period approximately 28% of the MTBE crossed Row A (Table 6.3). The percentage of hydrocarbons that crossed Row A was lower than MTBE, with a good

correlation between the effective solubility and the percentage that crossed Row A (Figure 6.28). Ethanol is the only compound that clearly does not follow this trend, indicating that the retention on the unsaturated zone in the source is a very significant process, even with a thin unsaturated zone.

6.4 Conclusions and Implications

After an E10 release most of the ethanol was retained in the unsaturated zone, above the capillary fringe. This retention was caused by ethanol partition out of the NAPL to the pore water above the water table, in regions where transport is limited due to the low water saturation and so low hydraulic conductivity. Ethanol retention was significant even with a thin (around 35 cm) unsaturated zone, with the water table at around 52 cm bgs. In contrast, most of the MTBE and hydrocarbons was transported downwards within the NAPL. MTBE retention in the unsaturated zone was limited by its lower solubility in comparison to ethanol, but it could be significant if the water table was deeper.

The time of arrival of the highest ethanol concentrations in the multilevel wells 2.3 m downgradient the source zone was delayed for around 150 days. Ethanol peak concentrations in the wells downgradient were similar to those of MTBE, despite the 100 times higher effective solubility of ethanol from the E10 gasoline released. Only about 6% of the mass of ethanol (including potential biodegradation products) was transported 2 m downgradient the source after 188 days, against 28% of the MTBE, 5% of the benzene and 0.2% of the naphthalene. The limited transport of ethanol from the source zone is likely a consequence of ethanol retention in the source zone, above the capillary fringe. Together with minor biodegradation, this can explain why in real sites impacted by ethanol spills, ethanol is hardly detected in high concentrations in the groundwater (McDowell et al. 2003; Chapter 3).

The observed ethanol behaviour contrasts with the assumption commonly made in previous studies (Molson et al. 2002; Mackay et al. 2006; Gomez et al. 2008) that ethanol fuels would reach the saturated zone with the same ethanol content as the initial mixture. While this might be the case in some sites, this study showed that ethanol retention in the unsaturated zone is significant, and therefore the conceptual models of ethanol fuel spills should be modified to include the effects of the unsaturated zone.

One of the main implications of the rapid ethanol partitioning to the pore water in the unsaturated zone is that it separates the high ethanol concentrations from the NAPL. The front of the dissolved hydrocarbon plumes was not associated with significant ethanol and so there was no enhanced solubility of hydrocarbons and no decrease in biodegradation rates for hydrocarbons is expected. However, oscillation in the water table and direct recharge on the source might cause a delayed transport of ethanol to the saturated zone, as observed in the field test, which can result in a sudden increase of hydrocarbons and ethanol concentrations.

The extent of ethanol retention on the source zone is dependent on the amount of water available between the release and the capillary fringe. Therefore, the percentage of ethanol that will reach the saturated zone is a function of depth to the water table, type of soil, presence of heterogeneities, spill volume, rate, and area.

6.5 Figures and Tables

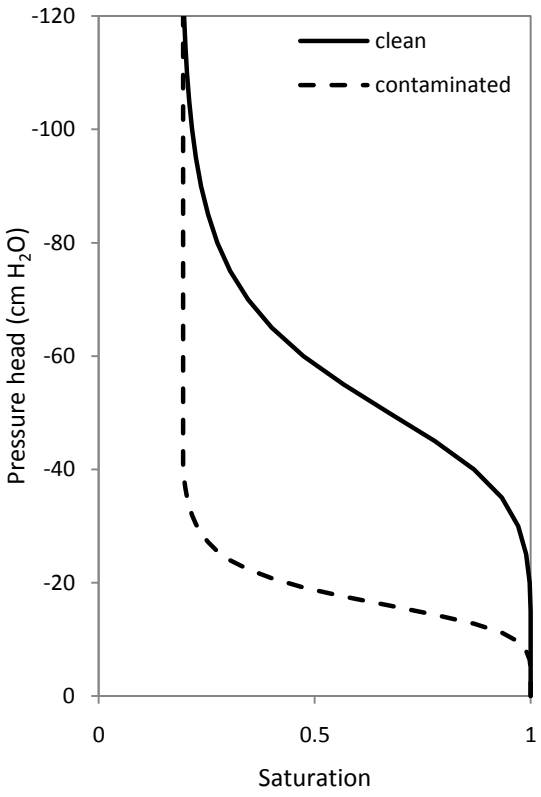

Figure 6.1: Pressure head - saturation profiles for clean (Mickle 2005) and gasoline contaminated Borden sand (estimated based on interfacial tension reduction and on Vakili 2008).

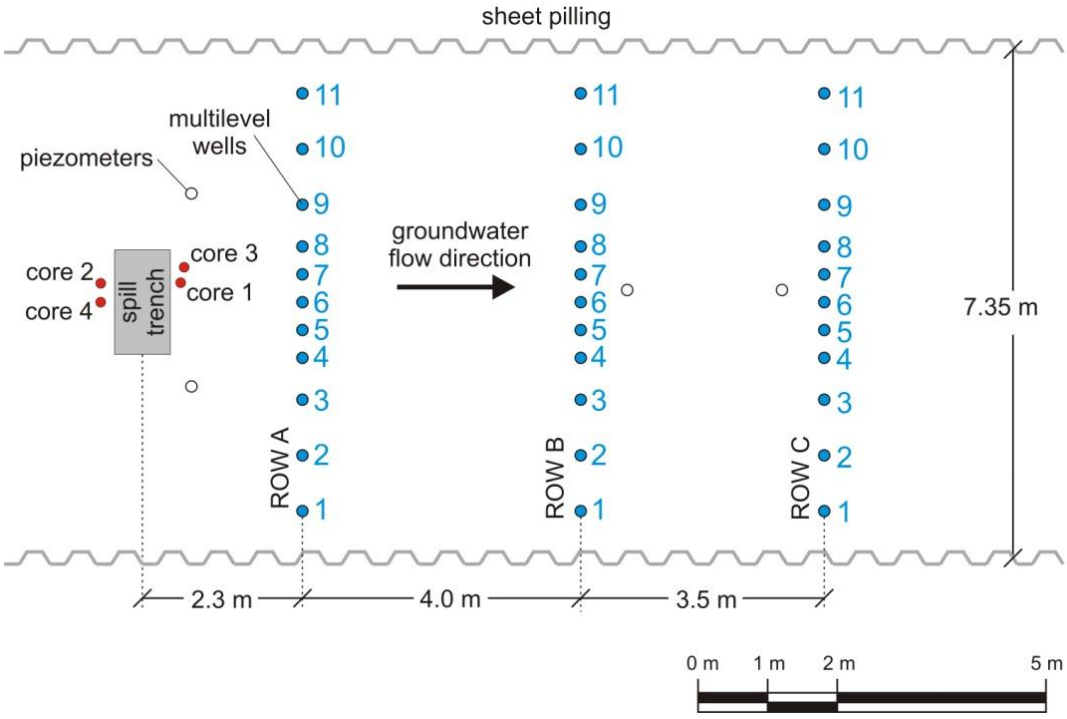

Figure 6.2: Site installations for groundwater monitoring and position of soil cores

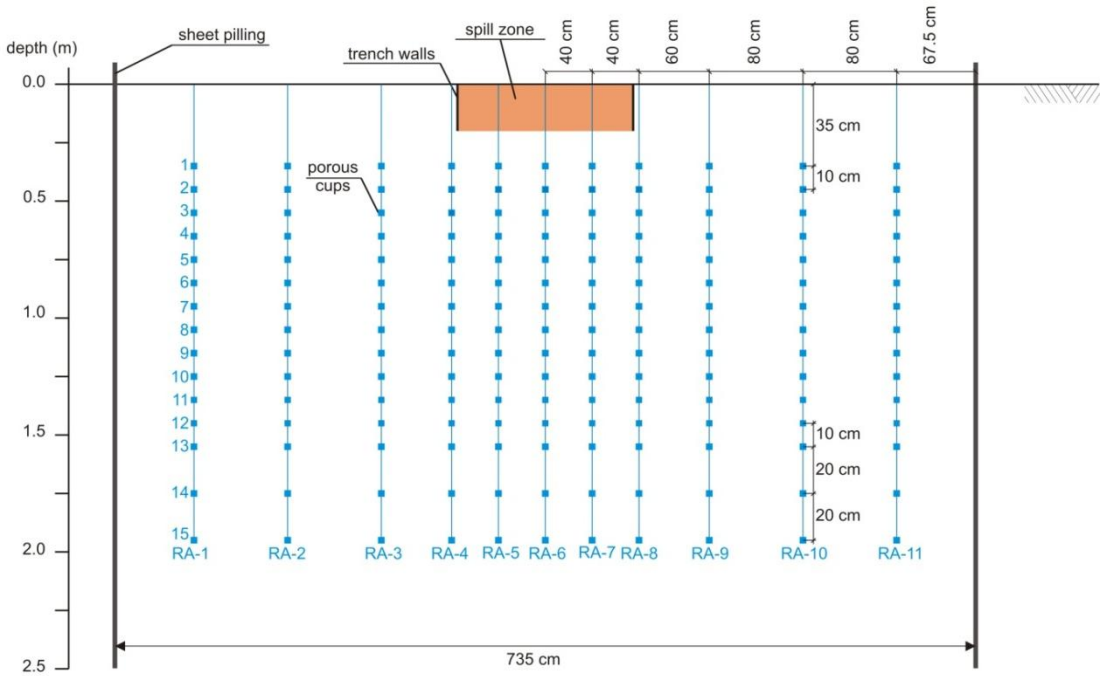

Figure 6.3: Row A cross section with the release zone projected onto the cross section

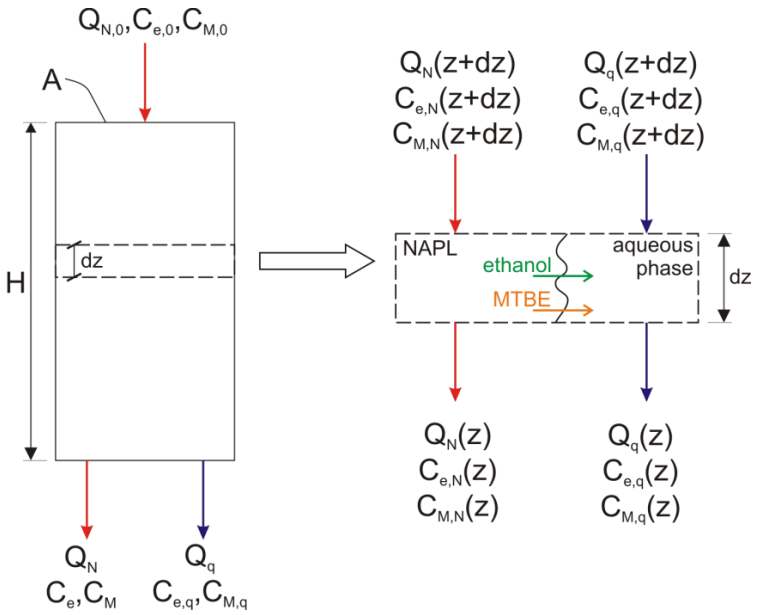

Figure 6.4: Conceptual model applied to estimate ethanol and MTBE retention in the unsaturated zone. Subscripts N and q refer to NAPL and aqueous phase respectively; subscripts e and M refer to ethanol and MTBE components.

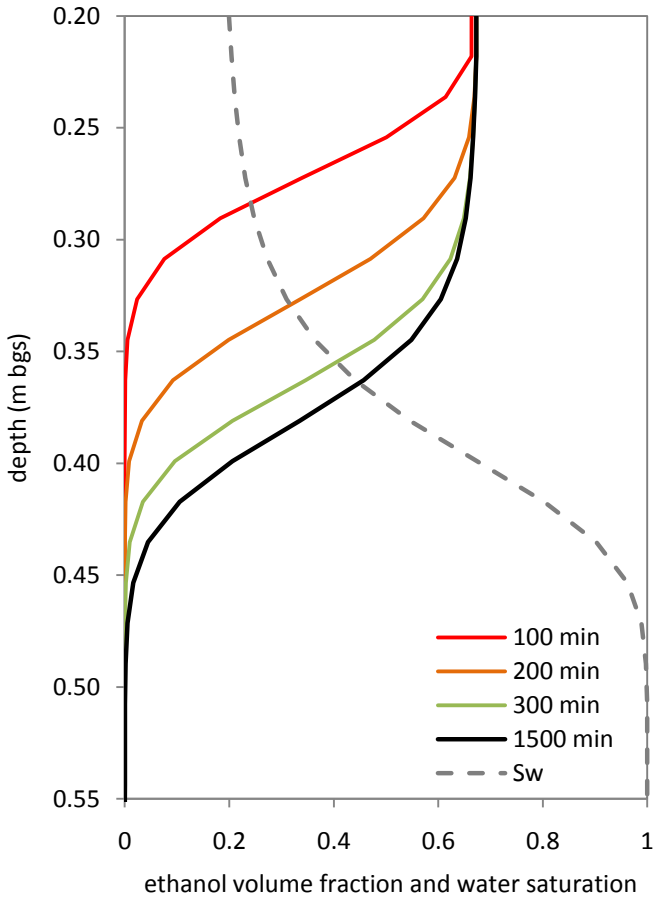

Figure 6.5: Calculated ethanol volume fraction in the aqueous phase and the water saturation profile (dashed line). The depth of 20 cm bgs corresponds to the bottom of the trench and the water table is at 55 cm bgs.

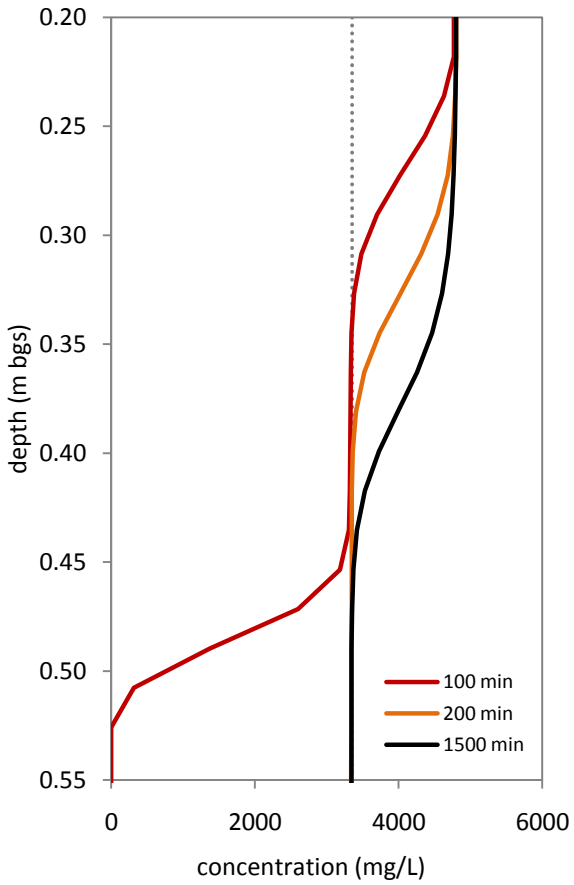

Figure 6.6: Calculated MTBE concentration (mg/L) in the aqueous phase. The dotted line represents the maximum MTBE concentration expected in the absence of ethanol.

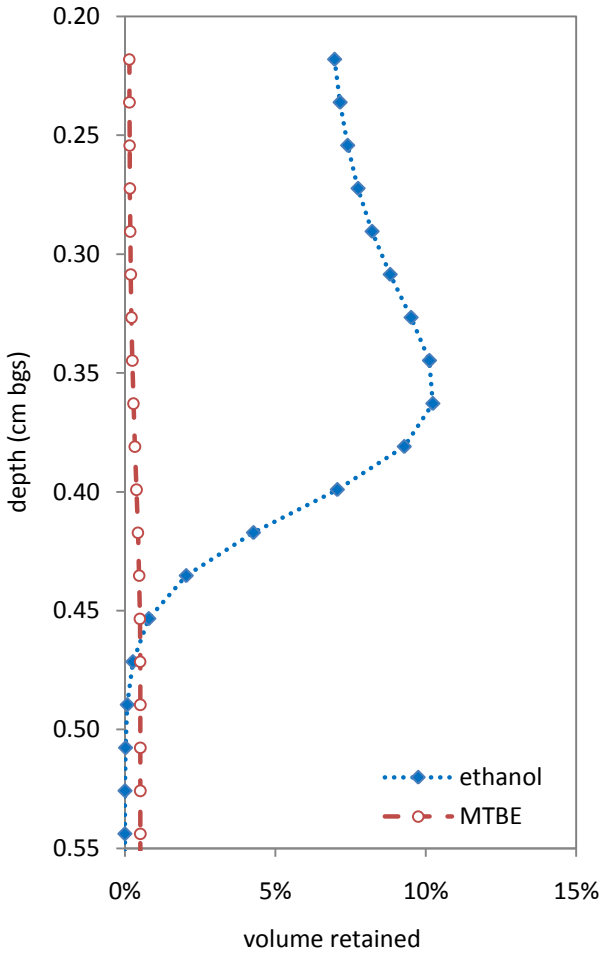

Figure 6.7: Profile of ethanol and MTBE retained in the aqueous phase in each layer after 1500 minutes, as percentage of the total released.

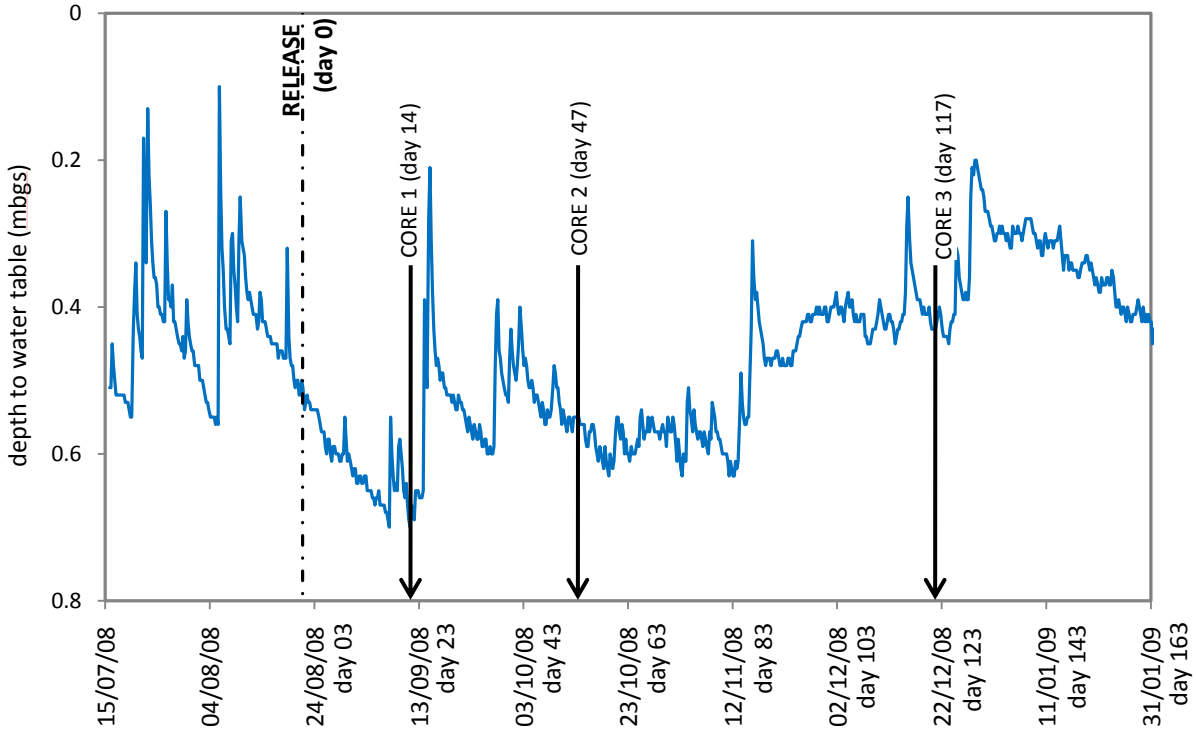

Figure 6.8: Water table position and coring dates (core 4 was collected on day 305, not shown)

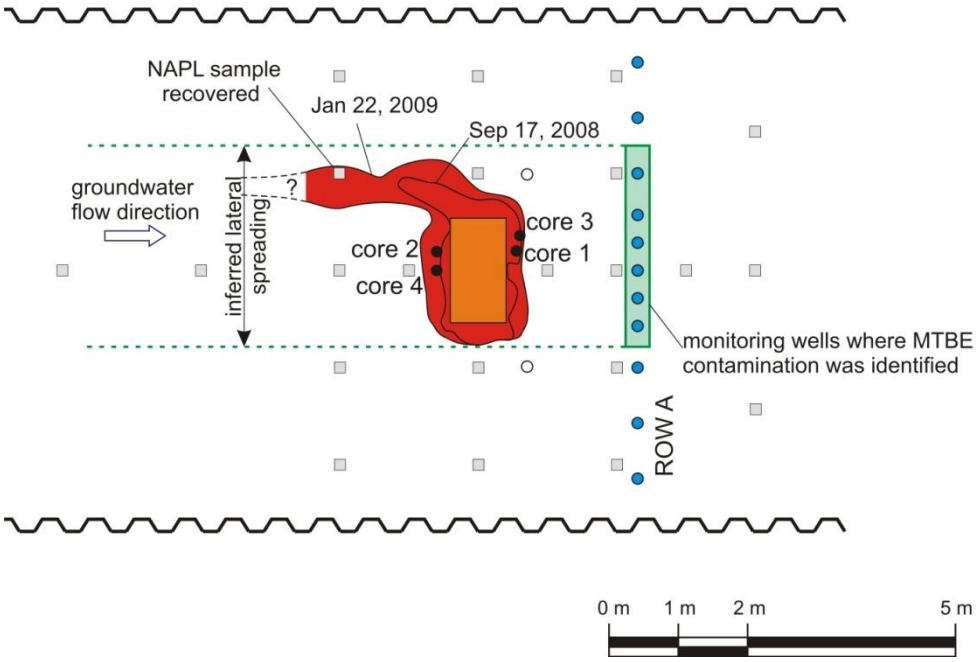

Figure 6.9: Contamination lateral extent: Dye ground stain and groundwater

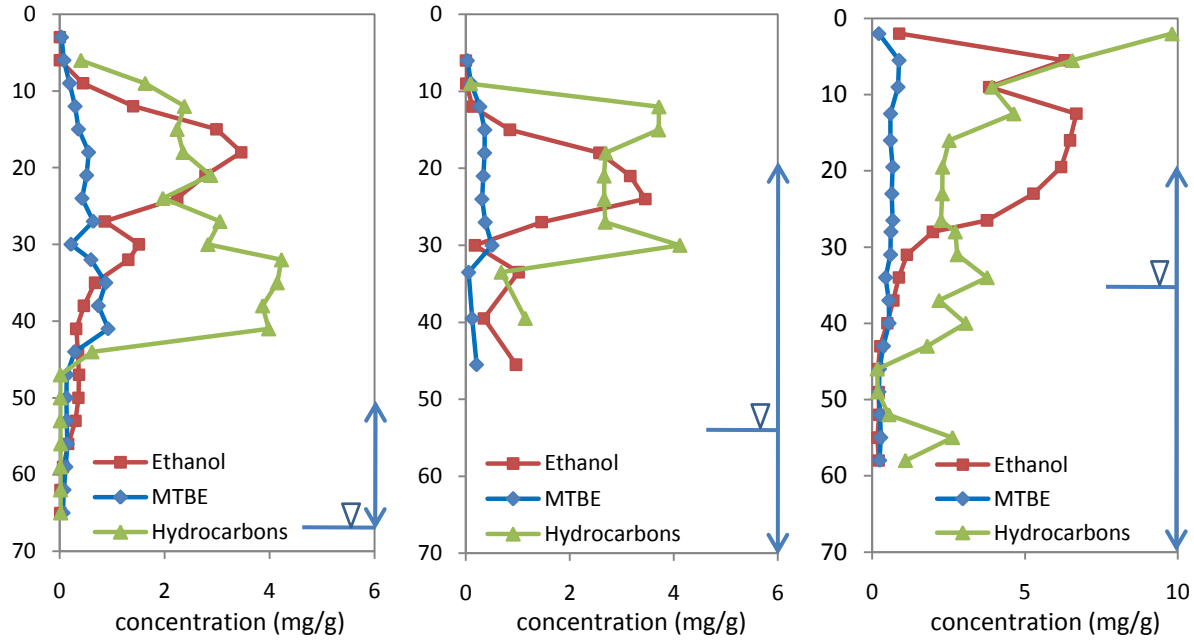

Core 1 – day 14 (04-Sep-08) Core 2 - day 47 (07-Oct-08) Core 3 - day 117 (16-Dec-08)

Figure 6.10: Concentration in soil cores (mg/g wet soil). Depth is on the y-axis (cm bgs). Hydrocarbons correspond to the sum of BTEX, TMBs and naphthalene. Vertical arrows indicate range of water table oscillation from the release to the day of the core.

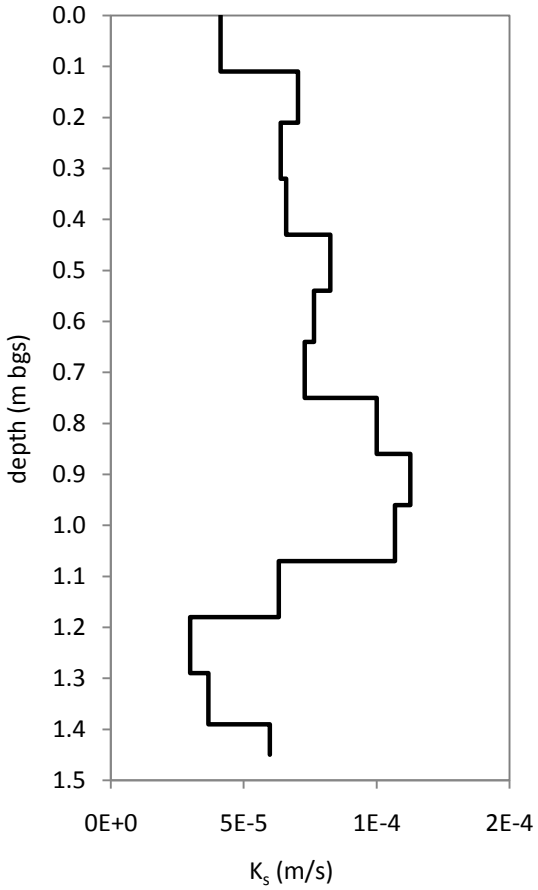

Figure 6.11: Saturated hydraulic conductivity (Ks) profile at core 4. Values were adjusted for water temperature of 10ºC.

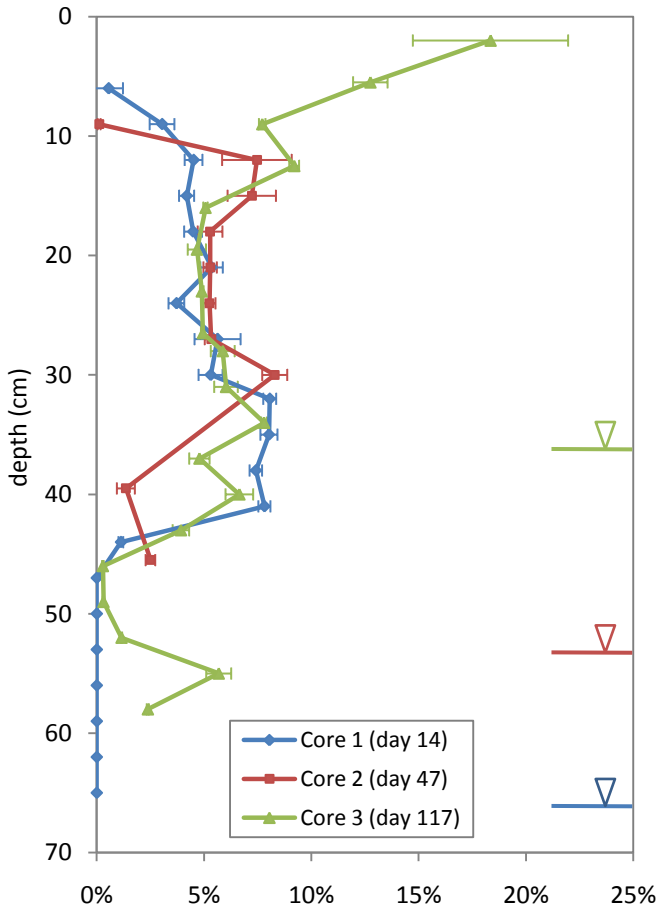

Figure 6.12: Calculated NAPL saturation profile (average of values determined based on toluene, ethylbenzene and o-xylene). Error bars represent 2 standard deviations. Water table position at the core date is indicated on the right side (color coded).

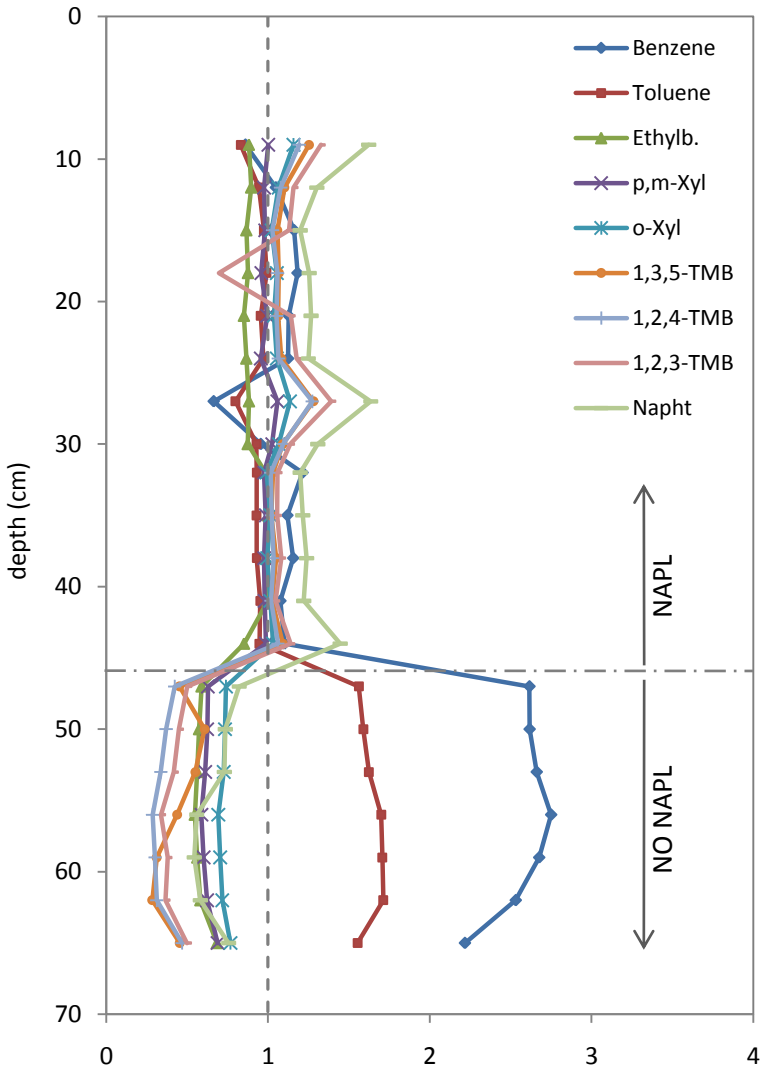

Figure 6.13: Measured ratio of C_i/C_t over expected ratio of C_i/C_t. Deviation from 1 indicates the absence of NAPL (data from soil core 1, obtained on 04-Sept-08)

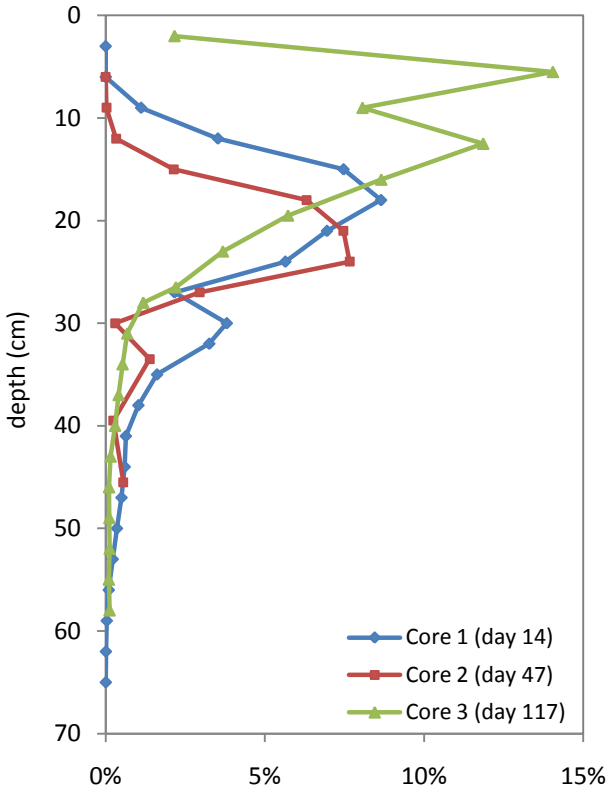

Figure 6.14: Ethanol mass fraction in pore water

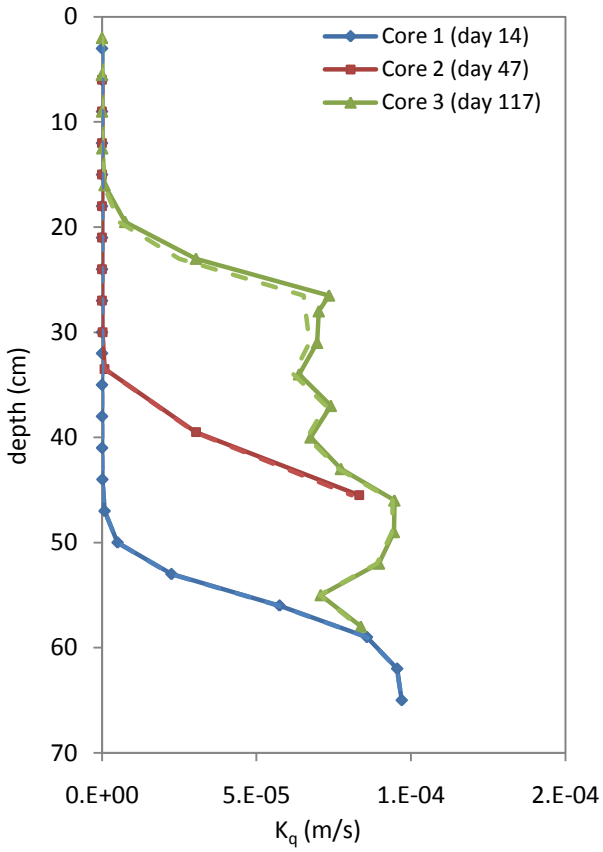

Figure 6.15: Effective hydraulic conductivity to aqueous phase (m/s). Dashed line indicates K_q considering changes due to solution density and viscosity.

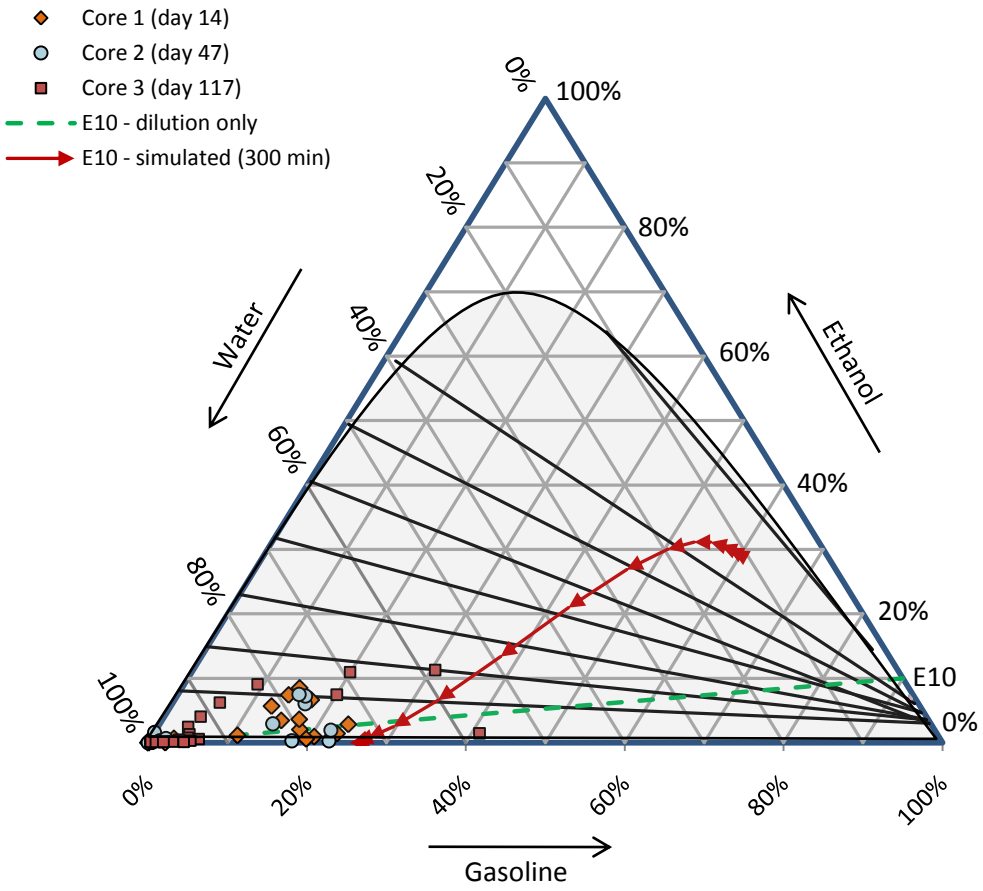

Figure 6.16: Gasoline-ethanol-water ternary diagram (adapted from Oliveira 1997) with the phase compositions inferred from soil cores, the calculated composition trend for E10 gasoline being diluted by mixing with water (dashed line) and model results (solid curve) at 300 min (see Subsection 6.3.1). Arrows indicate increasing depth.

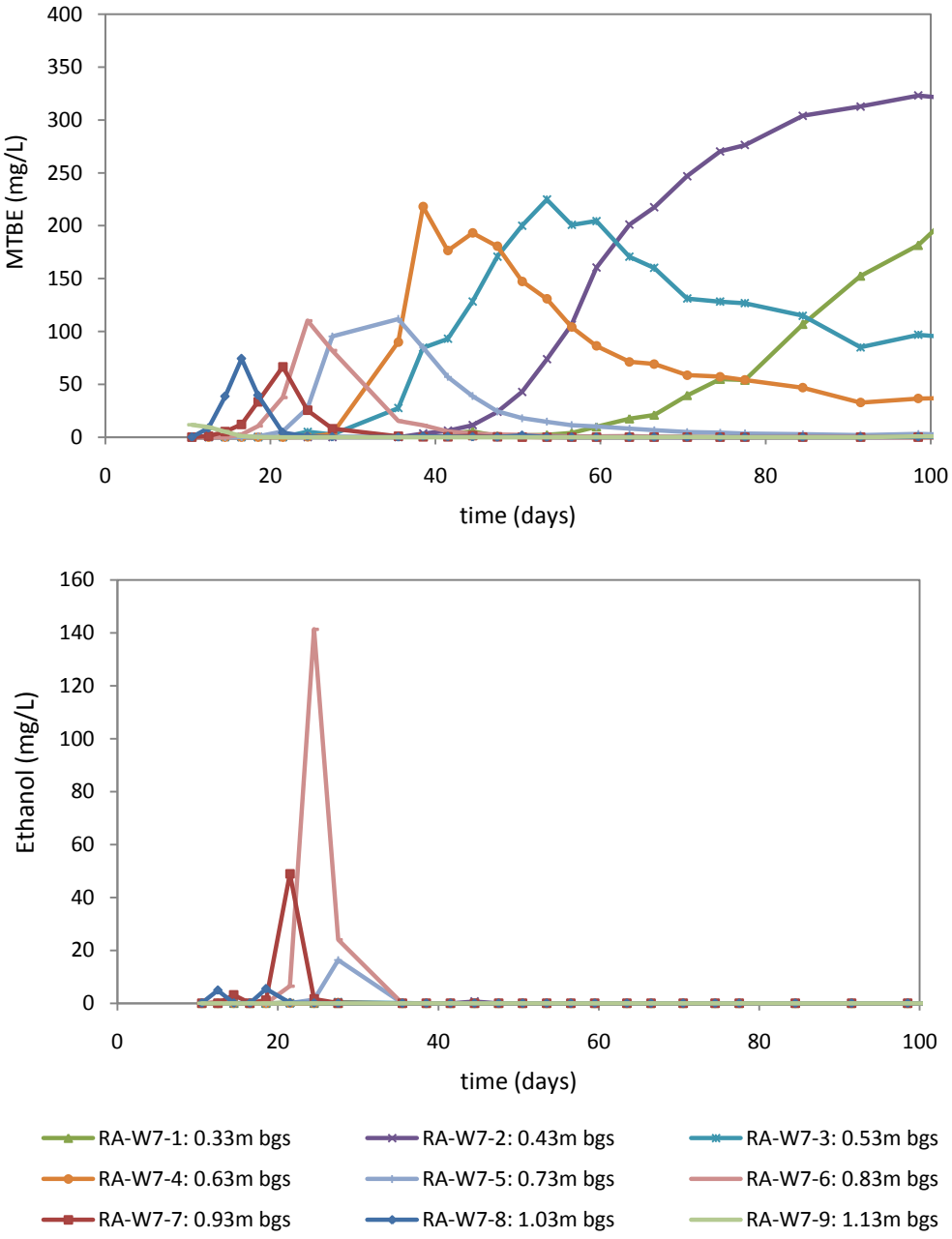

Figure 6.17: MTBE and ethanol breakthrough curves, well RA-W07.

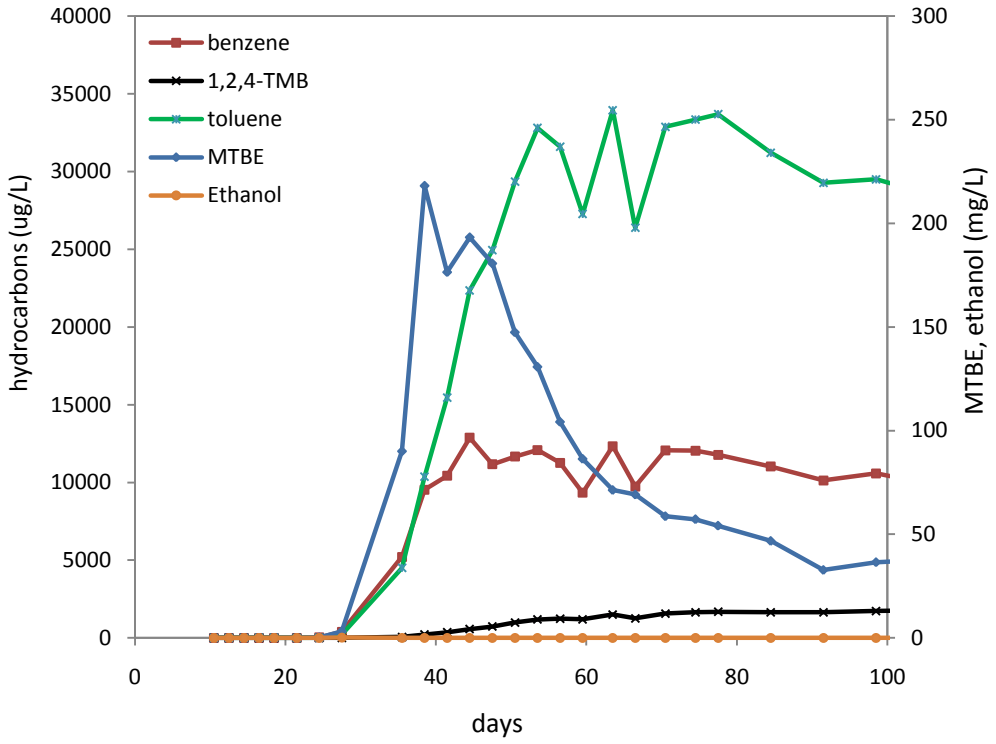

Figure 6.18: Breakthrough curves, well RA-W07-04 (0.63m bgs).

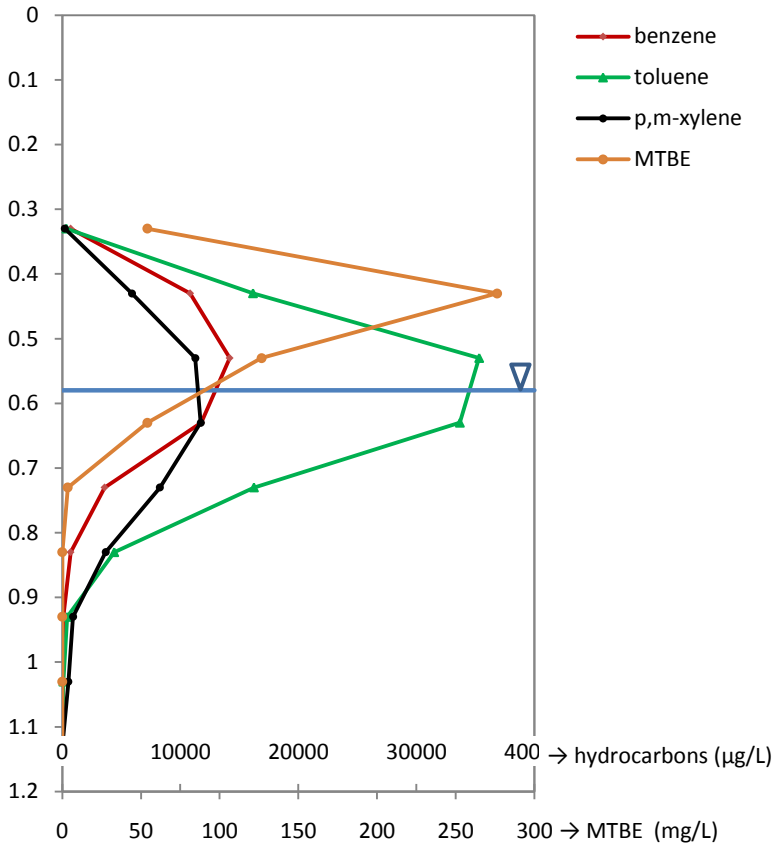

Figure 6.19: Concentrations profile at well RA-W07, day 77, with the water table at that day at about 0.58 m bgs.

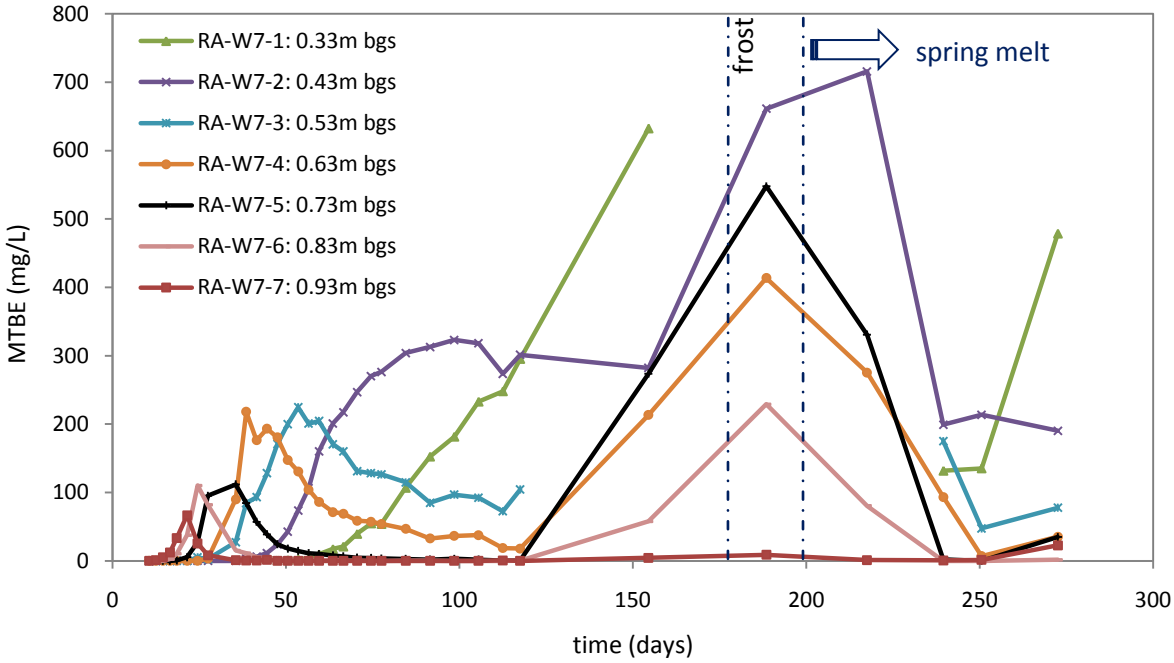

Figure 6.20: MTBE breakthrough curves, well RA-W07. Frost and spring melt times are estimated. Discontinuities on curves RA-W07-01 and RA-W07-03 reflect an inability to retrieve samples from these points, likely due to the frozen ground.

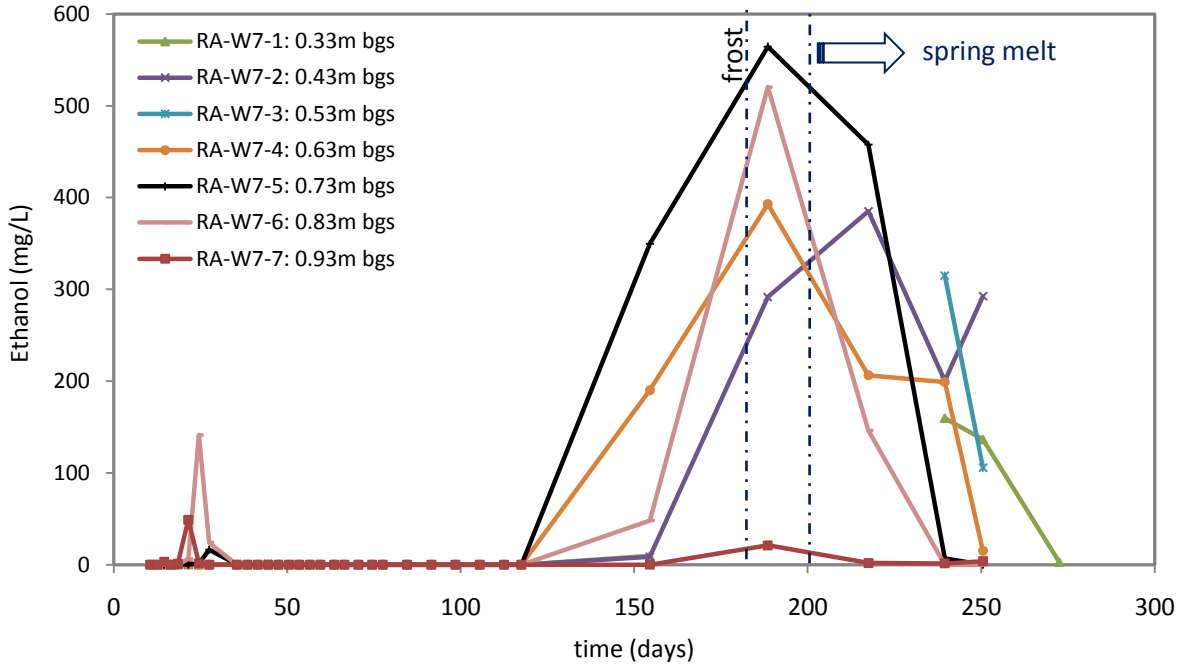

Figure 6.21: Ethanol breakthrough curves, well RA-W07. Frost and spring melt lines are estimated dates. Discontinuities on curves RA-W07-01 and RA-W07-03 reflect an inability to retrieve samples from these points, likely due to the frozen ground.

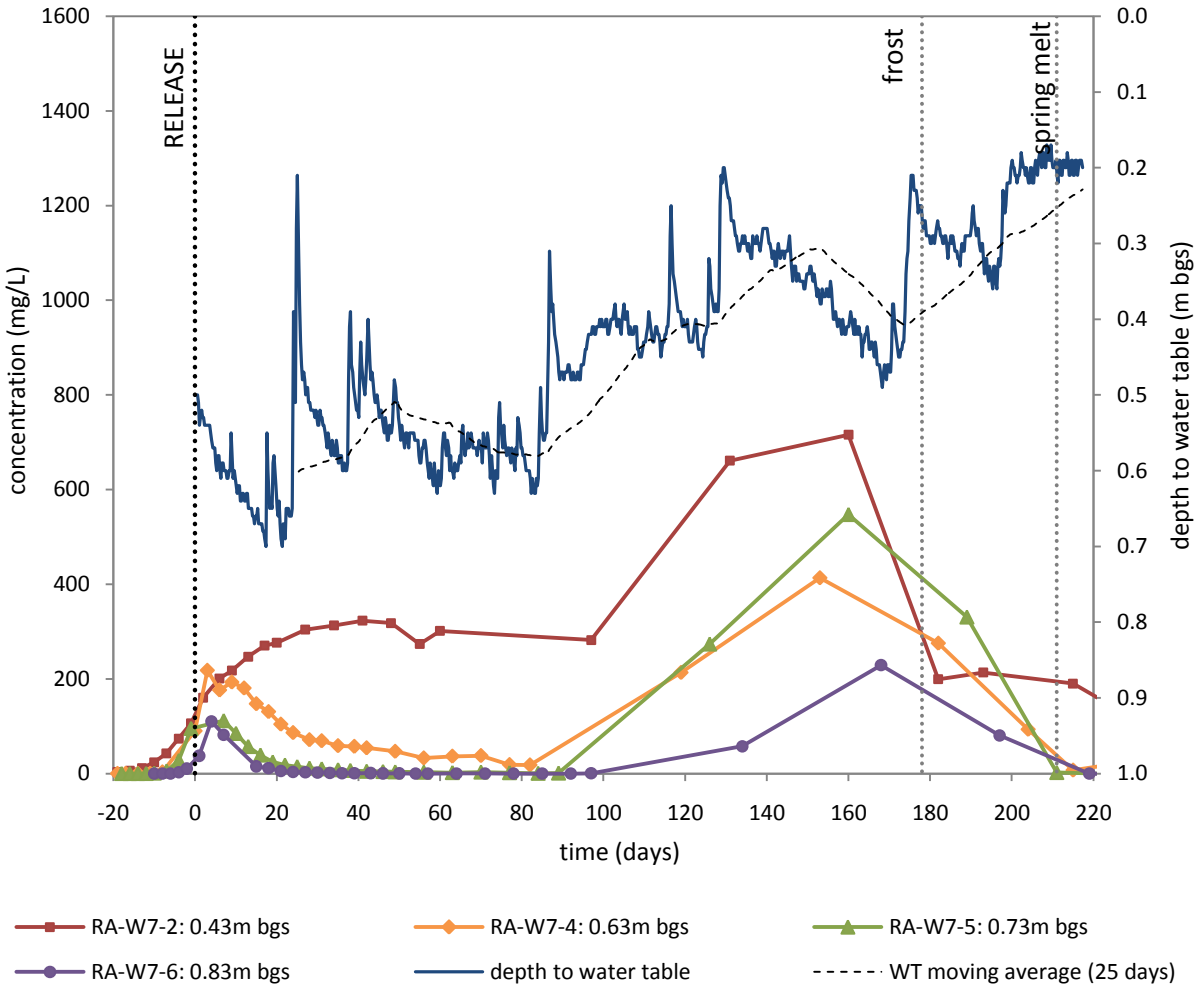

Figure 6.22: MTBE concentration at the source zone (calculated from breakthrough curves at well RA-W07) and depth to the water table. Moving average curve represents the average of the previous 25 days. Frost and spring melt lines are estimated.

day 27: no ethanol concentration above 50 mg/L

day 77: no ethanol concentration above 50 mg/L

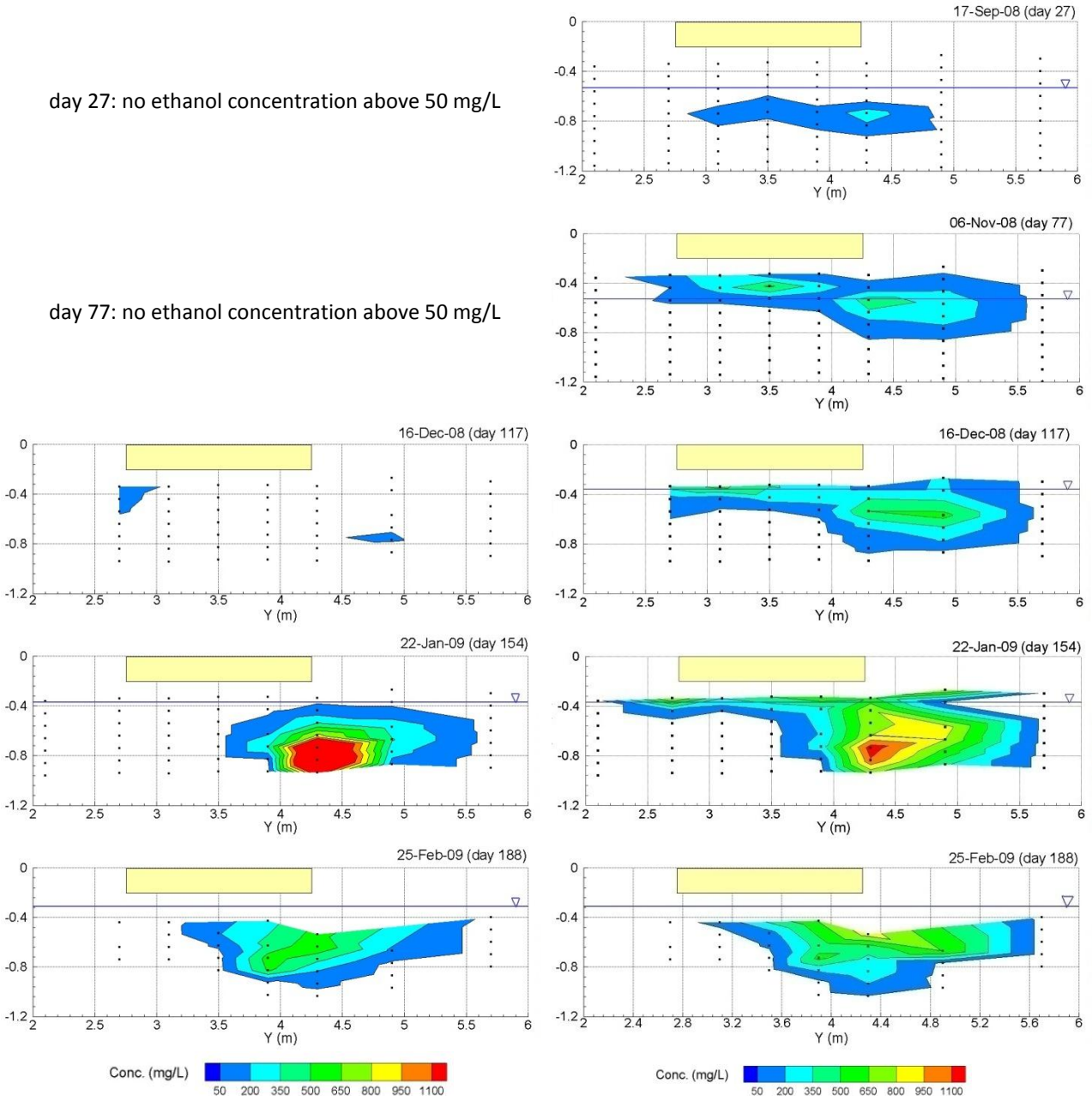

Ethanol MTBE

Figure 6.23: Contours at Row A, groundwater flows orthogonally, outwards from the page.

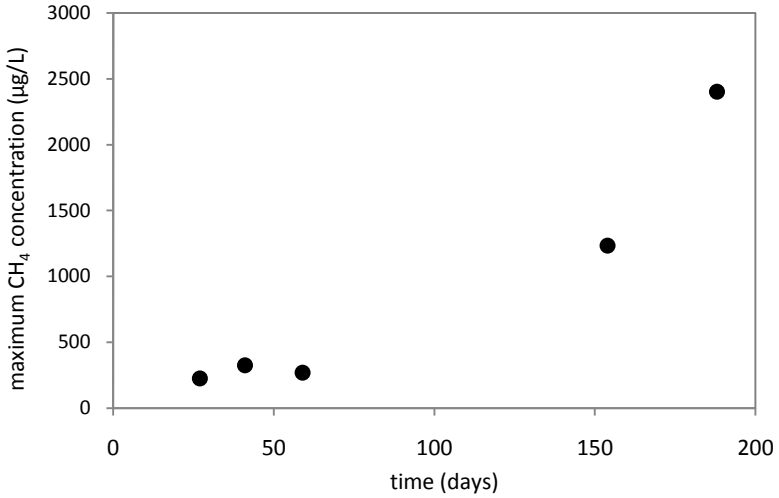

Figure 6.24**: Maximum methane concentrations detected in groundwater Samples for methane were collected from ports where concentrations were expected to be highest.**

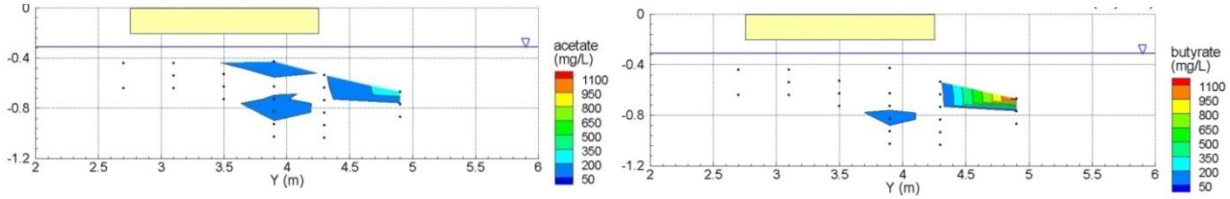

a) acetate concentration

b) butyrate concentration

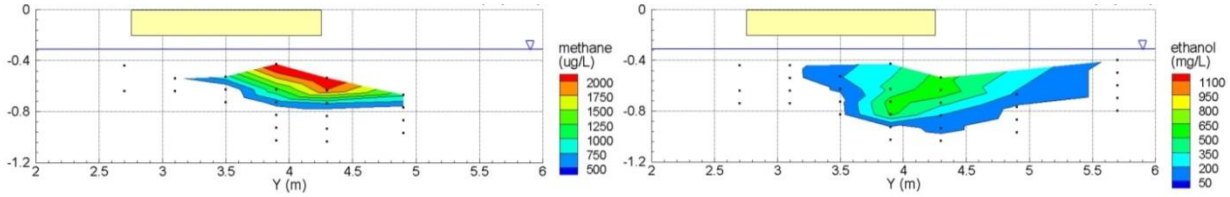

c) methane concentration

d) ethanol concentration

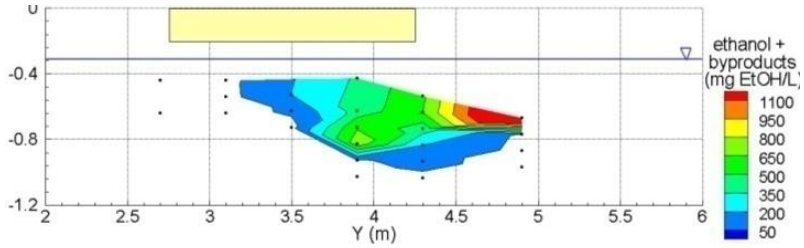

e) equivalent ethanol concentration

Figure 6.25: Distribution of ethanol and biodegradation products at row A, day 188 (25-Feb-09). Only those points actually sampled for the analyte are shown.

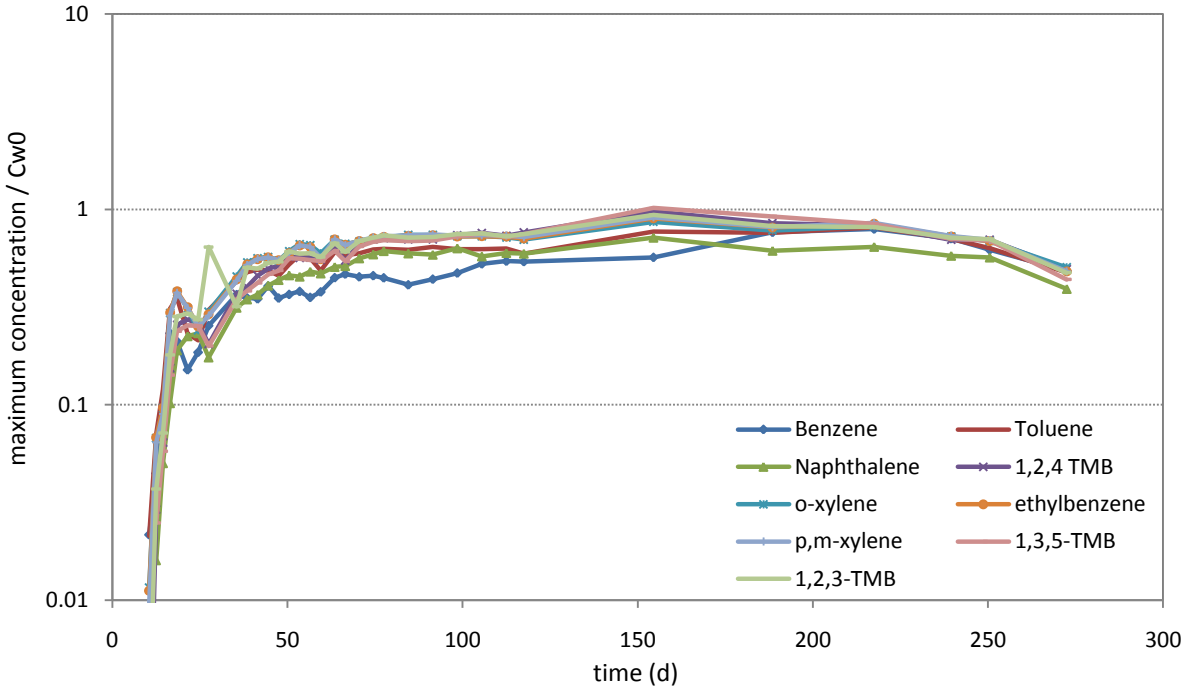

Figure 6.26: Ratio of maximum concentrations measured at well RA-W07 and expected concentrations, as determined in laboratory tests.

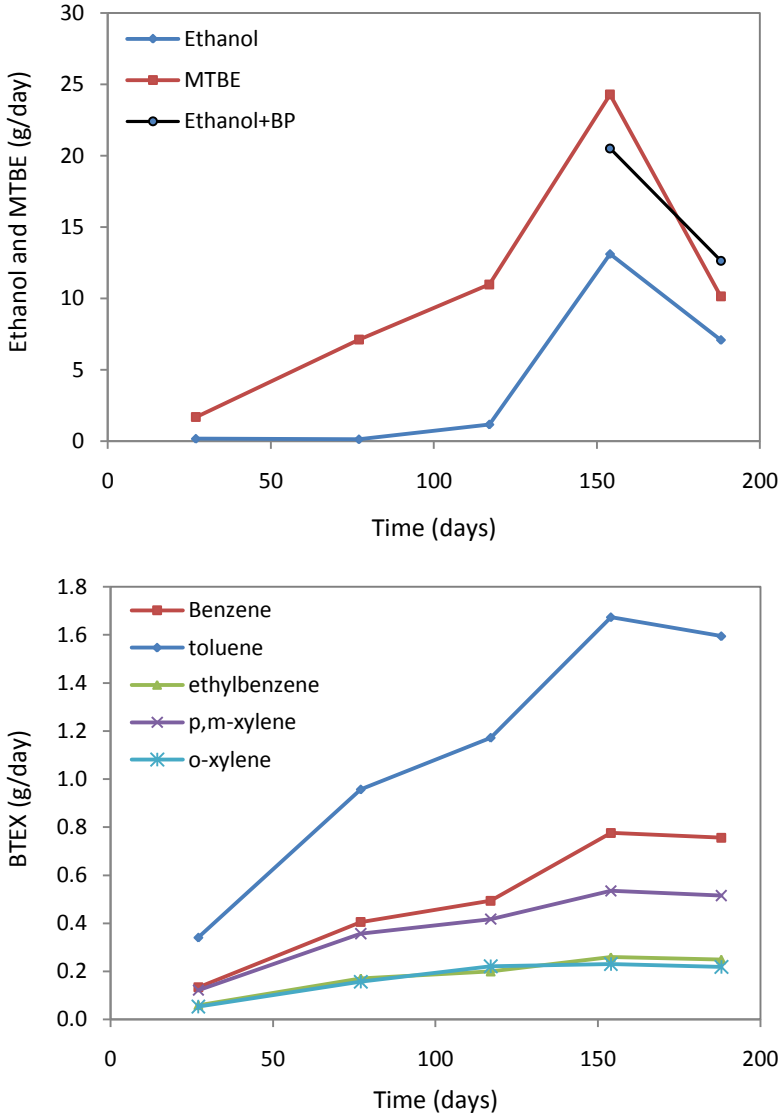

Figure 6.27: Mass discharge through time at Row A.

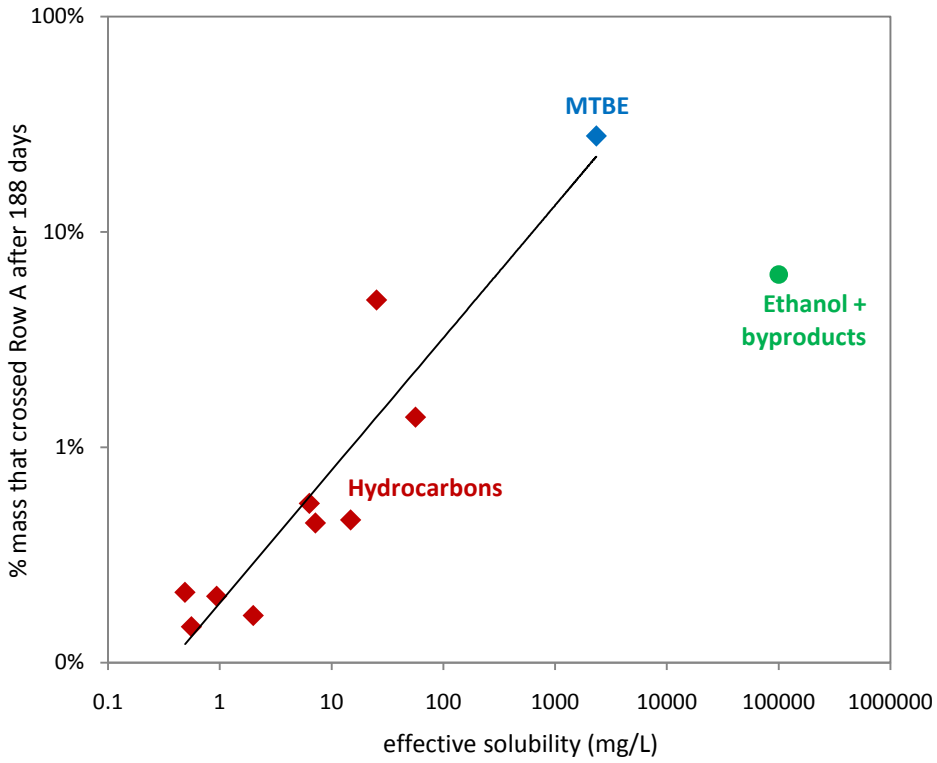

Figure 6.28: Effective solubility versus percentage mass that crossed Row A within the 188 days of monitoring. Correlation factors (R^2) are 0.976 excluding ethanol and 0.015 including ethanol. Note that ethanol's effective solubility was assumed equal to 10% (100,000 mg/L).

Table 6.1: Physical properties of the compounds investigated

	molecular weight [1]	density [1] (g/L)	solubility [1] (mg/L)	Henry constant [1] (atm L/ mol)	cosolvency power [2]	sorption distribution coefficient (K_d) [3] (L/kg)
Ethanol	46.068	789.3	infinite	0.00507		
MTBE	88.148	735.3	44000	0.70	0.3	
Benzene	78.112	876.5	1780	5.57	1.5	0.089
Toluene	92.139	866.8	531	6.60	1.5	0.088
Ethylbenzene	106.165	862.6	161	8.43	2	0.14
p,m-Xylene	106.165	858.1	171	7.1	2	0.187
o-Xylene	106.165	880.2	171	5.51	2	0.128
1,3,5-TMB	120.191	861.5	50	7.81	2	
1,2,4-TMB	120.191	875.8	57	5.69	2	
1,2,3-TMB	120.191	894.4	70	3.43	2	
Naphthalene	128.171	1025.3	86	0.43	2	

Sources: [1] Lide (2008); [2] estimated from Corseuil et al. (2004), Morris et al. (1988) and Freitas and Barker (2008). MTBE cosolvency power was determined from laboratory measurements (Appendix C); [3] Hubbard (1992). Naphthalene solubility obtained from Lide (2008) was corrected from the solid to the subcooled liquid (Schwarzenbach et al. 2003). Average values were adopted for p,m-xylenes.

Table 6.2: Methane concentration and carbon isotope.

Date	Port ID	CH_4 (mg/L)	$\delta^{13}C_{CH4}$ (‰)
19-Oct-08	V13-0.2	109	-20.2
	RA-W07-03	269	-40.2
22-Jan-09	RA-W04-01	870	-40.5
	RA-W04-03	112	-67.1
	RA-W09-04	915	-46.4

Table 6.3: Cumulative percentage of the mass that crossed Row A by each day

day →	**27**	**77**	**117**	**154**	**188**
Ethanol	0.01%	0.06%	0.23%	1.9%	4.1%
Ethanol+BP	0.01%	0.06%	0.23%	2.8%	6.3%
MTBE	0.34%	3.7%	9.1%	19%	28%
Benzene	0.11%	0.89%	1.9%	3.3%	4.8%
Toluene	0.03%	0.27%	0.59%	0.97%	1.4%
Ethylbenzene	0.01%	0.09%	0.20%	0.32%	0.45%
p,m-Xylene	0.01%	0.10%	0.21%	0.33%	0.46%
o-Xylene	0.01%	0.11%	0.25%	0.41%	0.55%
1,3,5-TMB	0.00%	0.03%	0.06%	0.10%	0.15%
1,2,4-TMB	0.00%	0.03%	0.07%	0.12%	0.17%
1,2,3-TMB	0.01%	0.04%	0.02%	0.15%	0.21%
Naphthalene	0.00%	0.04%	0.09%	0.15%	0.20%

Chapter 7
Summary and Recommendations

7.1 Summary of Accomplishments

The goal of this research was to improve the understanding of the behaviour of fuels containing ethanol in the subsurface and the impacts of ethanol to the fate of gasoline hydrocarbons. To accomplish that, new methods for ethanol contaminated sites investigation were developed, such as an isotopic tool for methane fingerprinting and unsaturated zone sampling techniques. The methods developed were applied to a controlled field test, where the ethanol behaviour in the unsaturated zone and capillary fringe was investigated in field scale for the first time. This research showed that the unsaturated zone can affect ethanol fate significantly, delaying its transport into the saturated zone and, therefore, decrease its impact on the fate of gasoline compounds. It is evident that assessment and remediation efforts in ethanol fuel contaminated sites must consider the retention and fate of ethanol in the unsaturated zone.

Specific contributions of this study are described below.

- Chapter 2 provides the first quantitative evaluation of the impact of ethanol on hydrocarbon biodegradation from NAPL sources at field scale. With support of numerical modeling, it was shown that 10% ethanol in gasoline is unlikely to impact BTEX, TMB and naphthalene biodegradation rates in initially pristine mildly aerobic aquifers. High ethanol fractions (95%), on the other hand, are likely to decrease hydrocarbon biodegradation rates significantly.

- This study presented the effect of heterogeneous K distribution on mass discharge through time. The mass discharge versus time was shown to be highly dependent on the hydraulic conductivity distribution, even for an aquifer with a low degree of heterogeneity.

- This research provided a tool to distinguish the origin of methane from gasoline or from ethanol biodegradation. This tool was applied and validated at ethanol fuel contaminated sites. Ethanol derived methane was found to be significantly enriched in ^{13}C in comparison to gasoline derived methane. Even though the methane stable carbon isotopic signature may vary with the microbial reactions involved and with the stage of ethanol biodegradation, the difference is sufficient to allow the distinction between the two sources.

- Methane in potentially explosive concentrations at sites impacted by ethanol fuels was, for the first time, demonstrated to be derived from ethanol biodegradation.
- A method for the correction of concentrations obtained using porous suction samplers for volatile organic compounds in the presence of ethanol was developed. The method allows the estimation of losses by volatilization when suction during sampling results in significant formation of bubbles in the sampling line, common when sampling from the vadose zone, where more negative pressures are required.
- Chapter 6 presents the first controlled field test where transport of organic compounds in the capillary fringe was evaluated. It was shown that transport in the capillary fringe can be significant, and concentrations in the capillary fringe can be higher than below the water table. Concentrations above the water table would likely be missed by conventional monitoring wells.
- Ethanol retention in the unsaturated zone was verified at field scale for the first time. Although ethanol retention was seen in lab tests and it was hypothesized that it could happen at field sites, its significance was never demonstrated. Ethanol retention in the unsaturated zone pore-water was verified through soil cores and NAPL recovered from the site was depleted of ethanol, as a consequence of ethanol partitioning to the unsaturated soil water.
- Downgradient transport of ethanol and selected gasoline hydrocarbons (BTEX, TMB and naphthalene) after an E10 (gasoline with 10% ethanol) release in the unsaturated zone was evaluated for the first time under well-defined field conditions. The retention of ethanol in the unsaturated zone resulted in ethanol being only detected at low concentrations downgradient, and no impact on dissolved hydrocarbon behaviour was evident.
- The effect of oscillations in the water table following an E10 spill was evaluated in the field. Oscillations of the water table with long duration were shown to bring a portion of the ethanol from the unsaturated zone to regions where horizontal transport is significant, causing slugs of ethanol to appear in the downgradient wells. Fast rise and decline of the water table only have a minor impact on ethanol distribution.

7.2 Conceptualization of Ethanol Fuel Spills

To conclude this study, a conceptual model of the fate of ethanol and gasoline hydrocarbons following an ethanol fuel spill is presented in this section.

To develop a conceptual model of ethanol fuel spills, it is useful to classify the spills into two categories: 1) spills where a significant portion of ethanol reaches the capillary fringe, and 2) spills where most of the ethanol is retained in the unsaturated zone. The consequences for groundwater contamination will be highly dependent on which of these two categories best describes the spill.

The criterion for the division is how much ethanol reaches the capillary fringe. Essentially, this is the difference between the volume of ethanol spilled and the volume of ethanol retained in the unsaturated zone. However, the volume retained in the unsaturated zone is not easily established, and it will depend on several factors, including: water content, type of soil, depth to water table, spill area, partitioning between phases and rate of infiltration. Nevertheless, a simple estimate can indicate which of the two categories is more likely.

When the mixture spilled has an ethanol fraction of less than 70%, the maximum ethanol fraction in the aqueous phase (f_e) will always be around 70%. So, the maximum volume of ethanol that can be retained in the unsaturated zone ($V_{e_{max}}$) can be approximated by equation 1, where A is the spill area, h is the distance between the spill and the top of the capillary fringe, n is porosity and $\bar{S}_w$ is the average water saturation over the height h. A more accurate estimate can be obtained applying the model described in Subsection 6.3.1.

$$V_{e_{max}} = A \cdot h \cdot n \cdot \bar{S}_w \cdot f_e \quad (1)$$

Application of equation 1 results in a prediction of the maximum value of ethanol that could be retained in the unsaturated zone, assuming that equilibrium between phases is reached during gasoline infiltration through the unsaturated zone. However, in some conditions this maximum capacity might not be attained. For example, preferential flow through fractures or macropores can limit the validity of equation 1. Also, heterogeneities in the unsaturated zone might affect the volume of porous media that is contacted by the infiltrating NAPL, also limiting the applicability of this estimate. Therefore, equation 1 provides a good way to identify spills type 1, but when the volume of ethanol spilled is less than the maximum volume that can be retained in the unsaturated zone, as estimated by equation 1, there is still a chance that significant volume of ethanol will reach the capillary fringe if equilibrium conditions are not attained or if preferential flow plays an important role.

To illustrate how this estimate can be used, equation 1 was applied for the controlled release of E10 at the Borden aquifer described in Chapter 6. The values adopted were 1.7 m^2 for the spill area, 20 cm as the distance to the top of capillary fringe, porosity of 33% and average water saturation of 30%. The maximum ethanol volume that could be retained in the unsaturated zone based on this equation is around 25 L. The volume of ethanol released was 20 L, therefore the unsaturated zone had the potential to retain all the ethanol released and the spill would be classified as type 2. This estimate is consistent with the field observations.

For spills where the ethanol fraction in the fuel is higher than 70%, aqueous concentrations as high as the concentration injected can be anticipated. For example, if the spill described at Borden was of E95 instead of E10, the maximum ethanol that could be retained in the unsaturated zone would increase to around 30 L. If the total volume of the spill is the same (200 L), the ethanol volume would also increase, to 190 L, and so the volume of ethanol reaching the capillary fringe would be around 160 L and the spill would be classified as type 1.

The same rationale can also be applied for other compounds, replacing f_e by the effective solubility of the compound. The limiting factor for the retention in the unsaturated zone will be the solubility of the compound. For example, MTBE is more soluble than any of the gasoline compounds. However, the MTBE concentration that could be expected in the unsaturated zone pore water for a gasoline containing 10% MTBE is around 6 g/L, or 0.6%. This value is 100 times less than the value expected for ethanol. Therefore, in order to have a significant retention of MTBE in the unsaturated zone, the unsaturated zone must have a very large retention capacity, which might happen in particular settings, like in sites with deep water table.

In ethanol fuel spills categorized as type 1, a significant volume of ethanol reaches the capillary fringe. This could happen for spills with high ethanol content (E95 spills, for example) or for large spill volumes of fuels with low ethanol content. Even though in spills type 1 most of the fuel mixture will reach the capillary fringe with the same composition as the initial mixture, the retention of ethanol in the unsaturated zone is likely to cause the composition of the fuel reaching the capillary fringe to vary in time. Initially, the mixture will be more depleted of its ethanol content due to ethanol retention. As the ethanol retention in the unsaturated zone approaches its maximum capacity, the concentration of ethanol in the fuel increases. The variability in the ethanol content of the fuel that reaches the saturated zone will result in a heterogeneous distribution of ethanol in the source.

In the case of spills with high ethanol content, as ethanol reaches the capillary fringe it travels downgradient at the top of the capillary fringe, as shown in the lab tests presented at Chapter 4. This ethanol is likely to transport hydrocarbons in high concentrations, due to cosolvency effects. Therefore, sampling the capillary fringe for volatile compounds will be of great importance in those cases. Chapter 5 presented a technique to allow sampling in the capillary fringe. After the ethanol that reached the capillary fringe has been transported, only the ethanol that was retained in the unsaturated zone will remain in the source (Chapter 4), and the ethanol will then behave as if the spill was initially type 2.

In spill type 1, ethanol dissolution from NAPL sources and transport downgradient from the source zone will happen quickly, with ethanol moving as a short slug (Chapter 2). In this situation, ethanol might coexist with gasoline hydrocarbon compounds in groundwater in high concentrations, and therefore the potential for ethanol impacting biodegradation is the highest. In Chapter 2 it was shown that 10% ethanol fraction in the gasoline is unlikely to impact biodegradation, but when the source is E95, the hydrocarbon biodegradation rates might be severely affected. Ethanol biodegradation might also lead to the formation of explosive levels of methane, as verified in Chapter 3.

For spills that fall within type 2, most of the ethanol in the spill is retained in the unsaturated zone pore water. The E10 release described on Chapter 6 is one example of such spills. In these cases, ethanol partitions out of the NAPL into the pore water above the capillary fringe as the NAPL infiltrates. Since the water saturation is low, the effective hydraulic conductivity to the aqueous phase is nil and ethanol is not transported horizontally. It was shown in Chapter 6 that the ethanol concentrations in the unsaturated zone remained relatively unaltered for more than 100 days, despite oscillations in the water table. The retention of most of the ethanol despite water table oscillations is likely promoted by instabilities caused by density and viscosity contrast with the clean water phase. Also, the lower density and higher viscosity of the regions with high ethanol concentration will decrease the effective hydraulic conductivity, and therefore groundwater flow will tend to go around these zones, further decreasing ethanol transport. Ethanol removal from the unsaturated zone by recharge is likely to be minimized by these processes. Therefore, most of the ethanol will likely remain in the same position in the unsaturated zone through long periods; and only small portions will be released following oscillations in the water table and recharge events.

The NAPL that reaches the capillary fringe will be significantly depleted of its ethanol content. Therefore, ethanol will not impact NAPL dissolution and hydrocarbon dissolved plumes. Cosolvency

and decrease in biodegradation are not expected. A rising water table that reaches the high ethanol concentrations in the previously unsaturated zone might bring some of the ethanol to the capillary fringe with potential for significant horizontal transport. Even though ethanol flushing is limited by the processes discussed previously, the effects of the water table oscillation might still be perceptible in the elevated groundwater concentrations of ethanol downgradient the source zone. The fraction of ethanol that is flushed by water table oscillation was shown to be dependent on the duration of the oscillation cycle. For example, in the release described in Chapter 6, when the water table went up and down in a few days no significant effect was noticed. However, when the water table persisted at a shallower position for more than one month, it caused a second slug of low concentrations of ethanol to migrate downgradient in the saturated zone. Therefore, in type 2 spills where most of the ethanol was retained in the unsaturated zone, the ethanol that is transported downgradient will be in pulses but with relatively low concentrations.

In conclusion, in spills where most of the ethanol reaches the capillary fringe (spill type 1), ethanol will be transported downgradient fast and possibly in high concentrations. Hydrocarbon might also be present in higher concentrations due to cosolvency. Ethanol will coexist with gasoline hydrocarbons in the dissolved plumes and ethanol might impact biodegradation. However, if most of the ethanol is retained in the unsaturated zone (spill type 2), the dissolved plumes will not contain significant ethanol mass and ethanol impacts on hydrocarbon plumes will be minimal.

7.3 Recommendations for Future Research

This research clarified some of the ethanol impacts on groundwater contamination, but some questions remain and others have arisen from this study.

Methane formation was shown to be significant in ethanol contaminated sites and carbon isotope signature was verified to be useful in determining the source of methane. However, the pathway of ethanol degradation under methanogenic condition seems to have a significant impact on the carbon isotope signature. The isotopic fractionation between ethanol and the different intermediate by-products was not evaluated in detail in this study. A carbon isotopic study of intermediate products might improve the understanding of ethanol biodegradation.

In the field study it was shown that most of the ethanol can be retained in the unsaturated zone and this will control its impacts on saturated zone plumes of ethanol and hydrocarbons. However, in spills where the volume of ethanol surpasses the volume that can be retained in the unsaturated zone, the impacts of ethanol on hydrocarbon are expected to be more pronounced. One situation where this is likely to happen is in E95 spills on top of gasoline residuals. These have been evaluated in lab scale and significant changes in gasoline residual distribution are expected. However, the consequences of the changes in the source zone configuration remain unclear and field-scale experiments would be critical to demonstrate the consequences to dissolved hydrocarbon plumes.

The effects of heterogeneities in the unsaturated zone should be investigated. Heterogeneities might play a major role on the fate of spilled ethanol. Heterogeneous layers might determine the amount of ethanol retained, the location where it is retained and how it is going to be released during recharge events or oscillations in the water table. The impact of heterogeneities on NAPL behaviour in the unsaturated zone has been evaluated in lab tests, but based on ethanol properties it can be anticipated that it will tend to accumulate in zones with higher water saturation, associated with smaller pore sizes, contrary to the behaviour expected for NAPL's. Laboratory and field tests should be conducted to evaluate the effects of heterogeneities in the fate of ethanol fuels.

Since the unsaturated zone appears to control the extent of the impacts of ethanol, incorporating the unsaturated zone in numerical models that aim to evaluate these impacts seems to be crucial. The implementation of such models might require more detailed quantitative characterization of the unsaturated zone, including measurements of transient data on saturation, pressure and

concentrations. Efforts to better describe the phase behaviour of ethanol in those models would also be important for better predictions.

The evaluation of ethanol behaviour in the unsaturated zone over larger periods of time and different recharge conditions should also be conducted to clarify what happens over time in type 2 spills. Characterization of the contamination in the unsaturated zone and transport in the capillary fringe at field sites impacted by ethanol spills would also be of interest. Sampling techniques adequate for different soil types, particularly with the presence of silts and clays in high fraction, need to be developed to facilitate investigation of ethanol fuel contaminated sites.

References

Chapter 1 References

ANP - Agencia Nacional do Petróleo, Gás Natural e Biocombustíveis (National Petroleum, Gas and Biofuels Agency). 2009. Biofuels. http://www.anp.gov.br/biocombustiveis/biocombustiveis.asp. (accessed August 3, 2009).

Berkowitz, B.; Silliman, S.E.; Dunn, A.M. 2004. Impact of capillary fringe on local flow, chemical migration, and microbiology. *Vadose Zone Journal* 3, no. 2: 354-548.

Brooks, M.C., M.D. Annable, Rao PSC, K. Hatfield, J.W. Jawitz, W.R. Wise, A.L.Wood and C.G. Enfield. 2004. Controlled release, blind test of DNAPL remediation by ethanol flushing. *Journal of Contaminant Hydrology* 69, no. 3-4: 281-297.

Chen, Y.D., J.F. Barker and L. Gui. 2008. A strategy for aromatic hydrocarbon bioremediation under anaerobic conditions and the impacts of ethanol: A microcosm study. *Journal of Contaminant Hydrology* 96, no. 1-4: 17–31.

Corseuil, H.X., C.S. Hunt, R.C.F. Santos and P.J.J. Alvarez. 1998. The influence of the gasoline oxygenate ethanol on aerobic and anaerobic BTX biodegradation. *Water Research* 32, no. 7: 2065-2072.

Corseuil, H.X., B.I.A. Kaipper and M. Fernandes. 2004. Cosolvency effect in subsurface systems contaminated with petroleum hydrocarbons and ethanol. *Water Research* 38, no. 6: 1449-1456.

Da Silva, M.L.B and P.J.J. Alvarez. 2002. Effects of ethanol versus MTBE on benzene, toluene, ethylbenzene, and xylene natural attenuation in aquifer columns. *Journal of Environmental Engineering* 128, no. 9: 862-867.

Deeb, R.A., J.O. Sharp, A. Stocking, S. McDonald, K.A. West, M. Laugier, P.J.J. Alvarez, M.C. Kavanaugh and L. Alvarez-Cohen. 2002. Impact of ethanol on benzene plume lengths: Microbial and modeling studies. *Journal of Environmental Engineering* 128, no. 9: 868-875.

Deeb, R.A., K.H. Chu, T. Shih, S. Linder and I. Suffet, M.C. Kavanaugh and L. Alvarez-Cohen. 2003. MTBE and other oxygenates: Environmental sources, analysis, occurrence, and treatment. *Environmental Engineering Science* 20, no. 5: 433-447.

Dominguez-Faus, R., S.E. Powers, J.G. Burken and P.J. Alvarez. 2009. The Water Footprint of Biofuels: A Drink or Drive Issue? *Environmental Science and Technology* 43, no. 9: 3005-3010.

Fletcher, B. 2007. Evaluation of carbon and hydrogen isotope fingerprinting of methane from ethanol degradation. MSc Thesis, Department of Earth Sciences, University of Waterloo.

Fraiture, C., M. Giordano and Y. Liao. 2008. Biofuels and implications for agricultural water use: Blue impacts of green energy. *Water Policy* 10, no. 1: 67–81.

Frazer, A.C., P.W. Coschigano and L.Y. Young. 1995. Toluene metabolism under anaerobic conditions: A review. *Anaerobe* 1, no. 6: 293-303.

Freitas, J.G. and J.F. Barker. 2008. Sampling VOCs with porous suction samplers in the presence of ethanol: How much are we losing? *Ground Water Monitoring & Remediation* 28, no. 3: 83-92.

Freitas, J.G., B. Fletcher, R. Aravena and J.F. Barker. in submission. Methane production and isotopic fingerprinting in ethanol fuel contaminated sites. *Ground Water*.

Goldemberg, J. 2008. The challenge of biofuels. *Energy & Environmental Science* 1, no. 5: 523-525.

Gomez, D.E., P.C. de Blanc, W.G. Rixey, P.B. Bedient and P.J.J. Alvarez. 2008. Modeling benzene plume elongation mechanisms exerted by ethanol using RT3D with a general substrate interaction module. *Water Resources Research* 44, no. 5: W05405.

Granda, C.B., L. Zhu and M.T. Holtzapple. 2007. Sustainable liquid biofuels and their environmental impact. *Environmental Progress* 26, no. 3: 233-250.

Heermann, S.E., and S.E. Powers. 1998. Modeling the Partitioning of BTEX in Water-Reformulated Gasoline Systems Containing Ethanol. *Journal of Contaminant Hydrology* 34, no. 4: 315–341.

Henry, E.J. and J.E. Smith. 2003. Surfactant-induced flow phenomena in the vadose zone: A review of data and numerical modeling. *Vadose Zone Journal* 2, no. 2: 154-167.

Hubbard, C.E., J.F. Barker, S.F. O'Hannesin, M. Vandergriendt and R.W. Gillham. 1994 Transport and fate of dissolved methanol, methyl-tertiary-butyl-ether, and monoaromatic hydrocarbons in a shallow sand aquifer. Washington, DC: API Publication 4601, American Petroleum Institute.

Jawitz, J.W., M.D. Annable and P.S.C. Rao. 1998. Miscible fluid displacement stability in unconfined porous media: Two-dimensional flow experiments and simulations. *Journal of Contaminant Hydrology* 31, no. 3-4: 211–230.

Jawitz, J.W., R.K. Sillan, M.D. Annable, P.S.C. Rao, K. Warner. 2000. In situ alcohol flushing of a DNAPL source zone at a dry cleaner site. *Environmental Science & Technology* 34, no. 17: 3722-3729.

Leite, M. 2008. Demon biofuel? Brazil disputes attacks. *The Interdependent* 6, no. 2: 14-15.

Lovanh, N., C.S. Hunt and P.J.J. Alvarez. 2002. Effect of ethanol on BTEX biodegradation kinetics: Aerobic continuous culture experiments. *Water Research* 36, no. 15: 3739–3746.

Luque, R., L. Herrero-Davila, J.M. Campelo, J.H. Clark, J.M. Hidalgo, D. Luna, J.M. Marinas and A.A. Romero. 2008. Biofuels: a technological perspective. *Energy & Environmental Science* 1, no. 5: 542–564.

Mackay, D.M., N.R. De Sieyes, M.D. Einarson, K.P. Feris, A.A. Pappas, I.A. Wood , L. Jacobson, L.G. Justice, M.N. Noske, K.M. Scow and J.T. Wilson. 2006. Impact of ethanol on the natural attenuation of benzene, toluene, and o-xylene in a normally sulfate-reducing aquifer. *Environmental Science & Technology* 40, no. 19: 6123-6130.

McDowell, C.J., T. Buschek, and S.E. Powers. 2003. Behaviour of Gasoline Pools Following a Denatured Ethanol Spill. *Ground Water* 41, no. 6: 746-757.

Mocanu, M.T. 2007. Behaviour of Oxygenates and Aromatic Hydrocarbons in Groundwater from Gasoline Residuals. M.Sc. Thesis, Department of Earth Sciences, University of Waterloo.

Molson J.W., J.F. Barker, E.O. Frind and M. Schirmer. 2002. Modeling the impact of ethanol on the persistence of benzene in gasoline-contaminated groundwater. *Water Resources Research* 38, no. 1: 1003.

Morris, K.R., R. Abramowitz, R. Pinal, P. Davis and S.H. Yalkowsky. 1988. Solubility of aromatic pollutants in mixed-solvents. *Chemosphere* 17, no. 2: 285-298.

Muller, A., J. Schmidhuber, J. Hoogeveen and P. Steduto. 2008. Some insights in the effect of growing bio-energy demand on global food security and natural resources. *Water Policy* 10, no. 1: 83-94.

Nadim, F., P. Zack, G.E. Hoag and S. Liu. 2001. United States experience with gasoline additives. *Energy Policy* 29, no. 1: 1-5.

Oliveira, E. 1997. Ethanol flushing of Gasoline Residuals: Microscale and Field Experiments. Ph.D dissertation, Department of Earth Sciences, University of Waterloo.

Palomino, A.M., and D.G. Grubb. 2004. Recovery of dodecane, octane and toluene spills in sandpacks using ethanol. *Journal of Hazardous Materials* 110, no. 1-3: 39–51.

Pantazidou, M., and N. Sitar. 1993. Emplacement of Nonaqueous Liquids in the Vadose Zone. *Water Resources Research* 29, no. 3: 705-722.

Parker J.C. 1989. Multiphase flow and transport in porous-media. *Reviews of Geophysics* 27, no. 3: 311-328.

Phelps, C.D. and L.Y. Young. 1999. Anaerobic biodegradation of BTEX and gasoline in various aquatic sediments. *Biodegradation* 10, no. 1: 15–25.

Powers, S.E., C.S. Hunt; S.E. Heermann, H.X. Corseuil, D. Rice and P.J.J. Alvarez. 2001. The transport and fate of ethanol and BTEX in groundwater contaminated by gasohol. *Critical Reviews in Environmental Science and Technology* 31, no. 1: 79–123.

Ronen, D.; Scher, H.; Blunt, M. 1997. On the structure and flow processes in the capillary fringe on phreatic aquifers. *Transport in Porous Media* 28, no. 2: 159-180.

Scharlemann, J.P.W. and W.F. Laurance. 2008. How Green Are Biofuels? *Science* 319, no. 5859: 43-44.

Schroth, M.H., J.D. Istok, S.J. Ahearn and J.S. Selker. 1995. Geometry and position of light nonaqueous-phase liquid lenses in water-wetted porous media. *Journal of Contaminant Hydrology* 19, no. 4: 269-287.

Stafford, B.P., N.L. Cápiro, P.J.J. Alvarez, and W.G. Rixey. 2009. Pore water characteristics following a release of neat ethanol onto pre-existing NAPL. *Ground Water Monitoring & Remediation* 29, no. 3: 93–104

Wilson, R.D., S.F. Thornton and D.M. Mackay. 2004. Challenges in monitoring the natural attenuation of spatially variable plumes. *Biodegradation* 15, no. 6: 359–369.

Yu, S., J.G. Freitas, A.J.A. Unger, J.F. Barker and J. Chatzis. 2009. Simulating the evolution of an ethanol and gasoline source zone within the capillary fringe. *Journal of Contaminant Hydrology* 105, no. 1-2: 1-17.

Zoby, J.L. 2006. Atenuação Natural de Pluma de Contaminação de Gasolina e Etanol em Água Subterrânea. Ph.D. Thesis, Universidade de São Paulo.

Chapter 2 References

Alvarez, P.J.J., P.J. Anid and T.M. Vogel. 1991. Kinetics of aerobic biodegradation of benzene and toluene in sandy aquifer material. *Biodegradation* 2, no. 1: 43-51.

Alvarez, P.J.J. and C.H. Hunt. 2002. The effect of fuel alcohol on monoaromatic hydrocarbon biodegradation and natural attenuation: Review article. *Revista Latinoamericana de Microbiologia* 44, no. 02: 83-104.

Barcelona, M.J., J.A. Helfrich, E.E. Garske and J.P. Gibb. 1984. A laboratory evaluation of ground water sampling mechanisms. *Ground Water Monitoring & Remediation* 4, no. 2: 32-41.

Barcelona, M.J., J. Lu and D.M. Tomczak. 1995. Organic acid derivatization techniques applied to petroleum hydrocarbon transformations in subsurface environments. *Ground Water Monitoring and Remediation* 15, no. 2: 114-124.

Barker, J.F., G.C. Patrick, L. Lemon and G.M. Travis. 1987. Some biases in sampling multilevel piezometers for volatile organics. Ground Water Monitoring & Remediation 7, no. 2: 48-54.

Bauer, R.D., M. Rolle, S. Bauer, C. Eberhardt, P. Grathwohl, O. Kolditz, R.U. Meckenstock, and C. Griebler. 2009. Enhanced biodegradation by hydraulic heterogeneities in petroleum hydrocarbon plumes. *Journal of Contaminant Hydrology* 105, no. 1-2: 56–68.

Bekins, B.A., E. Warren and M. Godsy. 1998. A comparison of zero-order, first-order, and Monod biotransformation models. *Ground Water* 36, no. 2: 261-268.

Chang, M.K., T.C. Voice and C.S. Criddle. Kinetics of competitive-inhibition and cometabolism in the biodegradation of benzene, toluene, and p-xylene by 2 pseudomonas isolates. *Biotechnology and Bioengineering* 41, no. 11: 1057-1065.

Chen, Y.D., J.F. Barker and L. Gui. 2008. A strategy for aromatic hydrocarbon bioremediation under anaerobic conditions and the impacts of ethanol: A microcosm study. *Journal of Contaminant Hydrology* 96, no. 1-4: 17-31.

Cirpka, O.A., Frind, E.O. and R. Helmig. 1999. Numerical simulation of biodegradation controlled by transverse mixing. *Journal of Contaminant Hydrology* 40, no. 2: 159-182.

Cirpka, O.A. and A.J. Valocchi. 2007. Two-dimensional concentration distribution for mixing-controlled bioreactive transport in steady state. *Advances in Water Resources* 30, no. 6-7: 1668-1679.

Corseuil, H.X., C.S. Hunt, R.C.F. Santos and P.J.J. Alvarez. 1998. The influence of the gasoline oxygenate ethanol on aerobic and anaerobic BTX biodegradation. *Water Research* 32, no. 7: 2065-2072.

Corseuil, H.X., B.I.A. Kaipper, and M. Fernandes. 2004. Cosolvency effect in subsurface systems contaminated with petroleum hydrocarbons and ethanol. *Water Research* 38, no. 6: 1449-1456.

Deeb, R.A., J.O. Sharp, A. Stocking, S. McDonald, K.A. West, M. Laugier, P.J.J. Alvarez, M.C. Kavanaugh, L. Alvarez-Cohen. 2002. Impact of ethanol on benzene plume lengths: microbial and modeling studies. *Journal of Environmental Engineering* 128, no. 9: 868-875.

Devlin, J.F., G. Tsoflias, M. McGlashan and P. Schillig. 2009. An inexpensive multilevel array of sensors for direct ground water velocity measurement. *Ground Water Monitoring & Remediation* 29, no. 2: 73-77.

Einarson, M.D. 2001. New low-cost, multi-level groundwater monitoring system. M.Sc. diss., Department of Earth Sciences, University of Waterloo.

Fang, J., M.J. Barcelona, R.V. Krishnamurthy and E.A. Atekwana. 2000. Stable carbon isotope biogeochemistry of a shallow sand aquifer contaminated with fuel hydrocarbons. *Applied Geochemistry* 15, no.2: 157-169

Fraser, M.J., J.F. Barker, B.J. Butler, F. Blaine, S. Joseph and C. Cook. 2008. Natural attenuation of a plume from an emplaced coal tar creosote source over 14 years. *Journal of Contaminant Hydrology* 100, no. 3-4: 101-115.

Gomez, D.E., P.C. de Blanc, W.G. Rixey, P.B. Bedient and P.J.J. Alvarez. 2008. Modeling benzene plume elongation mechanisms exerted by ethanol using RT3D with a general substrate interaction module. *Water Resources Research* 44, no. 5: W0545.

Grathwohl, P., C. Eberhardt, I. Klenk, H. Ruegner and U. Maier. 2000. Transverse vertical dispersivity in aquifer materials: Implications on mass transfer across the capillary fringe and the length of steady state plumes. In *Proceedings of the International Conference on Groundwater Research*, eds. P.L. Bjerg, P. Engesgaard and Th.D. Krom, 19-20. Rotterdam, Netherlands: A.A. Balkema.

Hubbard, C.E., J.F. Barker, S.F. O'Hannesin, M. Vandergriendt and R.W. Gillham. 1994 Transport and fate of dissolved methanol, methyl-tertiary-butyl-ether, and monoaromatic hydrocarbons in a shallow sand aquifer. Washington, DC: API Publication 4601, American Petroleum Institute.

Kim, I.S., Young, J.C., Tabak, H.H., 1994. Kinetics of acetogenesis and methanogenesis in anaerobic reactions under toxic conditions. *Water Environment Research* 66, no. 2: 119–132.

King, M.W.G., J.F. Barker, J.F. Devlin and B.J. Butler. 1999. Migration and natural fate of a coal tar creosote plume 2. Mass balance and biodegradation indicators. *Journal of Contaminant Hydrology* 39, no. 3-4: 281-307.

Kubert, M. and M. Finkel. 2006. Contaminant mass discharge estimation in groundwater based on multi-level point measurements: A numerical evaluation of expected errors. *Journal of Contaminant Hydrology* 84, no. 1-2: 55– 80.

Lovanh, N., C.S. Hunt and P.J.J. Alvarez. 2002. Effect of ethanol on BTEX biodegradation kinetics: aerobic continuous culture experiments. *Water Research* 36, no. 15: 3739–3746.

Li, K.B., Goovaerts, P. and L.M. Abriola. 2007. A geostatistical approach for quantification of contaminant mass discharge uncertainty using multilevel sampler measurements. *Water Resources Research* 43 (6): W06436.

Mackay, D.M., D.L. Freyberg, P.V. Roberts and J.A. Cherry. 1986. A natural gradient experiment on solute transport in a sand aquifer 1. Approach and overview of plume movement. *Water Resources Research* 22, no. 13: 2017-2029.

Mackay, D.M., N.R. De Sieyes, M.D. Einarson, K.P. Feris, A.A. Pappas, I.A. Wood , L. Jacobson, L.G. Justice, M.N. Noske, K.M. Scow and J.T. Wilson. 2006. Impact of ethanol on the natural attenuation of benzene, toluene, and o-xylene in a normally sulfate-reducing aquifer. *Environmental Science & Technology* 40 (19): 6123-6130.

Mocanu, M.T. 2007. Behaviour of Oxygenates and Aromatic Hydrocarbons in Groundwater from Gasoline Residuals. M.Sc. Thesis, Department of Earth Sciences, University of Waterloo.

Molson, J.W., J.F. Barker, E.O. Frind, M. Schirmer. 2002a. Modeling the impact of ethanol on the persistence of benzene in gasoline-contaminated groundwater. *Water Resources Research* 38, no. 1: 1003.

Molson, J.W., E.O. Frind, D.R. van Stempvoort and S. Lesage. 2002b. Humic acid-enhanced remediation of an emplaced diesel source in groundwater 2: Numerical model development and application. *Journal of Contaminant Hydrology* 54, no. 3-4: 277-305.

Molson, J.W. 2007. BIONAPL/3D User guide: A 3D model for groundwater flow, multi-component NAPL dissolution and biodegradation.

Molson, J.W., M.T. Mocanu and J.F. Barker. 2008. Numerical analysis of buoyancy effects during the dissolution and transport of oxygenated gasoline in groundwater. *Water Resources Research* 44, no 7: W07418.

Morris, K.R., R. Abramowitz, R. Pinal, P. Davis, and S.H. Yalkowsky. 1988. Solubility of aromatic pollutants in mixed solvents. *Chemosphere* 17, no.2: 285-298.

Parker, L.V. 1994. The effects of ground water sampling devices on water quality: A literature review. *Ground Water Monitoring & Remediation* 14, no.2: 130-141.

Patrick, G.C. 1986. A Natural Gradient Tracer Experiment of Dissolved Benzene, Toluene and Xylenes in a Shallow Sand Aquifer. M.Sc. thesis, Department of Earth Sciences, University of Waterloo.

Poulsen, M., L. Lemon and J.F. Barker. 1992. Dissolution of monoaromatics hydrocarbons into groundwater from gasoline-oxygenate mixtures. *Environmental Science and Technology* 26, no.12: 2483-2489.

Powers, S.E., C.S. Hunt, S.E. Heermann, H.X. Corseuil, D. Rice and P.J.J. Alvarez. 2001. The transport and fate of ethanol and BTEX in groundwater contaminated by gasohol. *Critical Reviews in Environmental Science and Technology* 31, no. 1:79–123.

Prince, R.C., T.F. Parkerton and C. Lee. 2007. The primary aerobic biodegradation of gasoline hydrocarbons. *Environmental Science & Technology* 41, no. 9: 3316-3321.

Renewable Fuels Association - RFA. 2008. Changing the Climate - Ethanol Industry Outlook 2008. Washington, DC: RFA.

Schirmer, M., J.W. Molson, E.O. Frind and J.F. Barker. 2000. Biodegradation modelling of a dissolved gasoline plume applying independent laboratory and field parameters. *Journal of Contaminant Hydrology* 46, no. 4: 339-374.

Schwarzenbach, R.P., P.M. Gschwend, and D.M. Imboden. 2003. *Environmental Organic Chemistry*, 2nd ed. Hoboken, N.J.: John Wiley & Sons.

Smith, M.R. 1990. The biodegradation of aromatic hydrocarbons by bacteria. *Biodegradation* 1, no. 2-3: 191-206.

Stafford, B.P., N.L. Cápiro, P.J.J. Alvarez, and W.G. Rixey. 2009. Pore water characteristics following a release of neat ethanol onto pre-existing NAPL. *Ground Water Monitoring & Remediation* 29, no. 3: 93–104.

Sudicky, E.A. 1986. A natural gradient experiment on solute transport in a sand aquifer: Spatial variability of hydraulic conductivity and its role in the dispersion process. *Water Resources Research*, 22, no. 13: 2069-2082.

Tao, Y., A. Fishman, W.E. Bentley and T.K. Wood. 2004. Oxidation of benzene to phenol, catechol, and 1,2,3-trihydroxybenzene by toluene 4-monooxygenase of *Pseudomonas mendocina* KR1 and toluene 3-Monooxygenase of *Ralstonia pickettii* PKO1. *Applied and Environmental Microbiology* 70, no.7: 3814–3820.

Tuxen, N., H.J. Albrechtsen and P.L. Bjerg. 2006. Identification of a reactive degradation zone at a landfill leachate plume fringe using high resolution sampling and incubation techniques. *Journal of Contaminant Hydrology* 85, no. 3-4: 179-194.

Yang, T. 2008. Investigation of residual gasoline in the GMT and E10 sources in Borden aquifer. MSc Thesis, Department of Earth Sciences, University of Waterloo, Ontario, Canada.

Yerushalmi L., J.F. Lascourreges and Guiot S.R. 2002. Kinetics of benzene biotransformation under microaerophilic and oxygen-limited conditions. *Biotechnology and Bioengineering* 79, no. 3: 347-355.

Yu, H., B.J. Kim and B.E. Rittmann. 2001a. The roles of intermediates in biodegradation of benzene, toluene and *p*-xylene by *Pseudomonas putida* F1. *Biodegradation* 12, no. 6: 455-463.

Yu, H., B.J. Kim and B.E. Rittmann. 2001b. A two-step model for the kinetics of BTX degradation and intermediate formation by *Pseudomonas putida* F1. *Biodegradation* 12, no. 6: 465-475.

Werth, C.J., O.A. Cirpka and P. Grathwohl. 2006. Enhanced mixing and reaction through flow focusing in heterogeneous porous media. *Water Resources Research* 42, no. 12: W12414.

Williams, E.C. 2007. Effect of ethanol on BTEX biodegradation in aerobic aquifer systems. M.Sc. thesis, Department of Earth Sciences, University of Waterloo.

Wu, M., Hickey, R., 1996. n-Propanol production during ethanol degradation using anaerobic granules. *Water Research* 30, no. 7: 1686–1694.

Zoby, J.L. 2006. Atenuação Natural de Pluma de Contaminação de Gasolina e Etanol em Água Subterrânea. Ph.D. Thesis, Universidade de São Paulo.

Chapter 3 References

Abrajano, T.A., N.C. Sturchio, B.M. Kennedy, G.L. Lyon, K. Muehlenbachs and J.K. Bohlke. 1990. Geochemistry of reduced gas related to serpentinization of the Zambales ophiolite, Philippines. *Applied Geochemistry* 5, no. 5-6: 625-630.

Ahad, J.M.E., B.S. Lollar, E.A. Edwards, G.F. Slater and B.E. Sleep. 2000. Carbon isotope fractionation during anaerobic biodegradation of toluene: implications for intrinsic bioremediation. *Environmental Science & Technology* 34, no. 5: 892-896.

Alvarez, P.J.J. and C.H. Hunt. 2002. The effect of fuel alcohol on monoaromatic hydrocarbon biodegradation and natural attenuation. Review article. *Revista Latinoamericana de Microbiologia* 44, no. 2: 83-104.

Aravena, R., and L.I. Wassenaar. 1993. Dissolved organic carbon and methane in a regional confined aquifer, Southern Ontario, Canada: Carbon isotope evidence for associated subsurface sources. *Applied Geochemistry* 8, no. 5: 483-493.

Aravena, R., L. Wassenaar and J.F. Barker. 1995. Distribution and isotopic characterization of methane in a confined aquifer in southern Ontario, Canada. *Journal of Hydrology* 173, no. 1-4: 51-71.

Aravena, R., S.M. Harrison, J.F. Barker, H. Abercrombie and D. Rudolph. 2003. Origin of methane in the Elk Valley coalfield, southeastern British Columbia, Canada. *Chemical Geology* 195, no. 1-4: 219– 227.

Barker, J.F. and P. Fritz. 1981a. Carbon isotope fractionation during microbial methane oxidation. *Nature* 293, no. 5830: 289-291.

Barker, J.F. and P. Fritz. 1981b. The occurrence and origin of methane in some groundwater flow systems. *Canadian Journal of Earth Sciences* 18, no. 12: 1802-1816.

Boutton, T.W., 1996. Stable carbon isotopes ratios of soil organic matter and their use of indicators of vegetation and climate change. In: *Mass Spectrometry of Soils*, ed. T.W. Boutton and S. Yamasaki, 47-82. New York: Dekker.

CETESB. 2007a. Processo CETESB (site BR1). Consulted on November 2007. Sao Paulo, SP: CETESB.

CETESB. 2007b. Processo CETESB (site BR4). Consulted on November 2007. Sao Paulo, SP: CETESB.

CETESB. 2007c. Processo CETESB (site BR3). Consulted on November 2007. Sao Paulo, SP: CETESB.

Chen, Y.D., J.F. Barker and L. Gui. 2008. A strategy for aromatic hydrocarbon bioremediation under anaerobic conditions and the impacts of ethanol: A microcosm study. *Journal of Contaminant Hydrology* 96, no. 1-4: 17-31.

Clark, I.D. and P. Fritz. 1997. Environmental Isotopes in Hydrogeology. Boca Raton: Lewis Publishers.

Coleman, D. D., C.L. Liu and K.M. Riley. 1988. Microbial methane in the shallow Paleozoic sediments and glacial deposits of Illinois, U.S.A. *Chemical Geology* 71, no. 1-3: 23-40.

Conrad, R., T.J. Phelps and J.G. Zeikus. 1985. Gas metabolism evidence in support of the juxtaposition of hydrogen-producing and methanogenic bacteria in sewage sludge and lake sediments. *Applied and Environmental Microbiology* 50, no. 3: 595-601.

Conrad, M.E., P.F. Daley, M.L. Fischer, B.B. Buchanan, T. Leighton and M. Kashgarian. 1997. Combined ^{14}C and $\delta^{13}C$ monitoring of in situ biodegradation of petroleum hydrocarbons. *Environmental Science and Technology* 31, no. 5: 1463-1469.

Conrad, M.E., P.F. Templeton, P.F. Daley and L. Alvarez-Cohen. 1999. Isotopic evidence for biological controls on migration of petroleum hydrocarbons. *Organic Geochemistry* 30, no. 8A: 843-859.

Corseuil, H.X., C.S. Hunt, R.C.F. Santos and P.J.J. Alvarez. 1998. The influence of the gasoline oxygenate ethanol on aerobic and anaerobic BTX biodegradation. *Water Research* 32, no. 7: 2065-2072.

Cramer, B., H.S. Poelchau, P. Gerlingb, N.V. Lopatin and R. Littke. 1999. Methane released from groundwater: the source of natural gas accumulations in northern West Siberia. *Marine and Petroleum Geology* 16, no. 3: 225-244.

Dempster, H.S., B.S. Lollar and S. Feenstra. 1997. Tracing organic contaminants in groundwater: A new methodology using compound-specific isotopic analysis. *Environmental Science and Technology* 31, no. 11: 3193-3197.

Edwards, E.A. and D. Grbic-Galic. 1994. Anaerobic degradation of toluene and o-xylene by a methanogenic consortium. *Applied and Environmental Microbiology* 60, no. 1: 313-322.

Ficker, M., K. Krastel, S. Orlicky and E. Edwards. 1999. Molecular characterization of a toluene-degrading methanogenic consortium. *Applied and Environmental Microbiology* 65, no. 12: 5576–5585.

Fletcher, B. 2007. Evaluation of carbon and hydrogen isotope fingerprinting of methane from ethanol degradation. MSc Thesis, Department of Earth Sciences, University of Waterloo.

Fraiture, C., M. Giordano and Y. Liao. 2008. Biofuels and implications for agricultural water use: Blue impacts of green energy. *Water Policy* 10, no. 1: 67–81.

Freitas, J.G. and J.F. Barker. 2008. Sampling VOCs with porous suction samplers in the presence of ethanol: How much are we losing? *Ground Water Monitoring & Remediation* 28, no. 3: 83-92.

Games, L.M. and J.M. Hayes. 1974. Carbon in ground water at the Columbus, Indiana landfill. In *Solid waste disposal by land burial in southern Indiana*, ed. D.B. Waldrip and R.V. Ruhe, 81-110. Bloomington, IN: Water Resources Research Center, Indiana University.

Gelwicks, J.T., B. Risatti and J.M. Hayes. 1989. Carbon isotope effects associated with autotrophic acetogenesis. *Organic Geochemistry* 14, no. 4: 441-446.

Granda, C.B., L. Zhu and M.T. Holtzapple. 2007. Sustainable liquid biofuels and their environmental impact. *Environmental Progress* 26, no. 3: 233-250.

Gooddy, D.C. and W.G. Darling. 2005. The potential for methane emissions from groundwaters of the UK. *Science of the Total Environment* 339, no. 1-3: 117– 126.

Harrington, R.R., S.R. Poulson, J.I. Drever, P.J.S. Colberg and E.F. Kelly. 1999. Carbon isotope systematics of monoaromatic hydrocarbons: Vaporization and adsorption experiments. *Organic Geochemistry* 30, no. 8A: 765-775.

Jenden, P.D. and I.R. Kaplan. 1986. Comparison of microbial gases from the Middle America Trench and Scripps Submarine Canyon: implications for the origin of natural gas. *Applied Geochemistry* 1, no. 6: 631-646.

Kelley, C.A., B.T. Hammer and R.B. Coffin. 1997. Concentrations and stable isotope values of BTEX in gasoline-contaminated groundwater. *Environmental Science and Technology* 31, no. 9: 2469-2472.

Kelley, C.A., N.B. DisIe and C.S. Martens. 1992. Temporal variations in the stable carbon isotopic composition of methane emitted from Minnesota peatlands. *Global Biogeochemical Cycles* 6, no. 3: 263-269.

Kim, I.S., J.C. Young, and H.H. Tabak. 1994. Kinetics of acetogenesis and methanogenesis in anaerobic reactions under toxic conditions. *Water Environment Research* 66, no. 2: 119–132.

Lide, D.R. (ed.). 2007. *Handbook of Chemistry and Physics. Internet Version 2007*, 87th ed. <http://www.hbcpnetbase.com>. Boca Raton, FL: Taylor and Francis.

LPT Enviro Inc. 2006. Summer 2006 Quarterly Monitoring Event: Denatured Alcohol Train Tanker Car Spill Project. October 2006. Ottawa, ON: LPT Enviro Inc.

McDowell, C.J., T. Buschek and S.E. Powers. 2003. Behaviour of gasoline pools following a denatured ethanol spill. *Ground Water* 41, no. 6: 746-757.

Müller, A., J. Schmidhuber, J. Hoogeveen and P. Steduto. 2008. Some insights in the effect of growing bio-energy demand on global food security and natural resources. *Water Policy* 10, no. 1: 83–94.

O'Leary, M.H. 1981. Review - Carbon isotope fractionation in plants. *Phytochemistry* 20, no. 4: 553-567.

Penning, H., P. Claus, P. Casper and R. Conrad. 2006. Carbon isotope fractionation during acetoclastic methanogenesis by *Methanosaeta concilii* in culture and a lake sediment. *Applied and Environmental Microbiology* 72, no. 8: 5648–5652.

Pessenda, L.C.R., A.S. Ribeiro, S.E.M. Gouveia, R. Aravena, R. Boulet and J.A. Bendassolli. 2004. Vegetation dynamics during the late Pleistocene in the Barreirinhas region, Maranhao State, northeastern Brazil, based on carbon isotopes in soil organic matter. *Quaternary Research* 62, no. 2: 183-193.

Powers, S.E., C.S. Hunt; S.E. Heermann, H.X. Corseuil, D. Rice and P.J.J. Alvarez. 2001. The transport and fate of ethanol and BTEX in groundwater contaminated by gasohol. *Critical Reviews in Environmental Science and Technology* 31, no. 1: 79–123.

RFA – Renewable Fuels Association. 2008. Changing the Climate - Ethanol Industry Outlook 2008. Washington, DC: RFA.

Schink, B., T.J. Phelps, B. Eichler and J.G. Zeikus. 1985. Comparison of ethanol degradation pathways in anoxic freshwater environments. *Journal of General Microbiology* 131, no. 3: 651-660.

Schoell, M. 1980. The hydrogen and carbon isotopic composition of methane from natural gases of various origins. *Geochimica et Cosmochimica Acta* 44, no. 5: 649-661.

Sherwood Lollar, B., S.K. Frape, S.M. Weise, P. Fritz, S.A. Macko and J.A. Welhan. 1993. Abiogenic methanogenesis in crystalline rocks. *Geochimica et Cosmochimica Acta* 57, no. 23-24: 5087-5097.

Smallwood, B.J., R.P. Philp and J.D. Allen. Stable carbon isotopic composition of gasolines determined by isotope ratio monitoring gas chromatography mass spectrometry. *Organic Geochemistry* 33, no. 2: 149–159.

Strapoc, D., M. Mastalerz, C. Eble, A. Schimmelmann. 2007. Characterization of the origin of coalbed gases in southeastern Illinois Basin by compound-specific carbon and hydrogen stable isotope ratios. *Organic Geochemistry* 38, no. 2: 267–287.

Sugimoto, A. and E. Wada. 1993. Carbon isotopic composition of bacterial methane in a soil incubation experiment: Contributions of acetate and CO_2/H_2. *Geochimica et Cosmochimica* Acta 57, no. 16: 4015-4027.

Thauer, R.K., K. Jungermann and K. Decker. 1977. Energy Conservation in Chemotrophic Anaerobic Bacteria. *Bacteriological Reviews* 41, no. 1: 100-180.

Van Breukelen, B.M. and J. Griffioen. 2004. Biogeochemical processes at the fringe of a landfill leachate pollution plume: potential for dissolved organic carbon, Fe(II), Mn(II), NH_4, and CH_4 oxidation. *Journal of Contaminant Hydrology* 73, no. 1-4: 181 - 205.

Ward, J.A.M., J.E. Ahad, G. Lacrampe-Couloume, G.F. Slater, E.A. Edwards and B. S. Lollar. 2000. Hydrogen isotope fractionation during methanogenic degradation of toluene: Potential for direct verification of bioremediation. *Environmental Science and Technology* 34, no. 21: 4577-4581.

Welhan, J.A. 1988. Origins of methane in hydrothermal systems. *Chemical Geology* 71, no. 1-3: 183-198

Whiticar, M.J., E. Faber and M. Schoell. 1986. Biogenic methane formation in marine and freshwater environments: CO_2 reduction vs. acetate fermentation - Isotope evidence. *Geochimica et Cosmochimica Acta* 50, no. 5: 693-709.

Widory, D. 2006. Combustibles, fuels and their combustion products: A view through carbon isotopes. *Combustion Theory and Modelling* 10, no. 5: 831 – 841.

Wu, M., Hickey, R., 1996. n-Propanol production during ethanol degradation using anaerobic granules. *Water Research* 30, no. 7, 1686–1694.

Yu, S., J.G. Freitas, A.J.A. Unger, J.F. Barker and J. Chatzis. 2009. Simulating the evolution of an ethanol and gasoline source zone within the capillary fringe. *Journal of Contaminant Hydrology* 105, no. 1-2: 1-17.

Chapter 4 References

Ageno M. and C. Frontali. 1967. Viscosity measurements of alcohol-water mixtures and the structure of water. *Proceedings of the National Academy of Sciences of the United States of America* 57 (4): 856-860.

Belda, R., J.V. Herraez and O. Diez. 2004. Rheological study and thermodynamic analysis of the binary system (water/ethanol): influence of concentration. *Physics and Chemistry of Liquids* 42 (5): 467–479.

Capiro, N.L., B.P. Stafford, W.G. Rixey, P.B. Bedient and P.J.J. Alvarez. 2007. Fuel-grade ethanol transport and impacts to groundwater in a pilot-scale aquifer tank. *Water Research* 41 (3): 656 - 664.

Conant, B.H., R.W. Gillham and C.A. Mendoza. 1996. Vapor transport of trichloroethylene in the unsaturated zone: Field and numerical modeling investigations. *Water Resources Research* 32 (1): 9-22.

Grathwohl, P., I.D. Klenk, U. Maier and S.B.F. Reckhorn. 2002. Natural attenuation of volatile hydrocarbons in the unsaturated zone and shallow groundwater plumes: Scenario-specific modelling and laboratory experiments. *Groundwater Quality: Natural and Enhanced Restoration of Groundwater Pollution* (Proceedings of the Groundwater Quality 2001 Conference held at Sheffield, UK, June 2001). IAHS Publ. 275: 141-146.

Henry, E.J., and J.E. Smith. 2002. The effect of surface-active solutes on water flow and contaminant transport in variably saturated porous media with capillary fringe effects. *Journal of Contaminant Hydrology* 56 (3-4) 247– 270.

Henry, E.J. and J.E. Smith. 2003. Surfactant-induced flow phenomena in the vadose zone: A review of data and numerical modeling. *Vadose Zone Journal* 2 (2): 154-167.

Jajuee, B., A. Margaritis, D. Karamanev and M.A. Bergougnou. 2006. Influence of dissolved hydrocarbons on volumetric oxygen mass transfer coefficient in a novel airlift contactor. *Chemical Engineering Science* 61 (12): 4111 – 4119.

Kechavarzi, C., K. Soga and T.H. Illangasekare. 2005. Two-dimensional laboratory simulation of LNAPL infiltration and redistribution in the vadose zone. *Journal of Contaminant Hydrology* 76 (3-4): 211-233.

Leverett, M.C. 1941. Capillary behavior in porous solids. Transactions of the American Institute of Mining and Metallurgical Engineers 142: 152-169.

Lide, D.R., ed. 2008. CRC Handbook of Chemistry and Physics, 88th ed. Boca Raton, FL: CRC Press/Taylor and Francis.

McDowell, C.J., T. Buschek, and S.E. Powers. 2003. Behaviour of gasoline pools following a denatured ethanol spill. *Ground Water* 41 (6): 746-757.

Oliveira, E. 1997. *Ethanol flushing of Gasoline Residuals: Microscale and Field Experiments*. Ph.D dissertation, University of Waterloo, Waterloo, Ontario, Canada. 1997.

Pantazidou, M., and N. Sitar. 1993. Emplacement of nonaqueous liquids in the vadose zone. *Water Resources Research* 29 (3): 705-722.

Parker, J.C., R.J. Lenhard and T. Kuppusamy. 1987. A parametric model for constitutive properties governing multiphase flow in porous-media. *Water Resources Research* 23 (4): 618-624.

Parker J.C. 1989. Multiphase flow and transport in porous-media. *Reviews of Geophysics* 27 (3): 311-328.

Powers, S.E., C.S. Hunt; S.E. Heermann, H.X. Corseuil, D. Rice and P.J.J. Alvarez. 2001. The transport and fate of ethanol and BTEX in groundwater contaminated by gasohol. *Critical Reviews in Environmental Science and Technology* 31 (1): 79–123.

Prince, R.C., T.F. Parkerton and C. Lee. 2007. The primary aerobic biodegradation of gasoline hydrocarbons. *Environmental Science & Technology* 41 (9): 3316-3321.

Schroth, M.H., J.D. Istok, S.J. Ahearn and J.S. Selker. 1995. Geometry and position of light nonaqueous-phase liquid lenses in water-wetted porous media. *Journal of Contaminant Hydrology* 19 (4): 269-287.

Stafford, B.P., N.L. Cápiro, P.J.J. Alvarez, and W.G. Rixey. 2009. Pore water characteristics following a release of neat ethanol onto pre-existing NAPL. *Ground Water Monitoring & Remediation* 29 (3): 93–104

Wyckoff, R.D., H.G. Botset and M. Muskat. 1932. Flow of liquids through porous media under the action of gravity. *Physics-A Journal of General and Applied Physics* 3 (1): 90-113.

Yu , S.Y., J.G. Freitas, A.J.A. Unger, J.F. Barker, J. Chatzis. 2009. Simulating the evolution of an ethanol and gasoline source zone within the capillary fringe. Journal of Contaminant Hydrology 105 (1-2): 1–17.

Chapter 5 References

Ballestero, T., B. Herzog, and G. Thompson. 2006. Monitoring and sampling the vadose zone. In *Practical Handbook of Environmental Site Characterization and Ground-Water Monitoring*, ed. D. M. Nielsen. 2nd ed., 207-247. USA: CRC Press, Taylor & Francis Group.

Barker, J.F., and R. Dickhout. 1988. An evaluation of some systems for sampling gas-charged ground-water for volatile organic analysis. *Ground Water Monitoring and Remediation* 8, no. 4: 112-120.

Beier, C., and K. Hansen. 1992. Evaluation of porous cup soil-water samplers under controlled field conditions: Comparison of ceramic and PTFE cups. *European Journal of Soil Science* 43, no. 2: 261-271.

Broholm, M.M., J.-A Gao, M. Christophersen, and P. Kjeldsen. 2002. Dissolution of hydrocarbon vapours in porewater in the vadose zone. Field experiment at Værløse Airforce Base, Denmark. In *Proceedings of the 1st International Workshop on Groundwater Risk Assessment at Contaminated Sites (GRACOS)*, ed. D. Halm and P. Grathwohl, 191-194. Tübingen: Dipl.-Geol. Björn Sack-Kühner.

Cápiro, N.L., B.P. Stafford, W.G. Rixey, P.B. Bedient, and P.J.J. Alvarez. 2007. Fuel-grade ethanol transport and impacts to groundwater in a pilot-scale aquifer tank. *Water Research*, 41, no. 3: 656-664.

Corseuil, H.X., B.I.A. Kaipper, and M. Fernandes. 2004. Cosolvency effect in subsurface systems contaminated with petroleum hydrocarbons and ethanol. *Water Research* 38, no. 6: 1449-1456.

Einarson, M.D. 2001. New low-cost, multi-level groundwater monitoring system. M.Sc. diss., Department of Earth Sciences, University of Waterloo.

Everett, L.G. and L.G. McMillion. 1985. Operational ranges for suction lysimeters. *Ground Water Monitoring & Remediation*, 5 no. 3: 4-80.

Everett, L.G., L.G. McMillion, and L.A. Eccles. 1988. Suction lysimeter operation at hazardous waste sites. In *Ground-water Contamination: Field Methods*, ed. A. G. Collins and A. I. Johnson, 304-327. Philadelphia: American Society for Testing and Materials.

Grossmann, J., and P. Udluft. 1991. The extraction of soil-water by the suction-cup method: A review. *European Journal of Soil Science* 42, no. 1: 83-93.

Harley, R.A., S.C. Coulter-Burke, and T.S. Yeung. 2000. Relating liquid fuel and headspace vapor composition for California reformulated gasoline samples containing ethanol. *Environmental Science & Technology* 34, no. 19: 4088-4094.

Heermann, S.E., and S.E. Powers. 1998. Modeling the partitioning of BTEX in water-reformulated gasoline systems containing ethanol. *Journal of Contaminant Hydrology* 34, no. 4: 315-341.

Helsel, D.R. and R.M. Hirsch. 1992. *Statistical Methods in Water Resources – Studies in Environmental Science 49*, Netherlands: Elsevier Science Publishers.

Jonge, H., P. Moldrup, M. Kjærgaard, and K. Dahlstrøm. 2003. Method evaluation of soil pore-water concentration estimates of some volatile organic compounds and phenanthrene. In *Proceedings of the 2nd International Workshop on Groundwater Risk Assessment at Contaminated Sites (GRACOS) and Integrated Soil and Water Protection (SOWA)*, ed. D. Halm and P. Grathwohl, 69-78. Tübingen: Dipl.-Geol. Björn Sack-Kühner.

Kohne, J.M. 2005. Mini suction cups and water-extraction effects on preferential solute transport. *Vadose Zone Journal* 4, no. 3: 866-880.

Lewis, D.L., A.P. Simons, W.B. Moore, and D.K. Gattie. 1992. Treating soil solution samplers to prevent microbial removal of analytes. *Applied and Environmental Microbiology* 58, no.1: 1-5.

Lide, D.R., ed. 2008. *CRC Handbook of Chemistry and Physics*, 88th ed. Boca Raton, FL: CRC Press/Taylor and Francis.

Linstrom, P.J. and W.G. Mallard, eds. 2005. *NIST Chemistry WebBook, NIST Standard Reference Database Number 69*, Gaithersburg MD: National Institute of Standards and Technology, (http://webbook.nist.gov).

McDowell, C.J., and S.E. Powers. 2003. Mechanisms affecting the infiltration and distribution of ethanol-blended gasoline in the vadose zone. *Environmental Science & Technology* 37, no. 9: 1803-1810.

Molson, J.W., J.F. Barker, E.O. Frind, and M. Schirmer. 2002. Modeling the impact of ethanol on the persistence of benzene in gasoline-contaminated groundwater. *Water Resources Research* 38, no. 1: 1003.

Morris, K.R., R. Abramowitz, R. Pinal, P. Davis, and S.H. Yalkowsky. 1988. Solubility of aromatic pollutants in mixed solvents. *Chemosphere* 17, no.2: 285-298.

Pankow, J.F. 1986. Magnitude of artifacts caused by bubbles and headspace in the determination of volatile compounds in water. *Analytical Chemistry* 58, no.8: 1822-1826.

Parker, L.V. 1994. The effects of ground water sampling devices on water quality: A literature review. *Ground Water Monitoring & Remediation* 14, no.2: 130-141.

Patterson, B.M., P.D. Franzmann, J.L. Rayner, and G.B. Davis. 2000. Combining coring and suction cup data to improve the monitoring of pesticides in sandy vadose zones: a field-release experiment. *Journal of Contaminant Hydrology* 46, no. 1-2: 187-204.

Perrin-Ganier, C., M. Schiavon, J.M. Portal, C. Breuzin, and M. Babut. 1993. Porous cups for pesticides monitoring in soil solution - laboratory tests. *Chemosphere* 26, no.12: 2231-2239

Poulsen, M., L. Lemon, and J.F. Barker. 1992. Dissolution of monoaromatic hydrocarbons into groundwater from gasoline-oxygenate mixtures. *Environmental Science & Technology* 26, no.12: 2483-2489.

Rais, D., B. Nowack, R. Schulin, and J. Luster. 2006. Sorption of trace metals by standard and micro suction cups in the absence and presence of dissolved organic carbon. *Journal of Environmental Quality* 35, 1:50-60

Schwarzenbach, R.P., P.M. Gschwend, and D.M. Imboden. 2003. *Environmental Organic Chemistry*, 2nd ed. Hoboken, N.J.: John Wiley & Sons.

Silkworth, D.R., and D.F. Grigal. 1981. Field comparison of soil solution samplers. *Soil Science Society of America Journal* 45, no. 2: 440-442.

Smith, J.A., H.J. Cho, P.R. Jaffé, C.L. MacLeod, and S.A. Koehlein. 1992. Sampling unsaturated-zone water for trichloroethylene at Picatinny Arsenal, New Jersey. *Journal of Environmental Quality* 21, no.2: 264-271.

Soil Moisture Equipment Corp. 2006. Porous Ceramics Catalog. http://www.soilmoisture.com/dlceramcat.html. (acessed February 23, 2006)

Strey, R., Y. Viisanen, M. Aratono, J.P. Kratohvil, Q. Yin, and S.E. Friberg. 1999. On the Necessity of Using Activities in the Gibbs Equation. *Journal of Physical Chemistry* 103, no. 43: 9112-9116.

Suarez, D.L. 1985. A soil water extractor that minimizes CO_2 degassing and pH errors. *Water Resources Research* 22, no.6: 876-880.

Weihermuller, L., R. Kasteel, J. Vanderborght, T. Putz, and H. Vereecken. 2005. Soil water extraction with a suction cup: Results of numerical simulations. *Vadose Zone Journal* 4, no.4: 899-907.

Wessel-Bothe, S. S. Patzold, C. Klein, G. Behre and G. Welp. 2000. Adsorption von Pflanzenschutzmitteln und DOC an Saugkerzen aus Glas und Keramik (Sorption of pesticides and DOC on glass and ceramic suction cups). *Journal of Plant Nutrition and Soil Science* 163, no. 1: 53-56.

Wilson, L.G., D.W. Dorrance, W.R. Bond, L.G. Everett, and S.J. Cullen. 1995. In situ pore-liquid sampling in the vadose zone. In *Handbook of Vadose Zone Characterization & Monitoring*, ed. L. G. Wilson, L. G. Everett and S. J. Cullen, 477-521. Boca Raton: Lewis Publishers.

Chapter 6 References

Abit, S.M., A. Amoozegar, M.J. Vepraskas and C.P. Niewoehner. 2008. Solute transport in the capillary fringe and shallow groundwater: Field evaluation. *Vadose Zone Journal* 7, no. 3: 890-898.

Ageno M. and C. Frontali. 1967. Viscosity measurements of alcohol-water mixtures and the structure of water. *Proceedings of the National Academy of Sciences of the United States of America* 57, no. 4: 856-860.

Alvarez, P.J.J. and C.H. Hunt. 2002. The effect of fuel alcohol on monoaromatic hydrocarbon biodegradation and natural attenuation. Review article. *Revista Latino Americana de Microbiologia* 44, no. 2: 83-104.

Araujo, D.B. 2000. Effect of fuel ethanol on subsurface microorganisms and its influence on biodegradation of BTEX compounds. MSc thesis, Department of Biology, University of Waterloo.

Barker, J.F. 1979. Methane in Groundwaters – A Carbon Isotope Geochemical Study. PhD Thesis, Department of Earth Sciences, University of Waterloo.

Belda, R., J.V. Herraez and O. Diez. 2004. Rheological study and thermodynamic analysis of the binary system (water/ethanol): influence of concentration. *Physics and Chemistry of Liquids* 42, no. 5: 467–479.

Berg, S. 2007. A device for measuring groundwater velocity in the capillary fringe. MSc thesis, Department of Earth Sciences, University of Waterloo.

Berkowitz, B., S.E. Silliman, A.M. Dunn. 2004. Impact of capillary fringe on local flow, chemical migration, and microbiology. *Vadose Zone Journal* 3, no. 2: 354-548.

Cápiro, N.L., B.P. Stafford, W.G. Rixey, P.B. Bedient and P.J.J. Alvarez. 2007. Fuel-grade ethanol transport and impacts to groundwater in a pilot-scale aquifer tank. *Water Research* 41, no. 3: 656 - 664.

Conant, B.H., R.W. Gillham and C.A. Mendoza. 1996. Vapor transport of trichloroethylene in the unsaturated zone: Field and numerical modeling investigations. *Water Resources Research* 32, no. 1: 9-22.

Corseuil, H.X., C.S. Hunt, R.C.F. Santos and P.J.J. Alvarez. 1998. The influence of the gasoline oxygenate ethanol on aerobic and anaerobic BTX biodegradation. *Water Research* 32, no. 7: 2065-2072.

Corseuil, H.X., B.I.A. Kaipper, and M. Fernandes. 2004. Cosolvency effect in subsurface systems contaminated with petroleum hydrocarbons and ethanol. *Water Research* 38, no. 6: 1449-1456.

Deeb, R.A.; J.O. Sharp, A. Stocking, S. McDonald, K.A. West, M. Laugier, P.J.J. Alvarez, M.C. Kavanaugh, and L. Alvarez-Cohen. 2002. Impact of ethanol on benzene plume lengths: microbial and modeling studies. *Journal of Environmental Engineering* 128, no. 9: 868-875.

Dullien, F.A.L. 1979. Porous Media – Fluid Transport and Pore Structure. 2nd edition. San Diego, CA: Academic Press Inc. 574 pg.

Feenstra, S., Mackay, D.M. and Cherry, J.A. 1991. A method for assessing residual NAPL based on organic chemical concentrations in soil samples. *Ground Water Monitoring and Remediation* 11, no. 2: 128-136.

Freitas, J.G. and J.F. Barker. 2008. Sampling VOCs with porous suction samplers in the presence of ethanol: How much are we losing? *Ground Water Monitoring & Remediation* 28, no. 3: 83-92.

Grathwohl, P., I.D. Klenk, U. Maier and S.B.F. Reckhorn. 2002. Natural attenuation of volatile hydrocarbons in the unsaturated zone and shallow groundwater plumes: Scenario-specific modelling and laboratory experiments. *Groundwater Quality: Natural and Enhanced Restoration of Groundwater Pollution* (Proceedings of the Groundwater Quality 2001 Conference held at Sheffield, UK, June 2001). IAHS Publ. 275: 141-146.

Gomez, D.E., P.C. de Blanc, W.G. Rixey, P.B. Bedient and P.J.J. Alvarez. 2008. Modeling benzene plume elongation mechanisms exerted by ethanol using RT3D with a general substrate interaction module. *Water Resources Research* 44, no. 5: W05405.

Heermann, S.E., and S.E. Powers. 1998. Modeling the partitioning of BTEX in water-reformulated gasoline systems containing ethanol. *Journal of Contaminant Hydrology* 34, no. 4: 315–341.

Heider, J., A.M. Spormann, H.R. Beller and F. Widdel. 1999. Review - Anaerobic bacterial metabolism of hydrocarbons. *FEMS Microbiology Reviews* 22 (1999): 459-473.

Henry, E.J. and J.E. Smith. 2003. Surfactant-induced flow phenomena in the vadose zone: A review of data and numerical modeling. *Vadose Zone Journal* 2, no. 2: 154-167.

Hewitt, A.D. 1996. Effect of collection and handling practices on concentrations of volatile organic compounds detected in soil subsamples. In *Volatile Organic Compounds in the Environment, ASTM STP 04-012610-16*, ed. W. Wang, J.L. Schnoor and J. Doi. West Conshohocken, PA: American Society for Testing and Materials. p. 170-180.

Hubbard, C.E. 1992. Transport and fate of dissolved methanol, methyl-tertiary-butyl-ether, and monoaromatic hydrocarbons in a shallow sand aquifer. MSc thesis, Department of Earth Sciences, University of Waterloo.

Jawitz, J.W., M.D. Annable, P.S.C. Rao. 1998. Miscible fluid displacement stability in unconfined porous media: two-dimensional flow experiments and simulations. *Journal of Contaminant Hydrology* 31, no. 3-4: 211–230.

Kueper, B.H., and E.O. Frind. 1988. An overview of immiscible fingering in porous media. *Journal of Contaminant Hydrology* 2, no. 2: 95-110.

Kueper, B.H., and E.O. Frind. 1991. Two-phase flow in heterogeneous porous media. 2. Model Application. *Water Resources Research* 27, no. 6: 1059-107.

Lenhard, R.J., and Parker J.C. 1990. Estimation of free hydrocarbon volume from fluid levels in monitoring wells. *Ground Water* 28, no. 1: 57-67.

Leverett, M.C. 1941. Capillary behavior in porous solids. *Transactions of the American Institute of Mining and Metallurgical Engineers* 142: 152-169.

Lide, D.R., ed. 2008. CRC Handbook of Chemistry and Physics, 88th ed. Boca Raton, FL: CRC Press/Taylor and Francis.

Lovanh, N., C.S. Hunt and P.J.J. Alvarez. 2002. Effect of ethanol on BTEX biodegradation kinetics: aerobic continuous culture experiments. *Water Research* 36, no. 15: 3739-3746.

MacFarlane, D.S. 1980. Hydrogeological Studies of an Abandoned Landfill on an Unconfined Aquifer: Physical Hydrogeology. MSc. Thesis, Department of Earth Sciences, University of Waterloo.

Mackay D.M., D.L. Freyberg and P.V. Roberts. 1986. A natural gradient experiment on solute transport in a sand aquifer: 1. Approach and overview of plume movement. *Water Resources Research* 22, no. 13: 2017-2029.

Mackay, D.M.; N.R. De Sieyes, M.D. Einarson, K.P. Feris, A.A. Pappas, I.A. Wood, L. Jacobson, L.G. Justice, M.N. Noske, K.M. Scow and J.T. Wilson. 2006. Impact of ethanol on the natural attenuation of benzene, toluene and o-xylene in a normally sulfate-reducing aquifer. *Environmental Science & Technology* 40, no. 19: 6123-6130.

McDowell, C.J., T. Buschek and S.E. Powers. 2003. Behaviour of gasoline pools following a denatured ethanol spill. *Ground Water* 41, no. 6: 746-757.

McDowell, C.J. and S.E. Powers. 2003. Mechanisms affecting the infiltration and distribution of ethanol-blended gasoline in the vadose zone. *Environmental Science and Technology* 37, no. 9: 1803-1810.

McNaughton, C.H. in preparation. High Frequency GPR Monitoring of a Shallow Gasoline Release. MSc thesis, Department of Earth and Environmental Sciences, University of Waterloo.

Mickle, R.J. 2005. A Coupled Hydrogeological-Petrophysical Analysis of Geophysical Variation in the Vadose Zone. MSc thesis, Department of Earth Sciences, University of Waterloo.

Mocanu, M.T. 2007. Behaviour of Oxygenates and Aromatic Hydrocarbons in Groundwater from Gasoline Residuals. MSc Thesis, Department of Earth Sciences, University of Waterloo.

Molson, J.W., J.F. Barker, E.O. Frind, M. Schirmer. 2002. Modeling the impact of ethanol on the persistence of benzene in gasoline-contaminated groundwater. *Water Resources Research* 38, no. 1: WR00589.

Molson, J., M. Mocanu and J. Barker. 2008 Numerical analysis of buoyancy effects during the dissolution and transport of oxygenated gasoline in groundwater. *Water Resources Research* 44, no. 7: W07418.

Morris, K.R., R. Abramowitz, R. Pinal, P. Davis, and S.H. Yalkowsky. 1988. Solubility of aromatic pollutants in mixed solvents. *Chemosphere* 17, no. 2: 285-298.

Oliveira, E. 1997. Ethanol flushing of Gasoline Residuals: Microscale and Field Experiments. Ph.D dissertation, Department of Earth Sciences, University of Waterloo.

Ott, J.B., J.R. Goates and B.A. Waite. 1979. (Solid + liquid) phase equilibria and solid-hydrate formation in water + methyl, + ethyl, + isopropyl, and + tertiary butyl alcohols. *The Journal of Chemical Thermodynamics* 11, no. 8: 739-746.

Prince, R.C., T.F. Parkerton and C. Lee. 2007. The primary aerobic biodegradation of gasoline hydrocarbons. *Environmental Science & Technology* 41, no. 9: 3316-3321.

Powers, S.E., C.S. Hunt; S.E. Heermann, H.X. Corseuil, D. Rice and P.J.J. Alvarez. 2001. The transport and fate of ethanol and BTEX in groundwater contaminated by gasohol. *Critical Reviews in Environmental Science and Technology* 31, no. 1: 79–123.

Reynolds, W.D. 2008. Chapter 75 - Saturated Hydraulic Properties: Laboratory Methods. in *Soil Sampling and Methods of Analysis*. ed. M.R. Carter and E.G. Gregorich, 1013-1024. Boca Raton, FL: CRC Press.

Ronen, D., H. Scher, M. Blunt. 1997. On the structure and flow processes in the capillary fringe on phreatic aquifers. *Transport in Porous Media* 28, no. 2: 159-180.

Schirmer, M., B.J. Butler, C.D. Church, J.F. Barker and N. Nadarajah. 2003. Laboratory evidence of MTBE biodegradation in Borden aquifer material. *Journal of Contaminant Hydrology* 60, no. 3-4: 229– 249.

Schmidt, T.C., M. Schirmer, H. Weiß and S.B. Haderlein. 2004. Microbial degradation of methyl tert-butyl ether and tert-butyl alcohol in the subsurface. *Journal of Contaminant Hydrology* 70, no. 3-4: 173– 203.

Schumacher, B.A. and M.M. Minnich. 2000. Extreme short-range variability in voc contaminated soils. *Environmental Science and Technology* 34, no. 17: 3611-3616.

Schwarzenbach, R.P., P.M. Gschwend, and D.M. Imboden. 2003. *Environmental Organic Chemistry*, 2nd ed. Hoboken, N.J.: John Wiley & Sons.

Silva, M.L.B. and P.J.J. Alvarez. 2002. Effects of ethanol versus MTBE on benzene, toluene, ethylbenzene, and xylene natural attenuation in aquifer columns. *Journal of Environmental Engineering* 128, no. 9: 862-867.

Smith, J.E., R.W. Gillham. 1999. Effects of solute concentration-dependent surface tension on unsaturated flow: Laboratory sand column experiments. *Water Resources Research* 35, no. 4: 973-982.

Soil Moisture Equipment Corp. 2006. Porous Ceramics Catalog. http://www.soilmoisture.com/dlceramcat.html. (acessed February 23, 2006).

Stafford, B.P., N.L. Cápiro, P.J.J. Alvarez, and W.G. Rixey. 2009. Pore water characteristics following a release of neat ethanol onto pre-existing NAPL. *Ground Water Monitoring & Remediation* 29, no. 3: 93–104

Sudicky, E.A. 1986. A natural gradient experiment on solute transport in a sand aquifer: spatial variability of hydraulic conductivity and its role in the dispersion process. *Water Resources Research* 22, no. 13: 2069-2082.

Thorbjarnarson, K.W., and D.M. Mackay. 1994. A forced-gradient experiment on solute transport in the Borden aquifer. 3. Nonequilibrium transport of the sorbing organic compounds. *Water Resources Research* 30, no. 2: 401-419.

Tuck, D.M., G.M. Iversen and W.A. Pirkle. 2003. Organic dye effects on dense nonaqueous phase liquids (DNAPL) entry pressure in water saturated porous media. *Water Resources Research* 39, no. 8: 1207.

van Genuchten, M.T. 1980. A closed-form equation for predicting the hydraulic conductivity of unsaturated soils. *Soil Science Society of America* 44, no. 5: 892-898.

Vakili, F. 2008. A Coupled Hydrogeological-Petrophysical Analysis of Geophysical Variation in the Vadose Zone. MSc thesis, Department of Earth Sciences, University of Waterloo.

Williams, E.C. 2007. Effect of Ethanol on BTEX Biodegradation in Aerobic Aquifer Systems. MSc thesis, Department of Earth Sciences, University of Waterloo.

Zhang, Yi, I.A. Khan, X.H. Chen and R.F. Spalding. 2006. Transport and degradation of ethanol in groundwater. *Journal of Contaminant Hydrology* 82, no. 3-4: 183– 194.

Yu, S., J.G. Freitas, A.J.A. Unger, J.F. Barker and J. Chatzis. 2009. Simulating the evolution of an ethanol and gasoline source zone within the capillary fringe. *Journal of Contaminant Hydrology* 105, no. 1-2: 1-17.

Appendices

Appendix A

Estimation of mass discharge standard deviation

$$Mass\ flux: F = \sum_{i=1}^{n} q_i \cdot C_i \cdot A_i$$

$$F = K \cdot \frac{dh}{dx} \cdot \sum_{i=1}^{n} C_i \cdot A_i$$

$$F = \underbrace{e^{lnK} \cdot \frac{dh}{dx}}_{u} \cdot \underbrace{\sum_{i=1}^{n} C_i \cdot A_i}_{v}$$

$$\sigma_u = e^{lnK} \cdot \frac{dh}{dx} \cdot \sigma_{lnK}$$

$$\sigma_v = \sqrt{\left(A_1 \cdot \sigma_{C_1}\right)^2 + \left(A_2 \cdot \sigma_{C_2}\right)^2 + \ldots + \left(A_i \cdot \sigma_{C_i}\right)^2 + \ldots + \left(A_n \cdot \sigma_{C_n}\right)^2}$$

$$\frac{\sigma_F}{F} = \sqrt{\left(\frac{\sigma_u}{u}\right)^2 + \left(\frac{\sigma_v}{v}\right)^2} = \sqrt{{\sigma_{lnK}}^2 + \left(\frac{\sigma_v}{v}\right)^2}$$

Appendix B

Ethanol partitioning based on ternary diagram

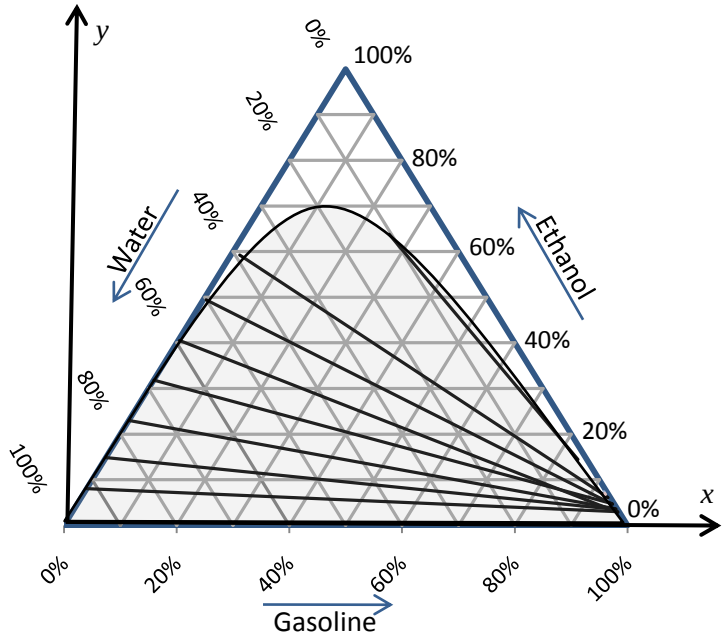

Ternary diagram describing equilibrium between ethanol, gasoline and water (after Oliveira 1997).

Position (x,y) of any mixture with ethanol, gasoline and water fractions: f_e, f_g, f_w:

$$x = f_g + f_e \cos 60°$$

$$y = f_e \sin 60°$$

Ethanol content in the aqueous phase ($c_{e,q}$) was estimated assuming that the left side of the binodal curve coincides with the water axis:

$$\frac{1}{c_{e,q}} = \sin 60° \left(\frac{1 - x}{y} + \frac{1}{\tan 60°} \right)$$

When the $c_{e,q}$ calculated was higher than 70%, the value of 70% was adopted. Comparison of calculated and experimental data is presented on the table below.

f_e	f_q	calculated $c_{e,q}$	experimental data *
7%	29%	9%	10%
16%	30%	22%	25%
23%	31%	33%	34%
28%	31%	40%	42%
36%	32%	52%	52%
43%	32%	63%	59%
49%	33%	70%	69%
54%	33%	70%	69%

* Oliveira (1997)

Appendix C

MTBE solubility and cosolvency power in the presence of ethanol

Both MTBE and ethanol act as cosolvents, increasing the solubility of hydrocarbons in water (Chen and Delfino 1997). Although MTBE has higher values of cosolvency power, usually its cosolvent effect is not important due to its relatively lower solubility in water (Chen and Delfino 1997). The phase equilibrium of water, ethanol and MTBE ternary system has been studied by Ashour (2005) and based on the ternary diagram, it was concluded that MTBE has greater affinity for the ethanol phase than for the water phase. The mole fraction of MTBE in the water phase increased from 0.78% to 3.94% when ethanol fraction in the water fraction went from 0 to 13%. Ethanol overall mole fractions higher than 20% resulted in a single phase.

Concentrations of MTBE and ethanol in the water in equilibrium with mixtures of API-91-01 gasoline, ethanol and MTBE were used to estimate MTBE solubility ($C_{i,dis}^{sol}$) and cosolvency factor (σ), using a log-linear model (equation 1) (Morris et al. 1988; Heermann and Powers 1998). The MTBE solubility and cosolvency power were determined as 66 g/L and 0.3, respectively. The results obtained are presented below.

$$\log C_i^m = \log C_{i,dis}^{sol} + \sigma \cdot f^c \quad (1)$$

measured ethanol (mg/L)	MTBE mol fraction in the NAPL	MTBE concentration		
		measured	with cosolvency	without cosolvency
1730	2.42%	1810	1600	1600
8890	2.37%	1650	1570	1560
76030	4.22%	2820	2930	2780
248000	4.57%	3630	3580	3020

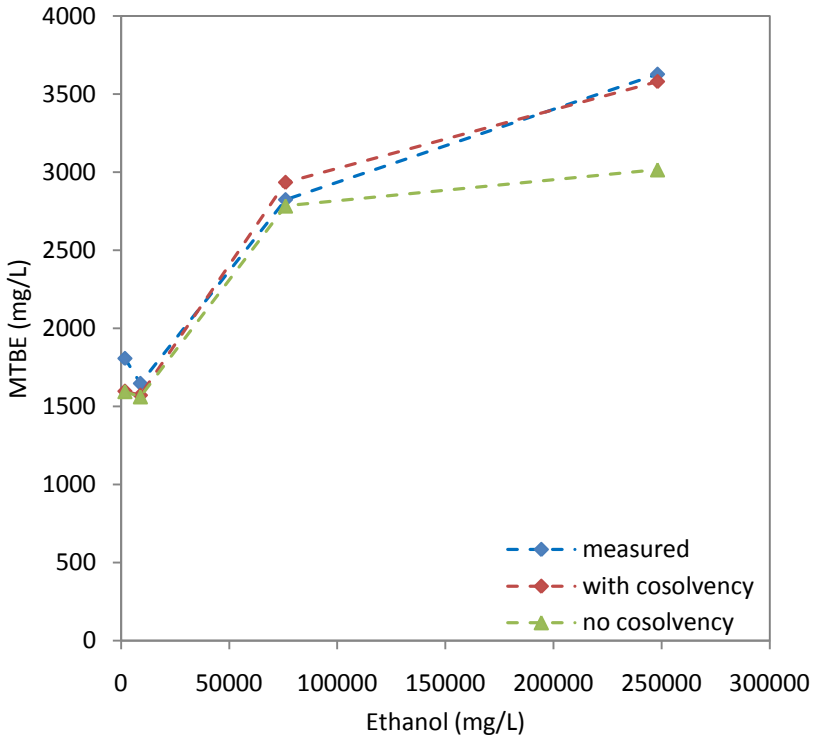

References

Ashour I. 2005. Liquid-liquid equilibrium of MTBE plus ethanol plus water and MTBE plus 1-hexanol plus water over the temperature range of 288.15 to 308.15 K. *Journal of Chemical and Engineering Data* 50, no. 1: 113-118.

Chen, C.S. and J.J. Delfino. 1997. Cosolvent effects of oxygenated fuels on PAH solubility. *Journal of Environmental Engineering – ASCE* 123, no. 4: 354-363.

Heermann, S.E., and S.E. Powers. 1998. Modeling the partitioning of BTEX in water-reformulated gasoline systems containing ethanol. *Journal of Contaminant Hydrology* 34, no. 4: 315–341.

Morris, K.R., R. Abramowitz, R. Pinal, P. Davis, and S.H. Yalkowsky. 1988. Solubility of aromatic pollutants in mixed solvents. *Chemosphere* 17, no. 2: 285-298.

Appendix D
Solution scheme for the 1-D model

Subscript definitions:

components (*c*): *e*: ethanol; *w*: water; *g*: gasoline; *m*: MTBE

phases (*p*): *q*: aqueous; *n*: NAPL

Other definitions:

V_c: volume of compound *c* in the layer;

$V_{c,p}$: volume of compound *c* in phase *p*;

V_{c/p_d}: volume of compound *c* (or phase *p*) drained from the layer;

V_{c/p_r}: volume of compound *c* (or phase *p*) remaining in the layer;

$V_{q_{max}}$: maximum volume of water that can be retained in the layer, as defined by the water saturation profile;

M_c: mass of compound *c* in the layer;

$C_{c,p}$: concentration of compound *c* in phase *p*;

f_c: overall fraction of compound *c* in the layer;

$f_{c,p}$: fraction of compound *c* in phase *p*;

Layers are identified by superscripts and timestep is presented in parentheses.

Assumptions:

phases are homogeneous and are in equilibrium within each layer, in each time step;

volume of gasoline retained is not significant;

aqueous saturation is constant;

partitioning to vapor phase is not significant;

water does not partition into the NAPL ($V_{w,n} = 0$); therefore: $V_{w,q} = V_w$;

volumes are cumulative;

For each layer, the calculations were performed at each time step as presented below, for ethanol, water and gasoline compounds and the two phases (aqueous and NAPL). The equations used for MTBE calculations are described later.

$$V_c^i(t) = \underbrace{V_c^i(t-\Delta t) - V_{c_d}^i(t-\Delta t)}_{initial\ vol.of\ c\ in\ the\ element} + \underbrace{V_{c_d}^{i-1}(t-\Delta t)}_{\substack{input\ from\ the \\ element\ above}}$$

$$f_c^i(t) = \frac{V_c^i(t)}{\sum_{c=e,w,g} V_c^i(t)}$$

With the overall fractions, the fraction of ethanol in the aqueous phase ($f_{e,q}$) was calculated as described in Appendix B. Then, the volume of ethanol in each phase is obtained as follow:

from:

$$f_{e,q}^i(t) = \frac{V_{e,q}^i(t)}{V_{w,q}^i(t) + V_{e,q}^i(t)}$$

comes:

$$V_{e,q}^i(t) = \frac{V_{w,q}^i(t)}{\frac{1}{f_{e,q}^i(t)} - 1}$$

$$V_{e,g}^i(t) = V_e^i(t) - V_{e,q}^i(t)$$

Determination of drainage volumes:

$$V_{q_d}^i(t) = V_{e,q}^i(t) + V_w^i(t) - V_{q_{max}}^i$$

$$V_{n_d}^i(t) = V_{e,g}^i(t) + V_g^i(t)$$

$$V_{w_d}^i(t) = V_{q_d}^i(t) \cdot \left(1 - f_{e,q}^i(t)\right)$$

$$V_{e_d}^i(t) = V_{q_d}^i(t) \cdot f_{e,q}^i + V_{e,g}^i(t)$$

$$V_{g_d}^i(t) = V_{n_d}^i(t) - V_{e,g}^i(t)$$

The equations used for MTBE are presented below.

$$M_m^i(t) = \underbrace{V_{n_d}^{i-1}(t-\Delta t)\cdot C_{m,n}^{i-1}(t-\Delta t)}_{\substack{input\ from\ the\ element\ above \\ through\ the\ NAPL\ phase}} + \underbrace{V_{q_d}^{i-1}(t-\Delta t)\cdot C_{m,q}^{i-1}(t-\Delta t)}_{\substack{input\ from\ the\ element\ above \\ through\ the\ aqueous\ phase}} + \underbrace{V_{q_{max}}^{i}\cdot C_{m,q}^{i}(t-\Delta t)}_{\substack{initial\ mass\ in\ the \\ element}}$$

The concentration of MTBE in the aqueous phase ($C_{m,q}$) was calculated considering that ethanol acts as a cosolvent, as described in Appendix C.

$$C_{m,n}^i(t) = \frac{M_m^i(t) - C_{m,q}^i(t)\cdot V_{q_{max}}^i(t) - C_{m,q}^i(t)\cdot V_{q_d}^i(t)}{V_n^i(t)}$$

Appendix E

Evolution of the hydrocarbon stain in the source zone with time

Aug. 21st, 2008 (day 0) – WT = 52cm bgs: Trench packing after E10 spill. Red stain on the sides indicates that some of the gasoline infiltrated through the sides of the trench.

Sep. 17th, 2008 (day 27) – WT = 49cm bgs: Red stain on the ground after water table rise. Blue arrow shows groundwater flow direction. Gasoline was recovered at the vapor sampling port indicated by the red arrow at 40 and 60cm bgs.

Dec. 03rd, 2008 (day 104) – WT = 41cm bgs: Red stain is stronger on the sides of the trench. Gasoline likely accumulated more on these regions due to less effective packing on the sides. Blue arrow shows groundwater flow direction.

Jan. 22nd, 2009 (day 154) – WT = 36cm bgs: Red stain is stronger and covers a bigger area. Stain is also seen outside of the temporary building. Blue arrow shows groundwater flow direction.

Appendix F

Equations for calculations using soil core data

Definitions:

s_i: dry soil concentration of compound *i* (mg/kg);

$s_{i,wet}$: wet soil concentration of compound *i* (mg/kg);

C_i: concentration of compound *i* in the aqueous phase (mg/kg);

ρ_b: soil bulk density = 1.81 g/cm^3;

S_i^{max}: maximum concentration of compound *i* in the soil without NAPL presence (mass of *i* / mass of soil);

$M_{i\_dis}^{eq}$: dissolved mass of compound *i* in the aqueous phase at equilibrium conditions;

$M_{i\_sor}^{eq}$: sorbed mass of compound *i* at equilibrium conditions;

M_i : total mass of compound *i*;

M_{solids}: mass of soil grains;

$C_{i\_dis}^{eq}$: dissolved concentration of compound *i* in the aqueous phase in equilibrium with NAPL (mass *i*/volume of water);

$C_{i\_dis}^{sol}$: solubility of compound *i* in the aqueous phase (mass *i*/volume of water);

$C_{i\_sor}^{eq}$: sorbed mass of compound *i* in equilibrium with NAPL (mass of *i* / mass of soil);

K_d: partition coefficient ($K_d = C_{i\_sor}^{eq}/C_{i\_dis}^{eq}$);

n: porosity = 0.33;

V_T: total volume;

ρ_b: soil bulk density = 1.81 g/cm^3;

x_i: molar fraction of compound *i* in the NAPL;

v_i: volume fraction of compound *i* in the NAPL;

S_w: water saturation;

m_w: water mass;

S_{NAPL}: NAPL saturation.

1: CONVERSION FROM WET SOIL CONCENTRATION TO DRY SOIL CONCENTRATION

$$s_{i,wet} = \frac{M_i}{M_{solids} + m_w} = \frac{M_i}{M_{solids} + \rho_w \cdot V_w} = \frac{M_i}{M_{solids} + \rho_w \cdot V_t \cdot n \cdot S_w}$$

$$s_{i,wet} = \frac{M_i}{M_{solids} + \frac{M_{solids}}{\rho_b} \cdot \rho_w \cdot n \cdot S_w} = \frac{M_i}{M_{solids}\left(1 + \frac{\rho_w}{\rho_b} \cdot n \cdot S_w\right)} = \frac{s_i}{1 + \frac{\rho_w}{\rho_b} \cdot n \cdot S_w}$$

$$s_i = s_{i,wet}\left(1 + \frac{\rho_w}{\rho_b} \cdot n \cdot S_w\right)$$

2: CHECK FOR NAPL PRESENCE

$$s_i^{max} = \frac{M_{i,dis}^{eq} + M_{i,sor}^{eq}}{M_{solids}}$$

$$s_i^{max} = \frac{C_{i,dis}^{eq} \cdot V_w + C_{i,sor}^{eq} \cdot M_{solids}}{M_{solids}}$$

$$s_i^{max} = \frac{C_{i,dis}^{eq} \cdot V_w + C_{i,dis}^{eq} \cdot K_d \cdot M_{solids}}{M_{solids}}$$

$$s_i^{max} = \frac{C_{i,dis}^{eq} \cdot n \cdot S_w \cdot V_T + C_{i,dis}^{eq} \cdot K_d \cdot M_{solids}}{M_{solids}}$$

$$s_i^{max} = C_{i,dis}^{eq}\left(\frac{n \cdot S_w \cdot V_T + K_d \cdot M_{solids}}{M_{solids}}\right)$$

$$s_i^{max} = C_{i,dis}^{eq}\left(n \cdot S_w \cdot \frac{V_T}{M_{solids}} + K_d\right)$$

$$s_i^{max} = C_{i,dis}^{eq}\left(\frac{n \cdot S_w}{\rho_b} + K_d\right)$$

$$s_i^{max} = C_{i,dis}^{sol} \cdot x_i\left(\frac{n \cdot S_w}{\rho_b} + K_d\right)$$

Maximum concentrations when $S_w = 1$ (fully saturated)

compound	$C_{i\_dis}^{sol}$ (mg/L)	x_i	K_d (L/kg)*	s_i^{max} (mg/kg)
toluene	519	7.9%	0.088	11.03
ethylbenzene	161	3.0%	0.14	1.56
o-xylene	171	2.3%	0.128	1.22

* Hubbard (1992)

3: NAPL SATURATION

$$M_i = M_{i,NAPL} + M_{i,dis} + M_{i,sorb}$$

$$M_i = V_{NAPL} \cdot v_{i,NAPL} \cdot \rho_i + C_{i,dis}^{sol} \cdot x_i \cdot V_w + C_{i,dis}^{sol} \cdot x_i \cdot K_d \cdot M_{solids}$$

$$M_i = S_{NAPL} \cdot V_{total} \cdot n \cdot v_{i,NAPL} \cdot \rho_i + C_{i,dis}^{sol} \cdot x_i \cdot n \cdot S_w \cdot V_{total} + C_{i,dis}^{sol} \cdot x_i \cdot K_d \cdot V_{total} \cdot \rho_b$$

$$\frac{M_i}{V_{total}} = S_{NAPL} \cdot v_{i,NAPL} \cdot n \cdot \rho_i + C_{i,dis}^{sol} \cdot x_i \cdot n \cdot S_w + C_{i,dis}^{sol} \cdot x_i \cdot K_d \cdot \rho_b$$

$$\frac{M_i}{\frac{M_{total}}{\rho_b}} = S_{NAPL} \cdot v_{i,NAPL} \cdot n \cdot \rho_i + C_{i,dis}^{sol} \cdot x_i \cdot n \cdot S_w + C_{i,dis}^{sol} \cdot x_i \cdot K_d \cdot \rho_b$$

$$s_i \cdot \rho_b = S_{NAPL} \cdot v_{i,NAPL} \cdot n \cdot \rho_i + C_{i,dis}^{sol} \cdot x_i \cdot n \cdot S_w + C_{i,dis}^{sol} \cdot x_i \cdot K_d \cdot \rho_b$$

$$S_{NAPL} \cdot v_{i,NAPL} \cdot n \cdot \rho_i = s_i \cdot \rho_b - C_{i,dis}^{sol} \cdot x_i \cdot n \cdot S_w - C_{i,dis}^{sol} \cdot x_i \cdot K_d \cdot \rho_b$$

$$S_{NAPL} \cdot v_{i,NAPL} \cdot n \cdot \rho_i = s_i \cdot \rho_b - C_{i,dis}^{sol} \cdot x_i \cdot (n \cdot S_w + K_d \cdot \rho_b)$$

$$S_{NAPL} = \frac{s_i \cdot \rho_b - C_{i,dis}^{sol} \cdot x_i (n \cdot S_w + K_d \cdot \rho_b)}{v_{i,NAPL} \cdot n \cdot \rho_i}$$

4: HYDRAULIC CONDUCTIVITY

$$k_{rw} = S_e^{0.5}\left[1-\left(1-S_e^{\frac{1}{m}}\right)^{m}\right]^2$$

$$S_e = \frac{S_w - S_{wr}}{1 - S_{wr}}$$

From Mickle (2005): m = 0.8276

Appendix G

Aqueous ethanol concentration from the soil core data

(Same definitions as presented in Appendix F)

To calculate the mass fraction of ethanol in the aqueous phase ($c_{e,q}$) as described in Appendix B, the overall phase composition had to be determined. The mass of each component (ethanol: m_e; NAPL: m_N; water: m_w) was determined for one unit area and height Δz, as follow:

$$m_e = s_e \cdot \rho_b \cdot \Delta z$$
$$m_N = S_N \cdot n \cdot \rho_N \cdot \Delta z$$
$$m_w = S_q \cdot n \cdot \rho_w \cdot \Delta z - m_e$$

The equation for water mass calculation implies that all ethanol is in the aqueous phase. This is based on the preferential partitioning of ethanol to the aqueous phase. As for most of the samples the mass of ethanol is small in comparison to the water mass and/or the NAPL saturation is small; meaning a small fraction of ethanol is in the NAPL; this assumption is not far from reality. The validity of this assumption was verified recalculating the mass of water after the ethanol partitioning between phases had been defined. When the difference in water mass was greater than 2%, the water mass was adjusted.

The overall fraction of each phase was then calculated and the ethanol concentration in the aqueous phase was obtained as described in Appendix B. The mass of ethanol in the aqueous phase, $m_{e,q}$, was obtained as follow:

$$f_{e,q} = \frac{m_{e,q}}{m_q}$$
$$f_{e,q} = \frac{m_{e,q}}{V_t \cdot n \cdot S_q \cdot \rho_q}$$
$$m_{e,q} = f_{e,q} \cdot V_t \cdot n \cdot S_q \cdot \rho_q$$
with: $\rho_q = 0.9989 \cdot X_w + 0.7845 \cdot X_e - 0.138 \cdot X_w \cdot X_e$ (Oliveira 1997)

The water mass was calculated considering the distribution of ethanol mass between the NAPL and aqueous phases and the validity of the assumption described before was verified.

The calculated concentration of ethanol is highly dependent on the assumed total aqueous concentration. To exemplify this, a different saturation profile was adopted, scaling the Borden characteristic curve based on the capillary fringe depression observed in laboratory experiments (Chapter 4). The concentration values obtained are much lower than calculated previously. Since the aqueous content was not directly measured, its estimation adds uncertainty on the estimated values. However, previous studies with Borden sand and the same gasoline have yielded similar saturation curves to what was estimated (Vakili 2008).

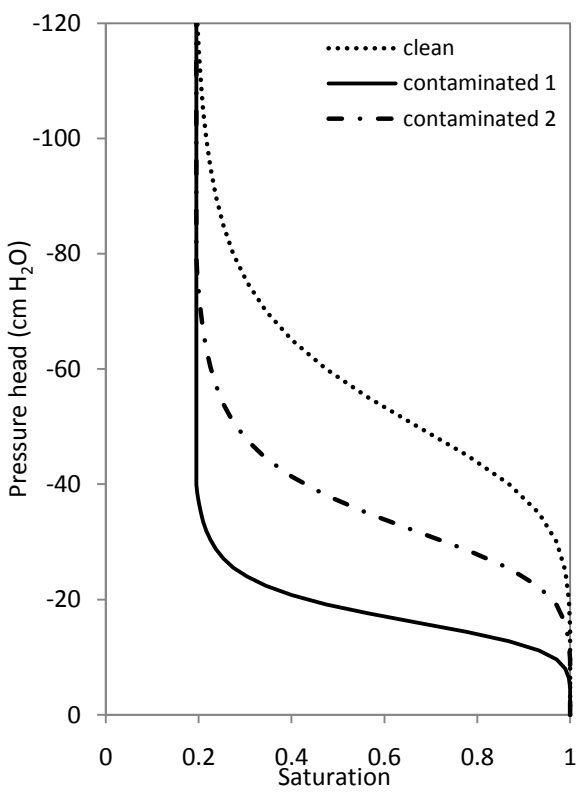

a) Aqueous saturation profile

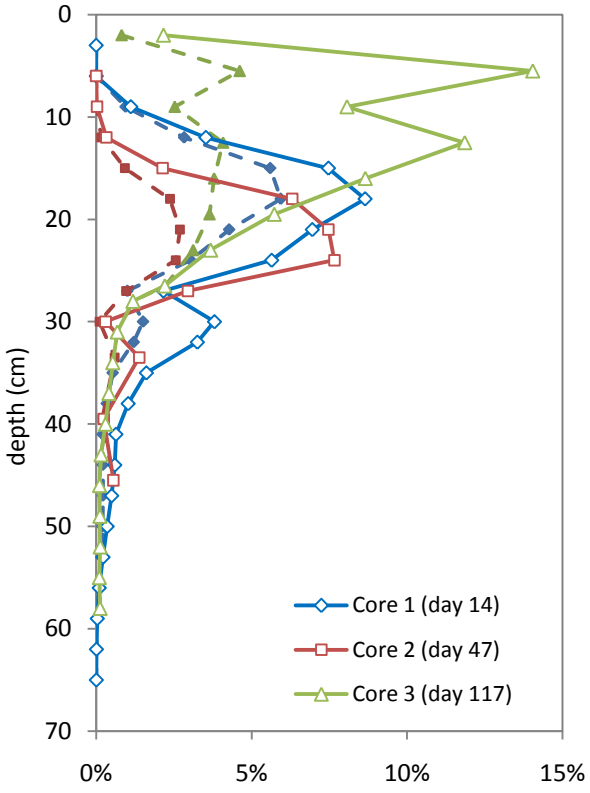

b) Ethanol concentration. Continuous line: contaminated 1; dashed line: contaminated 2.

Impact of the assumed water content profile on the ethanol pore water concentration estimate

References:

Oliveira, E. 1997. Ethanol flushing of Gasoline Residuals: Microscale and Field Experiments. Ph.D dissertation, Department of Earth Sciences, University of Waterloo.

Vakili, F. 2008. A Coupled Hydrogeological-Petrophysical Analysis of Geophysical Variation in the Vadose Zone. MSc thesis, Department of Earth Sciences, University of Waterloo.

Appendix H

MTBE breakthrough curves at wells RA-W06 and RB-W07

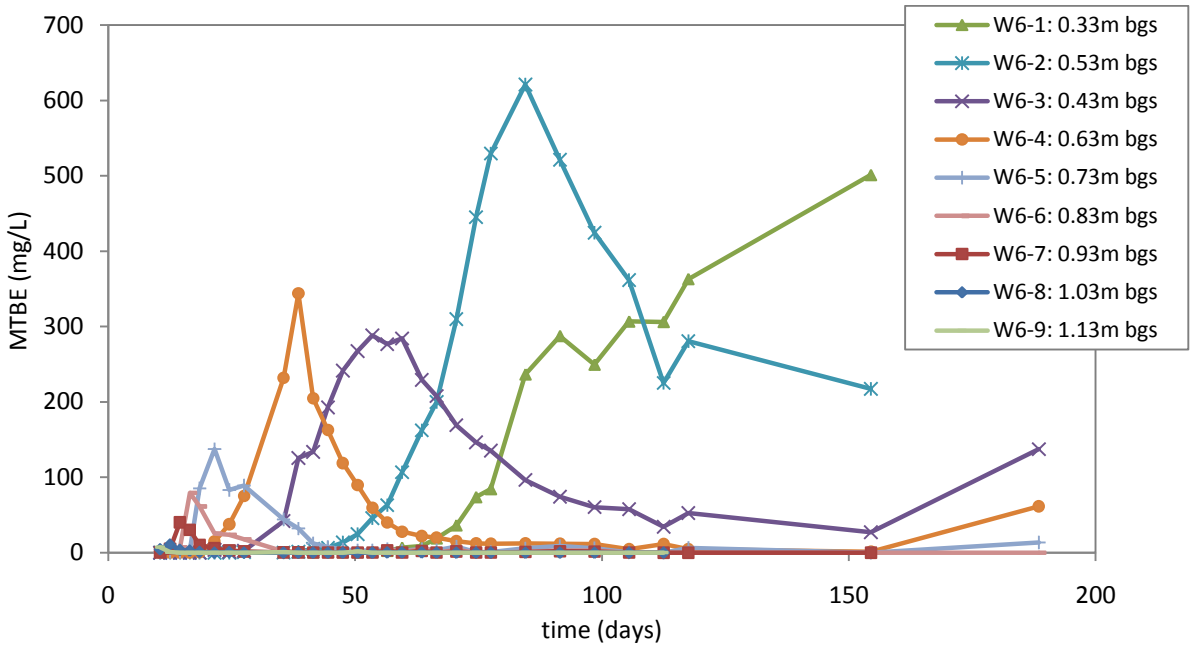

MTBE Breakthrough curve – Well RA-W06

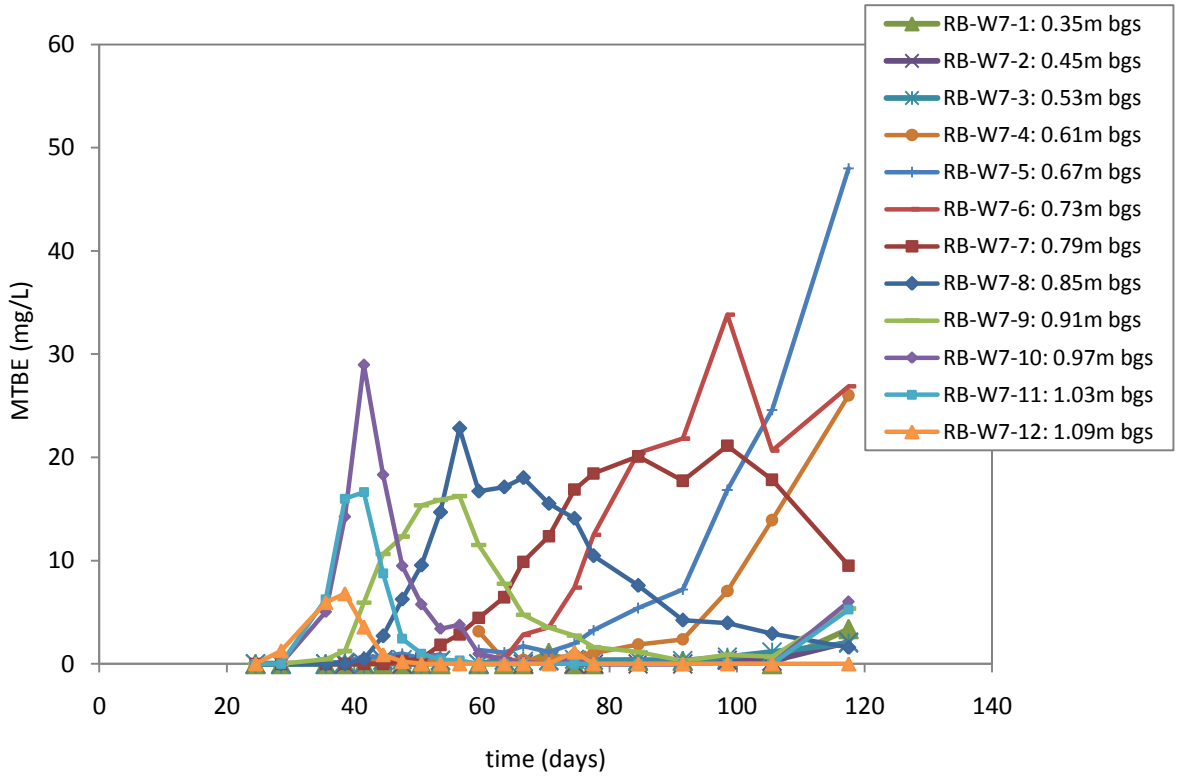

MTBE Breakthrough curve – Well RB-W07

Appendix I

Breakthrough curves at selected sampling ports

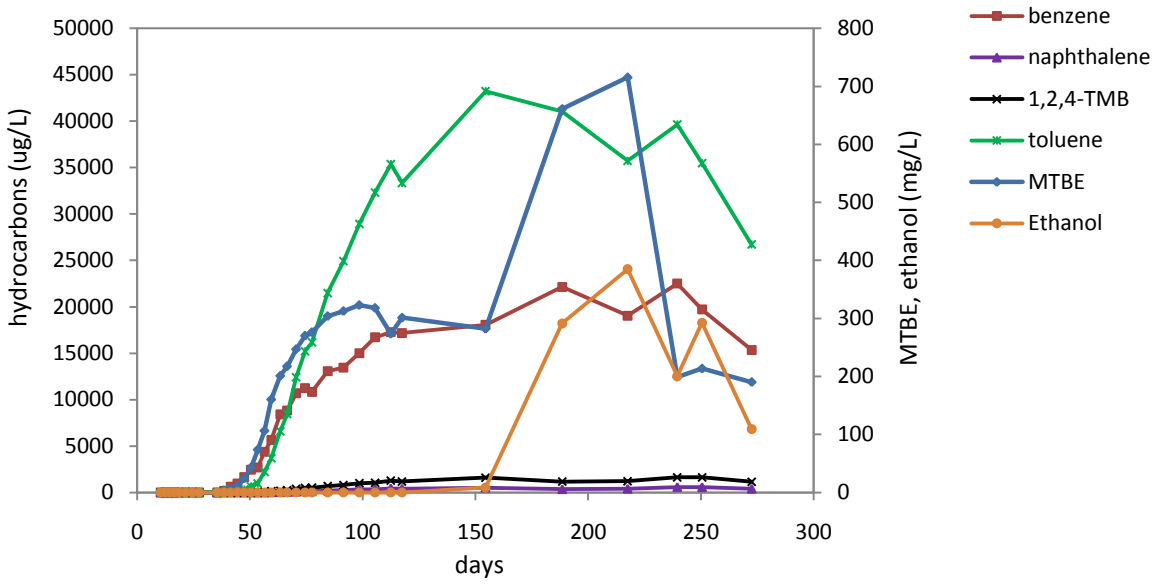

RA-W07-02: 0.43m bgs

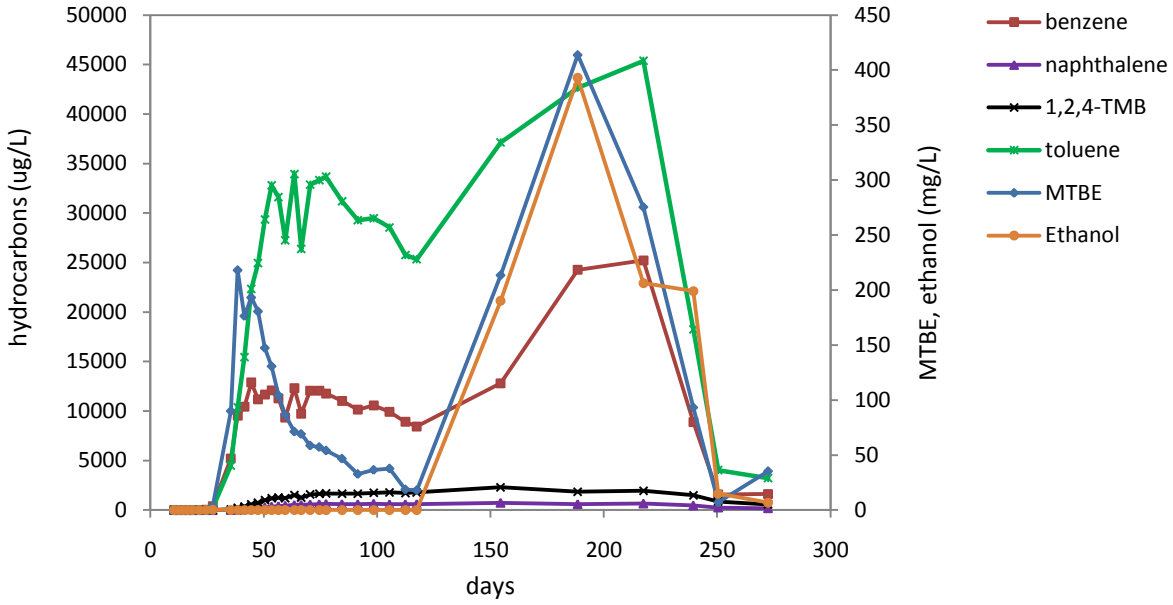

RA-W07-04: 0.63m bgs

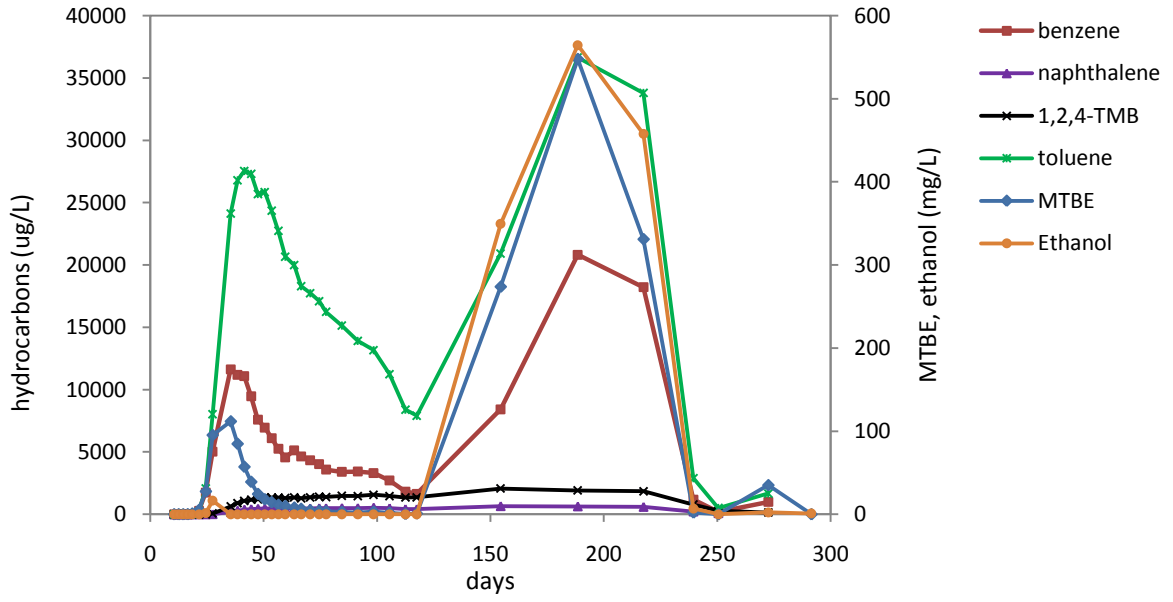

RA-W07-05: 0.63m bgs

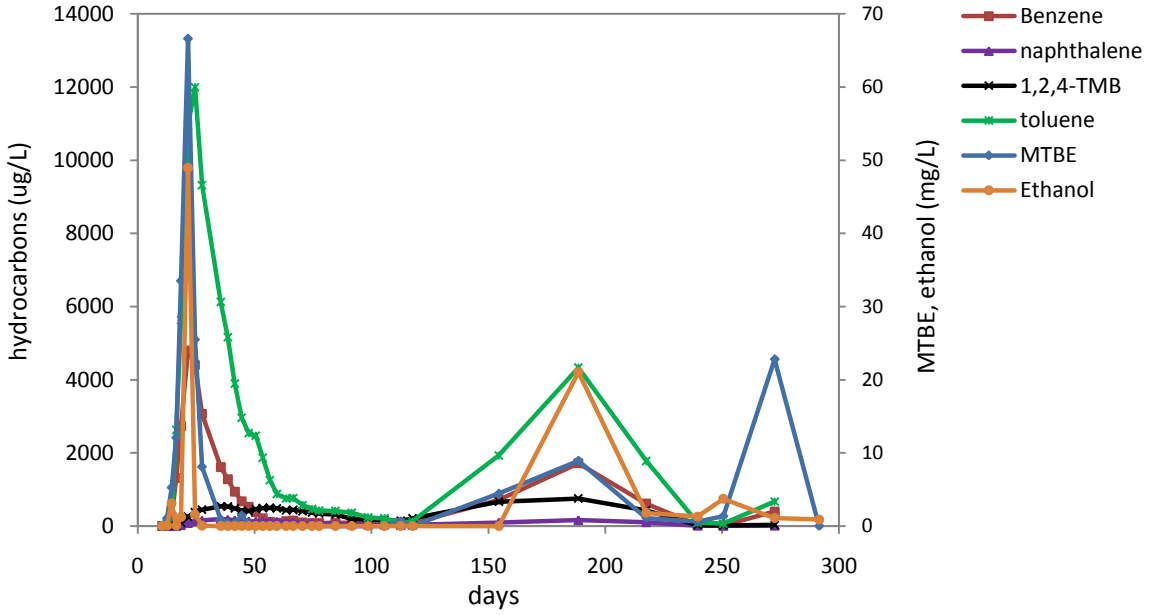

RA-W07-7: 0.83m bgs

Appendix J

Gasoline hydrocarbons snapshots

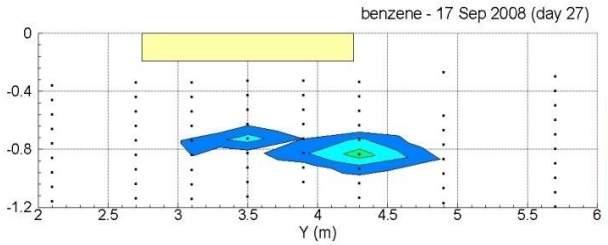

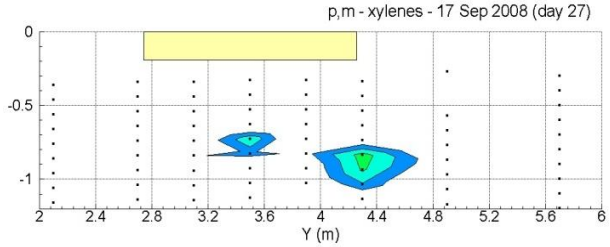

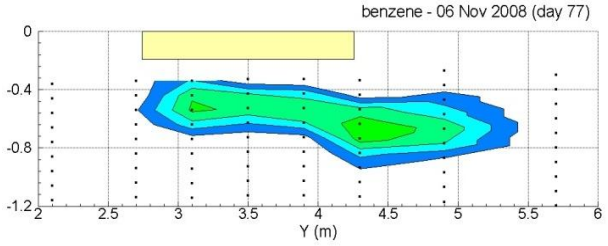

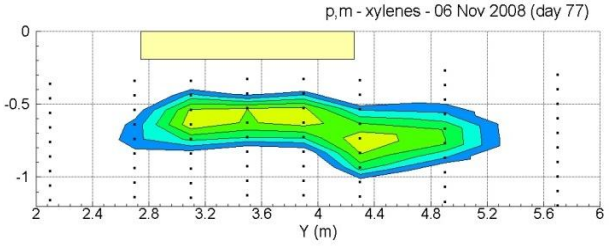

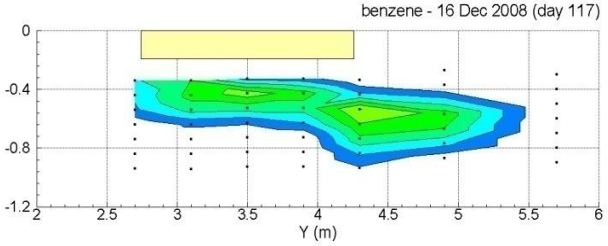

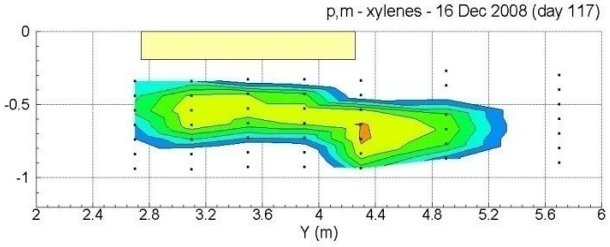

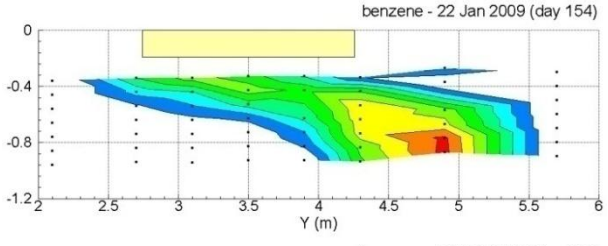

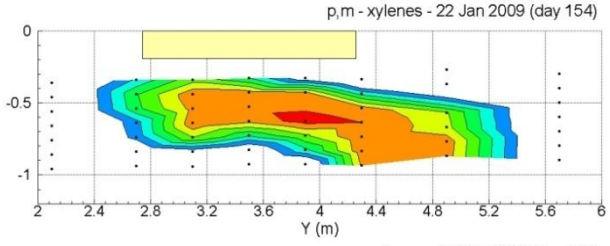

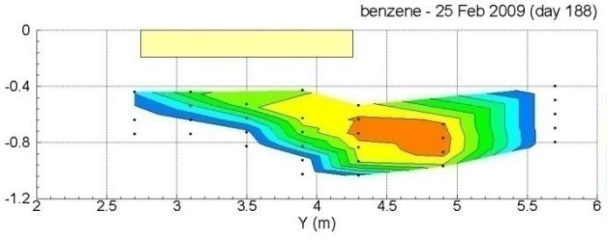

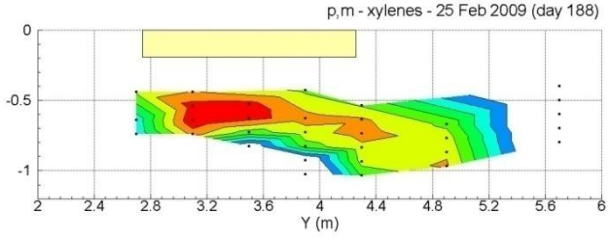

Benzene contours at Row A

p,m-Xylenes contours at Row A

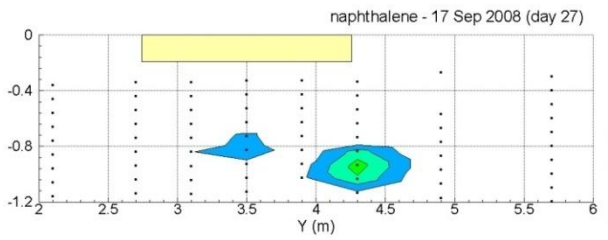

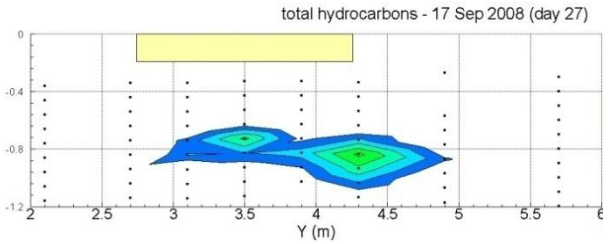

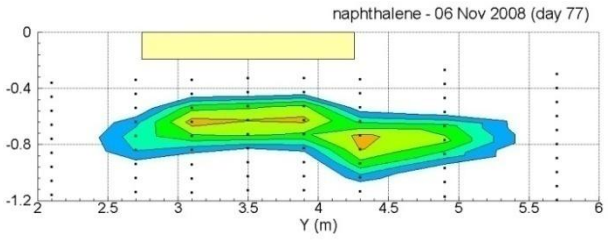

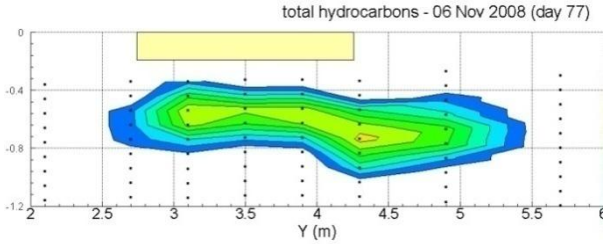

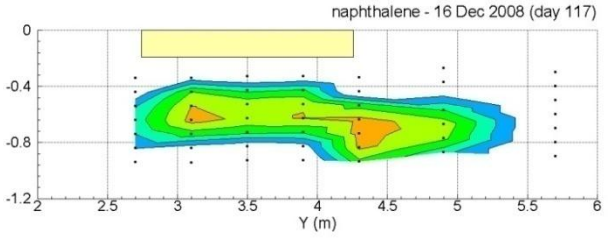

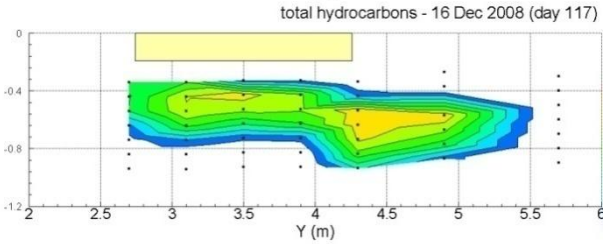

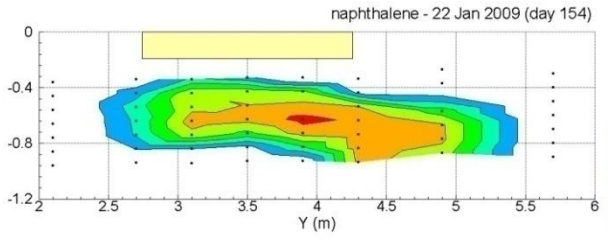

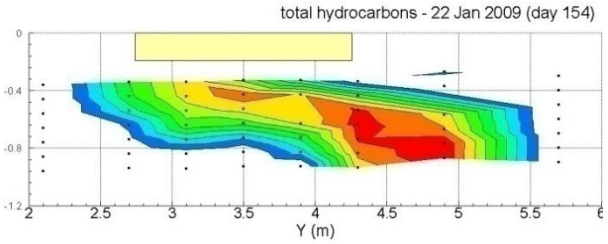

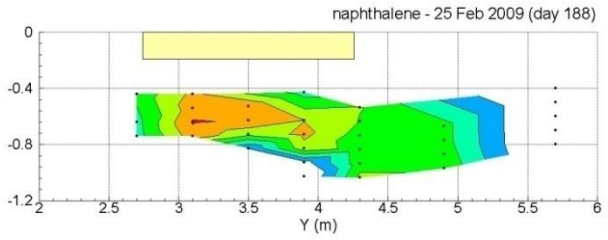

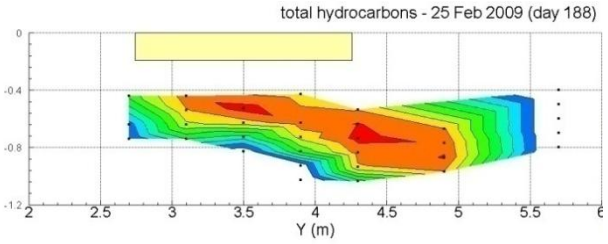

Naphthalene contours at Row A

Total hydrocarbons contours at Row A

Appendix K

Mass discharge calculation

Mass discharge was calculated according to the equation below:

$$Mass\ discharge = \sum_{i=1}^{n} q_i \cdot C_i \cdot A_i$$

q_i: darcy flux at sampling point i; average of 0.0297 m/day assumed equal for all points;

C_i: concentration at sampling point i;

A_i: cross sectional area of sampling point i perpendicular to flow direction.

The area A_i for each point was calculated as a rectangle with dimensions equal to half the distance to the closest sampling points in all directions.

Dimension in the vertical direction:

ports 1 and 13: 15cm

ports 2 to 12: 10 cm

ports 14 and 15: 20 cm

Dimension in the transverse direction:

wells 1 and 11: 107.5 cm

wells 2 and 10: 80 cm

wells 3 and 9: 70 cm

wells 4 and 8: 50 cm

wells 5, 6 and 7: 40 cm

The uncertainties associated with this approach to calculate the mass discharge are discussed on Chapter 2.

Appendix L

Field data: Groundwater and soil concentrations

(database included in a CD)